Analysis of multi-year ice loads Molikpaq data (1985-86 winter deployment): final report

Frederking, R.; Sudom, D.; Bruce, J.; Fuglem, M.; Jordaan, I; Hewitt, K.; Wright, B.

Publisher's version / Version de l'éditeur:
https://doi.org/10.4224/23002246
Controlled Technical Report (National Research Council of Canada. Canadian Hydraulics Centre); no. CHC-CTR-068, 2010-01

CANADIAN HYDRAULICS CENTRE
CENTRE D'HYDRAULIQUE CANADIEN

ANALYSIS OF MULTI-YEAR ICE LOADS MOLIKPAQ DATA (1985-86 WINTER DEPLOYMENT)

FINAL REPORT

R. Frederking and D. Sudom — **NRC-CHC**
J. Bruce, M. Fuglem and I. Jordaan — **Ian Jordaan and Associates Inc.**
K. Hewitt — **K. J. Hewitt & Associates Ltd.**
With some input from
B. Wright — **Brian Wright & Associates Ltd.**

Controlled Technical Report prepared for:
ConocoPhillips Canada
Shell International Exploration and Production
American Bureau of Shipping
Statoil
Keppel Offshore & Marine USA
ExxonMobil Upstream Research Company
Program for Energy Research and Development

Controlled Technical Report CHC-CTR-068
January 2010

Confidential until September 30, 2011

National Research Council Canada | Conseil national de recherches Canada

Canada

This page is intentionally left blank.

EXECUTIVE SUMMARY

This Joint Industry Project was initiated with the purpose of narrowing uncertainties associated with the 1986 multi-year ice loading events on the Molikpaq offshore structure in the Beaufort Sea. Insights gained from prior studies were built upon, and new thinking was applied to the issues. The project was aided by complete access to the extensive library of original Gulf Canada Resources and contractor reports on the Molikpaq deployments in the Beaufort Sea. This included access to the original data tapes, videos, Ice Observer notes, initial analysis notes, and contact with personnel who were involved during the events and had first-hand knowledge. Some of the reports had not been re-evaluated since they were originally prepared. A thorough review was carried out during the present project of the reports prepared in the Gulf Canada Resources Phases 1A/1B and Phase 2 JIPs on Dynamic Ice-Structure Interaction with the Molikpaq. Through these reviews, it became apparent that some of the original assumptions made in deriving ice loads from measured response of Molikpaq instruments could be questioned.

All previous analysis has taken MEDOF panel data as the basis for interpreting ice loading, either directly from the panels or indirectly for calibrating strain gauge and extensometer data. Questions had already been raised as to the state of the sand in the core and the limits on its ability to resist ice loading. The current study also identified softening of the material in the MEDOF panels as a reason why loads estimated using their original calibrations were so large.

The ice load estimates determined by the project team are based on the extensometer readings, combined with the finite element model in the Sandwell report; are supported by geotechnical estimates in the current and previous work of K. Hewitt; are consistent with the analysis of the May 12 decelerating floe impact; and are corroborated by a comparison between the MEDOF panel pressure results and local ice pressures measured in other regions. Ice loads initially determined by the above means were about 50% lower than those determined based on the original calibrations of the MEDOF panels. Analysis by the project team based on probabilistic averaging led to a 15% to 20% reduction of global ice loads. Where phase lock occurred, ice failure was simultaneous and loads were increased by 20% to 30% from the non-simultaneous case. The largest loads are associated with phase lock, and occurred on March 8, April 12 and May 12. Of these, the largest estimated load was for the April 12 event and was in the range of 200 to 250 MN.

The findings of the project team differ from the original Gulf Canada Resources evaluations of over 20 years ago and new analyses which are presented in the 2009 Klohn Crippen Berger report. The Klohn Crippen Berger evaluations conclude that, although the core was not densified, the partial liquefaction during the April 12 event was not due to the loose core. Instead, it was the result of the large cyclic loading experienced by the Molikpaq, on the order of 500 MN, which in turn is based on the assumption that the original MEDOF panels are reliable.

The load estimates based on the original calibration of the MEDOF panels have strongly influenced estimates in past publications regarding the Molikpaq. We believe that the ice loads determined by the present project team are an improved representation of multi-year ice loads on the Molikpaq over the 1985-86 season. New field measurements, either with improved panels on an offshore structure in the Arctic or impacts on a natural feature, are recommended.

This page is intentionally left blank.

EXTENDED ABSTRACT

This Joint Industry Project involved the detailed analysis of time series records to estimate ice forces and global pressures during periods of multi-year ice interaction with the Molikpaq caisson structure. Original data files, reports and videos from the 1985-86 deployment at the Amauligak I-65 location were used in the analysis. The objective of the JIP was to determine global ice loads and pressures resulting from multi-year ice interactions and relate them to ice conditions (thickness, feature shape, drift rate), ice failure mode (crushing, cyclic crushing, mixed modal, flexure, creep), and identify trends. Underlying this was a careful and critical review of all instrumentation systems, analysis methods and data sources used in previous analysis of ice loading on the Molikpaq.

New Findings

The work has identified factors which call into question the instrument calibration factors previously used in the interpretation of Molikpaq ice loads. Analysis of the deceleration of a second-year floe on May 12 gave substantially lower loads than those based on the original MEDOF calibrations. Comparison of local ice pressures from the MEDOF panels showed them to give average local ice pressures on average two times higher than the average local ice pressures from other comparable data sources and ice thicknesses. Softening of the MEDOF panels due to high local loading of the polyurethane buttons has been identified as a factor which explains this discrepancy. Additionally, geotechnical analysis indicated lower ice loads on the Molikpaq than loads predicted from MEDOF panel measurements. Placement of the sand core resulted in it being loose and unable to generate much resistance at the small deformations measured. It is our judgement that historical MEDOF panel derived ice loads are of the order of two times too high. We have developed new calibration factors to reflect this. In this report results are presented based on the new calibration factors, the "Best Estimate" case, and, for comparison with previous Molikpaq analysis based on original MEDOF panel calibration, the "Historical Case".

Event Selection

The first task of the project was to review all information sources to identify times when multi-year ice was likely interacting with the Molikpaq. This included the hourly ice observations made by environmental observers onboard the Molikpaq throughout the winter, and provided near continuous information on concentration, ice type by partial concentration, and drift speed and direction. They covered ice conditions in an area of a few kilometre radius around the Molikpaq. Because the distinction between second-year ice and multi-year ice is not generally clear, both were included in the inventory. Additionally, logs of videos, which identified multi-year ice that interacted with the Molikpaq, and ice interaction observation sheets or "rubble maps", which provided sketches and descriptions of ice type and failure mode, were reviewed. These latter records were more useful in identifying actual multi-year ice interactions with the Molikpaq. Twenty-one periods were identified for possible analysis. Within these time periods, when multi-year ice was present, events or Sub-events corresponding to a particular failure mode, drift speed, ice thickness, etc. were identified.

Ice Conditions

The 1985/86 winter season at the Amauligak I-65 location was judged to be more severe than normal. In late October, at the time of freeze-up, the edge of the polar pack was further south than normal, with some pockets of multi-year ice extending southwards across the same latitude as the Amauligak location. By early January the landfast ice edge was at the 20 m water depth contour, about 15 km south of the Molikpaq. In late February and early March, strong north-westerly winds brought second-year and multi-year ice southwards, into the vicinity of the Molikpaq's location. During the first week of March a mix of multi-year and second-year ice floes moved across the Amauligak location, impacting the Molikpaq in the process. On March 8, the southerly ice drift stopped, being constrained

by the landfast ice to the south. The ice then remained stationary, initiating a few creep loading events, until April 12, when the ice movement generated the largest loading event of the winter. During the remainder of the winter the ice was mobile and there were several encounters with second-year and multi-year ice.

Ice thicknesses for events were generally estimated by the Ice Observer and noted on sketches of interaction events. Video records were used to verify the visual observations. There is considerable uncertainty in the ice thickness observations, ± 0.5 m for ice around 2 m thick, and ± 1 m for ice 3 m and thicker. The ice which interacted with the Molikpaq on March 7-8 and April 12 was stationary for four weeks following March 8. This allowed access to the ice surface to measure ice thickness by drilling holes along the edges of the broken track and other areas, some that subsequently moved past the Molikpaq on April 12. It was for these events that the best measurements of ice thickness were obtained. Average thickness in specific areas related to loading events varied from 3.3 m to 5.9 m. The coefficient of variation from over 70 measurements of multi year and second-year ice in the region was 0.37. The feature which resulted in the largest load on the structure was a multi-year hummock 70 m long and with a 3 m sail height surrounded by ice with an average thickness of 3.3 m. The maximum load was limited by failure of thinner ice at the back side of the hummock.

Description of Molikpaq and Instrumentation

The Molikpaq is an annular steel caisson supporting a deck structure. The core of the annulus was filled with sand, which provided a portion of the horizontal resistance. The caisson has near vertical sides (7° from the vertical at the waterline) and is octagonal in plan. Because the structure was one of the earliest purpose-built structures for exploratory drilling in water depths greater than 20 m, it was extensively instrumented to gather information on the ice loading it experienced. A variety of sensors were installed in and around the structure:

- Ice load measurement systems on the caisson: MEDOF panels, strain gauges, extensometers, tiltmeters and accelerometers
- Geotechnical data measurement systems in the sand core and berm: pore pressure cells, total pressure cells, in-place inclinometers, manual inclinometers, electric piezometers and manual piezometers

There were 512 channels of instrumentation and a data acquisition system to record the output of the instruments. Depending upon trigger levels on instrument output, the recording system could record data in several modes:

- DAY files for which average, minimum and maximum values from a 1 Hz scan of all 512 channels were recorded every 5 minutes. This record was for periods of low or no ice loading, and was useful for establishing baseline or zero readings for the instruments.
- FAST files were triggered automatically when certain measured values were exceeded, or manually at the operators discretion. In this case all 512 channels were recorded at 1 Hz for 65 minutes.
- EVENT, or Burst, files were triggered by even more selective criteria, and a reduced selection of 128 channels was recorded at 50 Hz for about 60 seconds.

Another, and equally important part of the measurement program, was visual observations and video records of ice interaction to compliment the measurement data.

Evaluation of Instrumentation

Before determining ice forces, a comprehensive evaluation and assessment was made of the instrumentation used to measure ice loads on the Molikpaq caisson faces (MEDOF panels), and the Molikpaq caisson response (strain gauges, extensometers, accelerometers and tiltmeters). The instrumentation for measuring the response of the core was also examined (in-place-inclinometers and

manual inclinometers). In previous analyses, the MEDOF panels were taken as the basis for measurement of ice forces, and strain gauges and extensometers were calibrated from the MEDOF panel forces. In the original analysis projects by Gulf Canada Resources Limited (GCRL), extensive effort was put into verifying the response of the MEDOF panels, and identifying independent means of calibrating the strain gauges and extensometers. For the MEDOF panels, it focused primarily on evaluating and correcting for their creep behaviour. It was not until the latter phase of the GCR studies that an independent finite element calibration of the extensometers for determining ice loads was undertaken (Sandwell report in Appendix C of Rogers et al (1991b)). It used a 3-D finite element model of the caisson, friction under the base, and passive pressure resistance from the sand core on the loaded face and active pressure resistance from the sand core on the other faces. Even though the Sandwell report stated the sand core was dense, the actual stiffness values used in the analysis were likely for a loose sand. The analysis gave caisson ring stiffness values that were from one third to two thirds the value of 6 MN/mm obtained from MEDOF panel force measurements. This large difference in calibration factors led to a detailed examination of all factors which might explain the discrepancy.

Regardless of the instrument used for determining ice loads, there should be a fixed relation between them since they were responding to the same ice load. There is uncertainty, however, in the relation between load determined from extensometers, strain gauges and MEDOF panels. Using the MEDOF panels as a base, the factors relating MEDOF panels to extensometers have a coefficient of variance (COV) of 0.23 and the factors between strain gauges and MEDOF panels a COV of 0.34.

MEDOF Panel Softening

Because so much depended on the MEDOF panels, their performance was thoroughly assessed. Unfortunately the panels no longer exist, so they can not be recalibrated. Softening of the polyurethane buttons, which are the load supporting elements in the MEDOF panels, was identified by the Ian Jordaan and Associates team as a factor which could explain the discrepancies in estimated forces (see Chapter 3 of Appendix B). The literature on polymers has been searched and the work of Qi and Boyce (2005) on polyurethane was identified as the closest to describing the loading conditions to which the button material in the MEDOF panels was subjected. This publication presents measurements on polyurethane under high stresses of 20 MPa, and repeated loading. These loading conditions are similar to those experienced by the buttons in the MEDOF panels during ice crushing, when it is known that local pressures in “high pressure zones” are of the order of 10 to 20 MPa on areas 0.3 m by 0.3 m. Pressures on the polyurethane buttons themselves would be twice these values. The Qi and Boyce tests showed that polyurethane exhibited non-linear behaviour for stress above about 5 MPa. Furthermore, softening by about a factor of two after only a few repeats of these high load-unload cycles was observed. This behaviour, inherent in polyurethane, is convincing evidence that softening of the MEDOF panels is a real factor.

MEDOF panel and strain gauge data from the 1984-85 deployment of the Molikpaq at Tarsiut P-45 was thought to provide a means of verifying MEDOF performance before the panels were subjected to extensive loading. Review of the Tarsiut data indicated the MEDOF panels had already experienced extensive ice loads by the time the first measurements were recorded. The occurrence of softening, after only a few load cycles, is why analysis of the 1984-85 Tarsiut data did not help clarify the panel softening issue.

Extensometer Response

The Sandwell (1991) report was prepared for GCR to develop an independent calibration of extensometer measurements as a basis for the determination of ice loads. The report presents a finite element analysis (FEA) of the combined caisson and core of the Molikpaq, the only analysis of the total structure. It was done using COSMOS on a mini-computer. The original FEA for the design of the Molikpaq was done on a mainframe computer using STARDYNE with non-linear soil properties. In a comparison case, for the March 25 loading event, the results of the two programs compared closely. Subsequent cases were run using COSMOS to explore the influence of load magnitude, load distribution, core sand properties and stiffness on calculated extensometer response. COSMOS had the shortcoming that only linear soil properties could be included.

The Sandwell report considered three load distributions across the structure; a uniformly distributed load (UDL) just on the long face, a uniform distributed load (full UDL) across the whole structure including the corners, and a distribution, termed the "Most Likely", in which the corner loads were reduced. The latter two distributions generated lateral forces acting inwards on the corners, which significantly increased the apparent stiffness of the caisson (see Chapter 2 of Appendix B). For a given total load on the structure, all other factors being the same, a uniform load on the long face gave a ratio of 2.7 MN/mm. If the same load was distributed uniformly across the centre face and corners, the ratio was 3.9 MN/mm in terms of the global load and 2.3 MN/mm in terms of the long face load. In the case of the "Most Likely" distribution, the factors were 3.2 and 2.3 MN/mm. The proportion of load transmitted to base friction in the model had a significant effect. Increasing the base friction loading proportion from 20% to 40% to 60% increased the ratio from 3.6 MN/mm to 4.1 MN/mm to 4.5 MN/mm. These factors are all much lower than the "historical case" value of 6 MN/mm for face loading, but they demonstrate that determining a face load or global load from the caisson distortion ratio depends upon the assumptions used.

Shell also shared some of their experience with the redeployment of the Molikpaq to offshore Sakhalin. Direct comparisons were difficult because the Sakhalin configuration of the Molikpaq rested on a 15 m high annular spacer, the sand core was densified and the waterline was about 3 m lower on the caisson. Their extensometer calibration factor, from field measurements, averaged 6 MN/mm, but with large scatter. Based on the differences between Sakhalin and the Beaufort deployments, a lower value would have been expected from the Beaufort experience.

The IJA team used the results of the Sandwell (1991) FEA to determine a stiffness matrix which allows face and global loads to be determined under biaxial loading conditions; that is using deformations across both face pairs and corner pairs to determine loading. The methodology has been developed successfully, and was applied to four events. Where the load was predominantly normal to one of the faces, face load and global load were very similar. It had the largest affect for the March 7 event where there was loading on two faces. For event 0307B (late afternoon March 7) the matrix method gave a global load of 95 MN, compared to 80 MN on a single face.

Results of MEDOF panel and strain gauge measurements show that ice load is not uniform across the face. For example, on March 25 the distribution was U-shaped with the centre load only ¼ of the loads towards the edges, whereas on May 12 the centre load was 2 to 3 times greater than the load towards the edges. An analytical analysis in Appendix E indicates that such face load distributions can make a difference of ± 30% in the calibration factor for converting extensometer measurements of diametral change of the caisson to a face load.

May 12 Impact Event

The maximum force during the May 12 event was calculated by the IJA team based on the floe deceleration, assuming that an accurate time trace of the relative force can be obtained from the

extensometer readings. The mass and initial velocity of the free-floating floe were determined with reasonable accuracy from a helicopter survey of the extent of the floe and radar tracking of its drift. The caisson ring deformation was measured with extensometers, and can be converted to a global interaction force, knowing the stiffness of the caisson. Observers noted the time of initial impact and the time when the flow came to a halt. The momentum of the floe (mass times velocity) is equal to the impulse (area under the force-time curve from time of initial impact to when the floe stopped). Equating the momentum to the area under the force-time curve, global caisson stiffness was determined to be 2.2 MN/mm, substantially less that the historic value of 6 MN/mm used in previous analysis. The maximum force based on floe deceleration and ring deformation (global stiffness 2.2 MN/mm) was 105 MN, compared to 267 MN in previous analysis of extensometer data. Floe deceleration analysis for the May 12 event is presented in Section 11.12.

Local Ice Pressure Comparison

Another means of verifying the performance of the MEDOF panels is to compare the local ice pressures determined from the MEDOF panels with local ice pressures from other measurement sources such as the STRICE project in the northern Baltic. A rigorous basis for comparison of local pressures from several sources, covering a broad range of ice thicknesses is presented in the IJA report (Appendix B, Chapter 6), from the Ph.D. thesis of Rocky Taylor. This analysis takes into account the statistics of local pressures during an event, a weighting relating to the duration of the event, and the ice thickness. In this analysis, and other work, a trend of decreasing pressure with increasing ice thickness has been identified, a trend analogous to the familiar one of local pressure decreasing with increasing area. Mean local ice pressures from Molikpaq (MEDOF panel) and STRICE data are plotted below for a range of ice thicknesses and a power relation fit to each data set. The data sets do not overlap in thickness, but the trend lines demonstrate that the MEDOF panels over-predict local ice pressures by at least a factor of two.

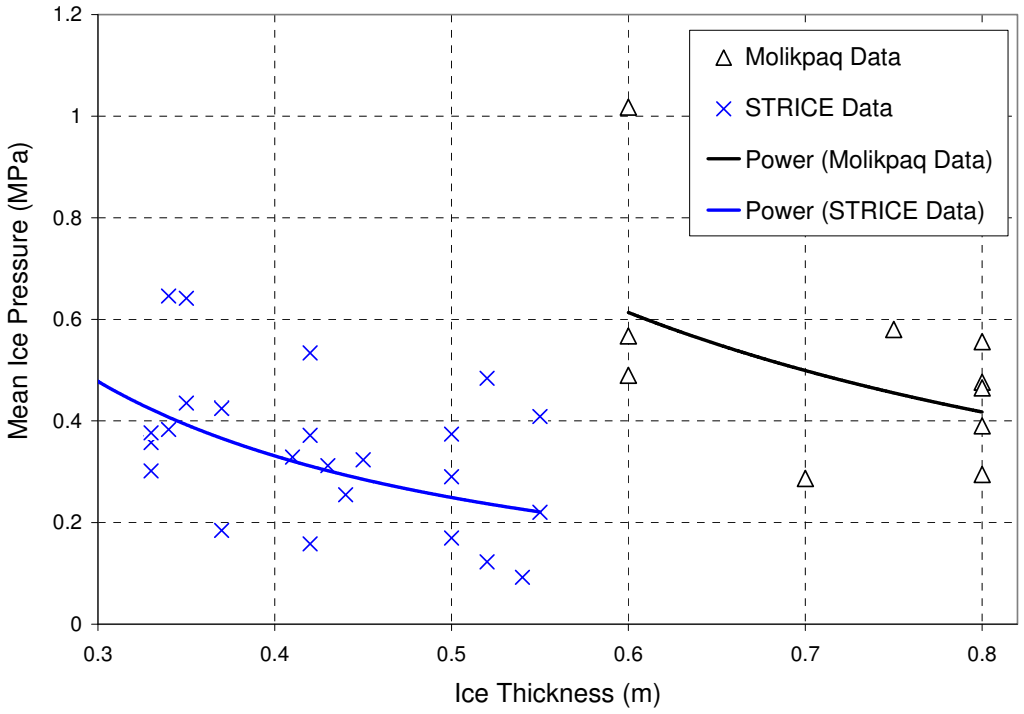

STRICE and Molikpaq column mean pressure vs. ice thickness data

Geotechnical Response

The geotechnical evaluation conducted by K.J Hewitt & Associates Ltd. included a review of:

- The initial design which emphasized the importance of the core sand properties.
- The as-placed (in situ) state of the core sand at Amauligak.
- Performance predictions based on various models, both geotechnical and structural.
- Measured displacements.

As a result, ice load estimates were made for several events. The largest load estimated by these means was during the event on the morning of April 12, 1986. It was concluded that since the global displacements were relatively small and that the sand core was in a loose state that this load was about 200 MN. However because of the inherent uncertainties in the evaluation of the properties of the composite unit combined with the uncertainties in determining displacements, it is believed that the actual load could differ from this estimate. Therefore it was concluded that the load could have been as high as 250 MN or as low as 150MN.

Klohn Crippen Berger Report and other Geotechnical input

ConocoPhillips Canada commissioned Klohn Crippen Berger to review select elements of the 1986 Molikpaq JIP work to provide a broader understanding of the geotechnical performance of the Molikpaq, as well as ice-structure interaction issues. The results of this review were presented to a meeting of Participants' geotechnical experts on February 25. The presentation and subsequent report covered an assessment of the core density, assessment of ice load and platform resistance for the April 12 event, methods and calibration used to estimate ice loads, and a treatment of ice crushing. The conclusion of the report was that, using previously published model calibrations for the Molikpaq core sand, the NorSand computed global load versus caisson ovalling was a good match to the central trend of the measured data for the March 25 and May 12 events. The inference from this match is that the MEDOF panel calibrations were as stated by GCRL, and that the MEDOF panels did not deteriorate during the first two deployments in the Canadian Beaufort Sea. Geotechnical experts from the three Participants, who attended the February 25 presentation, agreed with the KCB report conclusion that the sand core was dilative. Professor K.T. Law of Carleton University carried out an independent geotechnical review of K.J. Hewitt & Associates' 2008 and 2009 reports, as well as the Klohn Crippen Berger report. His reports are in Appendix J. He explained the different understandings of the core sand behaviour in the KCB report and by Hewitt. While acknowledging the core could be mildly dilative, he questioned some of the analysis in the KCB report, particularly the absence of an explanation of the high ice loads compared to the small measured horizontal movements.

Response to the Klohn Crippen Berger Report and other Geotechnical input

From a geotechnical perspective there was nothing in the KCB report that changed the opinions presented in the report by K.J. Hewitt & Associates Ltd. The main theme in the KCB report is that there have been significant advances in interpretation and modelling capabilities in the past twenty years and these advances verify GCRL's initial assessment of the as-placed condition and subsequent performance of the Molikpaq at I-65. However they did not directly address the issue of the 'stress level bias' which accounts for the difference between GCRL's initial assessment and our assessments which show the core sand to be contractive. The report also fails to make any mention that the performance of the Molikpaq at I-65 was exactly as anticipated in the initial design in 1982, if the unit was deployed with a loose sand core and subjected to relatively low ice loading. Likewise the Sandwell extensometer calibration study is dismissed as it did not match the MEDOF panel based load estimates. The KCB report also contained a review of the ice-structure interaction results and understanding of ice mechanics up to the time of the 1986 JIP. Understanding of ice mechanics has advanced since then.

Professor K.T. Law offers two opposing opinions regarding the state of the core sand. Based on his review of the KCB report he concludes that the core sand was dilative and not liquefiable. In contrast he states that 'Based on general evidence, the liquefaction potential of the core sand was high.' He acknowledges that this statement is consistent with the Hewitt report which concludes that the core sand was contractive and liquefiable. He does not offer an explanation for this discrepancy. He does however make the important observation that because of the small horizontal displacements, the estimated ice loads using various models are generally about half those proposed in the KCB report.

"Historical Case"

This JIP has established that geotechnical limitations on sand core behaviour and softening of the panels under normal service loading bring into question the use of original MEDOF calibration values to determine ice loads. Before establishing our "Best Estimate" of ice load and pressures, factors for relating extensometer, strain gauge and MEDOF panel results to each other are necessary. All previous analysis of ice loading on the Molikpaq has started with the MEDOF panels, since they directly measured ice forces on the outer faces of the caisson. MEDOF-based ice loads were subsequently used to calibrate strain response of bulkheads and deformation response of the caisson ring measured by extensometers, to ice loading. In spite of uncertainty of absolute values, MEDOF panel results do provide a basis for establishing relative values for calibrating the strain gauges and extensometers. In analysing and presenting results in this report we have presented two cases, one a "Historical Case" based on the original MEDOF calibration and relative values from strain gauge and extensometer measurements, and the other, a "Best Estimate" case, in which all results are adjusted to our best estimate of the load-caisson deformation relation from extensometer measurements. For the "Historical Case", a factor of 6 MN/mm was used to convert diametral change measured with the extensometers to a face load. The extensometer factor was determined from 20 calibration measurements, and has a coefficient of variation of 0.27. Strain gauge output was converted to a local ice load using an average factor of 24 kN/μs for a width of 2.44 m. This strain calibration factor was adjusted to take into account ice thickness and position on the caisson, and the factor was refined to take values from Table 2 of this report. The strain factor was determined from 39 measurements and had a coefficient of variation of 0.34. The "Historical Case" also provides a basis for comparing results from previously published work with those of this JIP.

"Historical Case" Ice Loads and Pressures

For this report, twenty-one time periods of interest where multi-year or second-year ice was present were investigated. Thirteen of these time periods have been broken down further into a number of events and Sub-events, and analysed in detail. Loads from each of the MEDOF panel, strain gauge and extensometer results have been calculated and presented separately. See Appendix K for time series plots of each event. Each Event or Sub-event includes a time series record of load related to periods when the size, thickness and shape of multi-year ice features are relatively uniform or defined; e.g. a hummock. Selected video records were viewed to verify documented failure behaviour. An event could be anywhere from a few minutes to 10s of minutes. Loading from the south and west, where there were no MEDOF panels, was analysed using strain gauge and/or extensometer data. The characterization of ice thickness was an important part of this task. Information from visual estimates and limited on-ice surveys was compiled from various sources and cross-checked, wherever possible.

Global pressures from the "Historical Case" approach are plotted as a function of ice thickness and compared to predictions of equation [A.8-22] of the *ISO DIS 19906 Arctic offshore structures* standard for a 58 m wide structure in Beaufort Sea conditions.

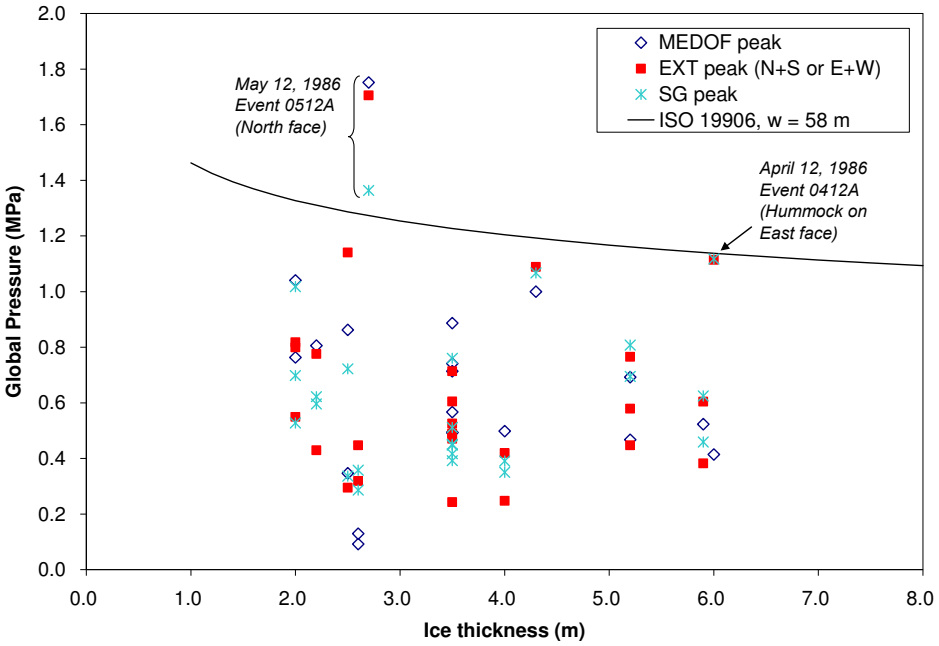

Global pressure "Historical Case" values compared with ISO DIS 19906 Eqn. [A.8-22]

"Best Estimate" Ice Loads and Pressures

The basis for establishing our "Best Estimate" of ice loads, as previously described, included the results of the local ice pressure comparison, geotechnical limitations of sand core response, May 12 floe impact analysis and a MEDOF panel softening mechanism. Our "Best Estimate" of the extensometer calibration used for ice load calculations was 3 MN/mm, 50% of the "Historical Case" value. This factor is likely at the upper end of the range of extensometer factors, but has been selected at this level to err on the side of caution. As a general rule all ice loads, whether determined from extensometers, strain gauges or recalibrated MEDOF panels should be treated as having a coefficient of variation of 1/4 to 1/3. Another method of dealing with this is through estimates of the statistical parameters in a probabilistic model. This is discussed briefly in the IJA report.

The "Best Estimate" face loads determined for the 19 events from the 13 time periods are presented below. Instances where only one or two strain gauges were available for measurement, are marked with an * or **. Note that after April 12 there were three active strain gauges on each face.

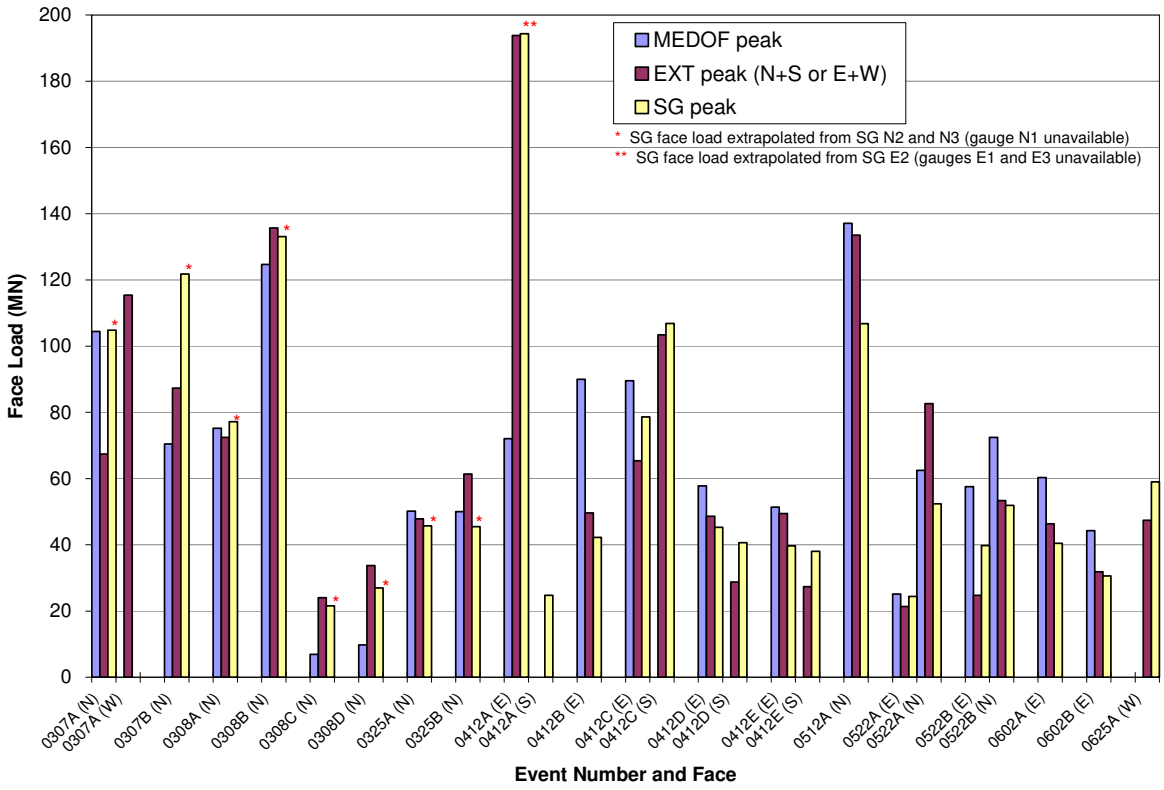

Face loads calculated using "Best Estimate" approach

Using ice thickness determined from visual estimates and limited on-ice surveys, maximum global pressures were determined from maximum loads on the 58 m long face for each event and plotted in the following figure.

The maximum global pressures from the 19 events, for our "Best Estimate" case of global pressures for each measurement system, have been plotted as a function of ice thickness in the figure below. For comparison purposes, global pressure as a function of ice thickness for a 58 m wide structure in Beaufort Sea conditions has been calculated using equation [A.8-22] from the *ISO DIS 19906 Arctic offshore structures* standard. All global pressure values fall below the prediction line. Any recommendation for change to the ISO standard is outside the scope of this project.

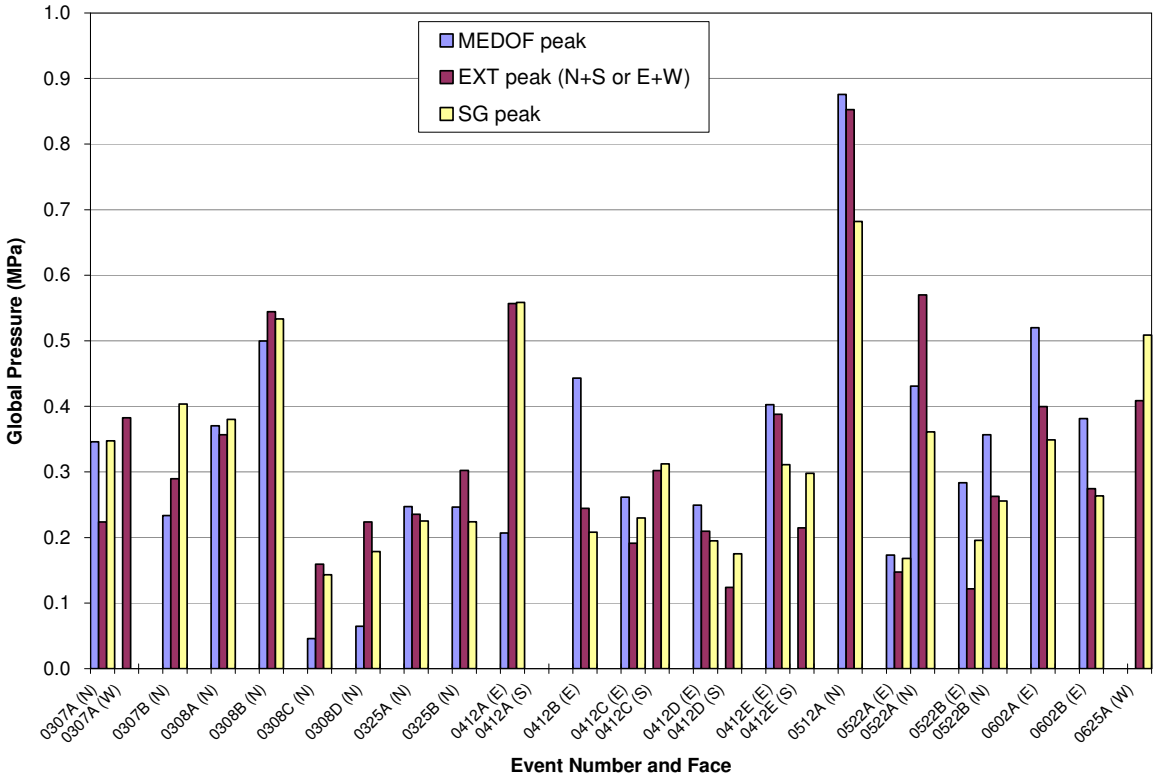

Global face pressures (for width of 58 m) calculated using "Best Estimate" approach

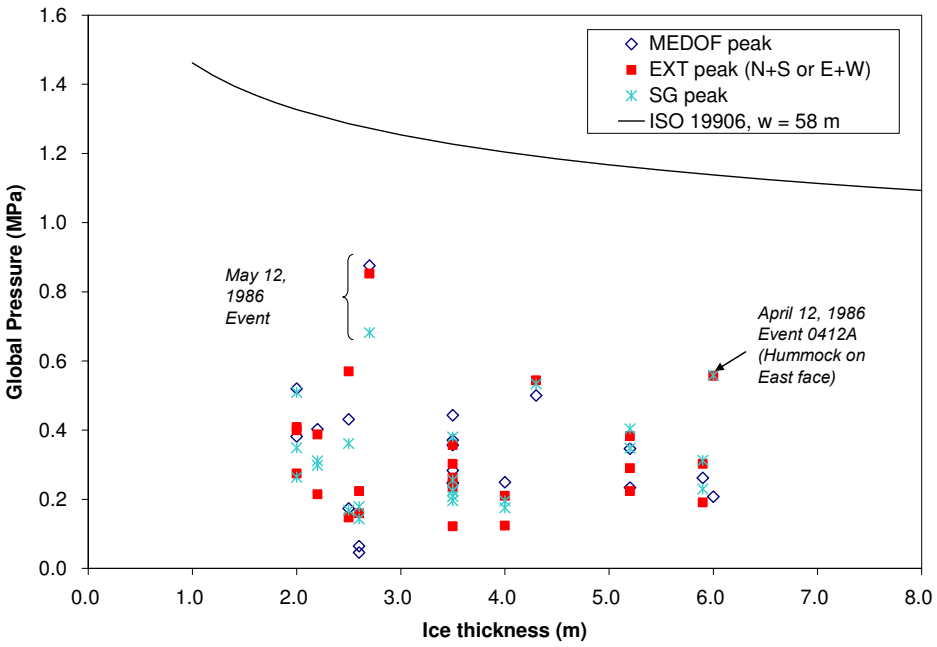

Global pressure "Best Estimate" values compared with ISO DIS 19906 En [A.8-22]

Probabilistic Averaging

The MEDOF panels and strain gauges only cover about 10% of the east and north faces. With random loading on each of the instruments, a linear averaging of the individual group pressures to get a face load may over-predict the load. A method of analysing the MEDOF panel and strain gauge data using probabilistic averaging has been applied and it results in lower face loads than linear averaging. The approach is described in detail in the IJA report (Chapter 5 of Appendix B). The results of this analysis are summarized in the Table below for a number of events. Two cases are presented, one using a linear averaging method for the MEDOF panel loads and the other using probabilistic averaging. In the "No Bottom" case the lower MEDOF panels were ignored and in the "Uniform" case they were included in the load calculation. For creep failure there was no reduction, however for crushing failure, where there was little or no correlation between panel group loads, the load reduction was between 15 and 20%. Note that the ice loads in the Table below are calculated using the "Historical Case" (extensometer calibration factor of 6 MN/mm). "Best estimate" ice load values would be 50% lower.

Maximum face loads (MN) with linear averaging (LA) and probabilistic averaging (PA)

Event	Failure Mode	Maximum Nominal Load		Maximum Nominal Load	
		LA	LA	PA	PA
		No Bottom	Uniform	No Bottom	Uniform
Mar-25-N-1	Creep	103	103	102	102
Apr-12-E-1	Crushing	169	169	139	139
Apr-12-E-2	Crushing	188	375	158	320
Apr-12-E-3	Crushing	84	92	73	82
May-12-N-1	Crushing	168	344	141	296
May-22-N-1	Creep	108	140	107	139
May-22-N-2	Crushing	123	214	103	180
Jun-02-E-1	Crushing	128	129	114	116
Jun-02-E-2	Creep	86	87	85	86

Phase Lock

The issue of phase lock has been examined. It is most clearly exemplified on May 12 when strain gauge results on the north face showed the simultaneous response of the three main bulkheads. This is clear in the EVENT files which were recorded at 50 Hz. Examining a few cases where phase lock was occurring, demonstrated that the peak loads were 20 to 30% greater than for times immediately before or after, when the loading across the face was random. Maximum loads on March 7 and 8, April 12, May 12, June 2 and June 25 were affected by phase lock. For structures not likely to have similar response to the Molikpaq (stiffer ones), measured loads could be reduced by 20 to 30%. Phase lock is discussed in Section 12 of this report.

This page is intentionally left blank.

TABLE OF CONTENTS

APPENDICES

LIST OF FIGURES

LIST OF TABLES

FINAL REPORT

1. INTRODUCTION

The presence of ice in the Arctic regions of Canada, USA, Greenland, Svalbard and Russia presents a unique set of obstacles to the safe and economic production of offshore oil and gas. Ice interaction with structures raises design, operational and regulatory issues, and if not understood properly, can lead to exceedingly expensive design and operational costs for offshore production. Global ice loads are needed for overall stability considerations of gravity based structures, caisson structures and floating production systems. Research on ice loads over the past several years has lead to significant understanding of these loads especially for level ice conditions. Recently, Timco and Croasdale (2006) invited twenty international ice mechanics specialists to predict loads for different full-scale scenarios. The results show general agreement in predicted loads generated by level first-year ice on a vertical-sided structure. However, predictions of loads for multi-year ice ranged over a factor of seven. Clearly this large uncertainty would lead to conservative assumptions regarding ice loads and significantly higher construction and operational costs in regions where multi-year is present. A better understanding of multi-year ice loads, and the factors that affect ice loads is the key to reducing this uncertainty.

The Molikpaq, which was designed and built in the early 1980s as an exploration structure, was extensively instrumented to measure its response to ice loading. This, combined with a program to obtain detailed ice information provided a unique data set for the study of ice loading. The data from measurements at Amauligak I-65 (70° 04' 40" N – 133° 48' 16" W) in 1985-86 were used in a Joint Industry Project conducted by Gulf Canada Resources Ltd. to analyse ice loads, and were reported in a series of confidential reports produced over the period 1987-81. ConocoPhillips Canada, now the owner of the still proprietary Molikpaq data, made the data available for this project, which focused on multi-year ice loading on the Molikpaq at Amauligak I-65. A study of the April 12, 1986 loading event on the Molikpaq (Frederking and Sudom, 2006) in which face loads and global loads were determined is a model of the detailed load analysis carried out in this project.

Previous analysis of ice loading on the Molikpaq has always started with the MEDOF panels, since they directly measured ice forces on the outer faces of the caisson. MEDOF-based ice loads were subsequently used to calibrate strain response of bulkheads and deformation of the caisson ring to ice loading. This JIP has established that geotechnical limitations on sand core behaviour and softening of the panels under normal service loading bring into question using the original MEDOF calibration values to determine ice loads. Nevertheless, MEDOF panel results provide a basis for establishing relative values for calibrating the strain gauges and extensometers. In analysing and presenting results in this report we will present two cases, one a "Historical Case" based on the original MEDOF calibration and relative values from strain gauge and extensometer measurements, and the other, a "Best Estimate" case, in which all results are adjusted to our best estimate of the load-caisson deformation relation from extensometer measurements.

1.1 Project task descriptions

The work for this project was divided into a number of tasks. The following six tasks comprised the initial scope of work for the JIP:

Task 1 – Selecting Appropriate Data: Hourly Ice Observer records, video logs, and daily event reports were reviewed to identify periods when multi-year ice was present, its concentration and floe size, its drift direction and drift rate, and whether it was interacting with the structure. From these records, periods of

multi-year ice loading were identified. Corresponding ice conditions were documented. Ice thicknesses were usually estimated visually or from video records, so a measure of their uncertainty is given.

Task 2 – Review of Instrumentation: All documentation on manufacture, selection and calibration of instrumentation was reviewed. Particular attention was paid to the MEDOF panels, the primary means of direct measurement of ice loads. Calibration of Molikpaq MEDOF panels and other MEDOF panels were checked for consistency and stability. Calibration of strain gauges and extensometers with respect to the MEDOF panels were established to allow relative determination of ice loads from them. Independent means of calibrating strain gauges and extensometers to produce ice loads were sought.

Task 3 – Detailed Analysis: Time series records from the MEDOF panels, strain gauges and extensometers were examined during the time periods of multi-year ice interaction with the structure. From these records, face loads were determined. Loads from MEDOF panel, strain gauge and extensometer results are calculated and presented separately. This has been done on an "Event" or "Sub-event" basis. Each Event, includes a time series record of load related to periods when the size, thickness and shape of multi-year ice features are relatively uniform or defined. An Event or Sub-event can be anywhere from a few 10s of seconds to 10s of minutes. Failure mode during the event was also described. MEDOF panels were on the north, northeast and east sides of the Molikpaq, so they were only used for loading from those directions. Loading from the south and west, where there were no MEDOF panels, were determined using strain gauge and extensometer data. Depending on the instrument, maximum face load or load on part of a face was combined with ice thickness to determine a maximum global pressure for each Event or Sub-event.

Task 4 – Video Analysis: Selected video records were reviewed with the assistance of Brian Wright, together with time series records of MEDOF panel group loads to identify ice failure modes and help divide Events into Sub-events of relatively consistent failure mode and/or ice thickness. Annotated descriptions of failure mode were prepared.

Task 5 – Probabilistic Averaging: The probabilistic averaging technique was applied by Ian Jordaan and colleagues to analyse the MEDOF panel results and calculate global loads. This involved examining the correlation structure of loads for each Event or Sub-event, which differs depending upon failure mode. The events and Sub-events were analysed for relevant statistics, and used as inputs into analyses of probabilistic averaging. Face loads predicted using probabilistic averaging were compared with loads determined from linear averaging.

Task 6 – Geotechnical Analysis: Kevin Hewitt analysed results from the geotechnical instrumentation and the properties of the sand core to estimate limits on ice loading. An assessment of uncertainty in estimating the ice load was made.

With additional Participants joining the JIP, Tasks 2 and 3 were enhanced by expanded MEDOF panel performance assessment and use of DAY files to verify "zero" values. The following three tasks were added:

Task 7 – Third Party Geotechnical Analysis and Review: ConocoPhillips Canada contracted Mike Jefferies to do a review of the original Amauligak geotechnical testing and analysis, and apply recent analysis methods which have become available, to address the issue of the state of the sand core. A presentation of the material was made to Participants. (ConocoPhillips Canada has made separate arrangements concerning access to this report by Participants) Professor K. T. Law of Carleton University was sub-contracted by CHC to make an assessment of the state of the sand core based on available information.

Task 8 – Identification of Phase Lock: Time periods when phase lock occurred were identified, ice thickness and drift speed associated with it noted, and increase in load quantified. In the summary of results, maximum global peak pressures that were associated with phase lock will be identified.

Task 9 – Local Ice Pressure Comparison: STRICE and Molikpaq local pressures were compared to help quantify the degree of MEDOF panel softening. Data from first-year ice loading on the Molikpaq with ice thicknesses similar to those of the STRICE project were used in the comparison.

1.2 Overview of previous work on Molikpaq ice loads

In the period 1986 to 1991 Gulf Canada Resources Ltd. conducted a Joint Industry Project to analyse ice loading on the Molikpaq. The project was carried out in three phases, Phase 1A, Phase 1B, and Phase 2 and documented in the following three sets of reports:

Dynamic Horizontal Ice Loading on and Offshore Structure
Phase 1A: Molikpaq Performance at Amauligak I-65
Frontier Development Division, Gulf Canada Resources Ltd., mid-July 1987
The report comprised 10 volumes covering as-deployed conditions, instrumentation and data acquisition, validation of ice force measurements, first-year ice event data, on-ice investigations, multi-year ice event data, geotechnical data, environmental monitoring, operational records, and a supplementary volume with reports from sub-contractors on MEDOF calibrations, FE analysis of strain gauge response, review of ice load measurement techniques, and re-analysis of ice loads.

Ice Loading on an Offshore Structure
Phase 1B: Dynamic Ice/Structure Interaction
Gulf Canada Resources Ltd., Summary Report; M.G. Jefferies and P.A Spencer, September 1989
The focus in this phase was characterization of ice/structure response data and the development of mathematical models to predict the nature of the interaction. The report comprised 2 volumes of the main report, followed by 8 volumes of appendices which addressed calibration issues, finite element modelling of the structure for dynamics, experiments on and discrete element modelling of crushed ice, and a dynamics model. The work in the appendices was done by Gulf personnel and contractors

Dynamic Ice/Structure Interaction with the Molikpaq at Amauligak I-65
Phase 2: Vol. 1: Main Report, Characterization of Sand Core Behaviour on April 12, 1986 and Development of Analysis Methodology, April 1991
Gulf Canada Resources Ltd., B.T. Rogers and C.A. Graham
Golder Associates, K. Been
Klohn Leonoff, M.G. Jefferies
This report characterized the core and berm sand properties and led to the development of a methodology to accurately describe the ice/structure/soil interaction occurring with Arctic gravity platforms.
Vol. 2: Ice Load Measurement on the Molikpaq at Amauligak I-65, April 1991
Gulf Canada Resources Ltd., B.T. Rogers, P.A. Spencer and M.D. Hardy
This report reviews the three methods (MEDOF panels, strain gauges and extensometers) used to measure ice loads, analysis techniques and presents some test cases of load calculation.
In addition to the first two volumes of the main report, there were seven more volumes of contracted out work covering geotechnical analysis, centrifuge testing, laboratory testing, and geotechnical assessment.

In the late 1980s a number of papers on the sand core properties and response of the core were published by the geotechnical community. The first of these (Sladen, 1989, Sladen and Hewitt, 1989) focused on problems in interpreting sand core properties from field tests, and the influence of placement method on *in situ* density of hydraulically placed sand. They pointed out that hydraulic placement of sand by

pipeline results in low relative density and loose state of the sand core. The first paper to present ice load results was Jefferies and Wright (1988). It mainly focused on ice loading dynamics, but presented maximum global loads of 230 MN, 320 MN, >500 MN and 250 MN for the March 7, March 8, April 12 and May 12 events, respectively. Brown et al (1992) presented a paper on dynamic ice interactions with the Molikpaq. It developed a finite element model of the structure and verified it against measured deformation of the caisson. For May 12 the model predicted an ice load of 160 MN which was amplified to 200 MN on the foundation. Hewitt (1994) published a conference paper stating the sand core was loose because it was placed by a hydraulic fill method and that "the ultimate resistance of the structure under dynamic loading was only 200 MN."

With funding support from the Canadian Government Program on Energy Research and Development, in 1995-96 Klohn-Crippen was contracted to archive Molikpaq data. This was done through preparation of a report and a CD with data from selected events from the deployment at Amauligak I-65. The report, DynaMAC: Molikpaq Ice Loading Experience (Klohn-Crippen, 1998) is publicly available and can be down loaded from the CHC website (http://www.nrc-cnrc.gc.ca/eng/ibp/chc/reports/beaufort.html). The distribution of the data CD is restricted. Table 5.4 and Figure 5.10 of the report provide maximum ice load estimates for the four main loading events at Amauligak I-65. The load values are face loads, but adjusting for structure width, are the same as those of Jefferies and Wright (1988). A compilation of time series records of Molikpaq loads derived from the DynaMAC CD was a component of the NRC Ice Load Catalogue (Timco et al, 1999), but remains a controlled distribution report. The original data tapes, from which the CD was prepared, were subsequently transferred to NRC-CHC for custodianship. The data tapes have been converted to ASCII format by CHC to facilitate analysis and long-term data preservation.

Because of the availability of the DynaMAC data, several journal and conference papers were published on results of analysed Molikpaq data. Note that the loads in the DynaMAC report and the following papers all are based on assuming the original MEDOF calibration factors are correct. Wright and Timco (2001) examined first-year ridge interaction with the Molikpaq and characterized failure modes from examining video records and found typical load levels ranged from 30 to 100 MN for first-year ridges with sail heights up to 2.5 m. Timco and Johnston (2003) presented detailed information on 188 ice loading events on the Molikpaq from both first-year and multi-year ice for different ice conditions including level ice, ridges, hummock ice and isolated floes. A consistent trend of increasing line load with ice thickness up to 7.8 MN/m for 7 m thick ice was presented in 8 summarizing figures. Timco and Johnston (2004) combined Molikpaq data with ice load results from four other offshore structures in the Beaufort Sea, showing consistent results of load as a function of ice thickness. Maximum global pressure was 1.9 MPa for 0.7 m thick ice and decreased to 1.1 MPa for 7 m thick ice. Timco et al (2005) looked at the May 12 impact event and presented a detailed description of the event, confirming the original estimate of a maximum impact force of 250 MN. Frederking and Sudom (2006) studied the April 12, 1986 event and determined a maximum global load of no more than 420 MN and most likely 380 MN. This was based on a re-analysis of extensometer and strain gauge data. Global ice pressures for the 8 to 12 m thick multi-year hummock crushing on the 58 m long east face was estimated to be not greater than 0.8 MPa. Jefferies et al (2008) returned to his earlier work on dynamic amplification of ice loads on the Molikpaq and determined a maximum east face load approaching 400 MN for a phase-locked event.

The loads from all previous analysis are generally consistent, since they all start from the same point of using the original calibration of the MEDOF panels.

2. SELECTED EVENTS FOR DETAILED ANALYSIS

2.1 Event selection

For Task 1 of this project, a list was prepared of time periods when multi-year ice was present and likely interacting with the Molikpaq. Because the distinction between second-year ice and multi-year ice is not clear, both have been included in the inventory. Twenty-one periods have been identified for possible analysis. From these general time periods, shorter periods, for which there was a detailed record, were selected. These were termed Events and corresponded to a particular failure mode, drift speed, ice thickness, etc. In some cases the Event was further divided into Sub-events where there was a noticeable change in failure mode, ice thickness or drift speed during the Event. Ice interaction details for the 21 time periods of interest are listed in the table in Appendix A. The time periods are numbered and these numbers will be referred to in Section 11. Some events were judged better suited for detailed analysis than others, based upon factors such as:

* Certainty of ice type (i.e. confirmation of multi-year or second-year ice interaction by more than one source)
* Availability of high-frequency ice load data (i.e. FAST or EVENT files, see Section 3)
* Information on failure mode (from video), ice thickness and ice drift speed and direction.

In this report, the abbreviations FY, SY and MY are often used for first-year, second-year and multi-year ice, respectively. The World Meteorological Organization ice classification refers to second-year ice as sea ice which has survived just one summer of melt, while multi-year ice has survived at least two summers of melt.

2.2 Winter 1985/86 ice season

The following description is taken from Klohn-Crippen, 1998.

During the 1985/86 winter season, the ice conditions encountered at Amauligak I-65 were more severe than normal. In late October, freeze-up began with the formation of thin first-year ice across the general offshore region. At the time, the edge of the polar pack was further south than normal, with some low to high concentration pockets of multi-year ice stretching southwards into the intermediate water depths, across the same latitude as the Amauligak location. In addition, there were a few areas of second-year ice (remnant first-year ice from the previous summer) drifting with the growing pack. Further to the south, the landfast ice formed over the October through late December period, reaching its maximum extent in early January, about 15 km south of the Molikpaq at the 20 m water depth contour.

Over the course of the freeze-up and early winter period, first-year pack ice, which occasionally contained small second-year ice floes, moved past the Molikpaq. Typical first-year ice thicknesses ranged from 0.3 to 1.3 m and drift speeds varied from 0.1 to 0.6 m/s. Predominant ice movements were from east to west, but on shorter time scales, movements from all directions occurred. During this period, there were no major offshore storms that moved the second-year ice and polar pack edge further to the north.

In late February and early March, the predominant east to west drift of the Beaufort's transition zone pack ice was interrupted by strong north-westerly winds, which brought variable concentrations of second and multi-year ice southwards, into the vicinity of the Molikpaq's deployment location. Over the first week of March, a number of multi-year and second-year ice floes moved across the Amauligak location, impacting the Molikpaq in the process. On March 8, the southerly ice drift stopped, being constrained by the landfast ice to the south. Over the next month, the ice around Amauligak remained stationary and did not begin moving until April 12, when strong offshore winds moved the pack to the northwest. As the ice

moved offshore, the Molikpaq encountered several more multi-year ice interactions, prior to entering the open waters of a lead that formed between the fast ice edge and the pack. For the remainder of the winter and spring, the ice cover continued to drift, with the Molikpaq encountering first-year ice which, on occasion, contained some multi-year ice floes. Break-up commenced in mid-May with the gradual loosening of the winter pack ice. Over the late May and June period, large floes continued to move against the Molikpaq but by early July, most of the winter ice had cleared and the Molikpaq was located in open water.

A stable grounded rubble field did not form around the Molikpaq at the Amauligak I-65 deployment location. A small grounded rubble pile did form on April 12, 1986, but was swept away shortly thereafter. The lack of a grounded rubble field is a significant observation and was a consequence of the Molikpaq's deep set-down draft (19.5 m) and relatively small berm crest, in combination with the nature of the ice action against its near vertical waterline faces. Since no protection was afforded by grounded ice rubble, the caisson was directly exposed to moving ice throughout the winter period.

3. INSTRUMENTATION AND DATA SOURCES

The Molikpaq is an annular steel caisson supporting a self-contained deck structure. The core of the annulus was filled with sand, which provided a portion of the horizontal resistance. The caisson has near vertical sides (7° from the vertical for the Amauligak I-65 location at the waterline) and is octagonal in plan, as shown in Fig. 1. At the water line, the long sides are about 58 m long and the cropped corners 22 m long. The minimum waterline width of the caisson was 90 m, and the maximum width across the diagonal was 104 m. For the 1985–86 deployment of the Molikpaq at Amauligak I-65, water depth was 31 m and the caisson was set down on a submarine berm, giving it a draft of 19.5 m. The lightship mass of the caisson and deck was 32,000 t, and with 100% consumables this would increase to 49,000 t. During April and May 1986, the estimated weight on berm was 37,361 t (Rogers et al, 1991a). The depth of the sand in the core was 21 m above base for a total volume of sand of 112,000 m^3. (Jefferies and Wright, 1988). The level of the sand was 1.5 m higher than mean sea level.

The deployment of the Molikpaq at Amauligak I-65 was the second winter season that it was in an ice environment. Much of the instrumentation to measure ice loads and caisson response had already experienced one ice season.

A variety of sensors were installed in and around the Molikpaq structure and soils, including:
- Ice load measurement systems: MEDOF panels, strain gauges, extensometers, tiltmeters and accelerometers
- Geotechnical data measurement systems: pore pressure cells, total pressure cells, in-place inclinometers, manual inclinometers, electric piezometers and manual piezometers
- Other instrumentation: ballast water and draft level gauges, dewatering flowmeters and suction head to monitor water within sand core, casing and plates to measure settlement, upward looking sonar to measure ice thickness, and sensors to measure temperature in the MEDOF panels, core and berm.

There were 512 channels of instrumentation and two data acquisition systems to condition and record the output of the instruments; one Hewlett-Packard-based, and the other referred to as the Weir-Jones. The Weir-Jones system provided real-time output of loads and also recorded data, but no data tapes from this system were available. Only tapes from the HP system were available.

In addition to the sensors for which data were captured in the data acquisition system files, other sources of data include:
- Time lapse video cameras (discussed in detail in Section 10)
- Reports on ice conditions, including Ice Observer reports

For this report, multi-year ice loads have been analysed based upon results from MEDOF panels, strain gauges and extensometers. In this Section an overview is given of the MEDOF panels, strain gauges and extensometers; the calibration of these systems is discussed in Section 5. The methodology for calculating face and global ice forces is described in Section 4. The geotechnical instrumentation is also briefly described in the following Section. The analysis of the geotechnical response and estimates of ice loading are treated in Section 6 and Appendix I.

In previous analysis of ice forces on the Molikpaq, the MEDOF panel results were taken as primary measurement of ice forces, and strain gauges and extensometers were calibrated against them. There were also efforts to calibrate the strain gauges and extensometers, independently from the MEDOF panels. These independent calibrations are discussed in Section 5 and methodologies for calculating ice forces from them described.

3.1 MEDOF panels

To obtain direct measurements of ice loading on the Molikpaq, a total of 31 MEDOF panels were installed on the north, northeast and east faces of the structure. It was anticipated that the most severe ice loadings would occur on these faces. Figures 1 and 2 show the location of the MEDOF panels deployed on the Molikpaq.

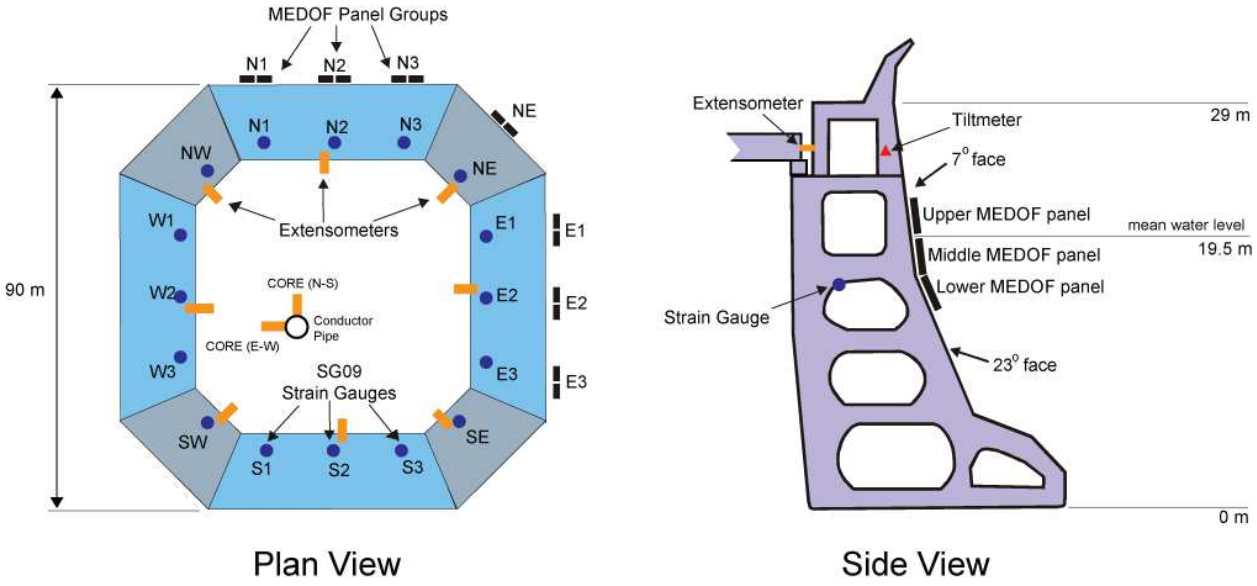

Figure 1 Placement of MEDOF panels, strain gauges, extensometers and tiltmeter on the Molikpaq

The MEDOF panels on the Molikpaq were composed of a steel back plate separated from the front plate by an array of polyurethane disks 2.54-mm thick, which deformed under load. The disks were 9.5 mm in diameter and spaced 12.7 mm on centres. The buttons occupy 44% of the space between the front and back plates. The front plate was 12.7 mm thick, a thickness selected to ensure no plastic deformation occurred in it under local ice pressures. The back plate was 4.55 mm thick. The front and back plates were welded together at the perimeter making for a closed system. The spaces between the disks contained a calcium-chloride solution which was displaced up a sight tube when a load was applied to a panel. Ice pressures on individual panels were determined with a sensitive pressure transducer that measured the pressure head at the base of the sight tube. The original sight tubes were 2000 mm long; however some of them were lengthened to 2400 mm in late 1985 because there was concern that fluid might overflow the top of the tubes under high loading.

The panels were 1.135 m wide and 2.715 m high, with a capacity of 20 MN, and were configured so that they measured the total force acting on the plate, regardless of how it was distributed or where it acted (Metge et al., 1983). The panels were clustered in groups of four or five as shown in Figure 2. Each array was two panels across and two panels vertically, with the water line passing across the lower part of the upper level of panels. One array on each of the faces had a fifth panel directly beneath the other four. The spacing between the centre of group N1 and N2 was 19.5 m and between N2 and N3 it was 17 m. The centres of E1, E2 and E3 were spaced 19.5 m apart. Panel groups N2 and E2 are offset from the centre of the north and east faces by 2.44 m to the west and north, respectively. Slightly more than 10% of the waterline length of each of the north and east faces were covered with panels.

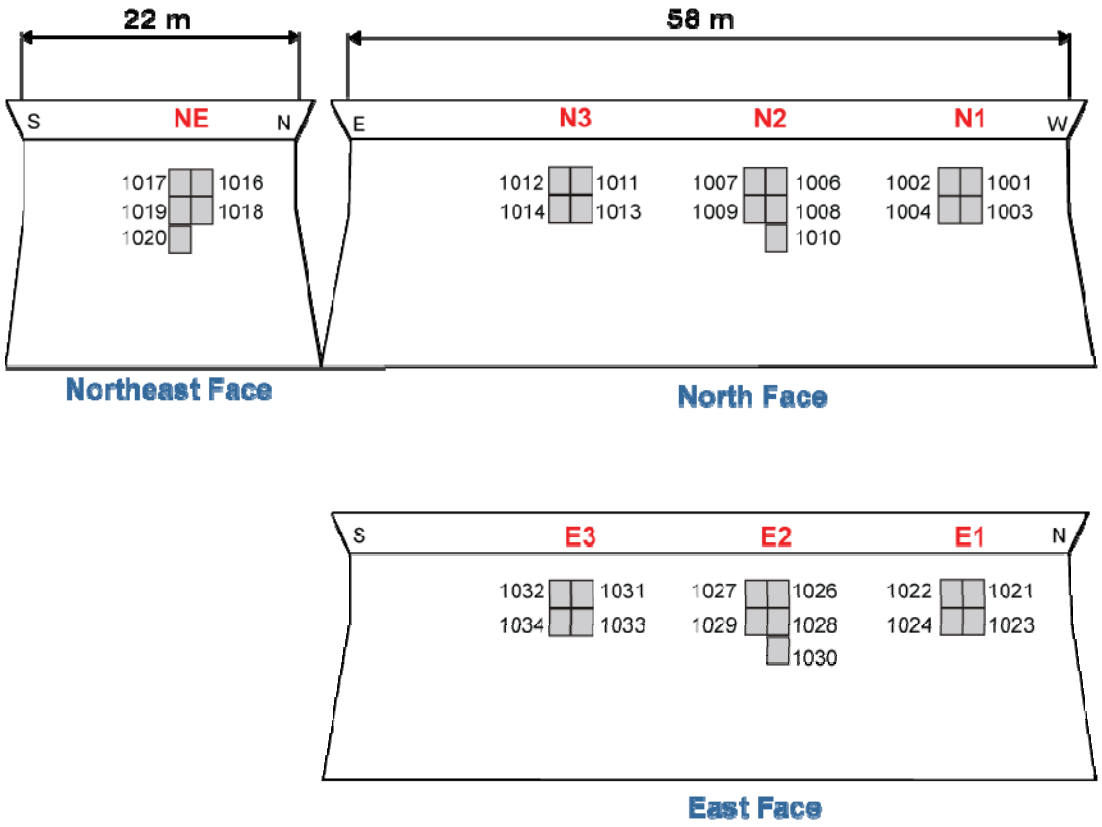

Figure 2 MEDOF panels on the North, Northeast and East faces of the Molikpaq

Panel 1019 (mid-level on the northeast face) did not function throughout the entire 1985/86 season at Amauligak I-65. Panels 1016 and 1017 (upper level on the northeast face) were damaged during flaring operations on December 20, 1985, and were not in working order after that time (Gulf Canada Ltd., 1987a). Thus for the majority of the monitoring program, 28 of the 31 MEDOF panels were functional.

At the time of the deployment of the MEDOF panels on the Molikpaq their inability to respond adequately to high-frequency loading changes and their susceptibility to creep when under long-term loading had been identified. Creep tests were done on the panels to determine their response characteristics and procedures developed for correcting for creep affects. During the course of this project another area of uncertainty with the MEDOF panel behaviour was uncovered by the Ian Jordaan and Associates (IJA) team – that of softening of the polyurethane buttons under cyclic loading. Details of this and other issues in relation to MEDOF panel performance are discussed in Appendix B from the IJA team and Appendix C from NRC-CHC.

3.2 Strain gauges

Although the MEDOF panels provided direct measurement of ice loading, their response time was approximately 5 to 10 seconds according to Jefferies and Wright (1988). Other sources (Rogers et al, 1998) indicate accurate response to 2 seconds. The rapidly fluctuating or dynamic ice loads were best measured by strain gauges. The strain gauges could also register loads up to 8 m below sea level (Gulf Canada Ltd., 1987b).

A total of 282 strain gauges were installed on the Molikpaq at the time of set-down at Amauligak I-65. Experience with the different locations of strain gauges showed that the '09 series' (also referred to as SG09) had the best sensitivity and linearity for measurements of loads from ice up to 5 m thick (Rogers et al, 1998). For the current project, data from the SG09 gauges are used.

The '09 series' strain gauges were installed on some of the main bulkhead struts supporting the external face of the Molikpaq. Initially the SG09 gauges were positioned on the bulkheads directly behind some of the MEDOF panels. From the beginning of the measurement program until April 12, 1986 the only SG09 gauges on the Molikpaq were at locations N2, N3, E2 and NE. On April 11, 1986 twelve new SG09 gauges were installed on the main bulkhead struts (Gulf Canada Ltd., 1987a). There were now SG09 strain gauges behind each MEDOF panel group. Note that the location of the E3 SG09 strain gauge did not coincide with MEDOF panel group E3, but was 4.88 m to the south of it. From this time onwards, '09 series' strain gauges were evenly distributed around the caisson with three gauges on each long face and one gauge on each corner face, as shown in Figure 1. The newly installed strain gauges were wired into channels with strain gauges that had expired. Data were available for all sixteen SG09 gauges in the FAST files and DAY files from April 11, 1986 onwards. As will be explained in Section 3.9, EVENT files were recorded on a separate system, and EVENT files up to and including the April 12 events only captured data from three of the four SG09 gauges; E2, N2, and NE. By the time that the next event triggered an EVENT file (May 12, 1986), the system was recording all 16 channels of SG09 data.

3.3 Extensometers

The deflection of the centre of each long face and corner face was measured using extensometers. There were a total of 10 extensometers, 8 measuring relative displacements of the faces with respect to the deck, and 2 for absolute movements of the deck relative to the assumedly fixed conductor casing (guide pipe). The deck was set on low friction elastomeric pads and was assumed to be rigid, but not transmit load from one face to another. The placement of the extensometers is shown in Figure 1. The extensometers were 6.6 m above mean sea level, which was 19.5 m above the base, and have a range of ±184 mm. Actual caisson displacement was calculated from the difference in the movement of the caisson face with respect to the guide pipe (Gulf Canada Ltd., 1987a). The effect of ice loading on any of the long faces was to cause the caisson ring to "oval", that is the diameter across the loaded direction became smaller and the diameter at right angle became greater. Relative movements of two opposite faces provided a measure of the total force on the face. When two orthogonal faces were loaded, this causes problems in interpreting the results. A methodology for interpreting extensometer results for this biaxial loading case is presented in Section 2.5 of the IJA report (see Appendix B). The extensometers had good frequency response so they accurately measured the deformation of the caisson ring.

3.4 Tiltmeters

Eight tiltmeters were located in the ice deflectors 5.8 m above mean sea level as shown in Figure 1, one tiltmeter in the centre of each face. The tiltmeter assembly was a biaxial tilt measuring instrument with two accelerometers mounted orthogonally. For static loading the tiltmeters responded by measuring the change in tilt of the upper part of the caisson. The sensors were originally installed to measure tilt, but could also measure both lateral and rotational accelerations (Gulf Canada Ltd., 1987a).

3.5 Accelerometers

Eight accelerometer units were installed at the base of the Molikpaq caisson and in the sand core. Four biaxial accelerometers were installed 2m above the base in the pump/valve rooms midway along the north, south and east faces of the Molikpaq. These sensors measured the acceleration at the base of the caisson, which could be compared with the tiltmeters at deck level. Another biaxial accelerometer was

installed in the inclinometer casing at the centre of the core 19.5 m below mean sea level. It monitored the lateral propagation of vibrations across the Molikpaq. A triaxial unit in a sealed container was buried 1 m deep in the centre of the core, and could measure accelerations in the vertical as well as horizontal plane. (Gulf Canada Ltd., 1987a)

3.6 Pore pressure cells and total pressure cells

Twelve pore pressure cells (PPC's) were mounted on the hull of the Molikpaq at the four major soil faces, adjacent to the core dewatering inlets. The PPC's measured pore pressures at the soil/structure interface, and were useful in monitoring any excess pore pressure during core filling, as well as providing redundancy to core instrumentation during normal operations. (Gulf Canada Ltd., 1987a)

Forty total pressure cells (TPC's) were uniformly distributed along the base of the Molikpaq to monitor base pressure on the caisson. These sensors were used mainly to detect hull overstressing during set-down, but were also used to monitor caisson overturning tendencies during ice loading. (Gulf Canada Ltd., 1987a)

3.7 In-place inclinometers and manual inclinometers

In-place inclinometers (IPI's) were located in the core, berm and foundation of the Molikpaq. Two in-place inclinometer (IPI) strings were installed inside the core, 5.5 m back from the middle of the north and south faces in the Molikpaq's sand core, to continuously monitor core deformation. The north face IPI string had six sensors, while the south face string had five. The sensors were located at various depths within the core and near the core-berm interface. There was also a sensor in the berm (depth 28.1 m) and two sensors placed just into the sub-cut (depths 40.5 m and 41.0 m). In addition to the IPI strings near the north and south faces, a third string was located near the centre of the structure. This string had one sensor in the core at 28.1 m below mean sea level.

Each IPI sensor used two precision closed-loop accelerometers to determine angular changes in the vertical plane (N-S and E-W directions). Some of the data were recorded in %g and others in mm of lateral movement over a 3-m-long base (Gulf Canada Ltd., 1987a).

For the three casings with in-place inclinometers the IPI strings and/or accelerometers could be temporarily removed to perform a survey using a manual inclinometer (Gulf Canada Ltd., 1987a). There were four additional inclinometer casings behind the east, west, northeast and south-west faces that were also used for periodic manual inclinometer readings. Together with the other three, these are the seven casings referred to in Section 6 and Appendix I.

3.8 Electric piezometers and manual piezometers

Six strings of electric piezometers were installed in the sand core and berm to monitor pore water pressure response to cyclic loading on the Molikpaq. These piezometers also measured the drawdown caused by the four core dewatering pumps. Each string contained three sensors at 10.5, 15.5 and 20.5 m below mean sea level (Gulf Canada Ltd., 1987a).

3.9 Data acquisition

The data tapes available for analysis in this project were from the HP system. The HP system logged data in two modes, 'slow' and 'burst'. The slow scan mode was used for long-term monitoring of all transducers. The slow scanner had two modes of operation, one scanning at 1 Hz with mean, minimum and maximum values stored at the end of five minute intervals. These files were termed DAY files, and

typically ran for one day, however, in some cases they were for shorter periods. For static or creep loading events, when the mean, minimum and maximum values were close together, they provided a reasonable indication of instrument response. For the other mode of scanning, a trigger activated either manually or by exceeding a threshold value of one of the instruments, started the recording of a FAST file. In this case all channels were recorded at a frequency of 1 Hz for 3900 readings, or about 65 minutes. Occasionally FAST files were recorded at 2 or 4 Hz, but still for 3900 readings. These two recording modes were mutually exclusive, either a DAY file or a FAST file were recorded, but never both at the same time.

The data acquisition system could also be triggered to record a limited number of channels (128) at 50 Hz for 90 seconds. These were referred to as EVENT files and were able to capture the dynamic nature of loading events. EVENT files were recorded in parallel with either DAY files or FAST files. Instrumentation that could respond at these frequencies were selected for recording, such as strain gauges, extensometers, piezometers, etc. MEDOF panels were not included in this subset because of their limited response characteristics. Note the EVENT files were also referred to a "Burst" files in earlier reporting.

For the 1985-86 deployment at Amauligak I-65, 140 data tapes with almost 900 DAY, FAST or EVENT files were available for analysis. A subset of the files associated with multi-year ice interactions was analysed in this project. Throughout this report, when referring to data files, DAY, FAST and EVENT will be in uppercase font.

3.10 Global response of Molikpaq to ice loading

The interpretation of various instruments depends on how the caisson and core respond to ice loading. Interpreting the measured response of extensometers, strain gauges, tilt meters, inclinometers and accelerometers is based on understanding the global response of the Molikpaq to ice loading. Therefore, having a "model" of the response of the caisson and core to ice loading is necessary. Figure 3 shows schematically a free-body-diagram of the caisson and core and where the resistance to ice loading is distributed. For static ice loading, resistance is generated by friction of the caisson base on the berm and passive and active soil pressures on the inner faces by the core. There is an apportioning of resistance between base friction and core pressure. The apportioning of the resistance probably changes as the ice load increases. The passive and active soil pressures may be represented by springs acting on the inner faces of the caisson. Base friction may be characterized by a friction coefficient, with no sliding until frictional resistance is exceeded.

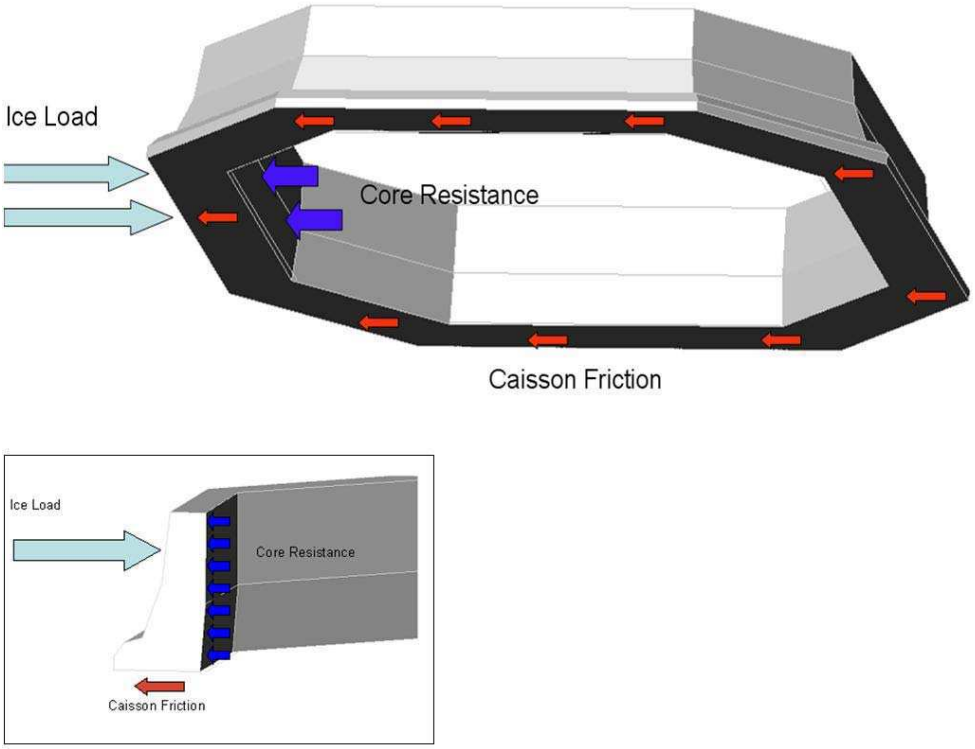

Figure 3 Ice load distribution into caisson and core (from IJA report, Appendix B)

The deformation of the caisson has been termed "ovalling", but the actual deformed shape is more a distorted ellipse. The loaded face moves away from the load, and the opposite (back) face also moves towards the centre, but not by as much. The two perpendicular faces move outwards, but also a lesser amount than the loaded face. The changing ellipsoidal shape based on extensometer measurements in illustrated in Figure 4.

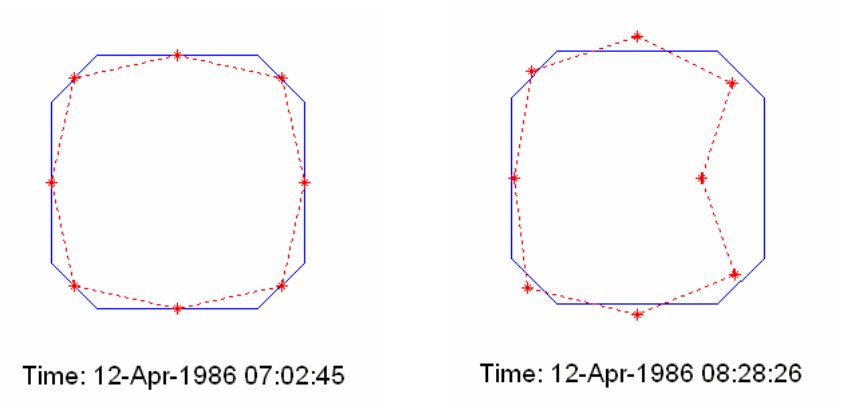

Figure 4 Relative deformation of the caisson from extensometer measurements under no-load condition (left), and with loading mainly on the east face (right). Extensometers are shown as red stars in the centre of each face. The deformation is scaled up by a factor of 667:1.

Ice load is applied across the face near the waterline on the caisson. It is expected that the top of the caisson, where the extensometers are located, will deform more than the base, which has a deeper section (see Figure 1) and whose movement is resisted by friction. Tilt measurements confirm that the caisson face does tilt inwards in response to ice loading. The actual deformed shape can be represented by the schematic of Figure 5. There are undoubtedly deformations of the caisson base, but these are probably small, and the in-place inclinometers that straddle the interface between the core and berm did not detect any relative movements. Slope indicator measurements, which were conducted periodically, did detect some localized movements at the interface between the core and the berm.

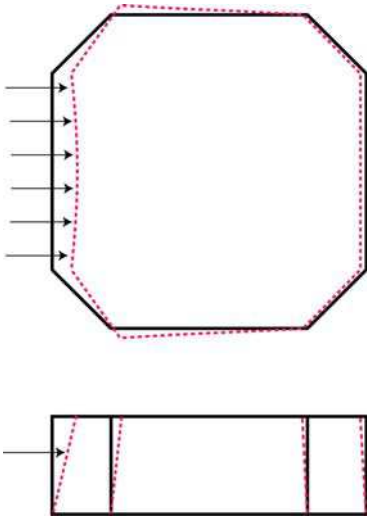

Figure 5 Plan and section views of caisson deformation

4. CALCULATION OF FACE LOADS

4.1 MEDOF panels

On the east and north faces of the Molikpaq, there were three groupings of MEDOF panels; on the northeast face there was one group of panels (see Figure 2). Ice load calculations using MEDOF panel results have been traditionally based upon the extrapolation of the load across an instrumented face using linear averaging. Note for this project, probabilistic averaging of the MEDOF results, as described in Section 5, will also be applied to determine loads on caisson faces. This Section deals only with load estimation using linear averaging.

The north face load, using linear averaging, is approximated by:

$$\frac{F_{N1} * (16.81\,\text{m}) + F_{N2} * (18.25\,\text{m}) + F_{N3} * (22.94\,\text{m})}{2.27\,\text{m}} \qquad \textbf{(4-1)}$$

where F_{N1}, F_{N2} and F_{N3} are forces calculated from the sums of each MEDOF panel grouping on the north face. The width of the long faces of the structure is 58 m, and the width of a grouping of MEDOF panels is 2.27 m. Panel groups were not spaced evenly on the faces. A tributary length for each of the panel groups is determined based upon the location of the centre of that panel group.

The east face load is calculated by:

$$\frac{F_{E1} * (16.81\,\text{m}) + F_{E2} * (19.5\,\text{m}) + F_{E3} * (21.69\,\text{m})}{2.27\,\text{m}} \qquad \textbf{(4-2)}$$

Note in Figure 2 that for the north and east faces, each panel group consists of four MEDOF panels except for the central group on each face, which has an additional lower panel. The treatment of the lower panel data is discussed later in this section.

For the northeast face, the load can be approximated by:

$$(F_{NE}) * \frac{22\,\text{m}}{2.27\,\text{m}} \qquad \textbf{(4-3)}$$

where F_{NE} is the sum of the group of five panels on the northeast face, and 22 m is the width of the shorter or corner face of the Molikpaq. Note that three of the five MEDOF panels on the northeast face were non-operational for most of the 1985-86 winter season, so for most events it is difficult to estimate the load on the northeast face. In these cases we do have one lower and one middle panel which can be used to extrapolate a face load.

The face loads for the north and east faces of the Molikpaq are calculated using the loads from the three panel groups on each face. The single lower panel in the centre panel group (E2 or N2) is used to estimate a force for the other "missing" lower panels shown in red in Figure 6. The rationale for including these "pseudopanels" where panels are missing is discussed in the following paragraphs. For the example of the north face, the force on panel group N1 is the sum of the forces on panels 1001, 1002, 1003, and 1004, plus the force on pseudopanels $N1_1$ and $N1_2$:

$$F_{N1} = F_{1001} + F_{1002} + F_{1003} + F_{1004} + F_{N1_1} + F_{N1_2} \qquad \textbf{(4-4)}$$

Data from the single deep panel on each long face are used to attribute a load to the missing panel in group E2 or N2, as well as to the panel groups without any deep panels. A proportion of the load measured by panel 1010 can be assigned to the missing panel $N2_1$. A proportion of the lower panel load recorded at location N2 can also be assigned to the missing panels $N1_1$ and $N1_2$ in group N1, and $N3_1$ and $N3_2$ in group N3. The same technique can be used with the east face panels.

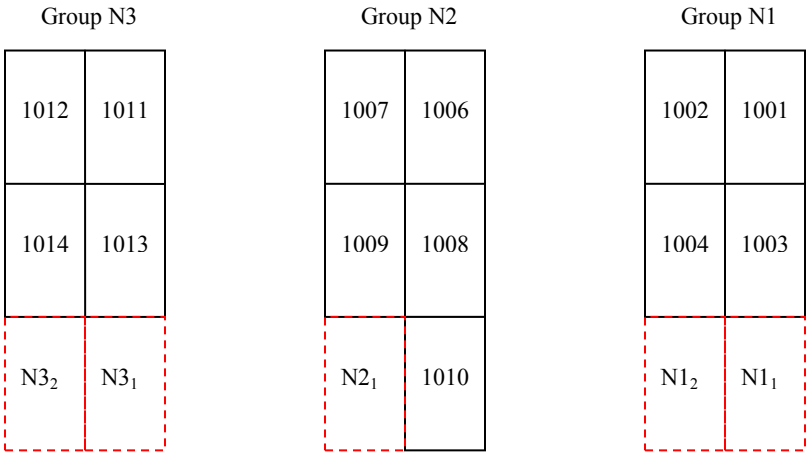

Figure 6 Panel groups on north face with pseudopanels shown in red

The rationale for introducing pseudopanels to include an effect of the lower panel, in the absence of direct measurement, is that when some load is measured on the one lower panel in the centre group (N2 or E2) it implies that there is a good chance that similar conditions exist for the other two groups. Ignoring the presence of the "missing" panels would result in a non-conservative estimate of ice loading on a face.

Different approaches may be used to determine the proportion of the lower panel load to be attributed to the missing panels. For this project, we will use the contact factors shown in Table 1 which were established by Rogers, Spencer and Hardy (1991). The contact factor is an estimate of what percentage of the lower portion of a panel group is loaded by ice. These factors were derived based on review of the time lapse video recordings for each face, accounting for ice thickness and contact length. The load on a missing lower panel is the contact factor for that panel group multiplied by the lower panel load. For the example of the north face:

$$F_{N2_1} = \text{(Contact factor for group N2) * (Load on panel 1010)} \quad \textbf{(4-5)}$$

$$F_{N1_1} = F_{N1_2} = \text{(Contact factor for group N1) * (Load on panel 1010)} \quad \textbf{(4-6)}$$

$$F_{N3_1} = F_{N3_2} = \text{(Contact factor for group N3) * (Load on panel 1010)} \quad \textbf{(4-7)}$$

This procedure was further modified by examining the force on the middle panels of N1 and N3. If the total force on N1 (panels 1003 + 1004) or N3 (panels 1013 + 1014) was less than 500 kN, no pseudopanel force was applied to that group for that instant in time. This adjustment and the contact factors in Table 1 were used to calculate the load-time results presented in Appendix K and Section 11.

Table 1 Contact factors for MEDOF panel groups (Rogers, Spencer and Hardy, 1991)

EVENTS	N1	N2	N3	E1	E2	E3
Nov 10	0	0	0	0.5	1	0.5
Mar 08	0.5	1	0.5	0.5	1	0.5
Mar 25	0.5	1	0.5	0.5	1	0.5
Apr 12 (am)	0	0	0	0.5	1	0.5
Apr 12 (pm)	0.5	1	0.5	0.4	1	0
May 12	0.35	1	0.4	0	1	0
May 22 (am)	0.4	1	0.5	0.5	1	0
May 22 (pm)	0	0.9	0.6	0.5	1	0
June 2	0.5	1	0.5	0	1	0

Other strategies based on ratios of panel loads can be used to estimate loads on the pseudopanels, see Section 8.8.1 for the IJA team discussion of this approach. The concern with ratios is that they can involve dividing by a small number which can lead to an unreasonable estimated pseudopanel load. Stochastic methods, also discussed by the IJA team in Section 8.8.1 probably represent the best approach. Regardless of the approach for dealing with the loads from the lower panels, whenever ice thickness is greater that 2.7 m (loading on the lower panels) there is greater uncertainty in estimating ice loads.

With loads on the north, northeast and east faces determined a vector sum of these loads can be taken to obtain a global load. However, since loads are only available on these three adjacent faces, there are limitations on determination of global loads. For ice moving from the northeast, all three faces are being loaded, and a global load can be determined. For loading from any other direction, there are loaded faces with no MEDOF panels and loads on the "un-instrumented" faces would have to be estimated. This would introduce another element of uncertainty.

4.2 Strain gauges

The face load from SG09 strain gauges is calculated by determining the force that acts over individual bulkhead spans of 2.44 m and extrapolating over the width of the structure. By the spring of 1986, there were three SG09 strain gauges on each long face of the Molikpaq. Similar to the MEDOF panels, the strain gauges were not placed symmetrically about the faces. A tributary length is calculated for each strain gauge, based on its location along the face. The total force on the east face is given by:

$$F_{SGE} = \frac{F_{SGE1} * (16.81\,\text{m}) + F_{SGE2} * (21.94\,\text{m}) + F_{SGE3} * (19.25\,\text{m})}{2.44\,\text{m}} \qquad \textbf{(4-8)}$$

where F_{SGE1}, F_{SGE2} and F_{SGE3} are forces calculated from SG09 strain gauges, using the calibration factor for each strain gauge to convert from raw units (microstrain) to force (kN). The calibration of strain gauges using MEDOF panel measurements is discussed in detail in Section 5.2.

Before April 11, 1986, the only SG09 gauge installed for the east face was located at E2 (see Section 3.2 for details). For events with only gauge SG09 E2 available, the face load is calculated by averaging the load over the full length:

$$F'_{SGE} = \frac{F_{SGE2} * (58\,\text{m})}{2.44\,\text{m}} \qquad \textbf{(4-9)}$$

Similar equations are used for calculating the force on each of the other three long faces. For events during which all three north face SG09 gauges were available, the north face load is given by:

$$F_{SGN} = \frac{F_{SGN1} * (16.81\,\text{m}) + F_{SGN2} * (18.25\,\text{m}) + F_{SGN3} * (22.94\,\text{m})}{2.44\,\text{m}} \quad \textbf{(4-10)}$$

Before April 11, 1986, only gauges SG09 N2 and N3 were available for the north face. In this case, the north face load is calculated by extrapolating F_{SGN2} over a greater length:

$$F'_{SGN} = \frac{F_{SGN2} * (35.06\text{m}) + F_{SGN3} * (22.94\,\text{m})}{2.44\,\text{m}} \quad \textbf{(4-11)}$$

On April 11, 1986, strain gauges were installed on the south and west faces. The south face load is given by:

$$F_{SGS} = \frac{F_{SGS1} * (15.5\text{m}) + F_{SGS2} * (22\,\text{m}) + F_{SGS3} * (20.5\text{m})}{2.44\,\text{m}} \quad \textbf{(4-12)}$$

The west face load is approximated by:

$$F_{SGW} = \frac{F_{SGW1} * (16.5\,\text{m}) + F_{SGW2} * (22\,\text{m}) + F_{SGW3} * (19.5\text{m})}{2.44\,\text{m}} \quad \textbf{(4-13)}$$

For the shorter faces, the method is similar except that only one strain gauge is used to extrapolate the force over a width of 22 m. In this case, the equation for the force on the northeast face, for example, is:

$$F_{NE} = (F_{SGNE1}) * \frac{22\,\text{m}}{2.44\,\text{m}} \quad \textbf{(4-14)}$$

Up until April 12, the coverage of the Molikpaq faces by strain gauges was so limited that determination of face loads was compromised. After 08:50 on April 12 a total of 12 strain gauges were connected to the data acquisition system. With calibration, this allowed not only loads on all faces, including corners, but also global loads by vector summing of face and corner loads.

4.3 Extensometers

Extensometers measure the overall response of the caisson to ice loading. Ice loading results in a change in the shape (ovalling) and displacement or the caisson as a whole. Equations (4-15) to (4-22) for the calculation of extensometer loads were derived by Gulf Canada Ltd. (1987b). The sign convention for the extensometers is as follows: deflection of the caisson towards the deck (gap closing) gives a decreasing or negative output; and movement of the deck towards the south and east with respect to the conductor casing or guide pipe (gap closing) gives a decreasing or negative output. Note that the sign convention for deck motions is the reversed from that in Gulf Canada (1987b). See Appendix D for an explanation of the sign convention used in this report. The formulas to determine face movement with respect to the guide pipe are:

$$N_C = N_R + GP(N-S) \quad \textbf{(4-15)}$$

$$E_C = E_R - GP(E-W) \quad \textbf{(4-16)}$$

$$S_C = S_R - GP(N-S) \quad \textbf{(4-17)}$$

$$W_C = W_R + GP(E-W) \quad \textbf{(4-18)}$$

$$NE_C = NE_R + (GP(N-S) - GP(E-W)) * \cos(45°) \quad \textbf{(4-19)}$$

$$SE_C = SE_R - (GP(N-S) + GP(E-W)) * \cos(45°) \quad \textbf{(4-20)}$$

$$SW_C = SW_R - (GP(N-S) - GP(E-W)) * \cos(45°) \quad \textbf{(4-21)}$$

$$NW_C = NW_R + (GP(N-S) + GP(E-W)) * \cos(45°) \quad \textbf{(4-22)}$$

where: N_R = north face extensometer response with respect to the deck
N_C = north face movement with respect to the guide pipe in North-South direction
GP (N - S) = guide pipe extensometer response in North-South direction
GP (E - W) = guide pipe extensometer response in East-West direction
(and so on)

Face loads in the East-West and North-South directions can be approximated with the formulas:

$$F_{E\text{-}W} = CF * (E_C + W_C) \quad \textbf{(4-23)}$$

$$F_{N\text{-}S} = CF * (N_C + S_C) \quad \textbf{(4-24)}$$

The parameter CF is the calibration factor (in MN/mm) used to convert the caisson displacement to a face load. Based on Sandwell (1991) finite element analysis the extensometer face load CF can be multiplied by 1.4 to get the equivalent global load across both the face and the two corners, assuming the most likely distribution of loading on the corners. Calibration of the extensometers is discussed in Section 5.3.

The foregoing analysis has only looked at the response of the caisson ring in the north-south and east-west directions. A 2-D matrix solution taking into account the additional deformations in the diagonal directions, northeast – south-west and north-west – south-east has been developed by Ian Jordaan and Associates, see Appendix B.

Additionally, the analysis assumes a uniform distributed load on the caisson faces. Measurements with the MEDOF panels and strain gauges show this is usually not the case. This is discussed in Appendix E, and it is shown that, depending on whether the distribution is U-shaped or peaked, the extensometer face load calibration factor could vary by ± 30%.

5. MEDOF PANEL, STRAIN GAUGE AND EXTENSOMETER RELATION

5.1 MEDOF panels

As detailed in Sections 5.2 and 5.3, the calibration of the strain gauges and extensometers is largely based upon the MEDOF panel values. It is therefore important to consider the accuracy and limitations of the MEDOF panels. The panels exhibited a tendency to creep over extended loading periods, and thermal effects were noted. For very thick ice, the panels would not capture the entire load. In addition, questions have been raised regarding the possibility of softening of the polyurethane within the panels. Still, the MEDOF panels were the only measure of direct ice loads on the Molikpaq at Amauligak I-65, and this is valuable data.

MEDOF panels were installed on the north, northeast and east faces of the Molikpaq as described in Section 3.1. The raw panel load outputs must be corrected using a pre-selected baseline because the hydrostatic column of the sight tubes was vulnerable to disturbances. Additionally, the panels were sensitive to thermal effects. Both thermal calibration and applied load versus fluid height calibration were obtained from testing of each panel in a laboratory prior to their deployment on the Molikpaq. An example of a calibration curve is given in Figure 7. A more detailed discussion of MEDOF panel characteristics and performance is provided in Appendix C. Another factor which should be considered is the tendency of the MEDOF panels to "creep" or exhibit an apparent increase in load when a static load is applied. This creep behaviour is not significant for ice loading events occurring over a relatively short period of time, but it can be an issue for longer term loading.

Smith and Spencer (1987) reviewed the use of MEDOF panels for determining local loads, looking at the calibration factor for each panel and its temperature dependency. There was less than a 2% difference between the calibration factors at 0° and -10°C, but at -20°C the panels were about 15% stiffer, thus they could under-predict load at lower temperatures. They also noted a substantial difference in the calibration factor from panel to panel, by as much as a factor of 3. They observed that the panels exhibited creep; that is a constant load applied for 24 hours resulted in an apparent increase of about 40%. Loads held constant for 10 to 20 minutes appeared to increase by 15% to 20%. Their conclusion was that the measured MEDOF panel loads were about 20% greater that the actual loads. In subsequent analysis and discussion of MEDOF panel response (Spencer et al., 1989) it was indicated that in the frequency range 1 Hz to 10^{-2} Hz measured MEDOF panel output could be taken as an accurate reflection of ice loading on them. For frequencies down to 10^{-3} Hz (about 15 minutes) creep results in the measured load amplitude being about 20% greater than the actual load. The best response from the MEDOF panels to load is in the interval of 10 to 100 seconds.

In addition to these calibration issues it should also be noted that for thicker ice the MEDOF panels may not capture the entire load on a given section of the structure. At locations E1, E3, N1 and N3 there were no lower panels installed, as shown in Figure 2. This means that the vertical height of the MEDOF panel group is 5.43 m, and the panels can only capture loading occurring over this height. Recall from Section 3.1 that the water level is just above the bottom of the upper level of panels. Therefore the MEDOF panels at locations E1, E3, N1 and N3 will not capture the entire load if the ice is thicker than 2.7 m, or if thinner ice fails and is pushed against the structure below the lowest panel. For cases where the MEDOF panels are used for calibration for events with thicker ice, a proportion of the load from the single lower panel is assigned to the "missing" lower panels. The method of calculating the load for the missing panels is discussed in Section 4.1.

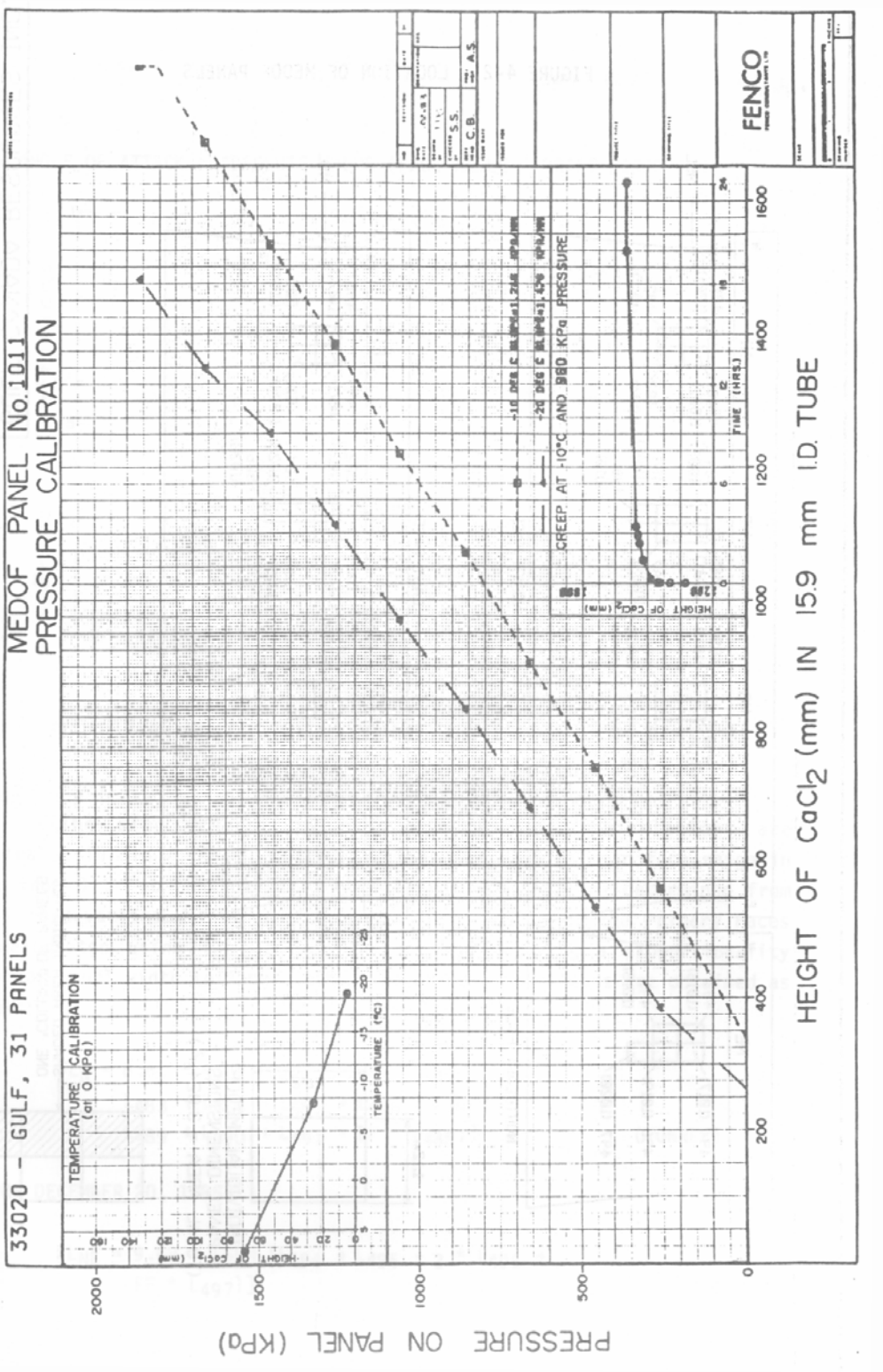

Figure 7 Example of calibration of a MEDOF Panel (Gulf Canada Ltd., 1987b)

5.1.1 Softening of polyurethane material in MEDOF panels (IJA Team)

MEDOF panel behaviour and response was examined extensively by the IJA team. A complete presentation of their assessment appears in Chapter 3.3 of Appendix B. An assessment of MEDOF panels by CHC is presented in Appendix C. The original calibration factors of the MEDOF panels, which were determined in the spring of 1983 immediately after they were manufactured, changed by the winter of 1985-86, as will be shown. Softening of the polyurethane (Adiprene-L100) buttons would lead to the MEDOF panels actual calibration factors in 1985-86 being substantially less than the original values. Because of the instrumentation arrangement of the MEDOF panels, all that can be measured is the height of the fluid in the sight glass, either by direct observation or by means of the pressure transducer. Softening of the buttons, or separation of the buttons from either the front or back faces of the panel, would still produce a similar increase in fluid height in the sight glass with the application of a lower load. This brings into question the absolute magnitude of face loads and global loads. Loads will be calculated in Section 11 for the "Historical Case" using the original calibration factors for the MEDOF panels, but their absolute values will be adjusted downwards in the "Best Estimate" case by a factor which will be described later in the report.

The literature on polymers was searched, and the work of Qi and Boyce (2005) identified as the closest to describing the actual loading of the button material in the MEDOF panels. This publication presents measurements on polyurethane under true stresses up to 20 MPa, and repeated loading. These loading conditions are similar to those experienced by the buttons in the MEDOF panels during ice crushing. The material exhibited non-linear behaviour for stress above about 5 MPa and additionally softened by about a factor of two after only a few of these high load cycles. In discussions with Prof. Qi at the University of Colorado, he suggested that softening of polyurethane could still be expected at stresses of 5 to 10 MPa, values which have been measured in high pressure zones during ice crushing (Frederking and Sudom, 2008).

5.1.2 MEDOF Panel and strain gauge calibration trends

Data from the Molikpaq deployment at Tarsiut P-45 in 1984-85, when the MEDOF panels were relatively new, were examined to see if any change in the relation between MEDOF and strain gauge results could be detected, compared to 1985-86 experience. Four DAY files from November 23 and 24, 1984 and one FAST file from May 9, 1985 were converted. Unfortunately, the four DAY files from November 1984 only contain MEDOF panel data. There are no strain gauge or reliable extensometer data in these DAY files so the comparisons could not be made.

The first DAY file available for analysis, at 20:30 on November 23, 1984, was about 10 hours after a loading event which had a reported maximum face load of 100 MN and a "lot of vibrations". The results of Qi and Boyce (2005) suggest even this small amount of loading could substantially change the stiffness of the urethane buttons, so it is not possible to get any sort of baseline performance data from the panels. The occurrence of softening, after only a few load cycles, is why further work on the 1984-85 Tarsiut data will not help clarify softening since the panels had already experienced extensive ice loads by the time of the first measurements.

Data from the 1985-86 season at Amauligak I-65 (Appendix F) were examined to see if any trends in panel response could be found. The MEDOF panel group loads were compared to the load from each strain gauge on the north and east faces in order to obtain a calibration factor. Since the strain gauges are affixed to the steel structure, it is unlikely they would change with time. If the MEDOF panels softened further in the 1985-86 season, they would tend to indicate a higher load than what was actually experienced, the strain gauge would give the same output for the same actual ice load, and the SG calibration factor would decrease with time. The MEDOF panel strain gauge calibration factor as a

function of time is plotted in Figure 8 and Figure 9 for the east or north faces respectively. A softening trend with time would tend to follow the dashed line shown in the figures. Although there is quite a bit of scatter in the data, there is no trend of decrease in calibration factors. As stated earlier, most of the MEDOF panel softening occurred during the initial loading episodes in November 1984.

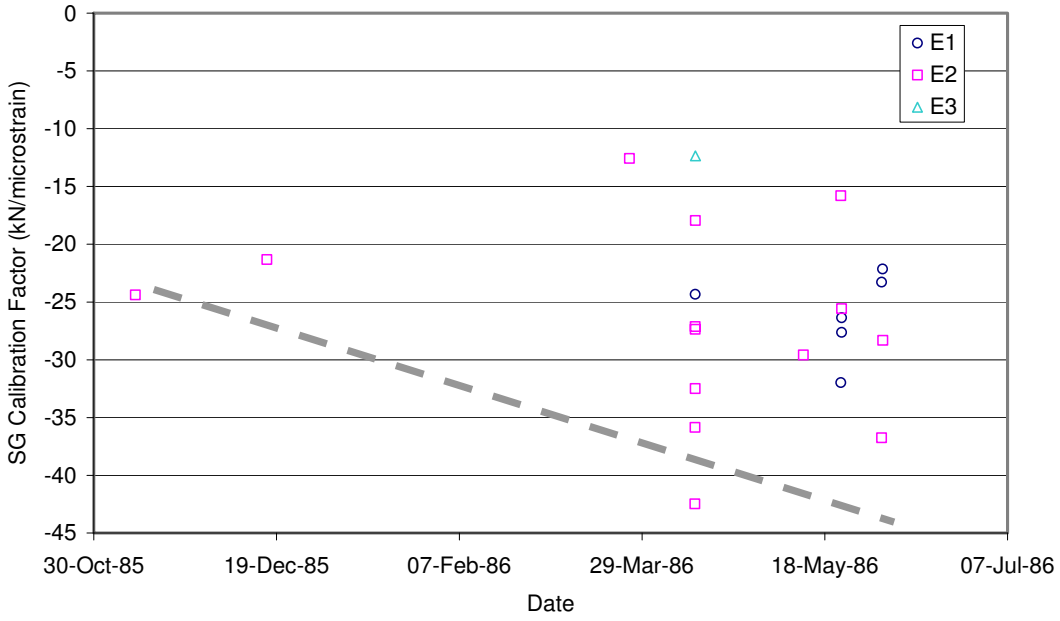

Figure 8 Strain gauge-MEDOF calibration factors for the east face over the 1985-86 season.

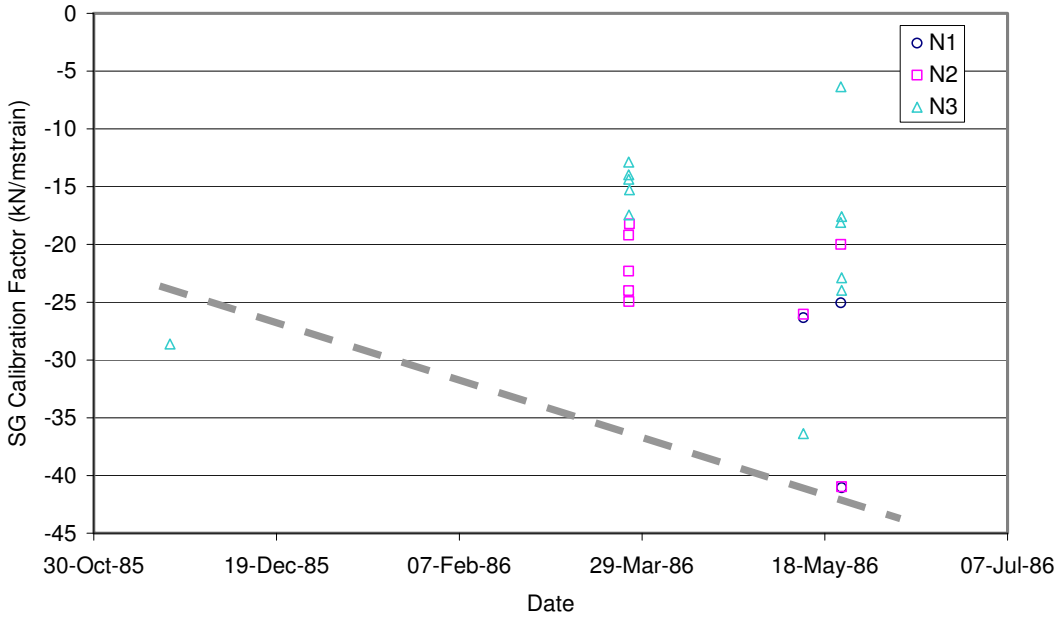

Figure 9 Strain gauge-MEDOF calibration factors for the north face over the 1985-86 season.

The FAST file from May 1985 at Tarsiut P-45, which had a full record of MEDOF, strain gauge and extensometer data, had a calibration factor of 26 kN/us for panel group E2, very similar to the 1985-86 values. The extensometer calibration for the east face was 11 MN/mm, a value greater than determined in the 1985-86 season.

5.2 Strain gauges

The strain gauge calibration factor is a constant which converts the strain gauge reading (in μstrain) to an ice load (in kN). The response of the '09' series strain gauges installed on the main bulkheads of the north, northeast and east sides of the Molikpaq correlated well with the MEDOF panels installed in corresponding locations on the exterior of the caisson. The effective or tributary width of each strain gauge can be taken as midway between adjacent main bulkheads, that is, 2.44m (Gulf Canada Ltd., 1987b). This tributary width is very close to the width of two MEDOF panels (2.27 m). Since there were strain gauges and MEDOF panels at seven locations (N1, N2, N3, NE, E1, E2 and E3), it was possible to calibrate the SG09 strain gauges by comparing the response of both types of instruments to a common ice load. Note that at location E3 the SG09 strain gauge was not directly behind the centre of the E3 MEDOF panel group, but was actually 4.88m towards the southeast corner of the caisson.

For this report, the calibration of the '09 series' (SG09) strain gauges was studied in depth in order to establish a level of confidence in ice loads derived from strain gauge measurements. Two main factors influencing the strain gauge calibration factor are the location of the gauge and the ice thickness during the loading event. A more extensive discussion of these factors is found in Appendix E.

Independent calibration factors for SG09 strain gauges were determined by finite element calculations and simulation of ice loading by deballasting. Finite element calculations by Smyth and Spencer (1987) showed the response of SG09 strain gauges to be sensitive to the elevation at which load was applied. However for ice thicknesses in the range 2 to 6 m they obtained a factor of about 14 kN/μstrain over a 2.44 m width. Their analysis assumed the majority of the ice load was resisted by the sand core. The deballasting tests simulated ice loading by pumping water out of caisson ballast tanks in order to generate a known exterior load due to water pressure on the Molikpaq. The loading created, however, was quite different from that generated by ice loading, so this approach could not be used to develop completely independent calibration factors. It was useful in establishing relative calibration factors for each gauge taking into account proximity to watertight bulkheads, pump rooms or corners which locally stiffen the structure.
The results of the evaluation of calibration factors in Appendix F have been divided such that an average calibration factor was calculated for time series with ice thickness of 2 to 5 m, and 5 to 6 m. Based on these results, best estimates of the calibration factors were determined as shown in Table 2. The calibration factors for strain gauges of the south and west faces are taken to be the same as for the east face, because their locations are similar to those of the east face.

Table 2 Strain gauge calibration factors determined for this project (kN/μstrain for width of 2.44 m)

Ice thickness	N1	N2	N3	E1	E2	E3
2 – 5 m	23	26	20	23	26	23
5 – 6 m	27	32	24	27	32	27

Note that the magnitude of these factors is related primarily to MEDOF panel measurements, while the relative values with position (N1, N2 and N3, for example) are related to independent deballasting tests. These factors are used for face load distributions, but bear in mind they are predicated on the original MEDOF calibrations. Calibration factors ranged from 6 to 43 kN/μs, and averaged 24 kN/μs with a

coefficient of variation of 0.34. The strain gauge at what was termed the E3 location was displaced by 4.88 m from the centre of the E3 MEDOF panel group, as noted in Section 3.2, so the strain gauge factor for the E3 location was taken to be the same as for E1 and N1 since its location with respect to bulkheads is similar to these strain gauges.

5.2.1 Strain gauge calibration experience at Sakhalin

It was suggested that experience from the Molikpaq deployment off Sakhalin could provide an opportunity to independently validate the calibration of strain gauges used to measure local response of the structure to ice loading. In the Sakhalin deployment an improved type of ice load measuring flat-jack panel developed by Sandwell (Frederking et al 2006) was used. This panel was not subject to the shortcomings of creep and softening and non-linearity under larger loads identified in the MEDOF panels used on the Molikpaq in the Beaufort. Shell was contacted about using some of the measurement data from Sakhalin to help validate the calibration of the strain gauges on the Molikpaq at Amauligak I-65.

This was done through an exchange of e-mails between Shell (Guido Kuiper) and CHC. In doing the comparison the following similarities and differences were identified:

Similarities for both locations

- The SG09 strain gauge is at the same position on a Main Bulkhead.
- A tributary loading width of 2.44 m was established for measurement data.

Differences

- At the Sakhalin location the water line is about 3.5 m lower on the structure than the case at Amauligak. Ice loading on 23° slope at Sakhalin versus 7° slope at Amauligak.
- At the Sakhalin location the Molikpaq sits on a 15-m high spacer.
- The sand core was denser at the Sakhalin location

From measurements at Amauligak in 1985-86 and FE calculations (Smyth and Spencer, 1987) it is known that the strain gauge calibration factor is sensitive to the elevation of load application on the structure. At the waterline elevation for Amauligak, the FE calculation gave a calibration factor of 14.4 kN/μs, whereas for loading about 3 m lower, similar to the water line elevation at Sakhalin, the factor was 19.9 kN/μs. (These numbers were reported in Table 2, Appendix E of our Draft Final Report in November 2008) The average calibration factor for the strain gauges at Amauligak was 25 kN/μs, based on field data and actual ice loading. The measurements at Sakhalin gave a lower calibration factor for the strain gauge. Even taking the elevation difference into consideration, the Sakhalin measurements still produced a lower SG09 calibration factor than the factor we determined from MEDOF panel measurements at Amauligak. This means that ice loads determined at Amauligak from MEDOF panel- based calibration factors, would appear greater than loads determined at Sakhalin from the Sandwell panel based calibration factor, given the same measured strain.

5.3 Extensometers

As discussed in Section 3.3 on extensometer setup, the caisson changed shape or 'ovalled' with a force on one of the long faces. The caisson displacement is calculated from the difference in the movement of the caisson face with respect to the immobile guide pipe:

$$d_{C-GP} = d_{C-D} - d_{D-GP} \qquad \textbf{(5-1)}$$

where: $d_{C\text{-}GP}$ = Movement of Caisson with respect to Guide Pipe
$d_{C\text{-}D}$ = Movement of Caisson with respect to Deck
$d_{D\text{-}GP}$ = Movement of Deck with respect to Guide Pipe

Displacements measured by the extensometers can be used to convert caisson ring deformation to a global load if a calibration factor is known. This calibration factor is also referred to as the "stiffness" of the structure. A discussion of previous calibration factors is given in Appendix E.

A detailed table with ice information and extensometer calibration factors for 11 files, as well as for individual segments of many files, is given in Appendix F. All face loads used for calculating the extensometer calibration factors are based on linear averaging of MEDOF panel results. Linear averaging provides a good estimate of face load where the loads from panel groups are well correlated, as is the case for March 25 in the afternoon. Where loading across the face is more random, as when crushing failure occurs, probabilistic averaging will result in a lower face load. The calibration factors determined for the "Historical Case" by NRC-CHC, and predicated on the original MEDOF calibrations adjusted for creep are shown in Table 3. These calibration factors were used to calculate the face loads presented in Section 14 and Appendix K. Extensometer deformation response to ice loading on a face is negative so a minus sign is introduced in the table to generate positive face loads for plotting purposes. Appendix E explains how the calibration factors have been reduced to take into account creep of the MEDOF panels, the means for calculating average values of the calibration factor and how our estimate of the factor was determined.

Table 3 Extensometer calibration factors for face loads (MN/mm)

	N-S	E-W
Range	-3.7 / -9.6	-5.5 / -9.2
Average	-6.2	-7.0
"Historical Case"	-6.0	-6.0

5.3.1 Extensometer calibration experience at Sakhalin

Shell agreed to share some of their experience with extensometer measurements at Sakhalin and interpretation ice load from them. After the June 2008 meeting they provided information that they determined an extensometer calibration factor of 2.6 MN/mm from FEM calculations. In subsequent communication with Shell they checked the soil stiffness used in their model and discovered it was too low, and concluded that the calibration factor from FEA should be higher at Sakhalin. Following our November 2008 meeting Shell examined a number of high load events at Sakhalin and determined an average extensometer value, based on load measuring panels that did not have the same problems as the MEDOF panels. There was considerable scatter in their results, like ours, but had a similar value to the one determined in our "Historical Case". Direct comparisons between the two deployments are difficult because the Sakhalin configuration of the Molikpaq rested on a 15 m high spacer, the sand core was densified and the waterline was about 3 m lower on the caisson. Based on the differences between the Sakhalin and Beaufort deployments, a lower value would have been expected from the Beaufort experience.

6. ICE LOADS FROM GEOTECHNICAL ANALYSIS AND RESPONSE (K.J HEWITT & ASSOCIATES LTD.)

The report prepared by K.J Hewitt & Associates Ltd. is in Appendix I of this report. The Summary and Conclusions of his report have been extracted and are reproduced here.

6.1 Summary

1. The report begins by reviewing the initial 1982 design of the Molikpaq which emphasized the importance of the core sand properties to the overall performance of the structure under ice loading. This 'Class A' prediction (a prediction made before an event) was that densification of the core fill sand to relative densities of about 70 percent was a sufficient condition to avoid serious cyclic mobility problems. It was also noted that such densification would require some advance upon the state-of-the-art in vibro-compaction and this had major implications both in terms of capital cost and schedule delay.

2. Methods of assessing in situ sand state are then presented. These methods include the CPT, the self-bored pressuremeter test and placement technique.

3. Using the above methods, and taking into account the amount of settlement and the marked increase in density achieved during subsequent blasting at Amauligak F-24 in 1987, it was concluded that the core sand as placed at Amauligak I-65 in 1985 was in a loose state (mean relative density of about 25 to 35 percent). GCRI had chosen not to use densification. Justification for this decision was provided by their new method of evaluating the 'state' of the core sand, which was subsequently shown to be in error (Sladen, 1989). This error was a minimum of at least 0.1 in terms of state parameter, or 25% in terms of relative density.

4. Numerous geotechnical models developed in the past to analyse the predicted deformations of the Molikpaq are then reviewed. All but one of these models are geotechnical models and only consider the response of the sand in the core and the berm. Because the properties of the steel caisson itself are not incorporated into these models they only predict the global deformations of the unit. The only means of measuring these global deformations is by slope indicators.

5. The other model reviewed is a structural model that was developed based on an analysis of the steel caisson itself with the properties of the core sand input as boundary conditions. The purpose of this 'Sandwell' model was to estimate the ring distortion behaviour of the Molikpaq to calibrate the extensometers to ice loads, as opposed to the slope indicators.

6. Performance predictions based on the geotechnical models are then reviewed. Although it is the author's opinion that all of the models discussed appear to be technically sound and could be useful tools in predicting field behaviour, this would only be true if the input parameters with respect to the insitu state of the sand and/or the ice loads were correct. Unfortunately the majority of the published analyses and associated physical model tests assumed that the insitu state of the core sand was medium dense to dense (mean relative density of around 65 percent). This is in contrast to all basic evidence that the core sand was in a loose state.

7. The exceptions to the above were one set of physical model tests conducted by GCRI where the sand is defined as loose and the EBA analyses which assume a core density on the border between loose and medium dense (relative density in the order of 35%).

8. The EBA analyses, however, do not model the stress/strain behaviour of the composite unit at low loads. As such a new 'Best Estimate' curve has been developed based on the EBA curve and taking into account strain compatibility at lower loads.

9. Using the Sandwell structural model, the load distortion ratios for the eleven most likely scenarios varied from 2.2 to 3.3 MN/mm with an average of 2.84 MN/mm. These calculated ratios are approximately half the ratios determined from data based on MEDOF panels.

10. The report discusses the inclinometer data and concludes that they are not reliable. Because of the looseness of the sand, the settlements within the core and the directions of movement of the slope indicators, previously quoted lateral deformations are not considered to be representative of actual deformations. However, even though the settlement of the loaded caisson face would indicate otherwise, there remains the possibility that there was some lateral deformation of the core (in the order of ten's of millimetres).

11. The maximum extensometer reading for the five significant events in 1986 was determined to be 60mm on the morning of April 12th. Because dynamics were involved, this value may be higher than the equivalent static value.

12. Ice load estimates have been made using both the 'best estimate' geotechnical model and the Sandwell structural model.

13. With respect to the geotechnical model, all indications are that if there were any permanent displacements of the Molikpaq in the direction of the ice loads they would have been small and could not be quantified from the inclinometer data. However if one were to assume an unrealistic, extreme worst case scenario whereby the:
    - Displacements tabled by GCRI were real.
    - These displacements were in the direction of the ice load.
    - That the residual displacements were one third of the 'elastic' displacements.

    then an extreme upperbound load estimate for the April 12th AM event of 290 MN could be deduced. However a more realistic extreme upperbound load for this event, assuming the residual displacements were two thirds of the 'elastic' displacements would be 220 MN. Such estimates for the three events associated with slope indicator data are shown in Table 4.

Table 4 Upperbound loads based on less extreme deflection scenarios.

DATE	DEFLECTION (mm)		UPPERBOUND LOAD(MN) (Assuming less extreme deflection scenarios)
	Residual	'Elastic'	
8th March	20	30	140
12th April AM	30	45	220
12th May	14	21	100

14. With respect to the Sandwell model, using an average load distortion ratio of 2.84 MN/mm (best conservative guess) and the maximum extensometer readings documented by the author for the five significant events in 1986, the ice load estimates are as shown in Table 5.

Table 5 Predicted ice loads based on extensometer readings.

DATE	DEFLECTION (mm)	PREDICTED ICE LOAD (MN)
8th March	37	105
25th March	20	57
12th April AM	60	170
12th April PM	30	85
12th May	45	128

15. As a reality check, the above estimated ice loads have been compared with ice loads derived from mass decelerations. Three examples are presented; one being the Molikpaq May 12th event, one concerns an impact of a multi-year feature on the SSDC in 1984, and the other is the largest recorded ice load on Hans Island in 1983. The ice loads so derived compare very well with those shown in Table 5.

6.2 Conclusions

Estimating ice loads on the Molikpaq at Amauligak I-65 based on geotechnical analyses and responses is not an exact science. However it has been shown that it is not the lack of modelling capability that is the issue. Instead it is the assessment of the insitu properties of the core sand and, at low load levels, the percentage of load being absorbed by base friction which provide the most significant areas of uncertainty.

The insitu properties of the core basically dictate the performance of the unit. The problem is that it is difficult to assess the core sand properties definitively. However the characteristic insitu density of the core sand, on which the properties of the core sand are primarily based, has been assessed with reasonable confidence to be in the range of 30% (i.e. loose). For comparison, the Klohn Crippen Berger report (Klohn Crippen Berger, 2009) states that the core sand had a mean relative density of about 35%. Based on this value the general performance of the Molikpaq under ice loading can be predicted based on both numerical and physical modelling undertaken both before and after the deployment at I-65 in 1985.

An indication of this predicted performance can be gleaned from the following statement made by Jefferies et al., 1985: '*significant performance shortfalls should be expected if the characteristic state of the sand core is (loose)…'* The Jefferies et al paper also provides an historical perspective that is worth repeating in light of the subsequent performance of the Molikpaq at I-65 on the morning of April 12th. '*The precedent for using undensified sand for artificial islands has been established in the Canadian Beaufort Sea by 22 surface piercing islands and 5 caisson type islands. However this precedent is not unequivocable (sic) because 5 failures occurred, all during construction.'*

Ice load estimates were made using both a 'best estimate' geotechnical model, assuming the core sand was in a loose to medium dense state, and the Sandwell structural model which assumed dense sand in the core.

The geotechnical model requires good inclinometer data as input. Such data are not available, for reasons outlined in the report, and therefore ice loads estimated from this model are quite speculative. However

there are strong indications that, if indeed there were any real deflections of the sand core they would have been small. If there was a real displacement then all the perimeter inclinometers would have recorded movements and these movements would have been in the direction of the ice load. This was not the case for any event. Even so, an extreme (conservative) deflection scenario was assumed. On this basis an upperbound ice load estimate of 220 MN has been assigned to the April 12th AM event.

Conversely the detailed structural model developed by the Molikpaq design team (the Sandwell model) requires extensometer data as input. Although the Sandwell model has several imperfections, the extensometer data appear quite reliable. Based on a best estimate of the load distortion ratio derived from this model, a conservative ice load estimate of 170 MN has been assigned to the April 12th AM event.

Having reviewed all of the analyses and data and taking into account the above comments, it is the author's overall opinion that the highest ice load occurred during the April 12th AM event and was about 200 MN.

However because of the inherent uncertainties in the evaluation of the properties of the composite unit combined with the uncertainties in determining displacements, it is believed that the actual load could differ from this estimate. Therefore it is the author's opinion that the load could have been as high as 250 MN or as low as 150MN.

The above ice load estimates are in the order of 50% or less than loads previously published which either directly or indirectly rely on MEDOF panel data. However such ice loads are consistent with loads based on floe decelerations including Hans Island data.

7. OTHER GEOTECHNICAL INPUTS TO THE JIP

Ryan Phillips at C-CORE was contracted by Ian Jordaan and Associates to review some of the background material on the geotechnical response of the Molikpaq caisson and sand core to ice loading. This report of November 2008 appears in the appendices of the Ian Jordaan and Associates report (Appendix B of this report) as Appendix C. The C-CORE report reviewed data from the DynaMAC CD, some papers on the Molikpaq geotechnical response in the open literature, and the thesis by Jeyatharan (1991) on centrifuge testing of the Molikpaq caisson and sand core system. The conclusion was that loading events were resisted mostly by caisson base shear and that displacements of the caisson were sufficiently small that little passive resistance would be mobilized in the core. At the November 2008 meeting with Participants, Ryan Phillips stated that an upper bound of 200 MN for the resistance of the caisson might be on the low side. This was clarified by Ryan Phillips in a C-CORE Technical Memorandum dated July 14, 2009, also in Appendix C of the IJA report. He looked at manual slope inclinometer readings, settlements, pore pressure and the small permanent movements from extensometer measurements, and concluded that "the 3 significant loading events exceeded the 200 MN basal shear resistance, but not by very much." Appendix D to the Ian Jordaan and Associates report contains a commentary by Kevin Hewitt that basically concurs with Ryan Philips' assessment that the majority of caisson resistance to the ice loads mobilized at Amauligak I-65 was from base shear or frictional resistance under the caisson.

Following the review of the November 2008 project report, ConocoPhillips Canada commissioned Klohn Crippen Berger to review select elements of the 1986 Molikpaq JIP work to provide a broader understanding of the geotechnical performance of the Molikpaq as well as ice-structure interaction issues. The results of this review were presented by Mike Jefferies to a meeting of Participants' geotechnical experts at a day-long seminar on February 25, 2009. Geotechnical experts from Shell, ExxonMobil and ConocoPhillips participated. The presentation covered an assessment of the core density and state, assessment of ice load and platform resistance for the April 12 event, methods and calibration used to estimate ice loads, and a treatment of ice crushing. Following the presentation, a teleconference was held on March 11, 2009, at which the Participants' geotechnical experts were polled for their assessment of the content of the presentation. They stated that, based on the information presented, they found the assessment of the core properties convincing and that the core would respond in a dilative manner under loading. Subject to confidentiality restrictions, ConocoPhillips Canada offered to make the report and presentation material available to the Participants and JIP project team for assessment. The Klohn Crippen Berger report was distributed to the JIP team for review in July 2009.

To obtain a third party review of the geotechnical work Professor K.T. Law of Carleton University carried out an independent geotechnical review of K.J. Hewitt & Associates' 2008 and 2009 reports, the original 1986 JIP geotechnical work, as well as the Klohn Crippen Berger report.. His reports are in Appendix J. He did support the conclusion that the sand core was loose; it could be mildly dilative and its state parameter would be close to the critical state line. He explained the different understandings of the core sand behaviour in the KCB report and by Hewitt, and identified questions relating to the analysis in the KCB report, particularly explaining high predicted ice loads compared to the small measured horizontal movements. K.J. Hewitt & Associates has provided a response to Law's review, which is included in Appendix I.

8. PROBABILISTIC AVERAGING (IAN JORDAAN AND ASSOCIATES TEAM)

This Section is taken from Chapter 4 of the Ian Jordaan & Associates report (Appendix B).

8.1 Introduction

When attempting to extrapolate to obtain global loads from local measurements, for instance those from the MEDOF panels, the question arises as to the appropriate measure of standard deviation. To take a simple example, consider first two adjacent panels. If the readings are fully correlated, then if one panel reads high, so does the other. If one reads low, so also does the other. In obtaining loads, one would not assume that one panel read high while the other reads low. The implication is that the mean and the standard deviation of readings for the average of the combined panels would be the same as for individual panels. In this case, simple (linear) extrapolation of the pressures to obtain the global load, i.e. multiplying the MEDOF reading by the structure width divided by the panel width, seems reasonable.

Now consider two distant panels: if they are uncorrelated, then there is no reason to assume that a high reading on one would imply a high reading on the other. The mean values, under similar loading conditions, would be the same, but averaging the two readings reduces the standard deviation. In fact, analysis shows that the standard deviation of the average is the standard deviation of an individual panel divided by $\sqrt{2}$. This will now be explained.

By considering a linear function of random quantities, it is possible to calculate the standard deviation of pressure distribution for a group of two panels or columns, whether they are correlated or not. If $Y = aX_1 + bX_2$, where X_1 and X_2 have a joint probability distribution, the variance is

$$\sigma_Y^2 = E\left(aX_1 + bX_2 - a\mu_{X_1} - b\mu_{X_2}\right)^2, \qquad \textbf{(8-1)}$$

where $E(\cdot)$ denotes expected value and the μ's denote mean values.

As a result,

$$\sigma_Y^2 = a^2\sigma_{X_1}^2 + \sigma_{X_2}^2 + 2ab\sigma_{X_1,X_2}, \qquad \textbf{(8-2)}$$

where σ_{X1}^2 and σ_{X2}^2 are variances and $\sigma_{X1,X2}$ the covariance.

If $Y = (X_1 + X_2)/2$, then, assuming equal variances σ and using Equation 8-2,

$$\sigma_Y^2 = \frac{1}{4}\left(\sigma^2 + \sigma^2\right) + \frac{1}{2}\sigma^2 \cdot \rho,$$

$$= \frac{1}{2} \cdot \sigma^2\left(1 + \rho\right),$$

in which ρ is the correlation coefficient.

As a result

$$\sigma_Y = \sigma\sqrt{\frac{1}{2}(1+\rho)} \qquad \textbf{(8-3)}$$

We see that if $\rho = 1$ (high correlation), $\sigma_Y = \sigma$ whereas if $\rho = 0$, $\sigma_Y = \sigma/\sqrt{(2)}$, as stated above.

If we consider eight panels, with means and individual standard deviations all equal to μ and σ respectively, knowing also that the pressures are stochastically independent, then the average pressure over eight panels will have a mean of μ with a standard deviation of $\sigma/\sqrt{(8)} = \sigma/2.83$. This shows that the standard deviation of an averaged load can be considerably less than the local standard deviation, and a much larger reduction can be expected for a wide face of the order of 90m. This example was based on the assumption of independence between panels, and it is important to consider correlation between adjacent panels.

To illustrate application of the method, an interaction involving mainly crushing is considered (Figure 10). The nominal interaction area represents the contact area that would occur without spalling of ice. The actual interaction area represents the area of contact with intact ice (after spalling). The high pressure zones represent areas of high pressure which are observed during crushing events. These high pressure zones can reach pressures up to the order of 70 MPa over smaller areas. Given the nature of the pressure distribution during crushing events, one expects the average pressure over a wide structure (shown in red) will have significantly less variance than the pressure measured over a single panel (shown in black).

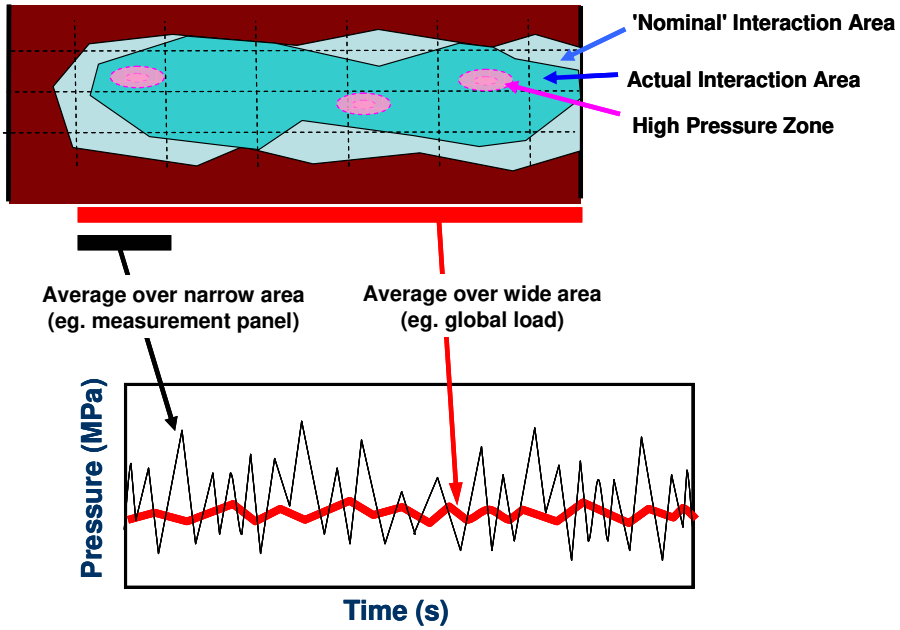

Figure 10 Pressure Averaging for Crushing Failure Model

8.2 Histograms for Individual MEDOF Columns

To provide background on the analysis to follow and to respond to client request, the histograms for selected individual MEDOF columns are provided. The trimmed event files (inhouse), corrected for panels not working, were used for this exercise. The three representative sample events given in Table 6 have been selected for further analysis.

Table 6 Events selected for analysis of column load distributions; h1 and h2 are lower and upper estimates, respectively, for ice thickness

Event No.	fastfile	h_1 (m)	h_2 (m)	v (m/s)	Ice Type	Loaded Face
01	f511121901	0.8	0.8	0.57	FY	N
23	f605120301	1.5	3.5	0.17	FY/MY	N
58	f603081731	4.3	4.3	0.04	MY	N

For each of the above events, histograms of loads acting on each column of the north face were generated and distributions were fitted to these data. Results of this analysis are shown in Figure 11, Figure 12 and Figure 13 for events 01, 23 and 58, respectively. The local column loads show a skewed and non-normal distribution. In the figures the data have been fitted to lognormal distributions, although other distributions such as Weibull or gamma may also be considered. Column to column variation in the load distributions are observed for all events. This likely results from local variations in ice thickness, physical properties, as well as from randomness of the failure processes.

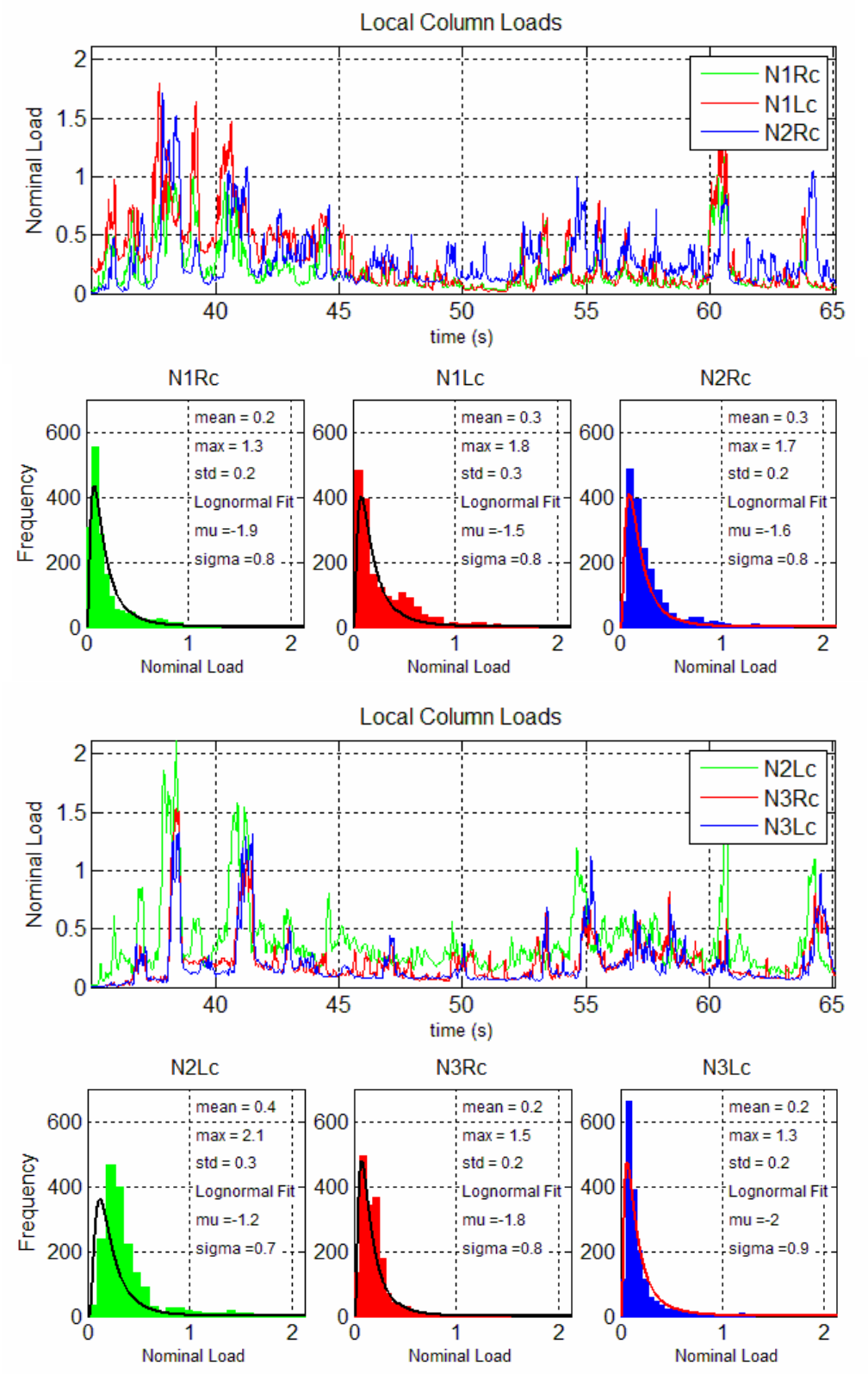

Figure 11 Histograms of nominal loads of columns for the North face during event 01

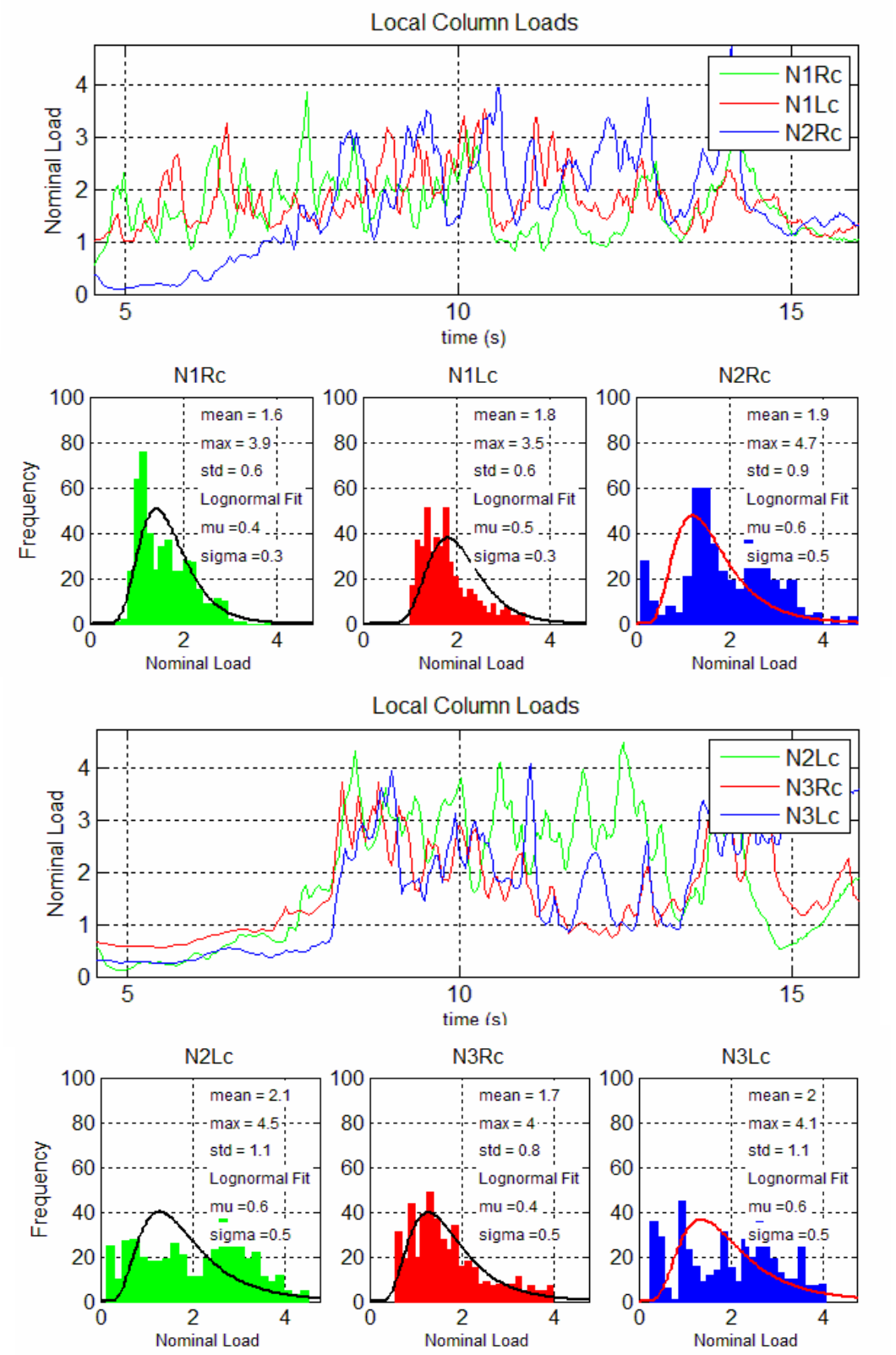

Figure 12 Histograms of nominal loads of columns for the North face during event 23

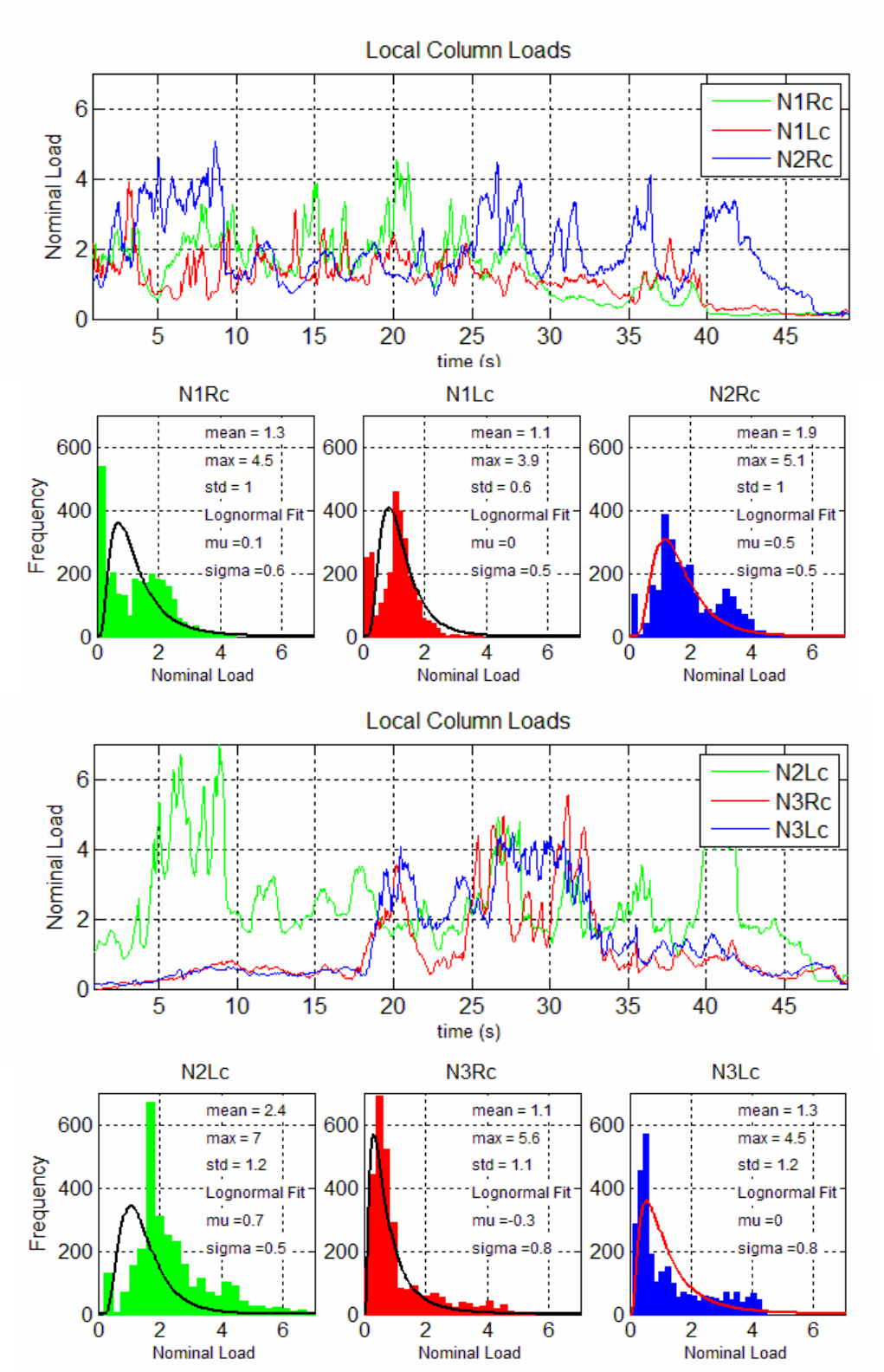

Figure 13 Histograms of nominal loads of columns for the North face during event 58

As can be seen, the ice force (or pressure) is not normally distributed. For large areas, a normal (or Gaussian) distribution follows as a result of the Central Limit Theorem (see Jordaan, 2005). If one adds together or averages many random quantities, one obtains a random quantity that approaches the normal distribution, regardless of the underlying distribution. In the case of ice loads acting on a structure, the global loads may be considered the sum of local loads across the structure width. The idea behind the Central Limit Theorem is illustrated in Figure 14. This notion is central in modelling global pressures as a random averaging process with a normal distribution defined by a mean and standard deviation.

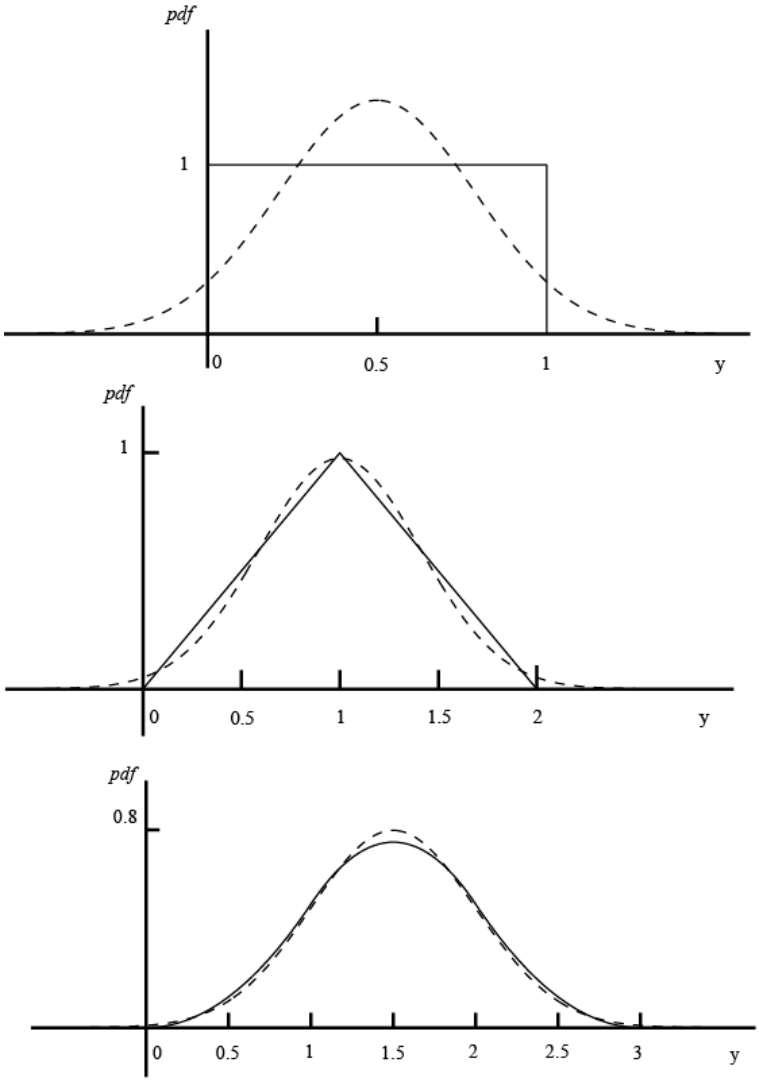

Figure 7.14 Addition of uniformly distributed random quantities (dotted line is normal distribution)

Reproduced with permission of Cambridge University Press

Figure 14 Addition of uniformly distributed random quantities; dotted line is normal distribution (Jordaan, 2005)

8.3 Autoregressive Method

Average ice failure pressures over wide structures can be estimated from measured load or pressure data over panels covering only part of the structure, using a "probabilistic averaging" method. A practical method needed to be developed to account for the fact that certain pairs of columns were adjacent while the pairs were also separated as noted in Figure 12.

The method that is proposed is based on a first-order autoregressive process (Vanmarcke, 1988). This is based on the Markov assumption. In a process in time, an event of a Markov process depends on the previous one and not those earlier in the process ("knowledge of the present makes the future independent of the past"). The correlation is directional because time moves forward only. The value at time *t* depends on the value at time $(t-1)$ plus an uncorrelated time series (usually white noise).

A process in space (such as ice pressure over a contact face) is distinct from a process in time since there is no preference of directionality. The following event correlates to both the preceding one and the following one (in a spatial sense). This can be expressed by the second-order difference equation:

$$X(t) = a\left[X(t-1) + X(t+1)\right] + U(t), \qquad \textbf{(8-4)}$$

where $X(t)$ is the random series and the *a* is a constant and $U(t)$ is an uncorrelated random series. If the process has a correlation function $\rho(\tau)$ where τ is the lag distance, which is the distance between two points noting that space rather than time is the key variable, then the associated covariance function is (Vanmarcke, 1988):

$$B_X(\tau) = \sigma_X^2 \rho(\tau),$$

where σ_X^2 is the variance at a given location. This will be denoted simply as σ^2 in the following. The variance σ_T^2 over an interval of length T after averaging of a one-dimensional random process with variance σ^2 is

$$\sigma_T^2 = \gamma(T)\sigma^2, \qquad \textbf{(8-5)}$$

where the variance function $\gamma(T)$ is obtained as (Vanmarke, 1983):

$$\gamma(T) = \frac{2}{T}\int_0^T (1-\frac{\tau}{T})\rho(\tau)d\tau. \qquad \textbf{(8-6)}$$

The square root of the variance function, $\left[\gamma(T)\right]^{1/2}$ is the "reduction factor" to be applied to the point standard deviation σ in order to obtain the variance for the structure as a whole. The quantities ρ and σ are to be obtained from the data (measured quantities).

Appropriate values of γ can be determined for both panel widths and structure widths; it is possible to estimate the variance in average pressure over the structure face given the variance in load over measurement panels. Since the panels were in separate groups, an alternative to Equation 8-4 has been used when considering the MEDOF panels, as described later on though the general principle still applies).

In their analysis of loads on the Molikpaq at Amauligak I-65, Jordaan et al. (2005) considered an exponential correlation function of the form

$$\rho(\tau) = \left[1 + \frac{|\tau|}{c}\right] e^{-|\tau|/c} \qquad \textbf{(8-7)}$$

to represent the correlation between pressures at separation distances τ, where c is a characteristic spacing which can be calibrated based on measured loads at different separation spacings c. The pressures considered were average pressures over the contact height. Based on analysis of a number of load events, Jordaan et al. (2005) recommended values of c in the range 0.82 to 1.37, corresponding to correlations of 0.6 to 0.8 between MEDOF panels at a spacing of 1.135 m.

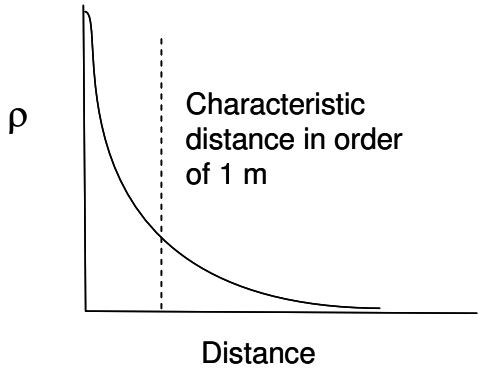

Figure 15 Illustration of exponential correlation function

Given the above exponential correlation function, the reduction function (Equation 8-6) for the process variance can be reduced to

$$\gamma(T) = 2\frac{c}{T}\left(2 + e^{-T/c} - 3\frac{c}{T}(1 - e^{-\frac{T}{c}})\right) \qquad \textbf{(8-8)}$$

This equation is used in determining the variance in load over the structure face, given the variance at a fixed point.

8.4 Direct Method

In determining the variance of a column load from that of a group, a direct method was used in the Jordaan et al. (2005) study exploiting the fact that the panels on a given face were separated into three groups of pairs. Given the small characteristic lengths c, the loads on the three groups on a face are essentially independent, so the variance $\sigma_M{}^2$ on the three groups equal the variance $\sigma_G{}^2$ on a single group, divided by the number of groups (Ng = 3), i.e.

$$\sigma_M{}^2 = \frac{\sigma_G{}^2}{N_G} \qquad \textbf{(8-9)}$$

The column loads are correlated since they are only 1.135 m apart. The variance σ_G^2 for a group of two adjacent columns is determined from the variance σ_C^2 of the column loads as follows. Defining the group load L_G as the average of the column loads L_{C1} and L_{C2}, Equation 8-3 may be used.

$$\sigma_G^2 = \sigma_C^2 \left[\frac{1}{2}(1+\rho) \right] \quad \textbf{(8-10)}$$

Then, using Equation 8-9,

$$\sigma_M^2 = \sigma_C^2 \left[\frac{1}{2}(1+\rho) \right] / N_G. \quad \textbf{(8-11)}$$

Using $\sigma_S^2 = \sigma_C^2 \cdot \gamma$ and Equation 8-11 above, one can estimate the variance σ_S^2 on the structure of width W_S from the variance σ_M^2 on the measured load as

$$\sigma_S^2 = \sigma_M^2 \cdot \frac{\gamma(W_S)}{\left[\frac{1}{2}(1+\rho) \right] / N_G}. \quad \textbf{(8-12)}$$

8.5 New Method for Project using Bi-functional Correlation Relationships

In the Jordaan et al. (2005) work, effort was concentrated on crushing type failures as it was assumed that these result in the highest loads. In order to make the method more general for the purposes of comparing loads estimates based on the different measurement devices (MEDOF panels, strain gauges and extensometers), and for different failure modes, it was extended as described in the following.

The exponential correlation function of Equation 8-7 does not provide the flexibility to model all the different failure events. To model more complex events, a bi-functional correlation function consisting of the weighted sum of two exponential correlation functions was found to provide better results.

$$\rho(\tau, q_1, c_1, c_2) = q_1 \cdot \left[1 + \frac{|\tau|}{c_1} \right] e^{\frac{-|\tau|}{c_1}} + (1-q_1) \cdot \left[1 + \frac{|\tau|}{c_2} \right] e^{\frac{-|\tau|}{c_2}} \quad \textbf{(8-13)}$$

The corresponding reduction function for the process variance is

$$\gamma(T) = q_1 \cdot \left[2\frac{c_1}{T}\left(2 + e^{-\frac{T}{c_1}} - 3\frac{c_1}{T}(1 - e^{-\frac{T}{c_1}}) \right) \right] + (1-q_1) \cdot \left[2\frac{c_2}{T}\left(2 + e^{-\frac{T}{c_2}} - 3\frac{c_2}{T}(1 - e^{-\frac{T}{c_2}}) \right) \right] \quad \textbf{(8-14)}$$

In determining line loads from the measured loads, the work of section 8.3 was extended for the case where the loads on the different panel groups are not independent. The variance σ_M^2 for the three groups

of panels on a face can be determined from the variance σ_G^2 of the group loads as follows. Defining the measured load L_M as the average of the group loads L_{G1}, L_{G2}, and L_{G3},

$$L_M = (L_{G1} + L_{G2} + L_{G3})/3, \quad \textbf{(8-15)}$$

The variance σ_M^2 is determined in a manner similar to Equation 8-1 and the following above; as a result

$$\sigma_M^2 = \left[\sigma_{G1}^2 + \sigma_{G2}^2 + \sigma_{G3}^2 + 2\sigma_{G1,G2} + 2\sigma_{G1,G3} + 2\sigma_{G2,G3}\right]/9$$

or

$$\sigma_M^2 = \sigma_G^2\left[\frac{1}{3}\left(1+\frac{2}{3}\rho_{1,2}+\frac{2}{3}\rho_{1,3}+\frac{2}{3}\rho_{2,3}\right)\right] \quad \textbf{(8-16)}$$

This can be approximated as,

$$\sigma_M^2 \approx \sigma_G^2\left[\frac{1}{3}\left(1+\frac{4}{3}\rho(18.5)+\frac{2}{3}\rho(37)\right)\right], \quad \textbf{(8-17)}$$

where the distance between groups is approximately 18.5m. Using $\sigma_S^2 = \sigma_C^2 \cdot \gamma$, Equation 8-10 and Equation 8-17 above, one can estimate the variance σ_S^2 on the structure from the variance σ_M^2 on the measured load as

$$\sigma_S^2 = \sigma_M^2 \cdot \frac{\gamma(W_S)}{\left[\frac{1}{2}\left(1+\rho(1.135)\right)\right]\cdot\left[\frac{1}{3}\left(1+\frac{4}{3}\rho(18.5)+\frac{2}{3}\rho(37)\right)\right]} \quad \textbf{(8-18)}$$

8.6 Determination of Model Parameters and Calibration

To evaluate and compare the different load related measures for the Molikpaq ice interaction events (MEDOF loads, extensometer readings, and strain gauge readings), analyses were conducted for the events and Sub-events agreed upon at the May 2008 meeting and summarized in Table 7 and Table 8 (B. Wright event classification). Only Sub-events involving predominantly creep and crushing failure modes were considered.

In this preliminary work, the MEDOF panel results were used to determine correlations. Since the calibration coefficients are not known, and the values of loads consequently uncertain, the values are designated as “Nominal”.

Table 7 Events considered for calibrations

Event	Faces Loaded		Event Duration	Ice Thickness		Sail Heights	Est. Contact Area	Load Obs. on Lower Panel
	Medof	No Medof		Min.	Max.	mean/max		
			min.	m	m	m	m2	Y/N
Mar-25-N-1	N, NE, E	NW	130	2.5	3.0		18.7	N
Apr-12-E-1	E	SE, S	73	4.0	6.0		22.8	Y
Apr-12-E-2	E	SE, S	61	4.0	6.0		22.8	Y
Apr-12-E-3	E	SE, S	16	4.0	6.0		22.8	Y
May-12-N-1	N, NE, E		48	1.7	2.0	1.5,2.5	17.0	Y
May-22-N-1	N, NE, E		71	2.0	3.0		17.0	Y
May-22-N-2	N, NE, E		73	3.0	4.0	1,2	17.0	Y
Jun-02-E-1	E		74	1.8	2.5		14.6	Y
Jun-02-E-2	E		68	1.8	2.5		14.6	Y

Event	Fast File	CHC Calibration Number	BW Event Number	Ice Type	Max nominal load	Modes (*Definitions found in Section 1)
Mar-25-N-1	f603251302	2	N/A	SY/MY ?	11.90	SLW
Apr-12-E-1	f604121101	9	14	MY	19.46	CC,CR,MM,SLW
Apr-12-E-2	f604121201	11	15A	MY	43.23	CR,M,SLD
Apr-12-E-3	f60412140A	10	15B	MY	10.63	CR,MM
May-12-N-1	f605120301	8	16	FY (MY inclusions)	47.57	CR, MM, SLW
May-22-N-1	f605220801	3	17	MY	16.19	SLW, MM
May-22-N-2	f605221301	5	18	MY	24.68	CR, SLD, SLW
Jun-02-E-1	f606021301	6	19	FY (MY inclusions)	14.89	CR, MM, SLW, SLD
Jun-02-E-2	f606022001	7	20	FY (MY inclusions)	10.06	SLW, CR, MM

Table 8 Sub-events Events Considered for Calibrations

Event	Subevent	Failure Mode	Subevent Duration	Load Obs. on Lower Panel	Max Nominal Load	Avg Nominal Load	No. Groups Loaded	Max. Extensometer Reading	Max. Summed Strain
			min.	(Y/N)				mm	uStrain
Mar-25-N-1	1	Creep	130.14	N	11.9	5.5	3	-0.8	370
Apr-12-E-1	3	Crushing	4.39	N	13.3	8.5	1	-2.0	403
Apr-12-E-2	1	Crushing	1.42	Y	10.6	8.2	1	-0.2	110
	2	Crushing	1.64	Y	12.8	11.0	2	-2.2	206
	3	Crushing	5.57	Y	22.9	15.8	3	-5.6	514
	4	Crushing	1.93	Y	17.3	12.4	2	0.3	427
	5	Crushing	4.21	Y	13.7	9.3	1	0.7	338
	6	Crushing	4.45	Y	43.2	20.0	2	-6.0	589
	8	Crushing	7.73	Y	27.7	17.9	2	-7.6	631
Apr-12-E-3	1	Crushing	1.5	Y	9.9	7.5	2	-6.1	393
May-12-N-1	2	Crushing	2.98	Y	30.1	23.0	3	-7.0	687
	4	Crushing	5.15	Y	47.6	32.7	3	-21.7	1232
	5	Creep	30.83	Y	43.3	15.3	3	-13.5	753
May-22-N-1	1	Creep	37.55	Y	16.2	13.4	3	-7.7	588
May-22-N-2	1	Crushing	2.95	Y	3.6	1.5	1	-1.2	94
	2	Crushing	5.63	Y	17.7	8.9	3	-2.7	505
	4	Crushing	2.05	Y	2.8	1.0	3	1.6	68
	5	Crushing	5.05	Y	11.7	5.8	3	1.4	390
	6	Creep	9.55	Y	24.7	19.7	3	-6.6	544
Jun-02-E-1	1	Creep	9.07	Y	6.4	5.2	1	-2.2	406
	2	Crushing	20.57	Y	14.9	7.1	2	-4.0	415
	4	Crushing	10.73	Y	11.4	9.0	3	-6.5	406
	5	Crushing	3.25	Y	7.6	6.8	2	-6.6	400
	7	Crushing	12.18	Y	14.6	8.3	2	-3.4	406
	8	Crushing	6.47	Y	9.9	5.5	1	-6.2	350
Jun-02-E-2	1	Creep	23.4	Y	6.4	5.4	3	-5.2	351
	2	Crushing	3.55	Y	10.1	5.9	3	-2.1	350

* Loads shown are measured loads on six MEDOF panel columns, calculated using the uniform method for missing lower panels.

The analysis steps carried out are summarized below and explained in more detail in the relevant subsections which follow.

Analysis Steps:

- Development of Correlation Functions
  - Correlations between column loads were determined based on the sum of the middle and top panel loads (i.e. loads associated with the lower panel on the middle right column were not included into order to maintain consistency).
  - Bi-functional correlation functions were developed separately for creep and crushing type Sub-events. First the average (over all Sub-events) correlations at specified panel separations were determined, and then bi-functional correlation functions were chosen which fit the data.
- Estimation of north and east Face Nominal Loads based on MEDOF Panels
  - Estimates of face loads were made for each sub-event, based on both linear and probabilistic averaging. Two models for treating thick ice cases were considered, as there is some uncertainty regarding loads below the middle row of panels (as there is only one lower panel).
- Calibration of MEDOF Panels
  - Because there is considerable uncertainty regarding MEDOF panel loads, as an alternative approach, MEDOF panel adjustment factors were determined based on the assumption that extensometer readings in conjunction with a structure stiffness of 3 MN/mm based on FEA results give correct loads.

8.7 Development of Correlation Functions

8.7.1 Comments on Load Distributions

The method implemented for probabilistic averaging is based on the assumption that certain statistical properties for the process being modelled, such as values of the mean, standard deviation and correlations are constant for the event under consideration. This is a reasonable assumption for events of reasonable duration. One aspect is whether the load is uniform across the contact face in the case of creep loads, as past experience has shown that loads might tend to be larger towards the outer edges of the contact face. These variations would not affect correlations but could affect the interpretation of results and resulting face load calculations.

To determine if there are variations in the load across the face, the mean load for each group has been determined for each MEDOF panel group. The results are summarized in Table 9. In 4 of 6 creep events, representing 201 of 241 minutes, the load on the middle group was smaller than the load on the outside groups. The most significant difference was for the 130 minute March 25, 1986 event.

Table 9 Variation in Nominal Panel Load with Location on Face

Event	Subevent	Failure Mode	Average Load		
			N1/E1 (Nominal)	N2/E2 (Nominal)	N3/E3 (Nominal)
Mar-25-N-1	1	Creep	2.47	0.83	2.18
Apr-12-E-1	3	Crushing	0.00	6.16	2.32
Apr-12-E-2	1	Crushing	2.29	1.82	4.10
	2	Crushing	2.29	3.79	4.96
	3	Crushing	5.14	6.13	4.52
	4	Crushing	3.43	4.82	4.17
	5	Crushing	2.07	2.81	4.43
	6	Crushing	5.06	7.62	7.28
	8	Crushing	6.13	6.21	5.61
Apr-12-E-3	1	Crushing	3.84	2.33	1.31
May-12-N-1	2	Crushing	8.20	7.46	7.37
	4	Crushing	10.19	10.91	11.65
	5	Creep	4.91	4.97	5.41
May-22-N-1	1	Creep	4.22	3.17	5.98
May-22-N-2	1	Crushing	0.13	0.07	1.33
	2	Crushing	0.39	3.59	4.92
	4	Crushing	0.05	0.12	0.86
	5	Crushing	0.29	2.38	3.12
	6	Creep	4.19	8.25	7.26
Jun-02-E-1	1	Creep	0.03	0.24	4.89
	2	Crushing	0.26	3.40	3.42
	4	Crushing	3.24	2.72	3.06
	5	Crushing	3.62	1.98	1.17
	7	Crushing	0.91	4.30	3.12
	8	Crushing	0.37	0.97	4.16
Jun-02-E-2	1	Creep	2.25	1.44	1.70
	2	Crushing	0.47	3.01	2.40
Average		Creep	3.01	3.15	4.57
		Crushing	2.78	3.93	4.06

8.7.2 Correlation between Columns based on Middle and Top Panel Loads

For each of the selected Sub-events, the correlation coefficient was calculated for each pair of columns. Example plots of correlation coefficient versus separation are shown in Figure 16a for a crushing type interaction and Figure 16b for a creep type interaction (the blue points indicate data). As a rule, for crushing type interactions the correlations fall off quite rapidly with separation distance, while for creep type interactions the correlations remain relatively high even at a 40 m spacing. It is of note that the correlations coefficients can be negative as the events are of limited duration.

It was considered that the methodology should be improved to provide better fits to the data. Accordingly, a method that is based on bi-functional functions for correlations has been applied.

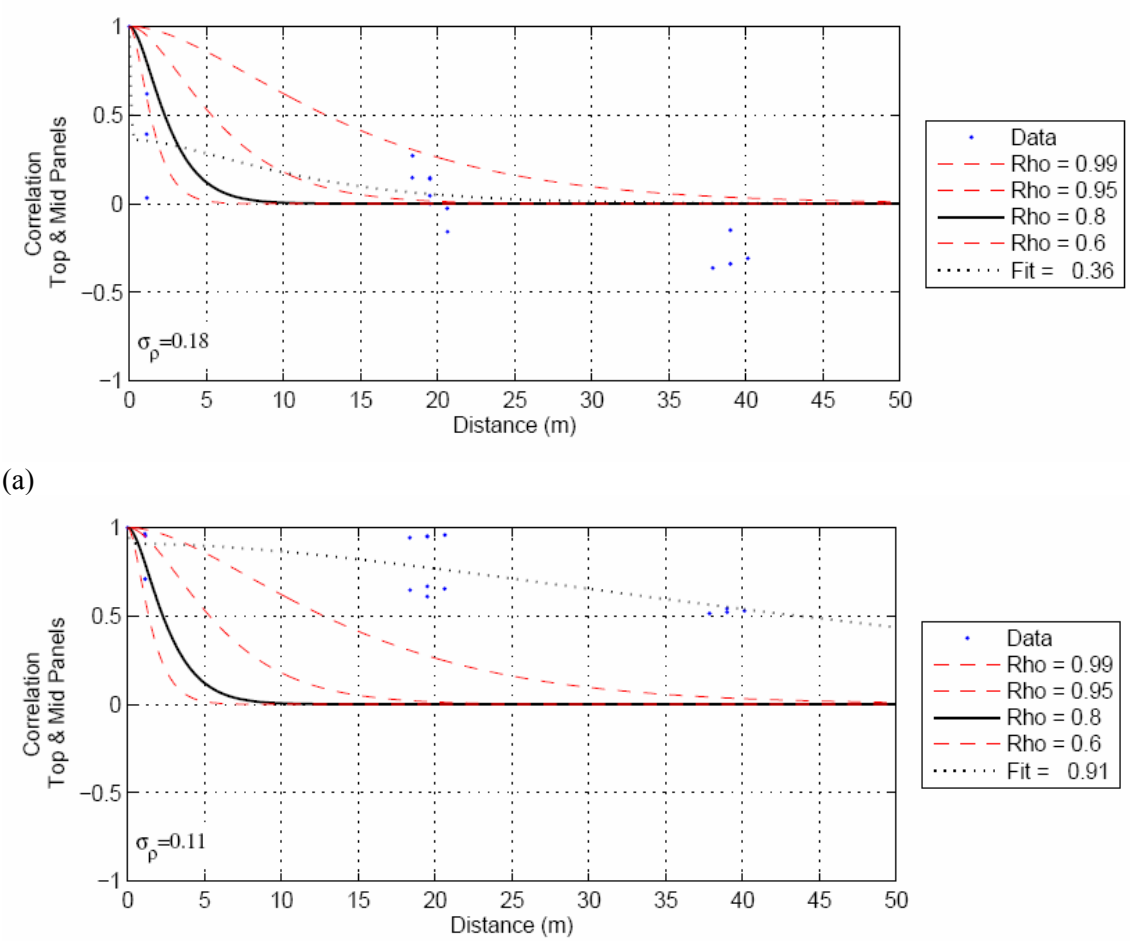

Figure 16 Examples of correlation coefficients as a function of separation for a) crushing and b) creep

8.7.3 Development of Bi-functional Correlation Functions for Creep and Crushing

The correlations at specified panel separations for duration-averaged crushing and creep events are shown in Figure 17 (a) and Figure 17 (b). The bi-functional correlation model described in Section 8.7.2 was then manually adjusted to give reasonable fits to the data (by adjusting the coefficients q_1, c_1 and c_2). The resulting fits are included in Figure 17 (a) and Figure 17 (b) and the associated coefficients are shown in Table 10.

It is seen that much improved fit has been obtained.

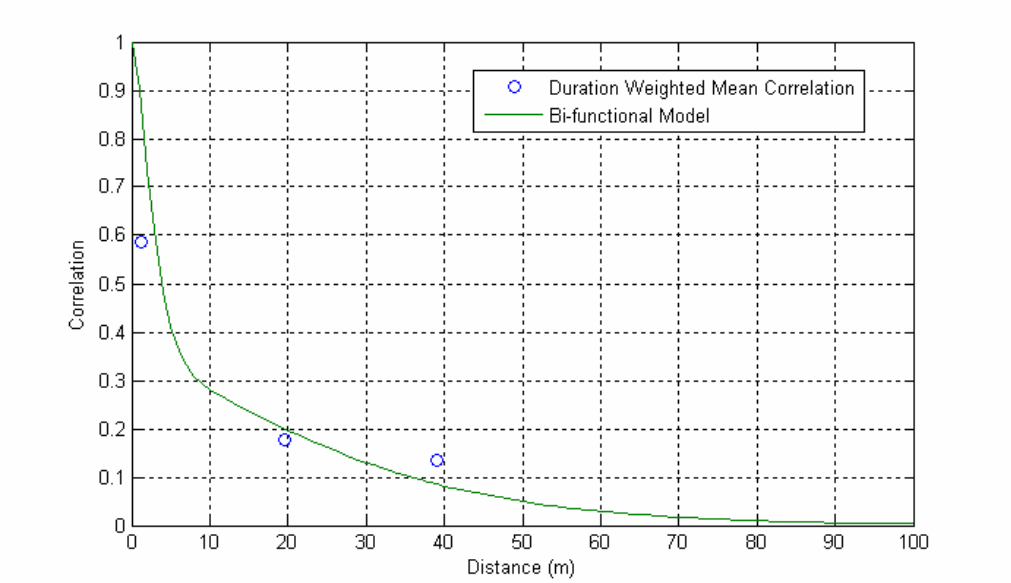

(a)

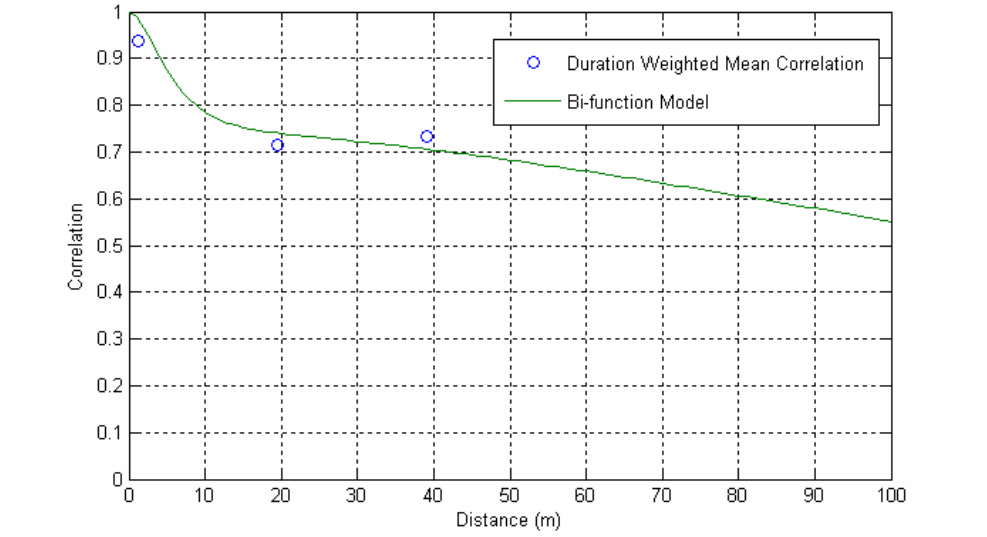

(b)

Figure 17 Bi-functional correlation models chosen for a) crushing type events and b) creep type events

Table 10 Coefficients for bi-functional correlation models

Failure Mode	q_1	c_1	c_2
		m	m
Crushing	0.68	1.5	15
Creep	0.25	3	100

8.8 Linear vs. Probabilistic Estimation of North and East Face Loads based on Nominal MEDOF Loads

8.8.1 Treatment of Bottom Panel Loads for Thick Ice

Except for the right column in the middle panel groups, the MEDOF panels reached depths of 2.915 m. The right column in the middle panel group on the north and east faces covered ice interactions to a depth of 5.63 m. In considering the relationship between actual loads and the loads measured on the MEDOF panels, consideration should be given to the possibility of ice thicker than the 2.915 and 5.63 m limits. Also there could be significant loading below these limits due to either rubble or intact ice pushed below the rubble.

Where loads were observed on the bottom panel of the middle right column on the east or north faces (Figure 18), the loads time traces columns without bottom panels were increased to include estimated bottom panel loads. The possibility of loads below the bottom panels was not considered and is unlikely given the quoted ice thickness values.

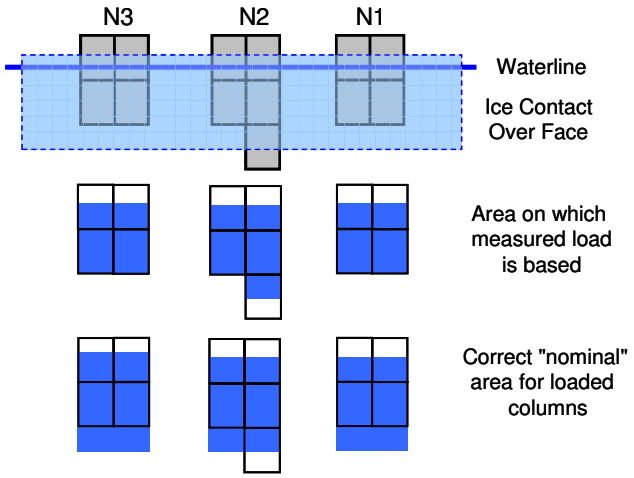

Figure 18 "Nominal" Contact Area for Columns given Uniform Thick Ice

Two assumptions have been implemented regarding loads on the bottom panels:

i) For each column, assume the bottom panel has the same load as the bottom panel for the right column in the centre group of the face, irrespective of the top and middle panel loads ("Uniform" Method for Bottom Panel Loads)

ii) For each column, assume the same ratio of total column load to the load on the top and middle panels as for the right column in the centre group of the face ("Ratio" Method for Bottom Panel Loads).

Neither of these methods is satisfactory, particularly for ice crushing. The ice failure process in a crushing failure consists of high pressure zones generally concentrated near the centre of the ice sheet, with occasional excursions towards the edges. Both methods fail to recognize this. Figure 19 illustrates the potential problems regarding bottom panel loads. The left and right columns of group N1 show significant middle panel loads at 40 minutes, whereas the middle group columns show moderate to small middle panel loads. At the same time, the lower panel of the middle right column shows a significant bottom panel load. Using the Ratio method can result in very large assumed loads on the N1 columns at 40 minutes.

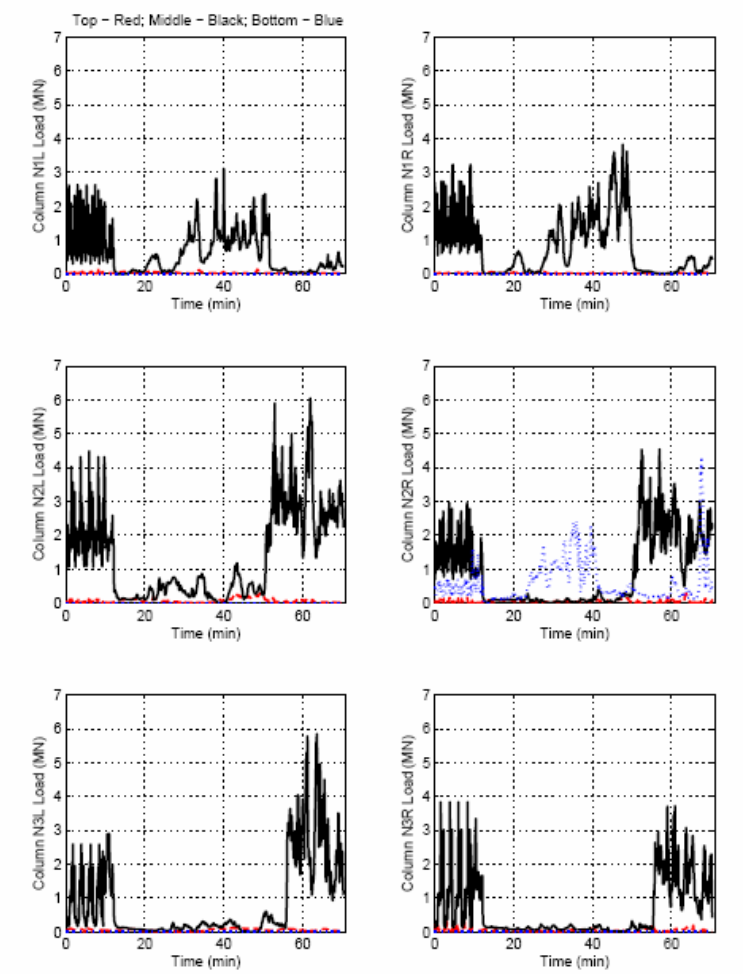

Figure 19 Illustration of effect of bottom areas with no panels

8.8.2 Linear vs. Probabilistic Averaging

Two methods were used for estimated time traces of face loads for the selected sub-events.

With "Linear Averaging", the load $L_C(t)$ over the contact width W_C is determined as

$$L_C = L_1 \cdot \frac{W_C}{W_1} \qquad \textbf{(8-19)}$$

where $L_1(t)$ is the average column load at each point of time t, W_C is the contact width (generally 58 m), and W_1 is the column width (1.135 m).

With "Probabilistic Averaging" the load $L_C(t)$ over the contact width W_C is determined as

$$L_C(t) = \frac{W_C}{W_1} \cdot \left[u + \Delta(t) \cdot \sqrt{\frac{\gamma(W_S)}{\left[\frac{1}{2}\left(1+\rho(1.135)\right)\right] \cdot \left[\frac{1}{3}\left(1+\frac{4}{3}\rho(18.5)+\frac{2}{3}\rho(37)\right)\right]}} \right] \qquad \textbf{(8-20)}$$

where u is the average (over time) of the mean column load and $\Delta(t)$ is the deviation $L(t)$ - u of the mean column load $L(t)$ from the mean u at each point of time,

8.8.3 Results for Linear and Pressure Averaging

The above methods were applied for the selected Sub-events. The maximum face loads for each event are summarized in Table 11. The largest load (375 MN) using the uniform bottom method occurs during the April 12th east face crushing event. Results are expressed in nominal MEDOF loads. Table 12 gives some earlier calibration results for the extensometers based on MEDOF panel nominal loads. This has been added to illustrate the extreme variety of results that are found if very short-duration events are used to calibrate.

Table 11 Linear and pressure averaging loads

Event	Failure Mode	Maximum Nominal Load		Maximum Nominal Load	
		LA	LA	PA	PA
		No Bottom	Uniform	No Bottom	Uniform
Mar-25-N-1	Creep	103	103	102	102
Apr-12-E-1	Crushing	169	169	139	139
Apr-12-E-2	Crushing	188	375	158	320
Apr-12-E-3	Crushing	84	92	73	82
May-12-N-1	Crushing	168	344	141	296
May-22-N-1	Creep	108	140	107	139
May-22-N-2	Crushing	123	214	103	180
Jun-02-E-1	Crushing	128	129	114	116
Jun-02-E-2	Creep	86	87	85	86

Table 12 Extensometer calibration results based on nominal MEDOF loads.

SUB EVENTS

Event	Subevent	Failure Mode	LA (Excluding Bottom Panel)	PA (Excluding Bottom Panel)
Mar-25-N-1	1	Creep	-5.52	-5.40
Apr-12-E-1	3	Crushing	-6.65	-5.37
Apr-12-E-2	1	Crushing	-7.82	-6.31
	2	Crushing	-4.25	-3.43
	3	Crushing	-8.26	-6.67
	4	Crushing	-4.42	-3.57
	5	Crushing	-3.23	-2.61
	6	Crushing	-3.64	-2.94
	8	Crushing	-4.68	-3.78
Apr-12-E-3	1	Crushing	4.19	3.39
May-12-N-1	2	Crushing	-6.55	-5.29
	4	Crushing	-0.96	-0.78
	5	Creep	-3.21	-3.14
May-22-N-1	1	Creep	-7.43	-7.26
May-22-N-2	1	Crushing	-13.89	-11.22
	2	Crushing	-8.16	-6.59
	4	Crushing	3.81	3.07
	5	Crushing	-2.62	-2.12
	6	Creep	-2.40	-2.34
Jun-02-E-1	1	Creep	-3.70	-3.62
	2	Crushing	-11.71	-9.46
	4	Crushing	-34.98	-28.26
	5	Crushing	10.84	8.76
	7	Crushing	-11.21	-9.06
	8	Crushing	-17.01	-13.74
Jun-02-E-2	1	Creep	-2.88	-2.82
	2	Crushing	-9.59	-9.38

FULL EVENTS

Event	Failure Mode	PA (Excluding Bottom Panel)	PA (Including Bottom Panel) Method 1	PA (Including Bottom Panel) Method 2
Mar-25-N-1	Creep	-5.40	-5.40	-5.40
Apr-12-E-1	Crushing	-6.41	-6.41	-6.41
Apr-12-E-2	Crushing	-3.27	-5.58	-6.76
Apr-12-E-3	Crushing	-6.22	-3.81	-8.88
May-12-N-1	Crushing	-2.60	-8.55	-10.41
May-22-N-1	Creep	-4.27	-5.48	-6.70
May-22-N-2	Crushing	-3.20	-8.40	-5.86
Jun-02-E-1	Crushing	-6.36	-5.83	-6.80
Jun-02-E-2	Creep	-5.28	-5.64	-6.35

8.9 Other Failure Modes and Factors

While the above method is reasonable for interactions which are predominantly crushing, other interaction and failure modes occur which involve correlations over different distance and time scales. At the same time, it should be noted that creep and crushing failures result in the greatest loads. A brief comparison is given below of the characteristics of the different modes:

Crushing:
Crushing events are characterized by random load traces on different panels that generally are uncorrelated as shown in Figure 20.

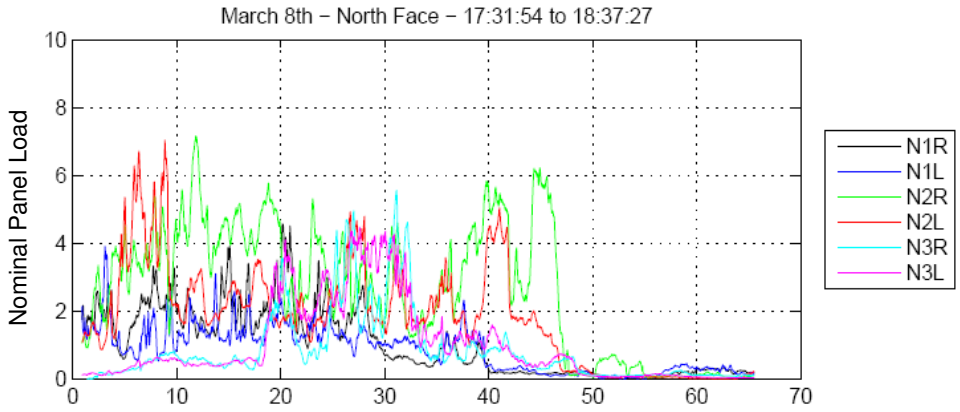

Figure 20 Example Crushing Event

Creep failure

Creep failure occurs at low velocities and shows highly correlated variations in pressure at different locations as can be seen in Figure 21. The characteristic distance in such cases can be as large as the structure width.

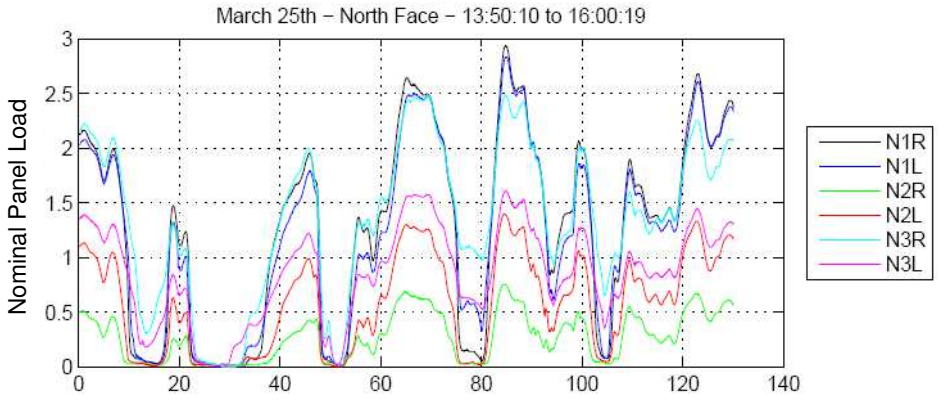

Figure 21 Example Creep Event

Flexural failure

Repeating flexural failures can result from buckling of the advancing ice or failure due to build-up and submersion of rubble and can occur across the width of the structure or locally (Figure 22).

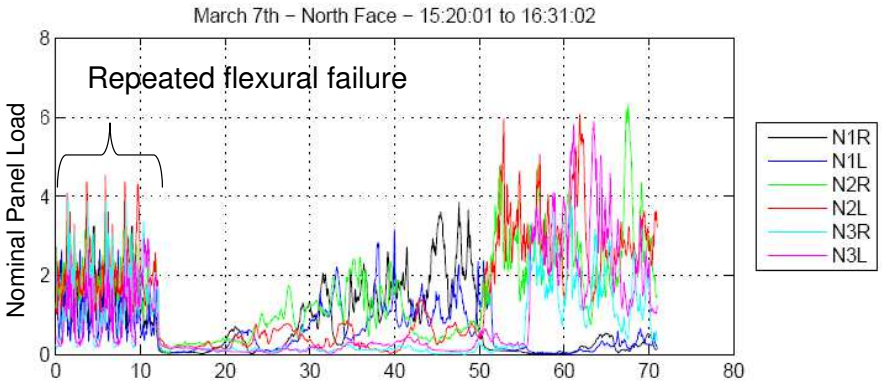

Figure 22 Example Flexure Event

Variation in thickness

Variations in the thickness of ice encountered can occur as a result of interaction with a multi-year ridge or embedded features (e.g. second-year or multi-year inclusions) as illustrated in Figure 23. These could appear as correlated variations in pressure across the structure face or part of the face if the thickness variation is not taken into account or if the strength of the new feature is different.

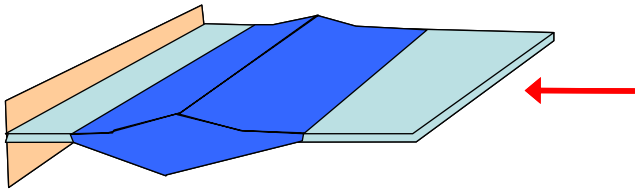

Figure 23 Variation in Contact Thickness

Variation in contact width

As a feature impacts the contact width will increase, enveloping additional panels (Figure 24). This can appear as negative or positive correlation in the load on different panels.

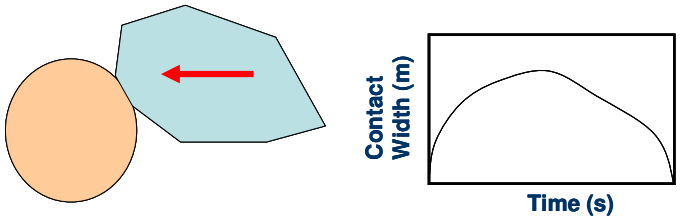

Figure 24 Variation in Contact Width

Splitting and spalling
Splitting and spalling events can cause a sudden change in actual contact area. Actual pressures could rise on the remaining ice, but nominal pressures might drop. These events may not be visually apparent to an observer, and could appear on panels, as positively or negatively correlated pressure changes on panels over durations considerably longer than those associated with the development of high pressure zones during crushing.

Additional factors
Examination of actual load time traces shows that the measured data can vary in a complicated manner when all of the above factors play a part. Different failure modes can occur at different locations at the same time, and areas of higher pressure can be seen to move across the contact face if the feature is moving at an angle to the face. At the same time, an ice-structure interaction event can be idealized as a random averaging process, and the assumption made that the process is stationary.

As noted, the data has many fluctuations, due to fractures, splits, and variations in ice thickness and other dimensions. If all of these aspects were measured, for instance if local variations in ice thickness were measured, one could develop a model to account for these effects. In the context of the present observations, the causes of the load fluctuations are considered as background random events within a stationary process, contributing to the variance. The process is therefore treated as stationary for a given time interval. This is considered to be a reasonable engineering approach. At the same time, caution should be exercised in using events that are of very short duration to estimate the statistical parameters of the process.

9. ICE INFORMATION AND CONDITIONS

Ice conditions are a very important factor in interpreting the face load results associated with each event. The main factors are ice thickness, movement rate and failure mode. There were four sources for this type of ice information. The first, and most general, was the hourly observations. Ice observers systematically characterized the ice conditions in the vicinity of the Molikpaq, but not necessarily the ice actually contacting any face. This was done visually, with the aid of radar and occasionally helicopter reconnaissance. The observations included partial concentration of each ice type using WMO ice categories, maximum ice thickness, ridging, drift rate and drift direction. The drift rate and drift direction were far field, generally taken from radar tracking of targets, and did not necessarily describe the rates and directions of interactions at the caisson faces. These data were reviewed and all periods when multi-year or second-year ice was present were noted. The second source of ice information was "caisson/ice interaction" reports or "rubble maps" which were prepared either on a daily basis, or at various stages during an event. Examples are presented in Figure 25 and Figure 26. They provided detailed information such as drift speed and direction, ice thickness and type, a sketch and such detailed notes an observer might record. They are quite useful and selected ones will be reproduced in this report. A third source of ice information was the summary of the 72 time lapse video records. There were two video cameras on the flare boom, showing ice interaction with the east and north faces, and one on the derrick top, showing interactions on any face. The video summary identified ice type, ice thickness, failure mode and other notes. Time periods when multi-year or second-year ice was present were noted for close examination and comparison with other information. The fourth source of ice information came from the detailed review of the video records with Brian Wright in January, 2008. These video tapes were selected from the 72 noted above. They were reviewed together with time series records of MEDOF panel forces, and annotated notes of failure behaviour were made. This detailed review helped divide Events into Sub-events, based on failure mode, and also identified the portion of a face being loaded. The results of this video analysis are presented in Section 10 and Appendix G.

CAISSON/ICE INTERACTION OBSERVATION #310

Date: APR 12/86.

Estimated start time of impact: 0800
Estimated finish time of impact: 0845

Local Ice at Caisson:

*Drift Speed: 0.12 knots (DRIFT INCREASE FROM 0 TO 0.12 knots in this time frame)
Drift Direction: 280 °T
Ice Type: MY.
mean/max
Ice Thickness 1.5m to 10m (HUMMOCK.)
Ridge Conc: singular/light (1-2/10)
moderate/heavy
(3-5/10) (≥ 6/10)
- Mean height: 6.5 m
- Extreme height: 10m m (estimates)

If ridge contacted caisson:
- Perpendicular to ~ face(s)
- Parallel to EAST face(s)
- If neither of the above, please indicate in the rubble map

Floe size: * SEE MULTI YEAR ICE DOCUMENTATION BY K. WOOLNER & B. O'DELL.

Rubble Map/Contact Area:
Time of Map: 0800

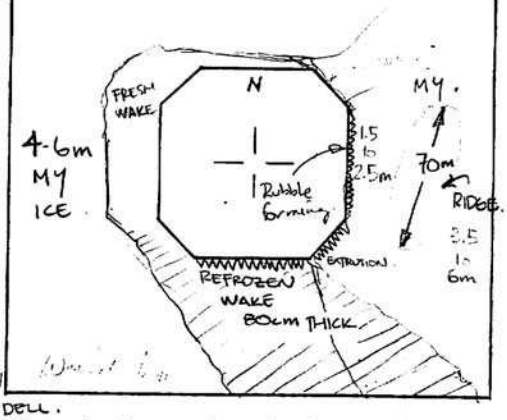

Contacted caisson face(s):

	% contact,		% contact,		% contact,		% contact
N	0	E	100% CRUSH.	S	100% CRUSH	W	0
NE	SLIDING, V. LITTLE PRESSURE	SE	100% CRUSH	SW	0	NW	0

DETAIL OBSERVATION & REMARKS (before, during and after the impact)

NOTE: Sketches with failure mode would be most helpful.

TIME — DESCRIPTION

0730 - 30 cm ICE MOVEMENT PAST HOUR.
0800 - ICE MOVING TO WNW
0805 - RED ALERT
0815 : MY ICE CRUSHING OVER WHOLE EAST FACE
RUBBLE FORMING ON EAST FACE (5m HIGH, EXTENDS 10m) (100%)
• EXTRUSION ON S.E. (100%)
• CRUSHING ON NE (100%)
TOTAL MOVEMENT 100m TO WNW.
0826 - PULSATING LOAD ~ 0.5 Hz.
— RIDGE/HUMMOCK PENETRATING RUBBLE - EAST FACE.
0828: RUBBLE UP TO TOP OF ICE DEFLECTOR — PULSATING @ 0.75 Hz.
0830 : PULSATING STOPPED
0834 : Large BUCKLING ON EAST FACE - AROUND HUMMOCK

Failure mode check list:
- *crushing
- flexure — see notes
- rubble/ridging
- rubble pile up
- sliding along side NE
- rafted/ridged areas that stopped
- ridges behind stopped feature
- wake conditions (pressure/no pressure)

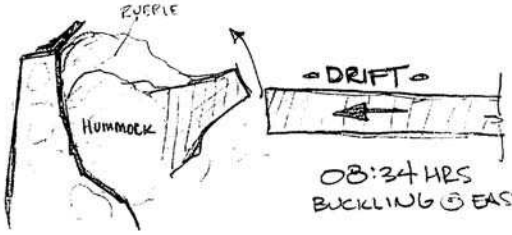

08:34 HRS
BUCKLING @ EAST FACE W/ CRUSHING & EXTRUSION ON NORTH EAST & SOUTH EAST FACES.

Figure 25 "Caisson/ice interaction" report for April 12 morning, 1986

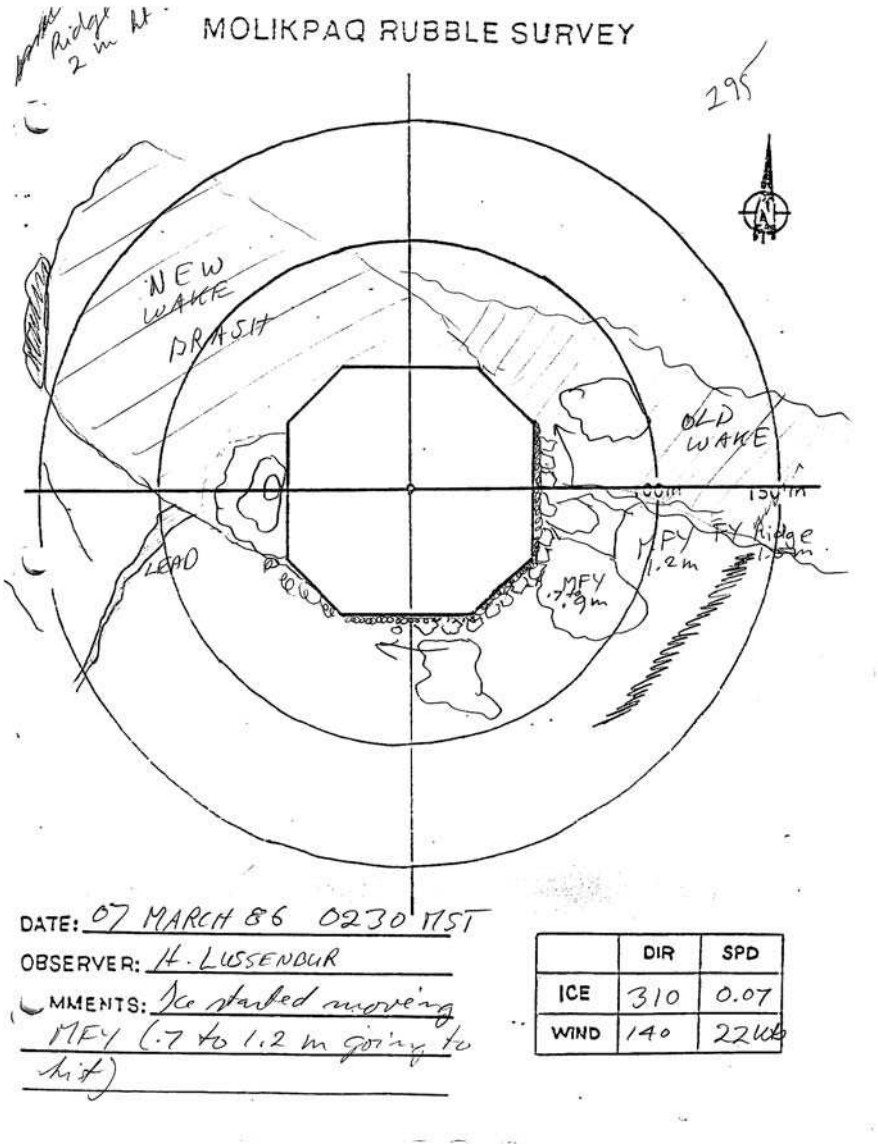

Figure 26 "Rubble map" from March 7, 1986

9.1 Multi-year ice thickness from March 1986 survey

The thickness of the multi-year ice interacting with the Molikpaq is a key factor in assessing the results, and making them useful for application to other locations and conditions. After the March 8 event, the Molikpaq was surrounded by a large field of multi-year and second-year ice floes imbedded in a first-year matrix. This ice field had interacted with the Molikpaq on March 7 and 8, and was now stationary. On March 9 twenty-six holes were drilled in a 100-m square immediately north of the Molikpaq. The average thickness was 2.6 m with a standard deviation of 0.6 m, however it was noted that in three cases the ice was thicker than 3.2 m (the maximum drill length at the time of measurement). On March 13 and 14 a more extensive survey of ice thickness around the Molikpaq was undertaken. Holes were drilled to measure ice thickness along a number of lines radiating out about 1000 m from the Molikpaq, providing additional quantitative measurements of ice thickness. The locations and thicknesses measured are noted in Figure 27. Review of reports identified some additional descriptive material, see Appendix H. The

drill hole numbers in Appendix H refer to the location numbers in Figure 27. With the exception of a few clearly first-year ice areas, the ice thickness measurements were of second-year or multi-year ice. A probability distribution of the 62 thicknesses is presented in Figure 28. The median ice thickness was 3.25 m, the average 3.8 m, the minimum 2 m and the maximum 10.5 m. There were 7 thicknesses measured at between 5 and 7 m. Ice thickness data from the same area as that measured March 9 indicated thicknesses greater than 3.2 m (presumably by this time a longer drill was available) and resulted in an average of 3.5 m and a standard deviation of 1.3 m, significantly greater than the March 9 results. The thickness measurements, even though taken after the March 7 and 8 events, provide a guide for quantitative estimates of thickness for the March 7, 8 and 25 events as well as April 12. We will try to relate specific ice thicknesses to particular events; however in a general sense these data provide an indication of multi-year ice thicknesses and their variability. Individual ice thickness measurements were accurate to about ± 0.1 m. There is considerable uncertainty, however in the average ice thickness attributed to individual events, ± 0.5 m for ice around 2 m thick, and ± 1 m for ice 3 m and thicker.

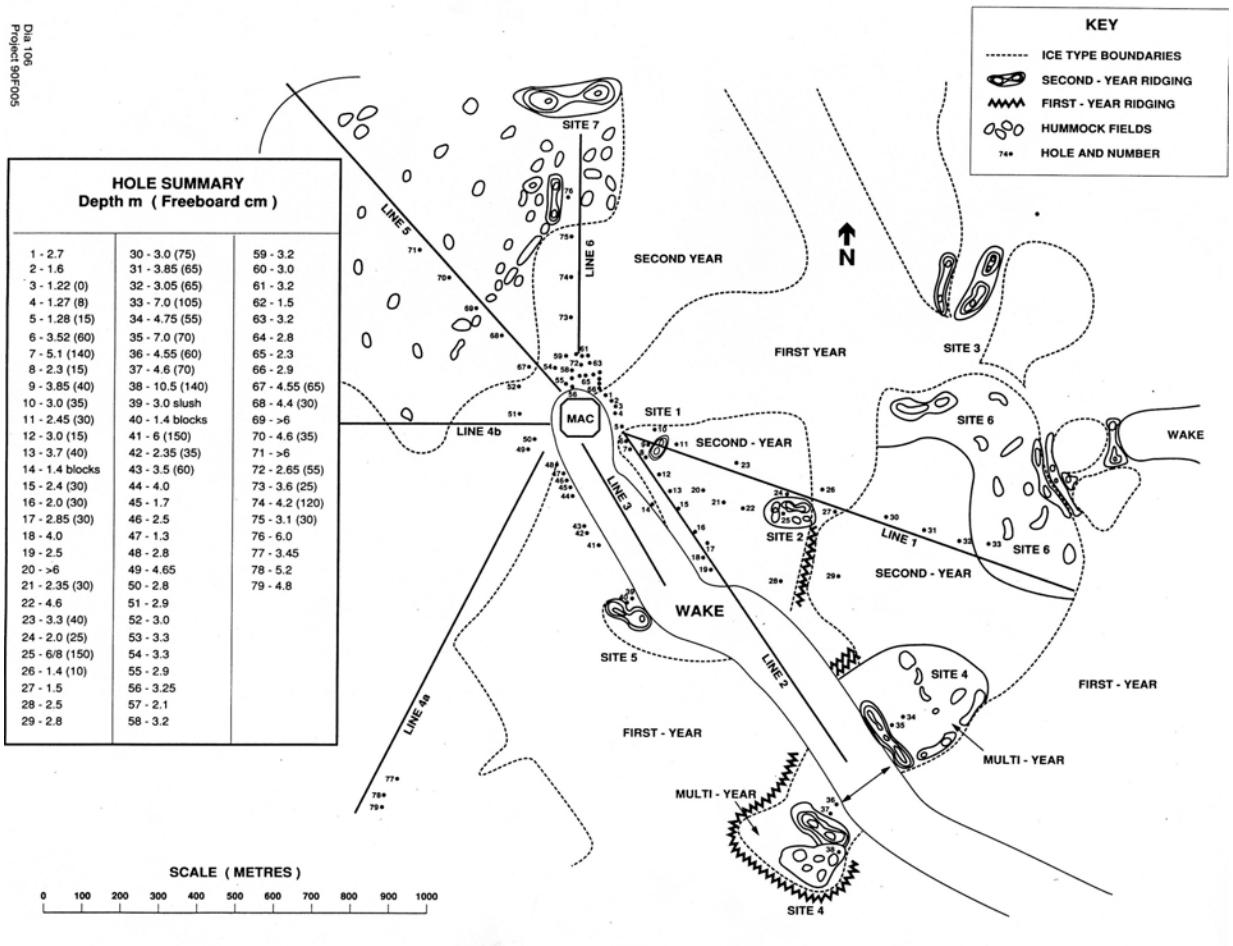

Figure 27 Survey of ice thicknesses surrounding the Molikpaq, March 1986

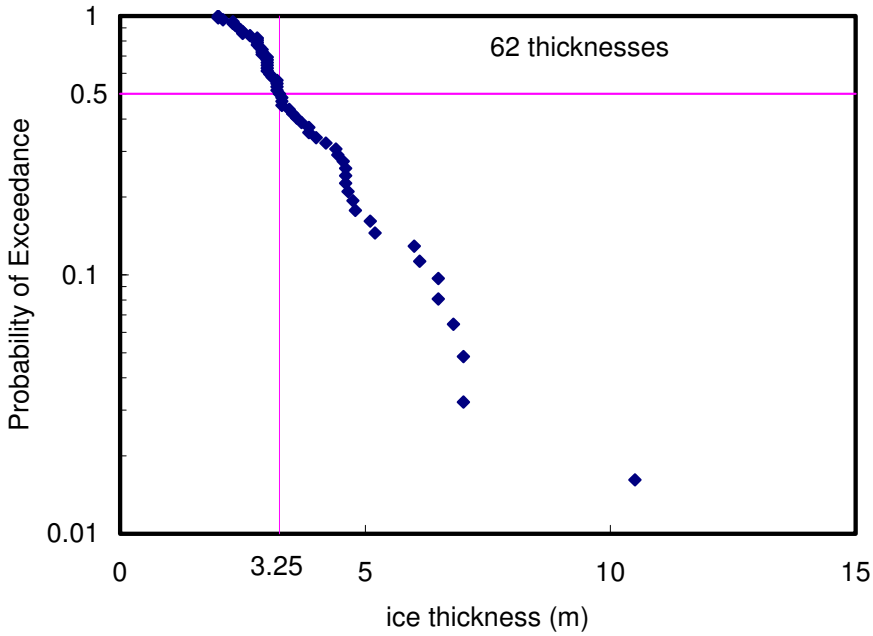

Figure 28 Probability distribution of second-year and multi-year ice around the Molikpaq in March – April 1986.

9.2 Multi-year ice thickness from Nares Strait

The ice thicknesses measured around the Molikpaq were 20 to 100 m apart, so while they are useful for establishing average values, they do not provide much information about spatial variability over distances comparable to the width of the Molikpaq, 100 m. Recently multi-year ice thickness surveys have been carried out in Nares Strait (Johnston, 2008). Thicknesses were measured on 10 m spacing, and provide a good indication of thickness variability. Figure 29 plots the elevation and draught of the top and bottom surface of a multi-year floe. Measurements are referenced to the water line. Lines 2 and 3 were at right angles to line 1 and at positions 20 m and 70 m with respect to the x-axis of line 1. The first point to observe is that the top surface of the ice does not give any indication of the thickness. The average of the 30 thicknesses was 4.8 m and the standard deviation 1.6 m, for a coefficient of variation of 0.33. Note that her COV of 0.33 is less than the COV of 0.37 obtained from the ice thickness measurements at the Amauligak I-65 site. For some events that will be presented in Section 11, only a few ice thickness measurements were available, so Johnston's results give an indication of the likely variability over distances equivalent to the width of the Molikpaq.

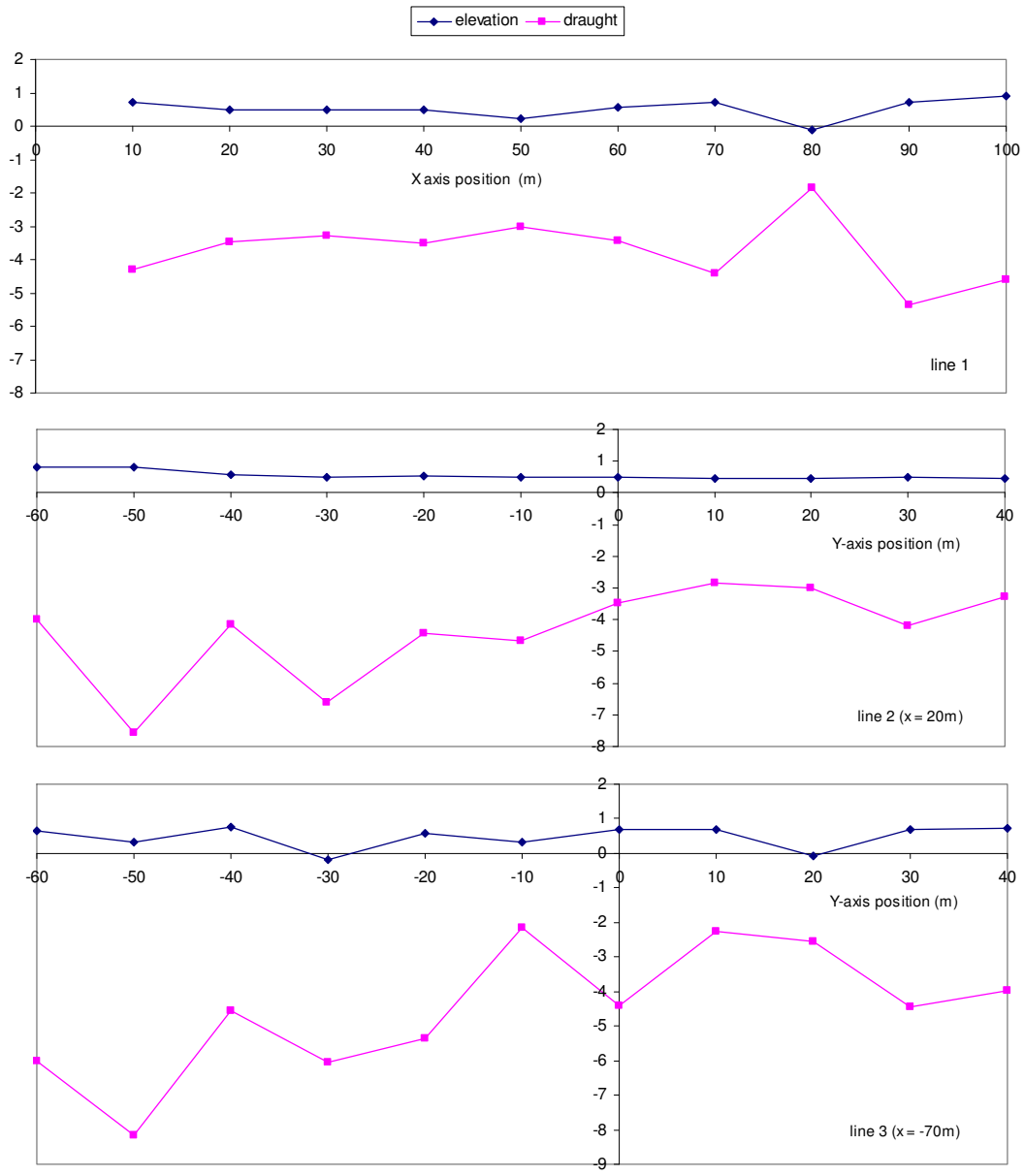

Figure 29 Plot of ice thickness variation

9.3 Amount of multi-year ice interaction with Molikpaq

Combining information from caisson/ice interaction reports, rubble maps, video records and hourly ice observations, it has been possible to estimate the amount of multi-year ice interacting with the structure for each event. These estimates are summarized in Table 13. For the time periods in Table 13, care has been taken to eliminate times when first-year ice was interacting with the structure. This explains why the for the interval times the ice velocity does not always equal the drift amount. About 2200 m of multi-year ice interacted with the Molikpaq from March through June 1986. Note that second-year ice interactions during November and December 1985 have not been included. Reference can also be made

to Frederking and Sudom (2009) for a more comprehensive presentation of multi-year ice flux past the Molikpaq in 1985-86.

Table 13 Amount of multi-year ice drift directly impinging on the Molikpaq

Event ID	Date	Time period	Ice velocity (m/s)	Drift Amount (m)
0307A	1986 Mar 07	15:20:41 – 16:31:01	0.05	150
0307B	1986 Mar 07	16:38:54 – 17:43:47	0.05	150
0308A	1986 Mar 08	16:03:13 – 17:14:12	0.1 to creep	500
0308B	1986 Mar 08	17:31:54 - 18:36:33	0.02 – 0.05	150
0308C	1986 Mar 08	21:11:21 - 22:22:20	creep ??	~
0308D	1986 Mar 08	22:26:08 - 23:02:07	creep ??	~
0325A	1986 Mar 25	08:30:39 – 09:44:13	creep	~
0325B	1986 Mar 25	13:50:10 – 16:00:08	creep	~
0412A	1986 Apr 12	08:23:30 – 08:45:00	0.06	150
0412B	1986 Apr 12	11:16:02 – 12:29:31	0.1	360
0412C	1986 Apr 12	13:00:07 – 14:01:04	0.06	200
0412D	1986 Apr 12	14:03:20 – 14:19:35	?	50
0412E	1986 Apr 12	14:19:35 – 14:35:31	?	50
0512A	1986 May 12	03:10:16 – 03:58:24	0.1 to creep	150
0522A	1986 May 22	08:39:23 – 09:50:27	creep	~
0522B	1986 May 22	13:58:07 – 15:11:32	creep to 0.05	200
0602A	1986 Jun 02	13:02:26 – 14:16:45	creep to 0.01	50
0602B	1986 Jun 02	20:16:55 – 21:24:33	creep to 0.01	50
0625A	1986 Jun 25	05:31:17 – 06:44:56	0.2 to creep	?
Total multi-year ice impinging from March to June 1986				~2200

10. VIDEO ANALYSIS BY BRIAN WRIGHT

The analysis of video records was performed by Brian Wright. Some results of his work are presented in this Section, with the full report provided in Appendix G. The Appendix gives annotated time series plots for all events.

10.1 Time Lapse Video Cameras

Three time lapse video camera systems were installed on the Molikpaq to document the ice conditions that it encountered and the types of ice failure modes that occurred. One of these cameras was placed on top of the drilling derrick and had pan and tilt features. This camera was sometimes used to "look out" at the oncoming ice cover. The other two cameras were usually mounted at the outer end of one of the rig's flare booms, which was located about 20m above the waterline off the NE corner of the caisson. These two video cameras were oriented in fixed directions, with one looking along the east long face of the caisson and the other looking along its north long face.

Figure 30 is a schematic illustration of the three camera locations and the approximate fields of view of the two cameras that were mounted on the flare boom. When the NE flare boom was in use, the two fixed cameras were relocated as shown. Figures 31 to 33 provide representative examples of individual frames taken from the time lapse video records.

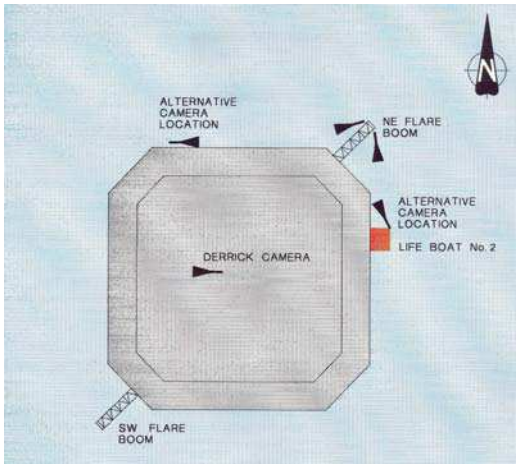

Figure 30 Schematic illustration of the primary and secondary locations of the three time lapse video cameras that were placed on the Molikpaq.

Figure 31 **A view of a first-year ridge interaction on the west side of the caisson, taken from the derrick top camera on March 3, 1986. The ice deflector is in the foreground.**

Figure 32 **A joint view of the east (left) and north (right) faces of the caisson taken from the two cameras mounted on the NE flare boom. The ice was crushing against the caisson's north face, with remnant debris sliding along its east face at the time.**

Figure 33 A similar view of the north and east faces of the caisson during darkness hours. In this case, the ice was failing against the east face in mixed modes, with broken ice debris sliding westwards along the caisson's north face.

Several points that should be noted about the video camera system onboard the Molikpaq are highlighted as follows.

- All of the cameras had a low light level capability, so that time lapse video records could be obtained throughout both the day-time and night-time hours
- The time lapse recorders were set to capture picture frames roughly once a second, which is a more than ample frequency to resolve all of the necessary ice interaction details
- The video cameras were hard wired to dedicated recorders and monitors that were located onboard the Molikpaq, in the DAS, and were periodically observed from there
- Since it was not practical to attend the time lapse camera on the derrick top (in terms of continuously changing its field of view to see the oncoming ice cover), a second monitor with pan and tilt controls was set up in the radio room. It was then primarily used as a tool for observing certain operations (helicopter landings, cranes activities, cargo transfer from vessels, etc.), and not to document ice-structure interactions.
- Hence, the two video cameras on the NE flare boom provided the best video records, but only along the N and E caisson faces, with no coverage obtained along the S or W faces during ice interactions associated with ice movements from the south or west
- The east face viewing camera looked straight along the east face, generally providing a profile view of the ice failure at the north end of the east face, while the north face viewing camera had a more oblique view, making it easier to determine ice loading lengths and separate out loading events on the N1, N2 and N3 MEDOF panel groups.
- Repositioning of the two video cameras on NE flare boom was also required several times throughout the winter of 1985/86 (because the flare boom was used and would have "torched them"), so the fields of view of the N and E faces are not exactly the same over the entire ice covered period
- Although the video records are very good, they do not always "see" the complete E and N faces, nor can the precise locations of the N1, N2, N3 and E1, E2, E3 MEDOF panel groups be identified (with exactness) on them
- As a result, practical and experienced judgements must be made when interpreting the ice interaction behaviours seen on the video records, in relation to the load time series derived from the instrument data

- Despite this caveat, the video coverage obtained along the N and E faces is generally of very high quality and in fact, is quite unique.

10.2 Analysis of Video Records

10.2.1 General

The information that is presented in the remainder of this section shows direct relationships between "cause and effect", on the basis of the Molikpaq videos and the recorded ice load instrument data. Firstly, the steps that were taken to analyse the time lapse videos in relation to different ice interaction events are outlined. The results of the analysis, which specify time periods of varying ice failure behaviours over certain widths of the caisson, are then given for a number of key events. This information should be recognized as fundamentally important, since it is used in subsequent sections of the report to assess global ice load levels on the caisson as a function of failure mode, and correlations in load levels across different widths of the caisson, for like ice failure behaviours, for probabilistic averaging applications.

10.2.2 Time Markers

The first step in the analysis procedure was to review the video records in relation to the instrument data time series that had been acquired. A good portion of this work was carried out jointly, at a project meeting January, 2008 in St. John's, with personnel from NRC-CHC, C-CORE and B. Wright & Associates being involved. At the outset, so-called time markers were found in the videos for all of the events under consideration, to ensure that the measured ice load time series and associated video records had common time stamps. Two representative examples of the type of time markers that were identified are highlighted as follows, for ice events on the north face of the caisson, on March 7 and May 22, 1986, respectively.

10.2.2.1 March 7, 1986

Figure 34 shows a "slice" of the ice load time series that was recorded by the instrumentation system on the Molikpaq for the March 7 event, starting at about 16:38. Here, the individual ice load traces are given for MEDOF panel groups N1, N2 and N3. Two video frames of the north face are also included, at specific times, to illustrate the type of ice action the caisson was experiencing. Comparisons between the ice load time series and video data indicated a very good time correspondence between both records as signified by the ice slump, to within a few seconds.

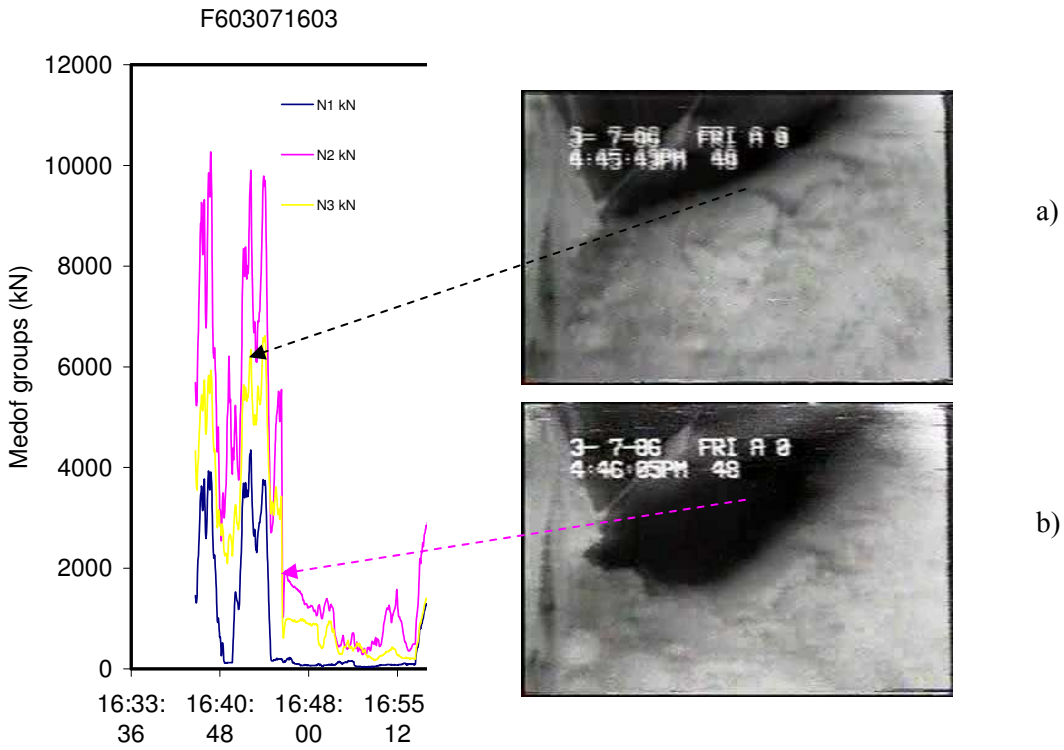

a) ice crushing on the north caisson face at the N3 (closest) and N2 (middle) panel groups
b) a slump of the crushed ice debris at N3 and N2, with an immediately reduction in loads

Figure 34 An example of the correspondence in time markers seen on the video records and on north face ice load group plots, in this case, on March 7, 1986.

10.2.2.2 May 22, 1986

Figure 35 shows a "slice" of the ice load time series that was recorded by the instrumentation system for the May 22 PM event. Here, individual ice load traces are given for MEDOF panel groups N1, N2 and N3. Several time lapse video frames are also included for specific times, to illustrate the type of ice action that the caisson was experiencing along its north face. This comparison also indicated a very good time correspondence between the details of the ice failures observed on the video records and the ice loads seen on the panel group plots, again to within a few seconds.

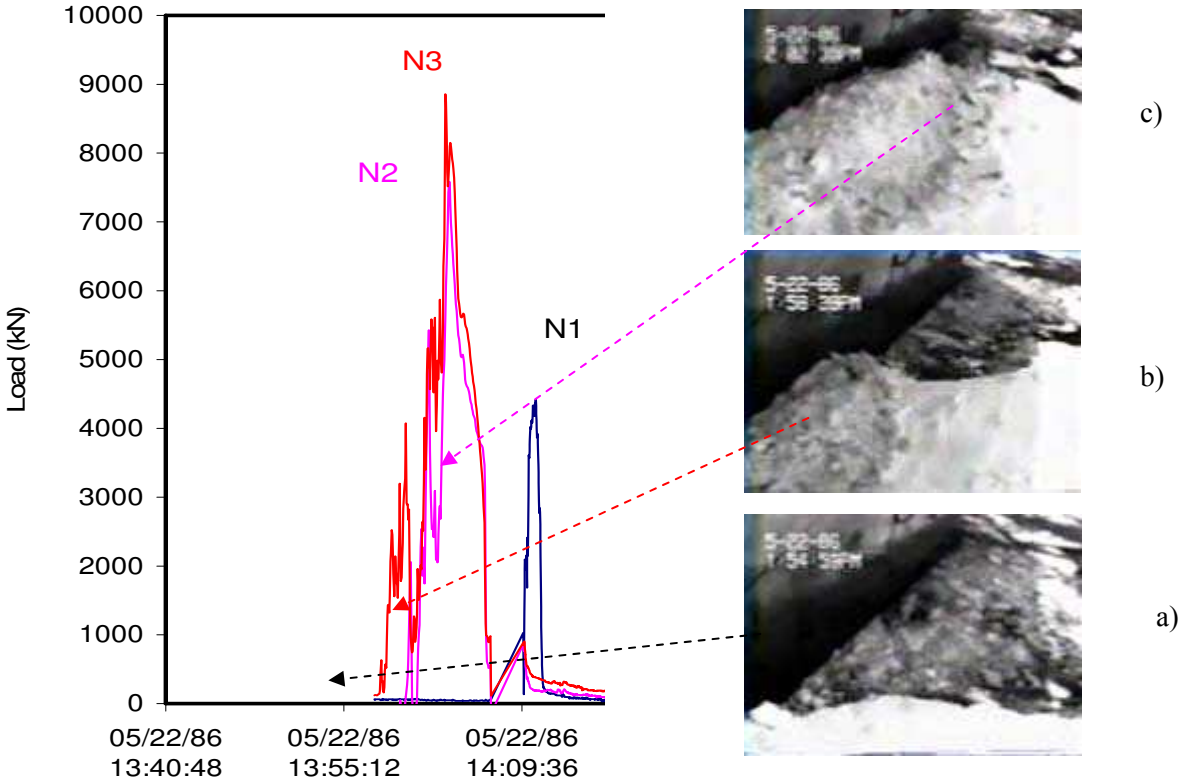

a) no ice action on the N face just prior to the event
b) crushing begins at the E end of the N face and spreads west to cover N3
c) crushing continues to spread west and reaches the N2 panel group (but not N1)

Figure 35 An example of the correspondence in time markers seen on the video records and on the ice load group plots, in this case, on May 22, 1986.

This type of time marker check between the ice load time series and time lapse video records was carried out for all of the events that were under consideration in this study. In most cases, the level of timing correspondence was very good, to within a few seconds. However, there were cases where there was a more substantial time difference between the two data sources. For example, on April 12, 1986, the ice load time series data lagged the time stamps on the video records by about four minutes.

10.2.3 Ice Failure Modes

The video records clearly showed that a wide range of ice failure behaviours across the loaded face (or faces) of the Molikpaq occurred over the course of each different ice event (FAST file). These failure modes were highly variable in both space and time. When reviewing the video data, it quickly became apparent that the ice interaction processes observed did not represent “stationary and random crushing”

over the duration of any particular FAST file record, as had been assumed in the probabilistic averaging methods used to date (Jordaan et al., 2006). [1]

For the purposes of this work, a decision was made to subdivide the ice interaction behaviours that were observed on the video records into a number of basic categories. These categories are highlighted as follows, and a few illustrations given to describe each one.

Continuous Ice Crushing

- evidenced by the ongoing creation of small ice pieces along the ice interaction front
- "paste-like extrusions" are commonly seen in thicker ice (e.g.: multi-year floes), but are not observed during most of the thinner first-year ice interactions
- ice clearance along the unloaded face(s) may appear to indicate crushing, but actually involves broken ice debris flowing around the caisson

ice crushing on the caisson's E face in thick second-year ice

note that the NE corner is not loaded but crushed ice debris is flowing around it

view of crushed ice debris taken from the caisson's ice deflector

large crushed ice extrusion clearing around the NE face of the caisson

view of a "crushed ice extrusion remnant in the caisson's wake

Cyclical Ice Crushing

- this ice interaction behaviour involves ice crushing, then a build-up of rubble debris, followed by a flexural failure in the oncoming level ice cover due to the weight of the rubble debris
- the cycle tends to repeat itself a number of times, until the ice cover fractures or more general rubble building or mixed modal ice failures take over

[1] The assumption of stationarity can be considered to apply to events with periods of mixed-mode failure – see Section 1.5 of IJA report. (Appendix B)

- this type of cyclical ice crushing is quite evident in thinner first-year ice, but is more difficult to discern in thicker first-year and old ice conditions
- it is important to note that this definition of cyclical crushing should not be confused with that of simultaneous ice crushing discussed by others (Jefferies & Wright, 1987) [RF comment; the period of cyclic crushing is a few minutes, much longer than the half to 3 second period seen in simultaneous ice crushing (phase lock)]

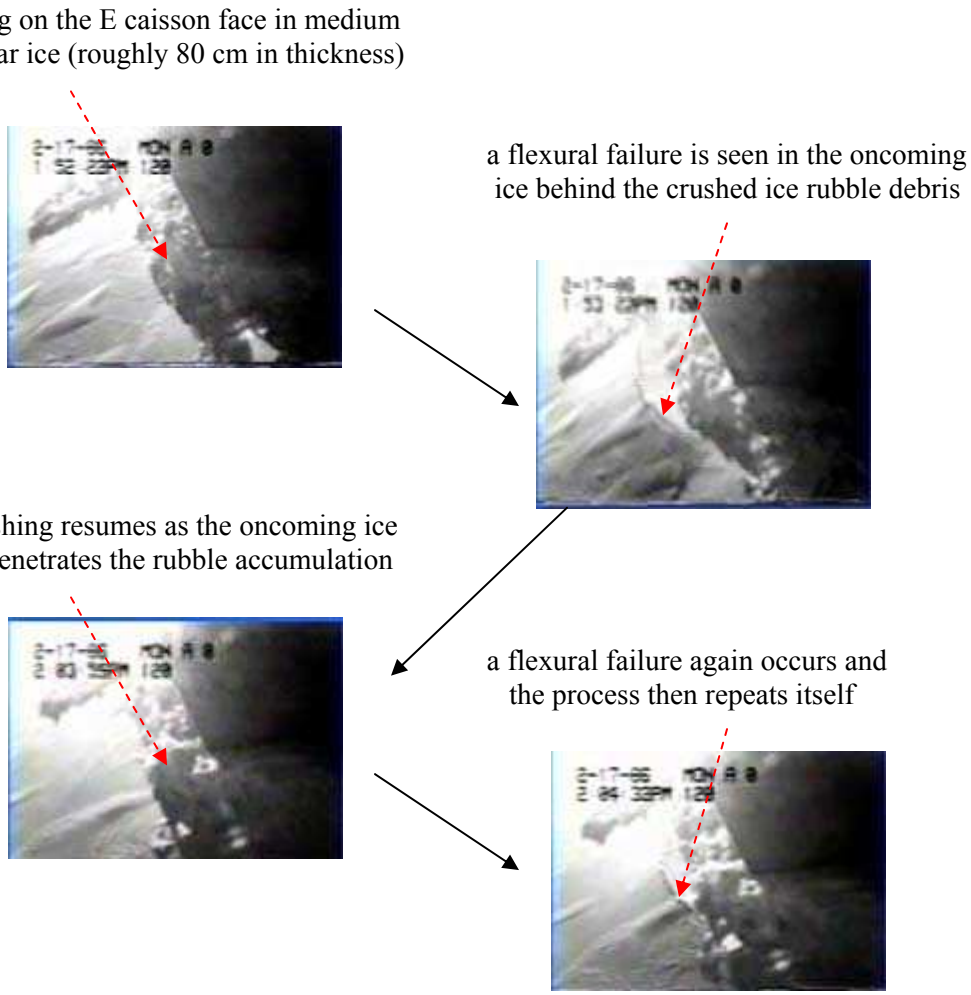

Mixed Modal Ice Failures

- mixed modal ice interaction behaviours involve a combination of failure modes across a caisson face, including out-of-plane bending failures, rubble building, fracture and at times, ice crushing across varying widths
- mixed modal ice failures are the type of ice interaction behaviour most commonly seen in first-year ice, and also during significant proportions of the time that thicker old ice floes failed against the Molikpaq
- ice load data that involves both mixed modal and the preceding ice crushing failure modes has been incorporated into some of the recent probabilistic ice load averaging work (Jordaan et al, 2006), perhaps tending to mix "apples with oranges" and producing some less than conservative global ice load prediction results

bending and splitting failures along the east face of the caisson

spatially varying bending and crushing failures against the north caisson face

Ice Sliding and Clearance

- a large number of the time lapse video records show ice sliding along the (largely) unloaded faces of the caisson (see Figure 32 and Figure 33)
- this is a natural part of the ice clearance process and should not be misinterpreted as ice failure against an unloaded caisson face
- when the ice attack angle on a given face is more than 50 degrees, it has been empirically estimated that the ice will begin to easily slide at low ice load levels

Slow Ice Loading

- various interaction events have been recorded where there is a very limited amount of ice movement (cm to tens of cm) over time frames of a few hours to a day or more, and also where the ice cover appears to stop moving (substantially) over periods of a few minutes
- these events have been classified as “slow ice pushes”, which likely involve loading across the ductile range
- no illustrations are provided here, since nothing appears to change in the time lapse video records of these types of ice interactions

10.3 Key Results

As noted earlier, additional ice load time series records and illustrative video frames are presented in Appendix G of this report. The key results of this time lapse video annotation work are summarized in Table 1 of Appendix G, which includes all ice interaction events that are under consideration in this work for which time lapse video coverage is available. The ice interaction failure modes have also been incorporated into a table with face loads in Appendix K.

11. DESCRIPTION OF ICE LOADING EVENTS

All time periods considered for ice loading analysis are listed in Appendix A. Details of the ice-structure interaction for each time period are provided in this Section.

Most of the ice information originates from caisson/ice interaction observations, or "rubble maps" made at the time of the events. Hourly records of ice type, thickness, concentration, and drift speed were also used. (These must be treated with caution since they detail all ice surrounding the Molikpaq, not necessarily just the ice interacting with the structure.) In addition, a summary of loading events by Klohn-Crippen (1995) was utilized. Analysis of the time lapse videos of the east and north faces for certain events was completed by Brian Wright. Video records are very useful in determining ice failure modes, but they cannot be used to establish ice thickness. For the events in November and December 1985 the videos were not analysed in detail. The video records were examined for many of the events in this section, and notes from the video analysis are included in the event summary tables. For further information refer back to Section 10 and Appendix G.

The data sources (video records, written observations and data acquisition system) all had slightly different time bases which were not synchronized. The exception is the day of April 12, 1986, for which a standardised time base was established (Rogers and Jefferies, 1986). The times given in this report correspond to the data acquisition system. Times are recorded as accurately as possible but could be off by several minutes.

A summary table of events for the "Historical Case" is given for each date which was analysed (see Table 1 in Appendix K). Note that Appendix K also contains time series plots of all events in a larger format than that of this section, as well as an expanded event table in Excel format for both the "Historical Case" and "Best Estimate" case. The Event ID numbers in the table of Appendix K are based upon sections of the available data files pertaining to particular ice failure modes (as in Section 10). The ID numbers for these selected events are also listed in the table in Appendix A which shows all time periods of potential interest.

Face loads calculated in this section are based on the "Historical Case", that is, using the original MEDOF calibrations and the derived calibration factors of Section 5.

11.1 November 10, 1985

11.1.1 Description of ice conditions and loading events

The first recorded encounter of second-year ice for the Molikpaq at Amauligak I-65 for the 1985/86 season occurred on November 10, 1985. On this day, up to $5/10^{ths}$ second-year ice was present in a first-year matrix. Various failure modes occurred at the east, southeast and south faces throughout the day, see Table 14. While it is not clear from the source, ridge heights are assumed to refer to ridge sail height. The information in the "Ice type & thickness" column of Table 14 and all other summary tables in this section comes from various sources including Ice Observer reports, as described above at the beginning of Section 11.

Table 14 Summary of ice loading on November 10, 1985

Time period # from Appendix A	Time		Drift speed, direction	Ice type & thickness	Ice conditions and failure behaviour
	From	To			
1	03:30	6:00	0.17 m/s to 300º	3/10^{ths} to 5/10^{ths} SY ice in a FY ice matrix. Thickness 0.7 – 1.5 m, with ridges up to 3m height	Crushing, flexure, and rubble pile-up on east, SE and south faces; sliding on northeast.
	06:00	10:20	0.25 m/s to 320º	5/10^{ths} SY ice in a FY ice matrix. Thickness 0.5 – 1.5 m	Mixed modal failure on east, southeast and south faces; low confining pressure with cracks opening up easily.
	10:20	10:50	0.4 m/s to 320º	Unknown concentration of SY ice in FY matrix.	Failure is mainly rafting and sliding
	13:30	17:00	0.4 m/s to 320º	Traces of SY in FY matrix. Thickness 0.7 – 1.2 m	Crushing and flexure on east, southeast and south faces; sliding at southwest. Drift rate begins to slow down during this period. Ice is mainly FY; traces of SY ice impact south and southeast faces
-	20:00		0.3 m/s to 350º	2/10^{ths} SY ice in a FY matrix. Thickness 0.5 – 1.5 m, with ridges up to 1.5 m high	Crushing and flexure on east, southeast and south faces; rubble pile-up at southeast face with sliding on south and east. SY hummock impacts east and southeast faces.

11.1.2 Event analysis

There was loading on the east face throughout the day of November 10, 1985. Ice conditions were well documented and several DAY, FAST and EVENT files are available for analysis. Load levels were relative low; the maximum deflection in the east-west loading direction was 10 mm. This corresponded to MEDOF-based peak load on the east face of 85 MN. The event was judged to be of lesser interest at this time.

11.2 November 19, 1985

11.2.1 Description of ice conditions and loading events

Rubble maps from the morning of November 19, 1985 indicate that there was a second-year hummock just off the west face. However, examination of the extensometer data for the west face shows very low loads for the time period during which the hummock may have interacted with the structure (maximum of 1.5 mm deflection ≈ 9 MN). At the north face were ridges and a rubble pile created by previous ice interactions, possibly containing traces of second-year ice. These ice features impacted the Molikpaq between 16:30 and 19:40 resulting in noticeable loading on the north face.

Table 15 Summary of ice loading on November 19, 1985

Time period # from Appendix A	Time		Drift speed, direction	Ice type & thickness	Ice conditions and failure behaviour
	From	To			
2	06:50	16:45	Creep (0.001 m/s) to 90º	Level FY and SY ice, 0.7 – 1.5 m thick, with ridges up to 4 m high	Very slow loading due to ice pressure to the west of the structure. Crushing on west face, with rafting and rubbling on the north and NW. At 10:30, the 1.5 m thick SY hummock is 35 m off the west face. Rubble and ridges at the north face. Negligible loads felt by the Molikpaq in this time period.
	16:45	19:40 (?)	0.06 m/s to 140º	Same as previous	Ridges containing traces of SY ice likely to have interacted with north face in this time period. SY hummock likely to have impacted west face in this time period. Ice surrounding Molikpaq becomes entirely FY at some point.
-	19:42		0.06 m/s to 140º	FY ice, 0.7 – 1 m thick with ridges up to 0.7 m high	Entirely FY ice, with FY ridges impacting north face

11.2.2 Event analysis

This event may not be ideal for analysis due to the lack of information regarding ice types and times at which interaction with known ice features occurred. No video records are available to resolve the uncertainties. Also, only DAY files are available for the periods in which the Molikpaq may have been in SY ice. No further analysis done at this time.

11.3 November 27, 1985

11.3.1 Description of ice conditions and loading events

For November 27, the ice observations or rubble maps indicate that a first-year floe interacted with the Molikpaq, but another source (Klohn-Crippen, 1995) clearly states that the ice is second-year.

Table 16 Summary of ice loading on November 27, 1985

Time period # from Appendix A	Time		Drift speed, direction	Ice type & thickness	Ice conditions and failure behaviour
	From	To			
3	12:06	1:06	0.75 m/s to 285º	SY ice, 1.2 m thick	3.7 km diameter floe impacts the east face after open water conditions. After 1 hour the floe completely passes the Molikpaq, leaving open water conditions again. Failure modes: milling, bending, crushing, rafting.

11.3.2 Event analysis

MEDOF panel, strain gauge and extensometer readings show high loads starting at approximately 12:00 when the second-year floe impacts the east face. The MEDOF panels and extensometer for the east face show loads earlier in the day starting around 09:00, while the SG09 gauges show no loads at all for this time. Because of uncertainty of ice type, further analysis has been deferred.

11.4 December 16, 1985

11.4.1 Description of ice conditions and loading events

The ice observations made at the time of this event (Gulf, 1989) indicate that only thick first-year ice was present, however a report by Klohn Crippen (1995) states that second-year ice was present in a thin first-year ice matrix. Examination of video records shows that thicker ice, possibly second-year, interacted with the Molikpaq between 09:00 and 10:15.

Table 17 Summary of ice loading on December 16, 1985

Time period # from Appendix A	Time		Drift speed, direction	Ice type & thickness	Ice conditions and failure behaviour
	From	To			
4	09:00	10:15	0.4 m/s to 300º	SY ice in thin FY matrix. Thickness: 0.3 - 1.2 m	Ice loading on south, SE, east, and NE faces. Mainly crushing, with flexural failure of ice under the weight of the crushed ice. At 09:33 radial cracks form and the floe splits in two, reducing load on the Molikpaq. East face video record shows interaction with thin FY ice until 09:00, when impact with some thicker ice begins (could be SY). Ice moves fairly rapidly, with variable thicknesses. Mixed modal failure at east face (finger rafting, crushing, flexure, rubbling).
-	10:15			FY ice	Mainly thin FY ice

11.4.2 Event analysis

Event judged to be of lesser interest at this time.

11.5 March 7, 1986

11.5.1 Description of ice conditions and loading events

During the winter of 1985/86 at Amauligak I-65, ice movement was predominantly from east to west. In early March 1986, strong north-westerly winds brought second and multi-year ice southwards toward the Molikpaq. Up to mid-day on March 7, only first-year ice interacted with the Molikpaq. After the loading events on March 7 and 8 the ice stopped, constrained by the landfast ice to the south. Figure 36 shows a survey of the ice types and thicknesses that passed the structure on March 7 and 8. These thicknesses are the ones described in Section 9.

On March 7 at approximately 15:30, the Molikpaq penetrated a heavily ridged multi-year floe resulting in dynamic loading on the west and north faces. The floe continued progressing past the Molikpaq, Site 4 in Figure 36 identified in blue, interacting with the structure for approximately two hours, and cleared Site 4 at about 17:30. Ice observations, video records and the survey of ice conditions were used to summarize the ice loading in Table 18. The average ice thickness from holes # 34 to #37 in Site 4 in Figure 36, on either side of the broken wake, was 5.2 m. Using Johnston's coefficient of variation of 0.33, the standard deviation on the 6.3 m mean thickness would be 1.7 m. The average air temperature for the three days preceding March 7 was -26 C.

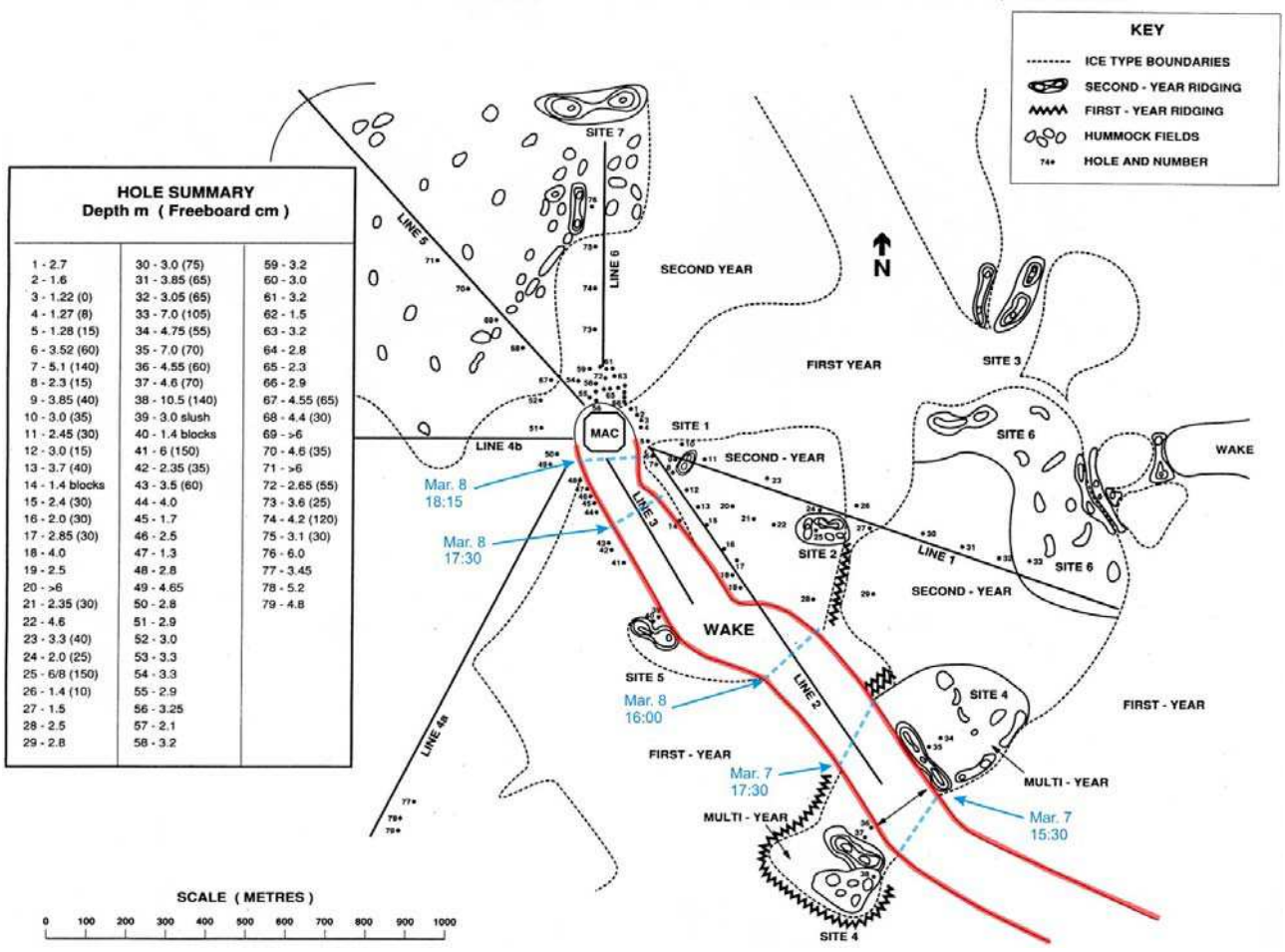

Figure 36 Survey of ice conditions surrounding the Molikpaq for March – April 1986. The wake or track of the ice past the structure on March 7 - 8, 1986 is outlined in red.

Table 18 Summary of ice loading on March 7, 1986

Time period # (and Event ID if applicable)	Time		Drift speed, direction	Ice type & thickness	Ice conditions and failure behaviour
	From	To			
-	15:20	15:32	?	FY ice	Video record shows crushing on entire north face.
5 (0307A)	15:32	15:44	0.05 m/s, to 130º	MY ice, 4 – 6 m thick (nearby hole surveys report ice 4.4 - 7 m thick, 5.2 m average)	Molikpaq penetrates MY floe. Video record shows sliding on entire north face.
	15:44	16:08	0.05 m/s, to 130º	MY ice, 4 – 6 m thick (nearby hole surveys report ice 4.4 - 7 m thick, 5.2 m average)	Crushing of MY ice floe on west and northwest faces. Dynamic loading on west face due to crushing of 50 m long, 2 m high hummock on its longitudinal axis. Rubble clearing around north and southwest faces, with some mixed modal failure on north face. Cracks form in floe but do not widen.
	16:08	16:16	0.05 m/s, to 160º	MY ice, 4 – 6 m thick (nearby hole surveys report ice 4.4 - 7 m thick, 5.2 m average)	Rubble piles form on west, northwest and north faces, dampening the dynamic loading. Global confinement of ice prevented rubble from clearing west face, and rubble pile was most likely grounded on the berm. Video record shows crushing on MEDOF panel group N2.
5 (0307A, 0307B)	16:16	16:46	0.05 m/s, to 160º	MY ice, 4 – 6 m thick (nearby hole surveys report ice 4.4 - 7 m thick, 5.2 m average)	MY floe fractures off northwest face; loads diminish on west face; dynamic loading on north face. Video record shows crushing on MEDOF panel groups N2 and N3 from 16:16 to 16:31, and then on all panel groups.
5 (0307B)	16:46	17:43	0.05 m/s, to 160º	MY ice, 4 – 6 m thick	Video record shows sliding and mixed modal failure on north face. Cracks in floe widen significantly by 17:00.

11.5.2 Event analysis

A number of DAY and FAST files were available for analysis of the loading events on March 7. In characterizing the factors affecting loads, the events and Sub-events identified in the video analysis of Section 10 are described in terms of time period, ice thickness, ice velocity, and failure mode in Table 19. The key to the abbreviations of failure mode, taken from Section 4 of Appendix G are as follows:

- CR: continuous ice crushing
- CC cyclic ice crushing
- MM mixed modal failures

- SLD ice sliding along a face
- SLW a creep or indiscernibly slow ice push

Table 19 Description of events and sub-events for March 7

Event ID	Sub-event number	Time period	Ice thickness (m)	Ice velocity (m/s)	Failure mode
0307A	full event	15:20:41 – 16:31:01	5.2m average (range: 4.3 – 6.3m)	0.05	CR, SLD & MM (north face)
0307A-1	1	15:20:41 – 15:32:21	FY ice		CR
0307A-2	2	15:32:22 – 15:44:32	5.2	0.05	SLD
0307A-3	3	15:44:33 – 16:10:25	5.2	0.05	MM
0307A-4	4	16:10:26 – 16:16:01	5.2	0.05	CR
0307A-5	5	16:16:02 – 16:31:01	5.2	0.05	CR
0307B	full event	16:38:54 – 17:43:47	5.2	0.05	CR, MM & SLD (north face)
0307B-1	1	16:38:54 – 16:45:05	5.2	0.05	CR
0307B-2	2	16:45:06 – 17:43:47	5.2	0.05	SLD & MM

The DAY file preceding Event **0307A** indicated loading commenced at about 11:30 on March 7 and was exclusively on the north face. Starting at 15:20 for Event **0307A** loading on the north face (Figure 38) was probably FY ice, giving quite large loads from linear averaging of MEDOF panels. At 15:32 loading on the north face dropped off to zero. At about 15:35 loading shifted to the west face (Figure 37) and began to increase. This is inferred from the East-West extensometer results since the West face extensometer showed the greatest response, and the east face MEDOF panels did not register any load. As the loading on the west face increased further, at about 15:45 it started to induce an outward deformation of the north face which shows as a negative face load from extensometers. However, the MEDOF panels indicate a north face load of ~100 MN. The extensometer record indicted a maximum force on the west face of ~230 MN at 16:02 while the MEDOF panels give a load of ~100 MN on the north face at the same time. There are only two SG09 strain gauges on the north face so the estimated load from them is over a 40 m length of the north face. At 16:15 the loading on the west face drops off abruptly to zero and from that point onwards loading is on the north face. Note that Event **0307B** immediately follows Event **0307A**. From about 16:15 to 16:45 the extensometer response on the north face increases to the point where the west face extensometer load goes “negative” (Figure 37 and Figure 39). This illustrates the limitation of estimating face load from the extensometer when two faces are loaded at the same time. Note that there is a further load on the north face from 17:05 to 17:15, which generates a negative response from the East-West extensometers. Pulsations at 0.5 to 1 Hz were reported during the loading on March 7.

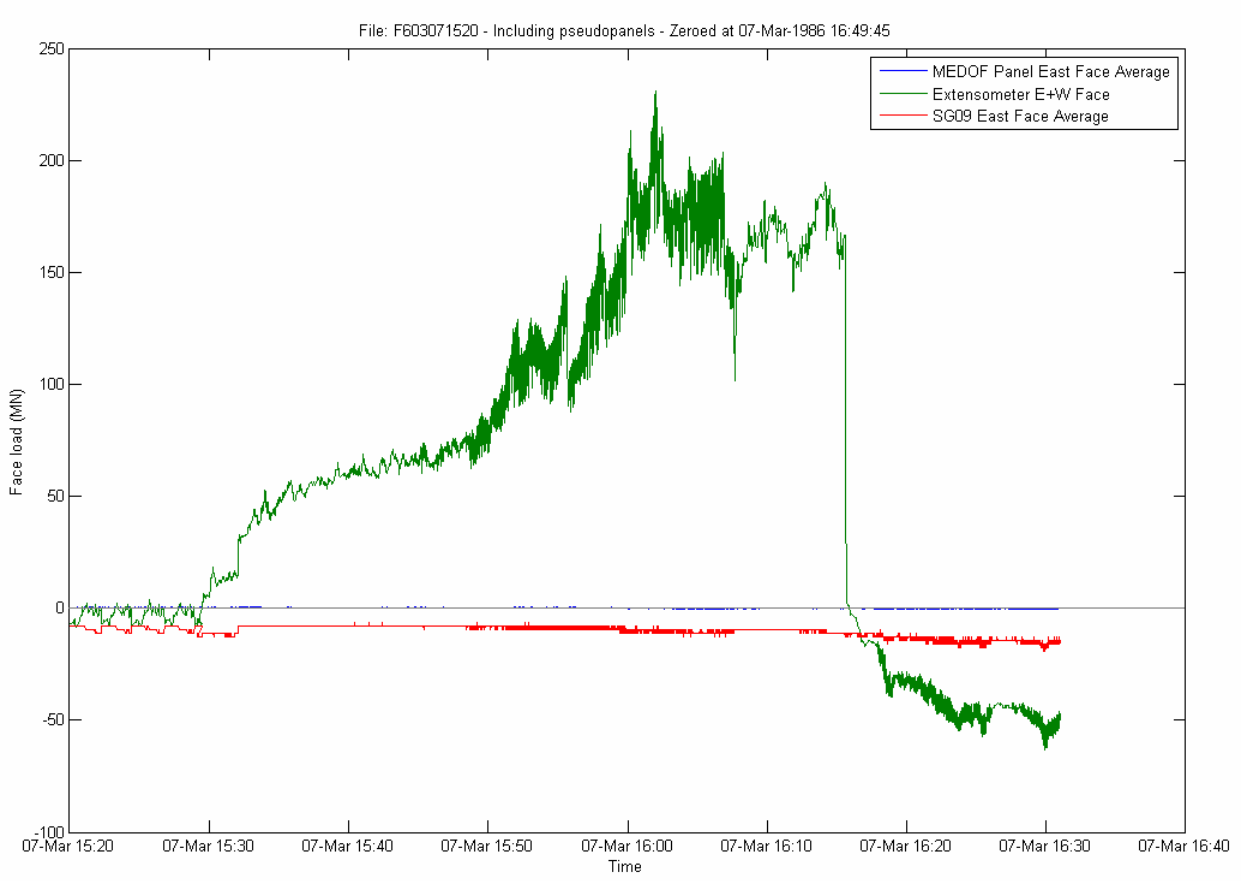

Figure 37 March 7 – West face loading, Event 0307A

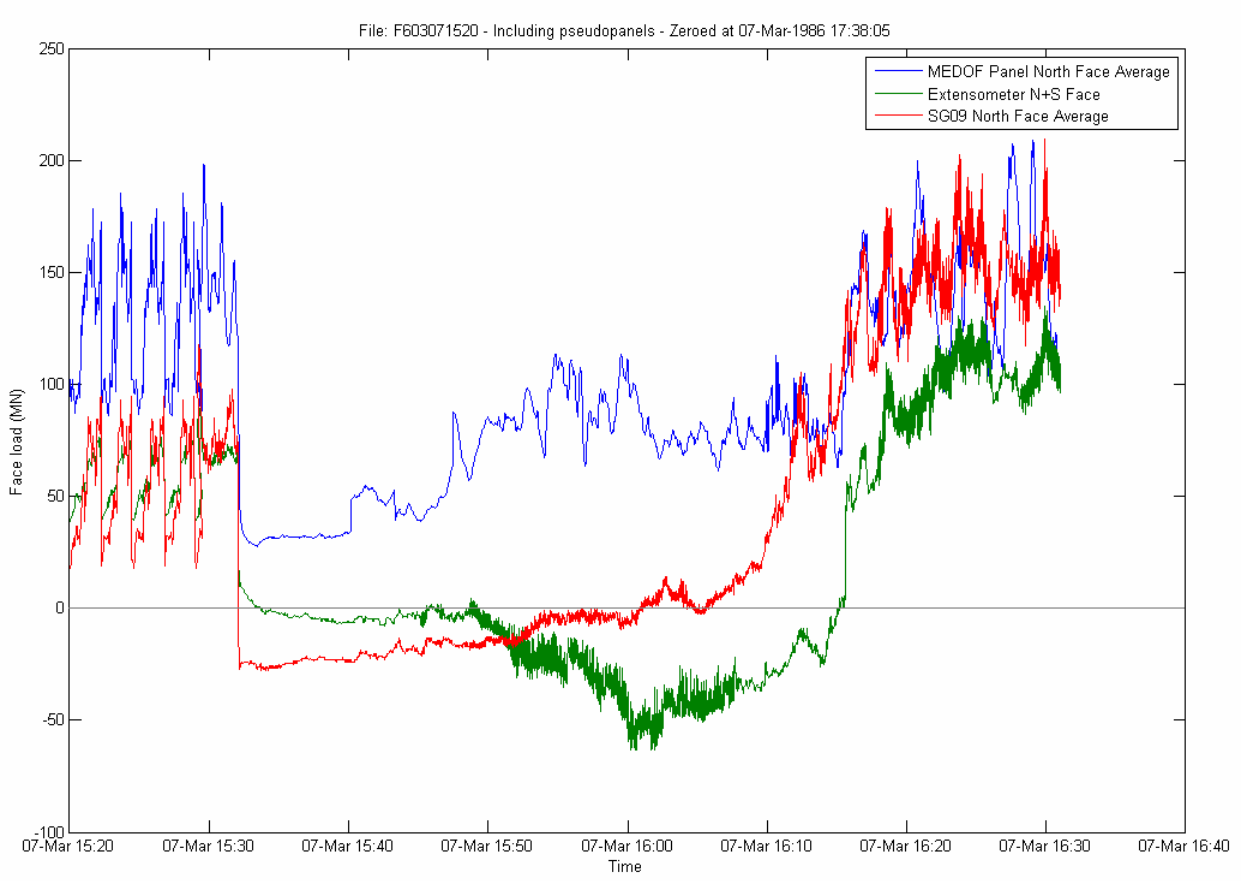

Figure 38 March 7 - North face loading, Event 0307A

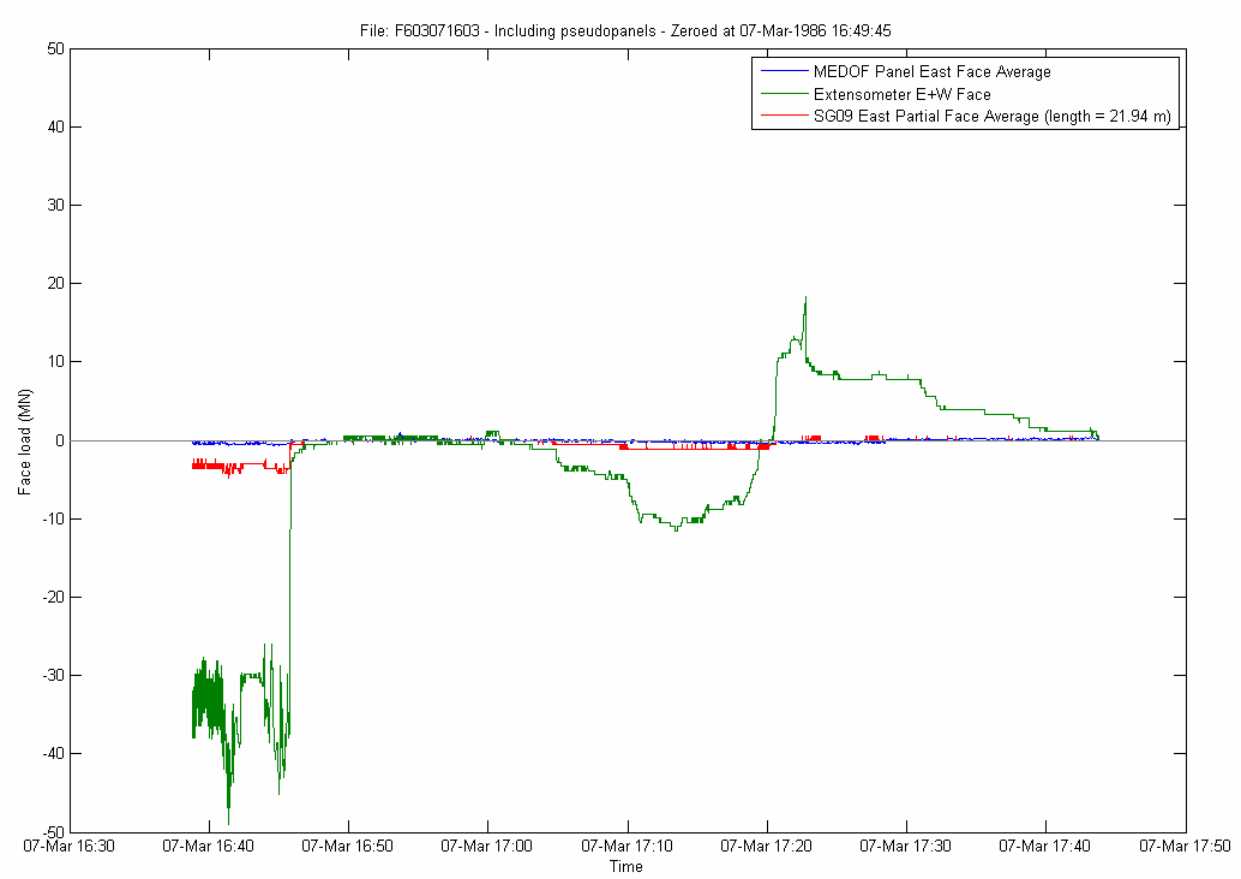

Figure 39 March 7 - East face loading, Event 0307B

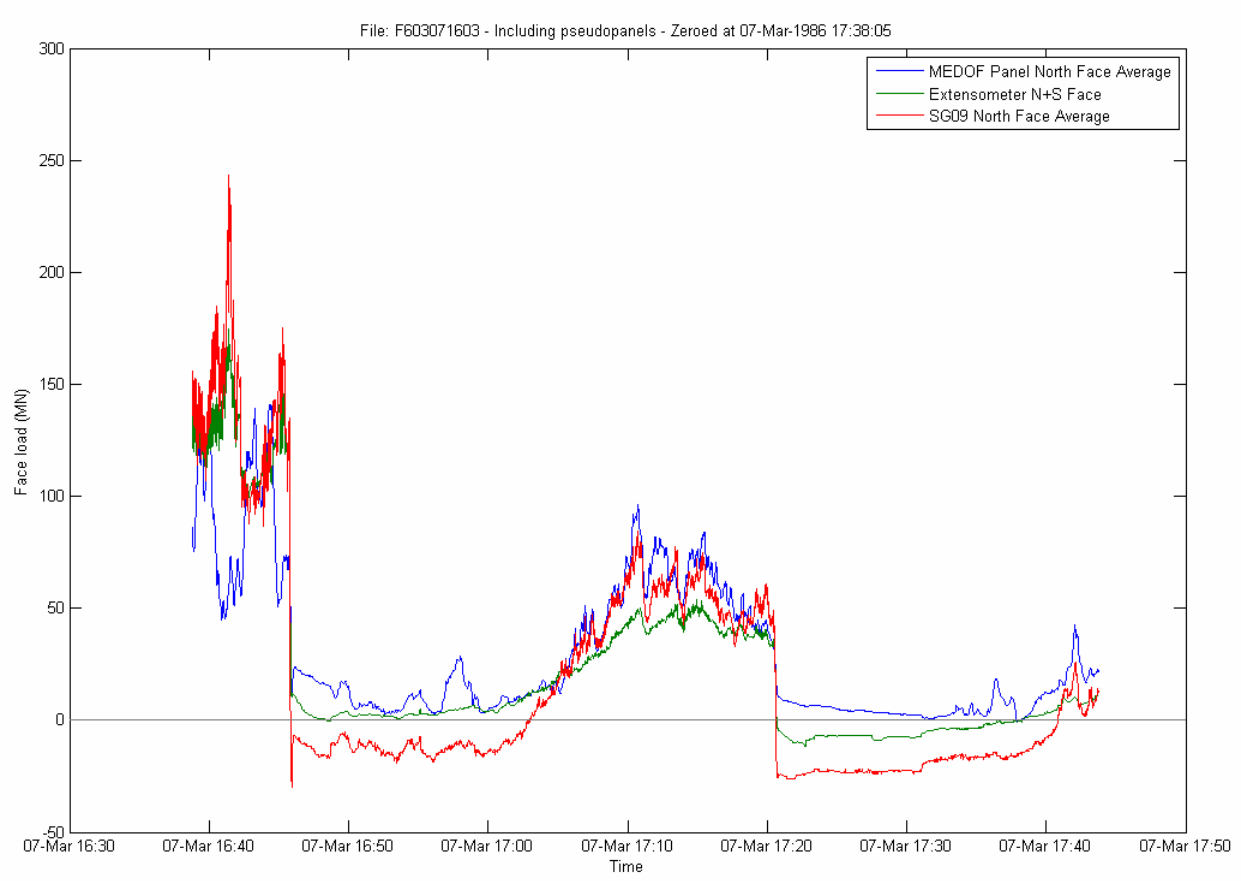

Figure 40 March 7 - North face loading, Event 0307B

11.6 March 8, 1986

11.6.1 Description of ice conditions and loading events

For March 8, 1986, a caisson/ice interaction report (Gulf, 1989) and partial video coverage are available. This information, combined with the ice survey shown in Figure 36, was used to summarize the ice loading events in Table 20. Figure 36 shows that on March 8 an area of SY ice passed the structure followed by a short interval of FY ice before coming to a halt in another area of SY ice. This event has some uncertainty about times of interaction with specific ice features, ice drift speed, and ice type. Our best estimates of the ice location are at various times on the afternoon of March 8 are indicated in blue on Figure 36. The ice observation and hourly reports indicate that only second-year ice was present near the Molikpaq, while an event summary (Klohn-Crippen, 1995) states that the ice was multi-year. Examination of the video records shows that multi-year ice may have interacted with the structure. In either case, this event involved 3-4 m thick older ice in a 2 km by 1 km floe, resulting in high loads on the north face.

Table 20 Summary of ice loading on March 8, 1986

Time period # (and Event ID if applicable)	Time		Drift speed, direction	Ice type & thickness	Ice conditions and failure behaviour
	From	To			
6 (0308A)	15:00	17:30	0.1 m/s – creep, to 160º	SY ice: 2 – 4 m thick; FY ice: 1.3 – 1.7 m thick	Large SY floe surrounds Molikpaq. Crushing on west, NW and north faces, with rubble piles 2 – 5 m high. Drift slows to creep during this time interval. For the latter part of this time period (exact time is unknown), FY ice is interacting with the Molikpaq.
6 (0308B)	17:30	18:00	0.02 – 0.05 m/s, to 160º	SY or MY ice: 3 – 4 m thick	Penetration of SY or MY floe begins. Crushing on west, NW and north faces, with crushing and sliding on NE. Extrusion-collapse cycles, with major collapse at 17:41 (video time). Rubble piles 2 – 3 m high on west face, 4 m high on NW face, and 10 m high (deck level) on north face. High confining pressures; loads pulsating at 1 Hz. Failure mode changes from crushing to flexure; cracks form in floe.
	18:00	18:45	0.05 – 0.005 m/s, to 180º	SY or MY ice: 3 – 4 m thick	Drift begins to slow down. Ride up and failure of ice sheet on north face, with rubble pile continuing to form. Load diminishes when cracks to the north and northwest occur at 18:20. Ice sheet behind the rubble pile on north face begins to fail at edge near NE face. Radial cracks form off west face. Crushing and sliding on northeast face. Video record shows rubble clearing down NE face toward the east. Larger blocks of ice seen toward the end of this time period suggest that flexural failure has occurred.

11.6.2 Event analysis

The DAY file for the period between the March 7 and March 8 events indicated loading on the north face between 20:00 and 22:00 on March 7 of a magnitude approaching that of earlier in the day. Four FAST files were recorded on March 8. Using failure modes events identified in the video analysis of Section 10 each file is treated as an event and described in terms of time period, ice thickness, ice velocity, and failure mode in Table 21.

Table 21 Description of events for March 8

Event ID	Sub-event number	Time period	Ice thickness (m)	Ice velocity (m/s)	Failure mode
0308A	full event	16:03:13 – 17:14:12	3.5* (FY ice at end of time period)	0.1, then slows to creep	CR & SLW
0308B	full event	17:31:54 - 18:36:33	4.3	0.02 – 0.05	CR, CC, SLD & MM
0308C	full event	21:11:21 - 22:22:20	2.6*	?	no video
0308D	full event	22:26:08 - 23:02:07	2.6*	?	no video

* no load on lower panel

The four events on March 8 (Events **0308A**, **0308B**, **0308C** and **0308D**), were all for loading exclusively on the north face. Even though some crushing was reported for the west face, the East-West extensometers did not detect any loading; however extensometers measurements in the east-west directions may have been masked by the influence of large loading on the north face. There were four cycles of cyclic crushing load on the north face from 16:05 to 16:15, of maximum magnitude ~100 MN (see Figure 41). From 17:30 to 18:15 there was crushing on the north face with loads reaching about 270 MN (see Figure 42. The two plots (Figure 43and Figure 44) for loading in the evening of March 8 indicate relatively low load levels associated with slow creep.

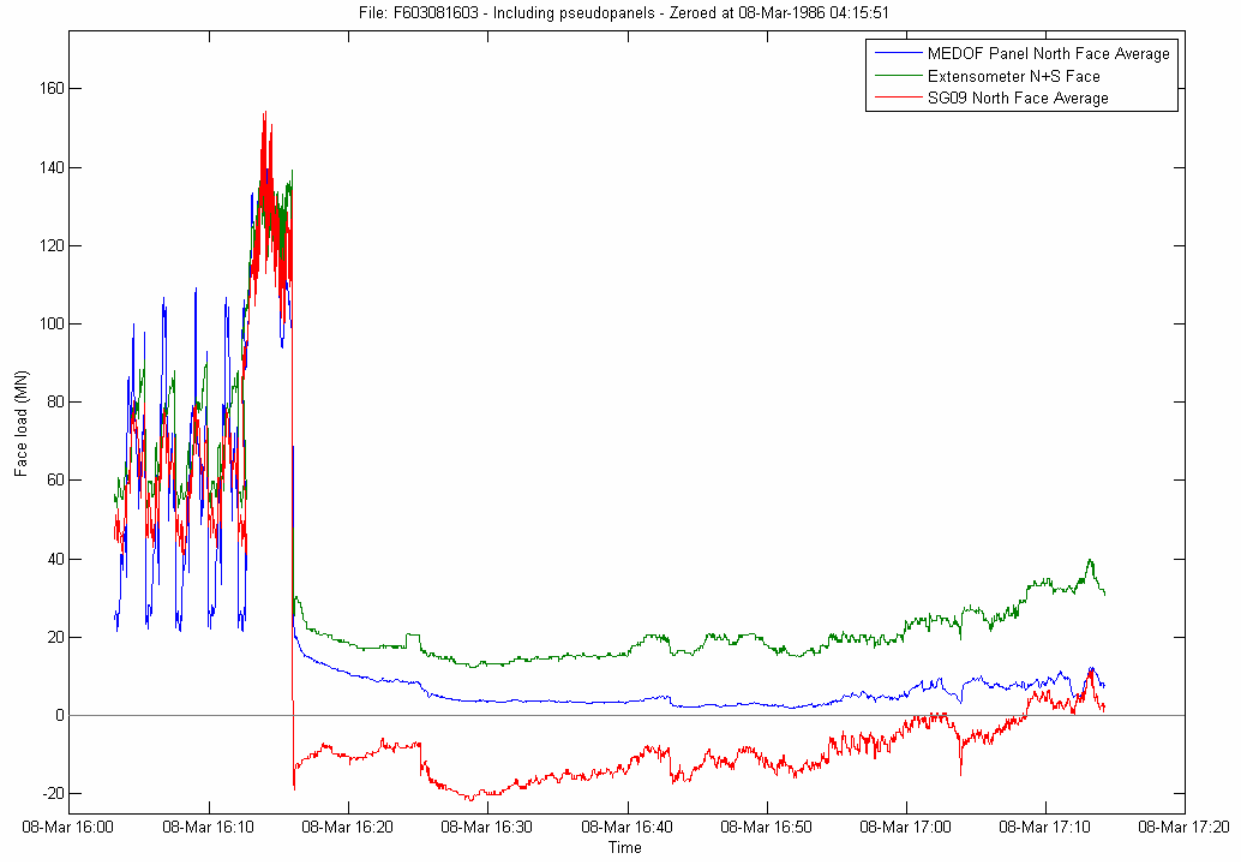

Figure 41 March 8 - North face loading, Event 0308A

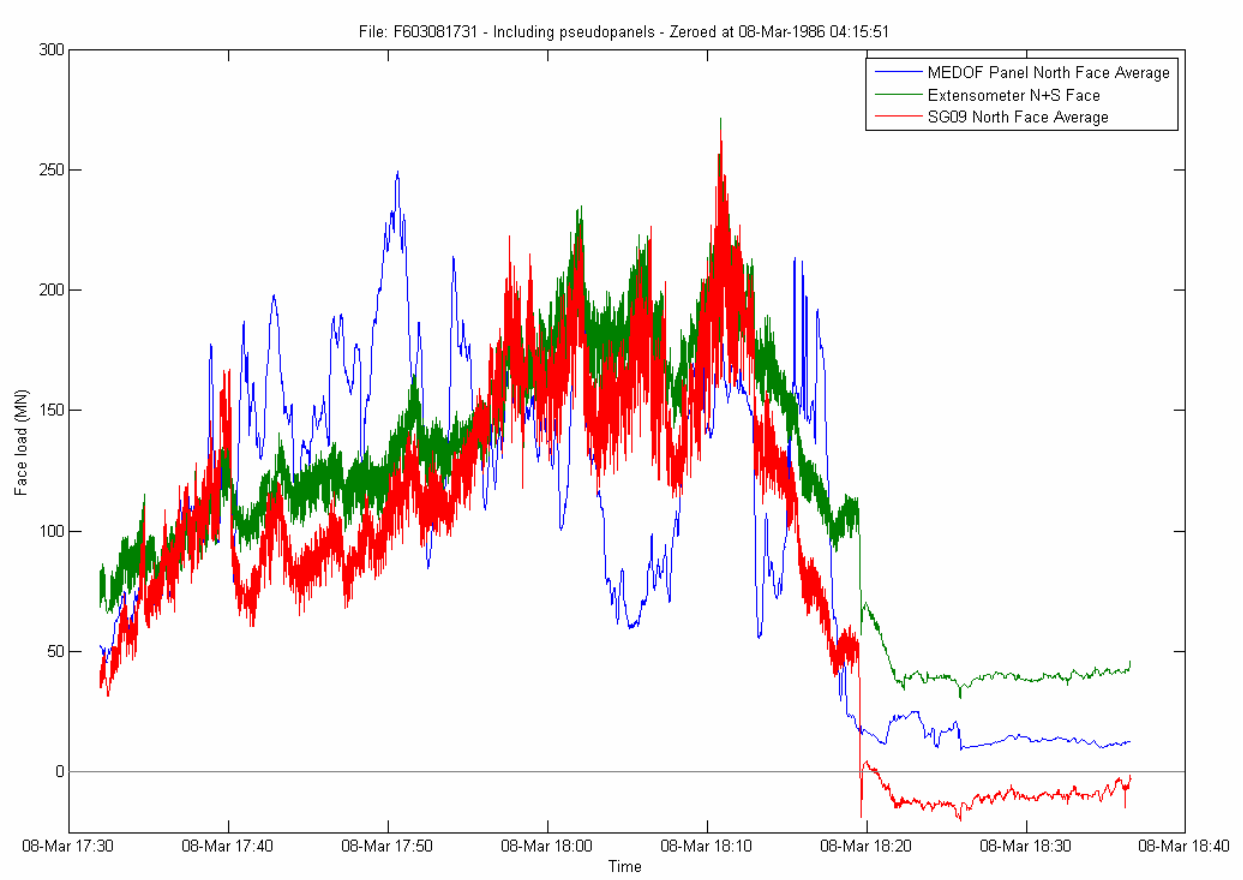

Figure 42 March 8 - North face loading, Event 0308B

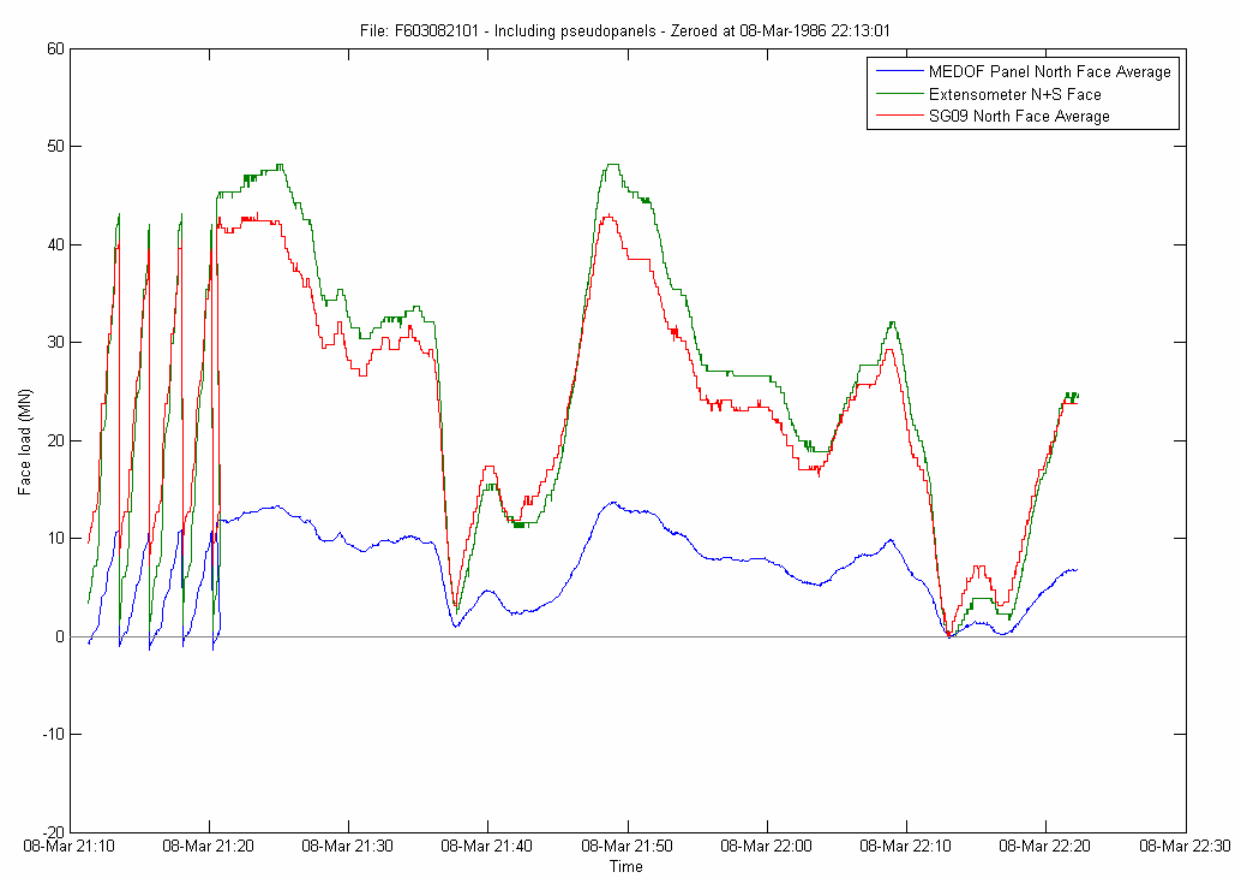

Figure 43 March 8 - North face loading, Event 0308C

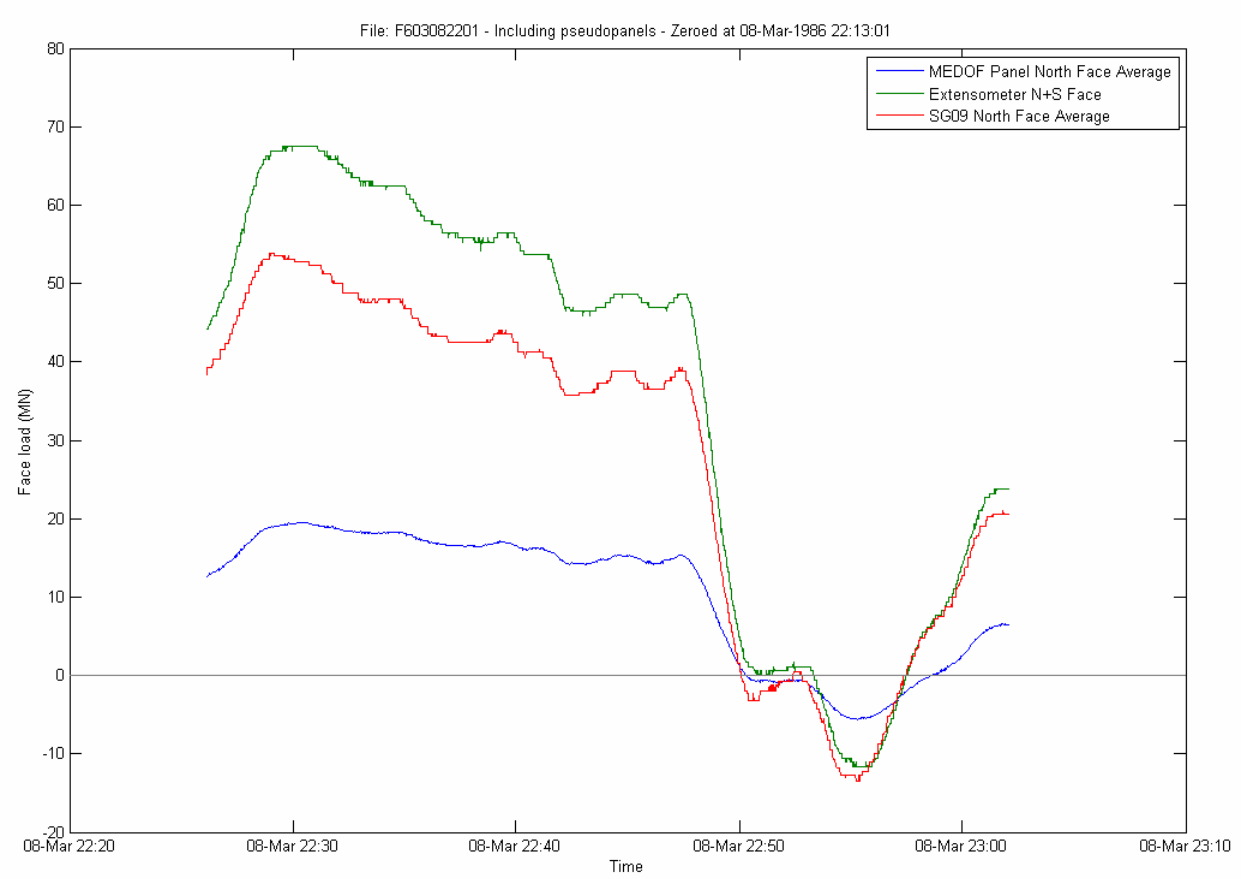

Figure 44 March 8 - North face loading, Event 0308D

11.7 March 22-24, 1986

11.7.1 Description of ice conditions and loading events

From March 22 to 24, 1986 the second-year ice slowly crept towards the south-southwest, resulting in loading mainly on the north face. One rubble map, for 0830 on March 23, was available for this time period. The information on it described the drift speed as "creep" with crushing on the NW, N and NE faces. The Ice Observer data indicated 20 cm of creep to 240° True for the previous 2.5 hours at 1300 on March 23, but no loading response was detected on the east face MEDOF panels.

Table 22 Summary of ice loading on March 22-24, 1986

Time period # from Appendix A	Time		Drift speed, direction	Ice type & thickness	Ice conditions and failure behaviour
	From	To			
7	10:00 March 22	14:00 March 24	Creep to 200º	SY ice: 2.5 – 3 m thick, with hummocks up to 3.5 m high	Slow loading during this time interval

11.7.2 Event analysis

Only DAY files were recorded for this time period. The 5-minute average, minimum and maximum values of the MEDOF panels were examined and typically the maximum was about 5% greater than the average and the minimum 15% less. No load was measured on the lower MEDOF panels; 1010(N2) and 1020(NE), so the ice thickness was 2.7 m or less. From Figure 45, maximum load on the north face was about 55 MN on March 22, 80 MN on March 23, and 70 MN on March 24. The N-S extensometer deflection on March 23 was ~7 mm, equivalent to ~42 MN. There was no evidence of any loading on the east face for this period.

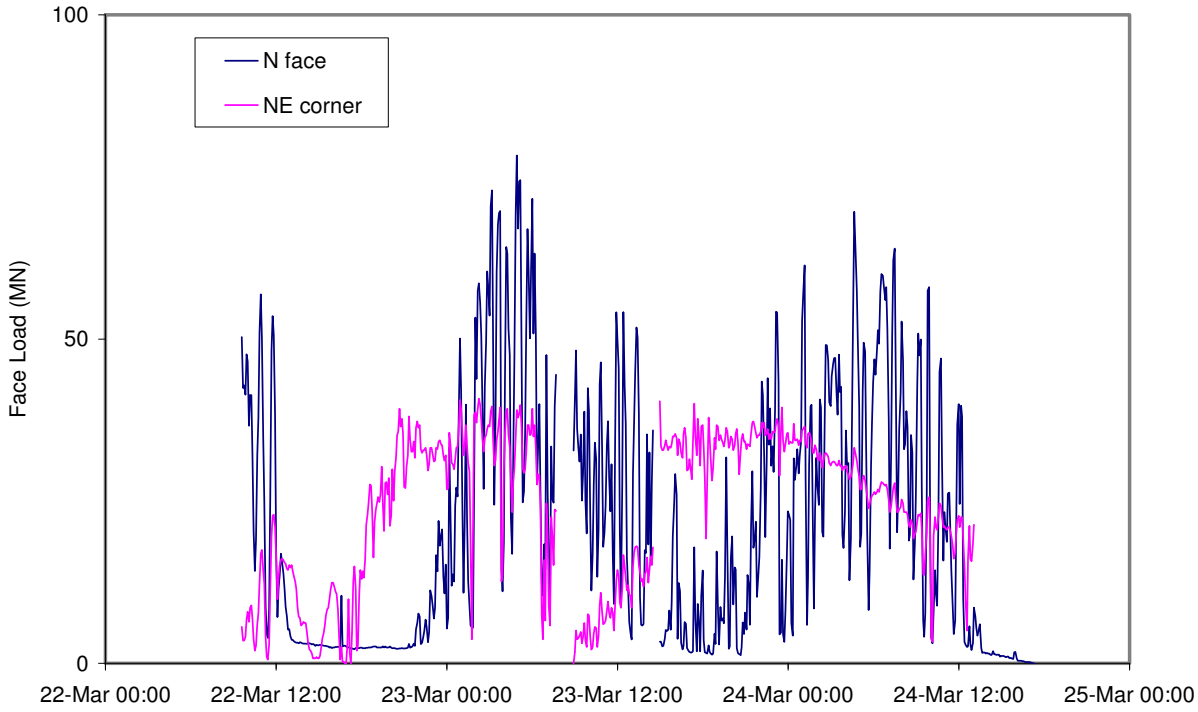

Figure 45 Loads on North face and Northeast corner, March 22-24

11.8 March 25, 1986

11.8.1 Description of ice conditions and loading events

On March 25, 1986, the second-year ice immediately surrounding the Molikpaq started to slowly move southwards. Caisson/ice interaction reports (Gulf, 1989) and the ice survey in Figure 36 were used to determine the ice behaviour described in Table 23. Average air temperature for the preceding three days was -24 C.

Table 23 Summary of ice loading on March 25, 1986

Time period # (and Event ID if applicable)	Time		Drift speed, direction	Ice type & thickness	Ice conditions and failure behaviour
	From	To			
8	02:00	08:15	Creep to 180º	SY ice, 2.5 – 3.5 m thick	Ice loading mainly on north face
8	08:15	08:30	Creep to 200º	SY ice, 2.5 – 3.5 m thick	Loading mainly on the north face, with some loading on the NW, NE and east faces. Cyclic loading (3 minute period) thought to be the result of a floe pressing on the north face.(see March 25 load trace in Appendix K)
8 (0325A)	08:30	10:30	Creep (0.00006 m/s) to 200º	SY ice, 2.5 – 3.5 m thick	Ice moves 20 cm in this time interval. Very small cracks form in ice on NW face. Ice heaves slowly due to buckling under the surface. No failure modes apparent on the surface of the ice. Video record shows creep loading across entire north face.
9 (0325B)	16:00 (approx.)		Creep to 220º	SY ice, 2.5 – 3.5 m thick	Ice continues to creep, with drift direction shifting more to the SW.

11.8.2 Event analysis

Review of the video indicated failure behaviour for the events on March 25 was creep, see Table 24. The DAY files prior to the first FAST file for March 25 indicated creep loading from 04:00 to 08:30, with load peaks reaching 80% of those in Event **0325A**.

Table 24 Description of events for March 25

Event ID	Sub-event number	Time period	Ice thickness (m)	Ice velocity (m/s)	Failure mode
0325A	full event	08:30:39 – 09:44:13	3.5*	creep	SLW
0325B	full event	13:50:10 – 16:00:08	3.5*	creep	SLW

Time series plots for the two March 25 loading events on the north face are presented in Figure 46 and Figure 47. Event **0325A** in the morning indicated loads of about 110 MN for slow creep. In the afternoon, Event **0325B,** higher loads of about 120 MN were attained, again for creep at a rate of about 20 cm per hour. No adjustment of the MEDOF panel loads has been made due to creep of button material in the panels. Because of the loading periods of 2 to 10 minutes these events are particularly useful for calibration of strain gauges and extensometers against MEDOF panels. Also noteworthy is the similarity

of the form of the load time curves from MEDOF panel, Extensometer and SG09 strain gauge measurements.

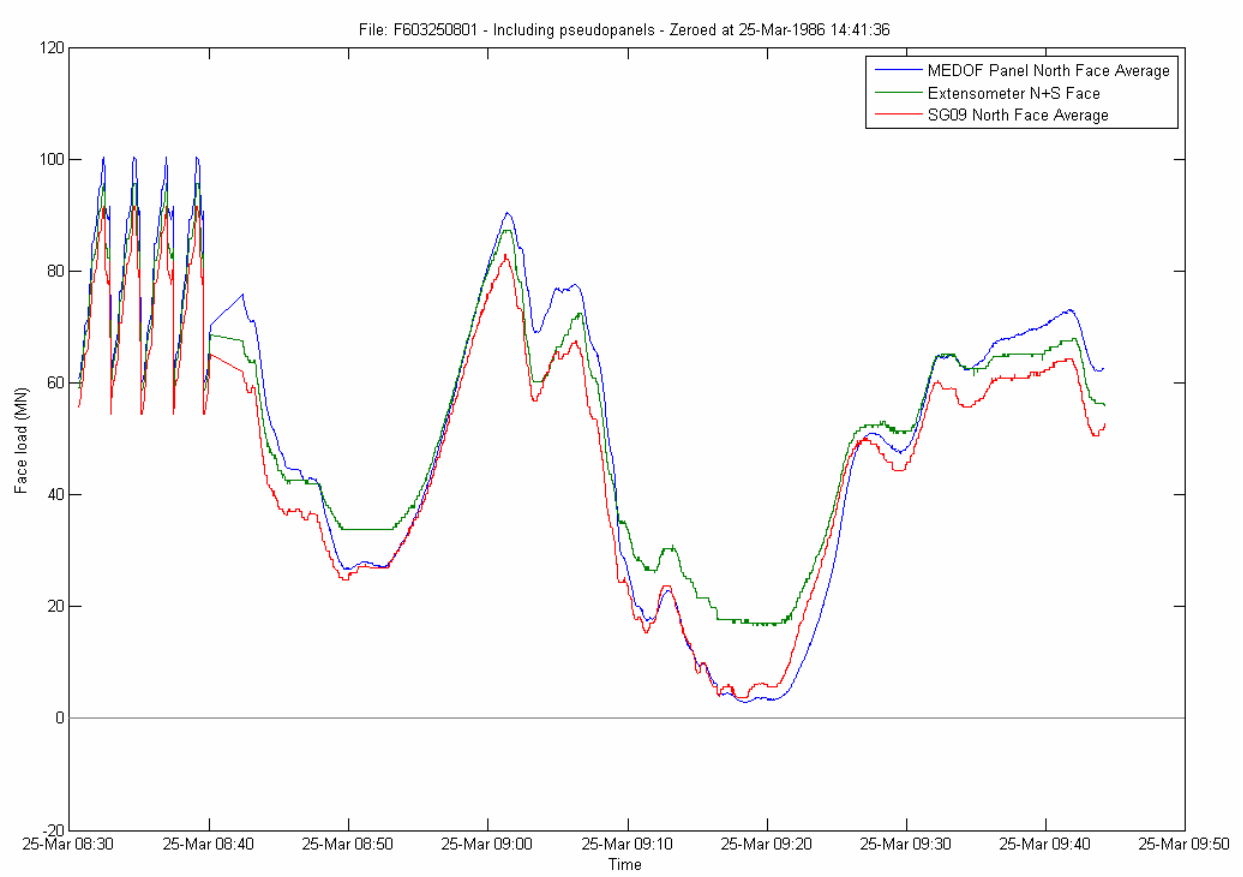

Figure 46 March 25 - North face loading, Event 0325A

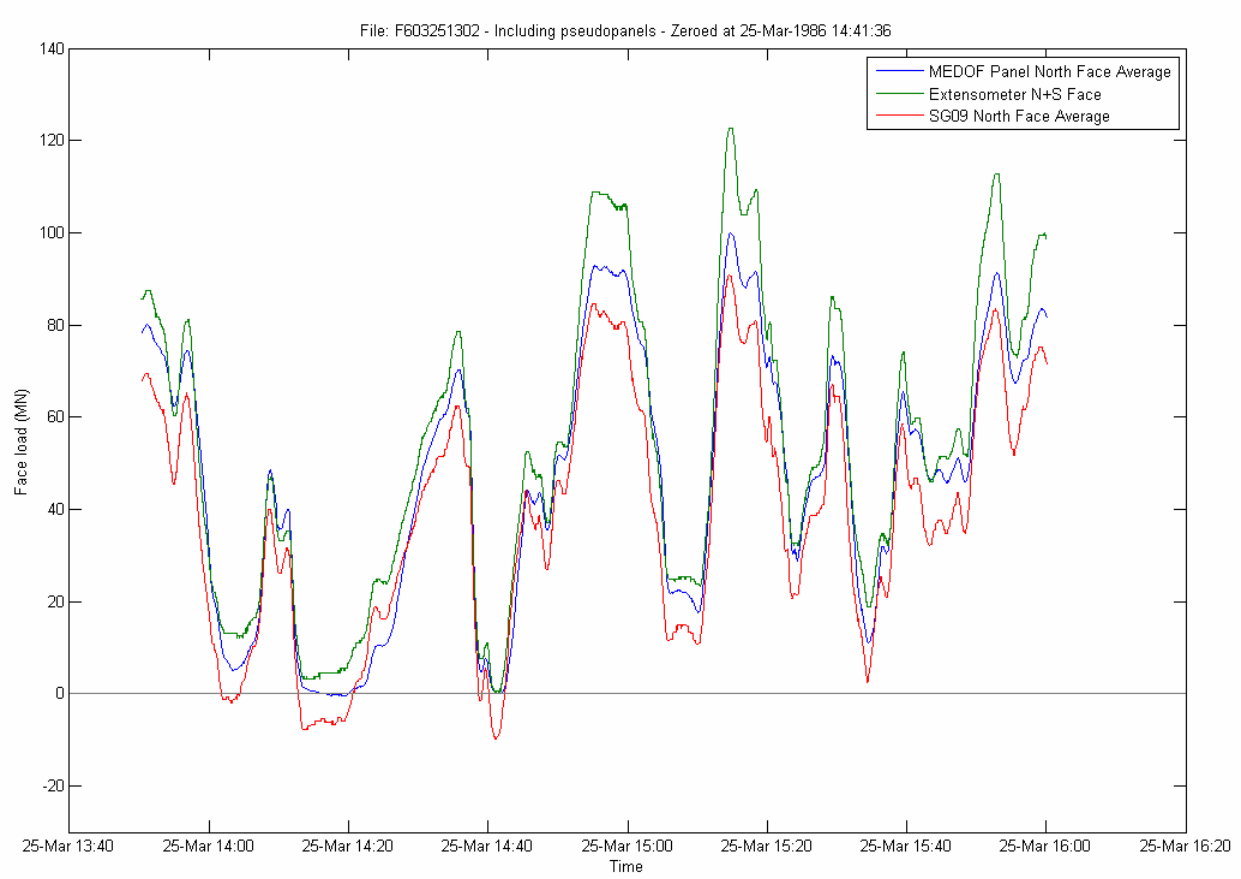

Figure 47 March 25 - North face loading, Event 0325B

Since the afternoon of March 25 provided a significant static loading event, the north and south face movements with respect to the Guide Pipe and north face tiltmeter results were compared, Figure 48. Referring back to Figure 47, it can be seen that the north face movement and tilt are directly related to the north face load, in fact they are well synchronized. The maximum north face movement is about 19 mm to the south, while the maximum south face movement is about 1.5 mm to the north. Also they are related, the south face moves inwards (to the north) whenever the north face moves inwards(to the south), but to a much smaller extent. The maximum tilt change of the north face is 0.04 % g, which is equivalent to an offset of about 14 mm over the 23 m distance from the base to the tiltmeter, compared to the 19 mm movement of the top of the north face. This implies that the base of the north face may have slid 5 mm to the south.

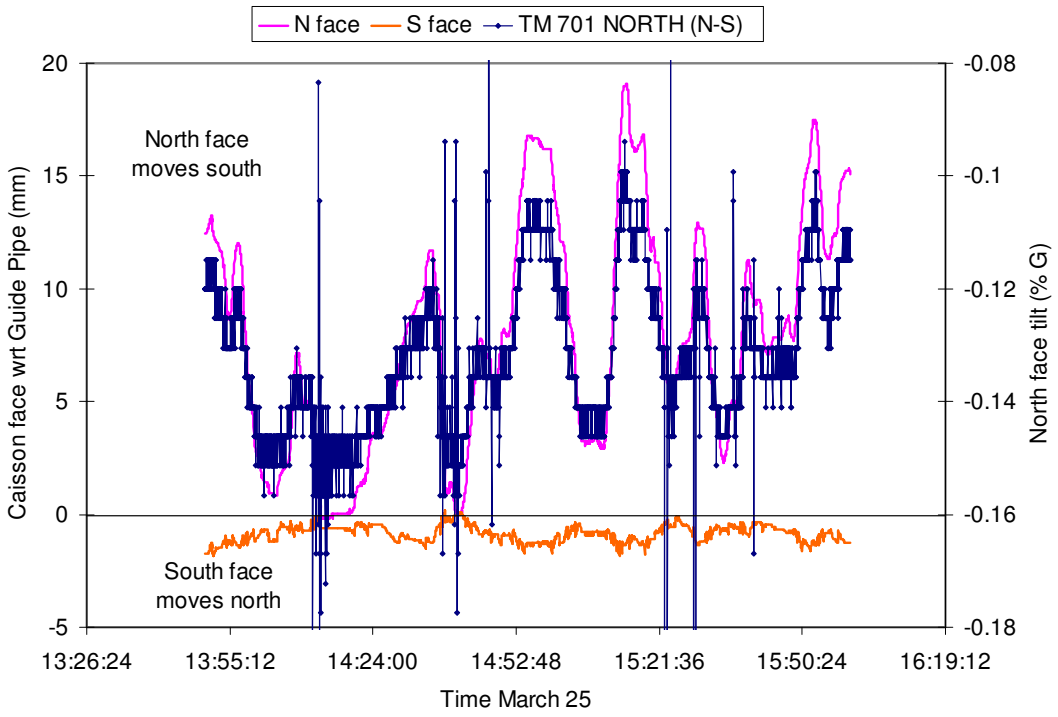

Figure 48 Comparison of caisson face movement and tilt on March 25

11.9 March 27, 1986

11.9.1 Description of ice conditions and loading events

On March 27 the second-year ice surrounding the Molikpaq slowly moved towards the northwest.

Table 25 Summary of ice loading on March 27, 1986

Time period # from Appendix A	Time		Drift speed, direction	Ice type & thickness	Ice conditions and failure behaviour
	From	To			
10	12:00	17:35	Creep to 315º	SY ice, 2.5 – 3.5 m thick	Ice creeps 30 cm in this time interval

11.9.2 Event analysis

For the slow creep event on March 27, 1986, only DAY files were recorded. This event is not amenable to further analysis since the ice movement did not result in measurable response from any of the instrumentation on the Molikpaq.

11.10 April 6-7, 1986

11.10.1 Description of ice conditions and loading events

No ice interaction observations are available for April 6-7, 1986. This is likely due to the fact that ice loading was very slow and failure of the ice at the walls of the Molikpaq was probably not obvious. As mentioned in Table 26, dynamic loading did occur for a short time on April 7.

Table 26 Summary of ice loading on April 6-7, 1986

Time period # from Appendix A	Time		Drift speed, direction	Ice type & thickness	Ice conditions and failure behaviour
	From	To			
11	22:00 Apr. 6	05:00 Apr. 7	Creep to 180º	SY ice, 2.5 – 3 m thick	Slow creep event. Some cyclic loading on north face on Apr. 7 from 02:10 – 02:30.

11.10.2 Event analysis

Three FAST files were recorded for this time period, but it is not clear why they were triggered. DAY files for the period April 1-12 were reviewed and a maximum load of 26 MN on the north face was measured on April 5 at 09:50, see Figure 49. The nature of the load record indicates creep behaviour on April 5 and the first half of April 6, but no information on rate is available. During time period # 11 (Apr. 6, 22:00 to Apr. 7, 05:00), loads on the north face varied from 5 to 15 MN. Some cyclic loading, with a period of about 2 minutes, was detected in the strain records in the time period 02:10 to 02:30. The amplitude and magnitude were small.

An explanation for cyclic loading at this time: from late March to April 12 there were some observations of gaps of the order of 30 cm opening between the face of the Molikpaq and the ice cover. It is likely that these gaps refroze, and when ice movements in the opposite direction occurred, this thin first-year ice interacted with the structure, failing in a cyclic fashion. The sensitivity of the instrumentation permitted these load cycles to be detected.

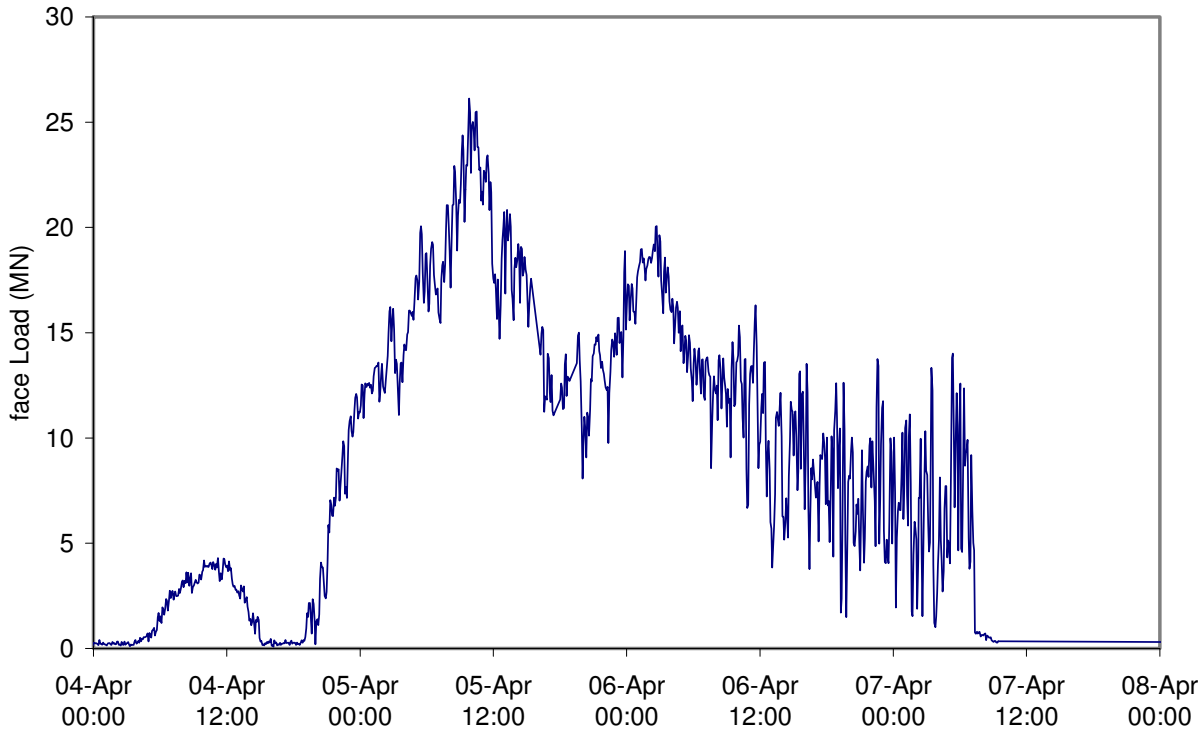

Figure 49 April 4-8, North face load

11.11 April 12, 1986

11.11.1 Description of ice conditions and loading events

As mentioned in Section 11.5.1, the ice surrounding the Molikpaq was essentially stationary (aside from some creep movement) from March 8 to April 12, 1986. A survey of the ice conditions near the Molikpaq during this time period is shown in Figure 50. This figure shows the path of the ice impacting the structure on April 12 (shaded strip extending from the caisson to the southeast). The hole numbers correspond to thicknesses given in the Hole Summary table in the same figure. The ice around the Molikpaq did not experience significant movement after March 8 until strong winds began to move the pack ice to the northwest on April 12. Air temperature for the preceding three days was -23 C.

The ice feature on April 12, which interacted with the Molikpaq between 08:15 and 08:35, was a multi-year hummock about 70 m long, 3 m sail height and estimated to have a total thickness of 12 m. It was surrounded by ice ranging in thickness from 2.5 to 5 m and averaging 3.3 m. Later in the morning, ice ranging in thickness from 2.5 to more than 6 m and averaging 3.5 m failed against the east face. In the afternoon, Site 4 ice 4.75 to 7 m thick interacted with the south and east faces.

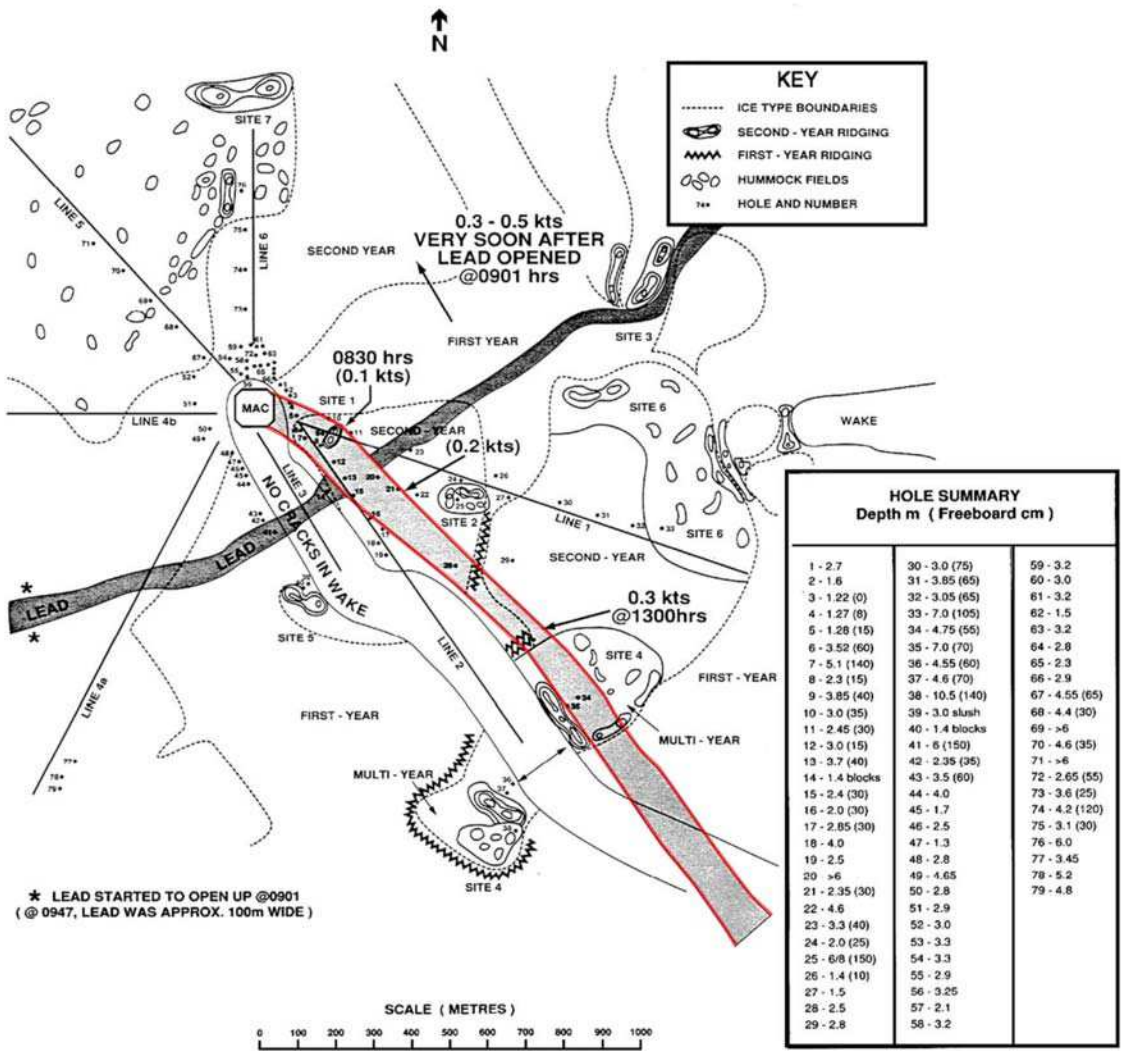

Figure 50 Survey of ice conditions surrounding the Molikpaq for March – April 1986. The track of the ice past the structure on April 12, 1986 is outlined in red

The ice interactions of April 12 were documented in greater detail than any other day for the Molikpaq at Amauligak I-65; therefore many sources of information about the events are available. These sources include caisson/ice interaction observations, video records and ice thickness surveys. A summary of events on April 11-12 based on the various sources is given in Table 27.

Table 27 Summary of ice loading on April 11-12, 1986

Time period # (and Event ID if applicable)	Time		Drift speed, direction	Ice type & thickness	Ice conditions and failure behaviour
	From	To			
12	11 Apr 21:30	12 Apr 07:00	Creep to 360º	SY ice: 1.5 to 2.5 m	No significant loading on Molikpaq
13	12 Apr 07:00	12 Apr 08:00	Creep to 280º	SY ice: 1.5 to 2.5 m	Ice begins to move towards west-northwest; 1 m of ice drift in this time interval

Time period # (and Event ID if applicable)	Time		Drift speed, direction	Ice type & thickness	Ice conditions and failure behaviour
	From	To			
	08:00	08:23	0.06 m/s to 280º	SY/MY ice: 1.5 to 2.5 m (refrozen wake is 0.8 m thick)	Multi-year ice crushing over entire east and southeast faces; some sliding and crushing on northeast; crushing of refrozen wake on south
13 (0412A)	08:23	08:27	0.06 m/s to 280º	MY ice: 6.5 to 10 m	Hummock approaches the structure and disappears under rubble pile; load pulsates at approximately 0.5 Hz, increasing to 0.75 Hz; load is dampened after several minutes and vibration of the structure stops
	08:27	08:45	0.06 m/s to 280º	2 to 4 m (rubble pile 10 m)	Ice fails in flexure/buckling 50 m from east face behind rubble pile; crushing on northeast and southeast faces
13	08:45	09:27	0.08 m/s to 290º	2 to 4 m (rubble pile 10 m)	First crack starts in the ice off the north end of the east face, reducing confining pressure; ice riding over rubble at east face; rubble begins to collapse; crushing and rubble pile-up on southeast; crushing and sliding on south face; random vibrations of structure
	09:27	09:42	0.1 m/s to 290º	2 to 4 m (rubble pile 10 m)	Lead continues to open up; rubble on east face flows into lead; crushing on southeast face and southern half of east face; low loads on south face
	09:42	10:14	0.1 m/s to 290º	3 to 4 m	Ice loading on southeast and south faces; open water (lead) at east face
14 (0412B)	10:14	12:00 (approx.)	0.1 m/s to 290º	3 to 4 m (rubble piles 2-3 m high on east, 5-6 m high on southeast)	Loading and rubble pile-up on east and southeast faces

Time period # (and Event ID if applicable)	Time		Drift speed, direction	Ice type & thickness	Ice conditions and failure behaviour
	From	To			
15 (0412C)	12:57	14:12?	0.06 m/s to 290º	East face: MY ice 4 to 6 m (rubble pile 8 m); South face: MY ice, followed by refrozen wake	FY ice impacts southeast face and part of east and south faces at 12:57, followed by MY ice impact several minutes later. Crack forms off east face at approx. 13:04; multi-year ice crushing and rubble build-up on southeast face and 25% of east and south faces. East face video shows mixed crushing, mixed modal failure and sliding of MY ice on east face from 14:00 – 14:12. At some point between 13:30 and 14:05, the old wake from the March 7-8 events makes contact with the south face. (Video is available only for the south face starting at 14:05.) The wake moves past the structure, followed by FY ice impact on the south face at 15:00.
15 (0412D, 0412E)	14:12?	15:00	?	East face: FY ice, possibly still some MY ice interaction; south face: refrozen wake	Ice begins to transition to FY at approximately 14:12. East face video shows FY ice crushing on northern half of east face from 14:15 – 14:17, followed by mixed modal failure until the video record ends at 14:19. Bending failure occurs behind the crushing ice.
-	15:00	19:57	0.15 m/s to 290º	FY ice, 1.7 m; MY rubble pile 10 m high	Grounded rubble pile on east face from earlier events; thick first-year ice failing on rubble pile on east face; crushing on southeast face; crushing/sliding on northeast face. Video record shows FY ice failing by fracture at south face.
-	19:57	21:27	0.15 m/s to 290º	FY ice, 1.5 m; MY rubble pile 10 m high	Lead opens up behind rubble pile on east face, extending far to the east
-	21:27	21:43	N/A	MY rubble pile 10 m high	Open water around structure; rubble pile still intact

Time period # (and Event ID if applicable)	Time		Drift speed, direction	Ice type & thickness	Ice conditions and failure behaviour
	From	To			
-	21:43	?	0.13 m/s to 270º	FY/MY ice, 3.5 to 10 m thick	"Alpha" floe containing some multi-year ice impacts rubble pile at east face; crack forms in floe several minutes later

11.11.2 Event analysis

A DAY file starting on April 11 was used to establish zeros for instrument responses on April 12. A combination of DAY, FAST and EVENT files were available for analysis of the loading events during the day itself. In characterizing the factors affecting loads, the events and Sub-events identified in the video analysis of Section 10 are described in terms of time period, ice thickness, ice velocity, and failure mode in Table 28.

Table 28 Description of events and sub-events for April 12

Event ID	Sub-event number	Time Period	Ice thickness (m)	Ice velocity (m/s)	Failure Mode
0412A	full event	08:23:30 – 08:45:00	East face: 6m average (range: 3.3m to 10m with hummock) South face: FY ice (refrozen wake)	0.06	CR & CC (east face)
0412A -1	1	08:23:30 – 08:25:00	6	0.06	CR & CC
0412A -2	2	08:27:02 – 08:28:24	6	0.06	CR & CC
0412A -3	3	08:28:26 – 08:29:56	6	0.06	CR & CC
0412A -4	4	08:33:59 – 08:45:00	6		CR
0412B	full event	11:16:02 – 12:29:31	3.5 m average (range: 2.5 – 6m)	0.1	CC, CR, MM & SLW (east face)
0412B -1	1	11:16:02 – 11:24:51	3.5	0.1	CC
0412B -2	2	11:24:52 – 11:52:48	3.5	0.1	SLW & MM
0412B -3	3	11:52:49 – 11:57:12	3.5	0.1	CR
0412B -4	4	11:57:13 – 12:29:31	3.5	0.1	SLD
0412C	full event	13:00:07 – 14:01:04	5.9	0.06	CR, MM & SLD (East face)
0412C -1	1	13:00:07 – 13:01:32	5.9	0.06	CR
0412C -2	2	13:01:33 – 13:03:11	5.9	0.06	CR
0412C -3	3	13:03:12 – 13:08:46	5.9	0.06	CR
0412C -4	4	13:08:47 – 13:10:43	5.9	0.06	CR
0412C -5	5	13:10:44 – 13:14:57	5.9	0.06	CR
0412C -6	6	13:14:58 – 13:19:25	5.9	0.06	CR
0412C -7	7	13:19:26 – 13:42:30	5.9	0.06	SLD
0412C -8	8	13:42:31 – 13:50:15	5.9	0.06	CR
0412C -9	9	13:50:16 – 14:01:04	5.9	0.06	SLD & MM
0412D	full event	14:03:20 – 14:19:35	MY or SY ice, followed by FY	?	CR, SLD & MM (east face)
0412D-1	1	14:03:20 – 14:10:10	Thinner MY or SY ice (<5.9m)	?	CR, MM, SLD
0412D-2	2	14:10:10 – 14:19:35	Likely to be FY ice	?	CR, SLD
0412E	full event	14:19:35 – 14:35:31	2.2m average; mainly FY ice – possibly some MY rubble	?	CR & MM (East face)
0412E-1	1	14:19:35 – 14:20:56	2.2	?	CR
0412E-2	2	14:20:57 – 14:35:31	2.2	?	MM

Event **0412A** was the most active loading event of the season. In this event a hummock with a 3 m sail height failed against the east face of the Molikpaq, generating the highest load on the structure. An average ice thickness of 6 m has been estimated for this event. Three EVENT files at 50 Hz and a FAST "Weir-Jones" file at 1 Hz cover part of the interval between 08:18 and 08:48, the end and start of neighbouring DAY files, see Figure 51. This event involved dynamic loading on the east face during the 3 EVENT files (between 08:23 and 08:30), and represents the highest response from a strain gauge or

extensometer for the entire season. The loads up to 08:30 are based on one SG09 strain gauge, E2, and the east and west extensometers. For the latter part of this event, data from three strain gauges on the east face and the east face MEDOF panels are available for determining face loads. Where face load is only dependent on the E2 SG09 strain gauge, previous analysis of this event (Frederking and Sudom, 2007) indicated that it over predicts the face load. No adjustment is made here, but Section 13.1 describes a reduction factor for the one strain gauge, E2. The record for the lower MEDOF panel, 1030(E2), showed significant loading on it, however as the load on it increased, the load on its two neighbouring middle panels (1028 and 1029) was decreasing. When panel 1030 experienced its maximum load, about 08:36, load on panels 1028 and 1029 was almost back to zero. At 08:36:35 MEDOF panels, SG09 strain gauges and extensometers all experienced a sharp trop off to near zero loads. This is likely when the ice failed in flexure at the back side of the hummock, where the thickness was about 3.5m. Also of note, all MEDOF panels and strain gauges returned to close to their original zero values. Only the extensometers showed a zero shift over the event; the east face displaced about 15 mm to the west and the west face about 5 mm to the east, for a net East-West diameter decrease of 10 mm. Which translates to a force of 60 MN.

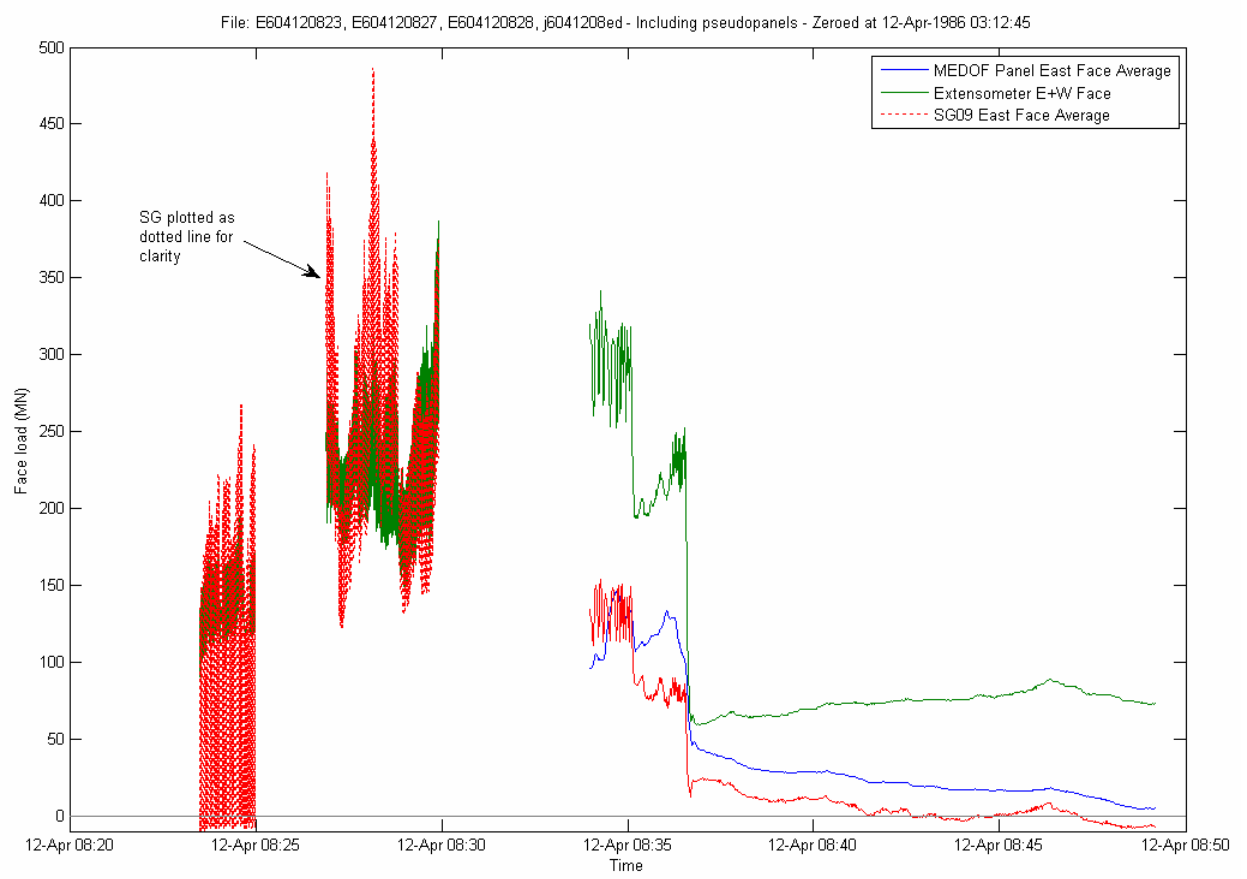

Figure 51 April 12 - East face loading, Event 0412A

The extensometer record in Figure 52 indicated negative loading on the south face around 08:35. This is due to the high loading on the east face at this time which causes an increase in the north-south diameter. The strain gauges on the south face indicate small compressive loading on the south face.

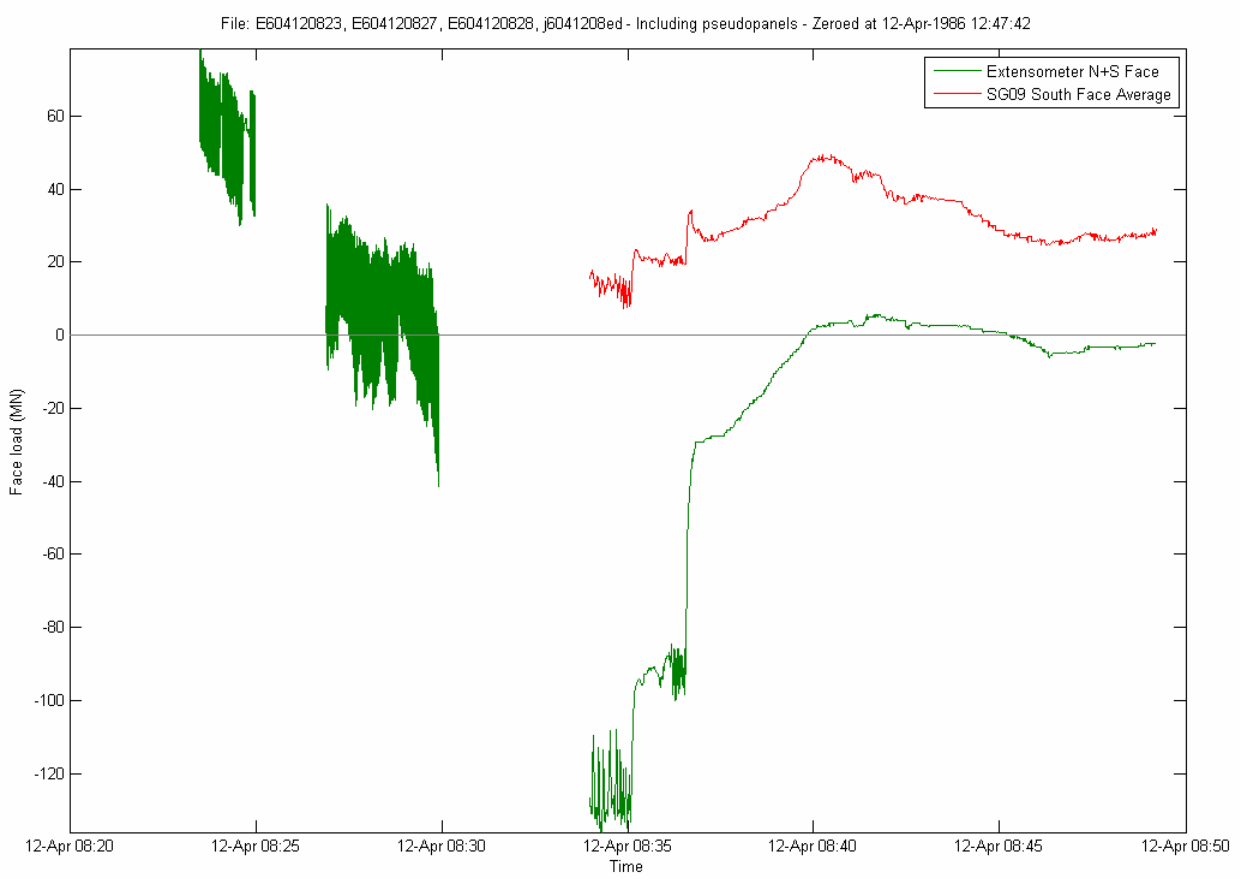

Figure 52 April 12 - South face loading, Event 0412A

The DAY file between 08:48 and the next FAST file, which started at 11:16, indicated forces in the range 100 to 200 MN on the south and east faces. These forces are upper bound values, since they were determined assuming maximum values on all panels were occurring simultaneously on MEDOF panels or SG09 strain gauges within each 5-minute recording interval. Event **0412B** involved loading on the east face in late morning, see Figure 53. Initially there was cyclic crushing with a period of about 2 minutes.

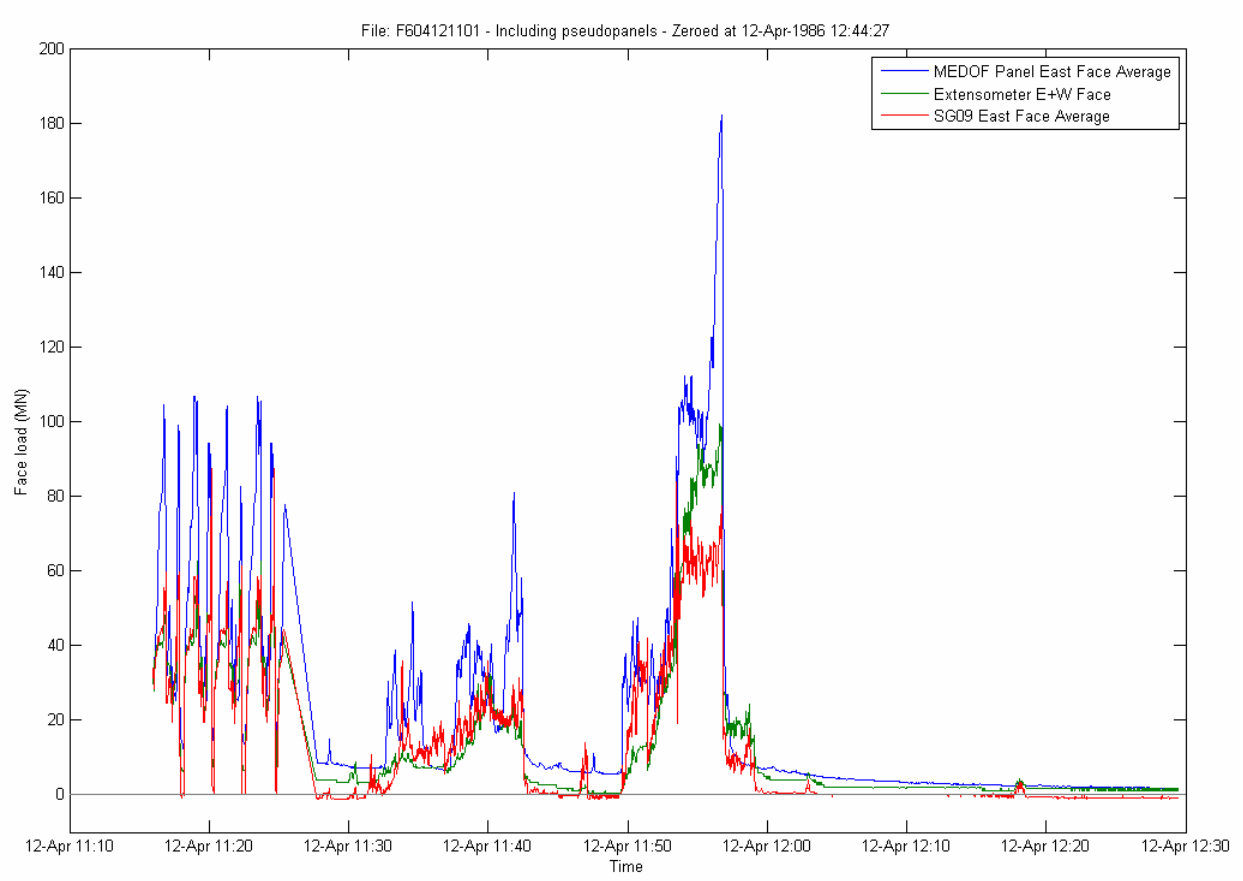

Figure 53 April 12 - East face loading, Event 0412B

Event **0412C** involved loading on the east and south faces in early afternoon. Higher loading was experienced on the south face than the east face.

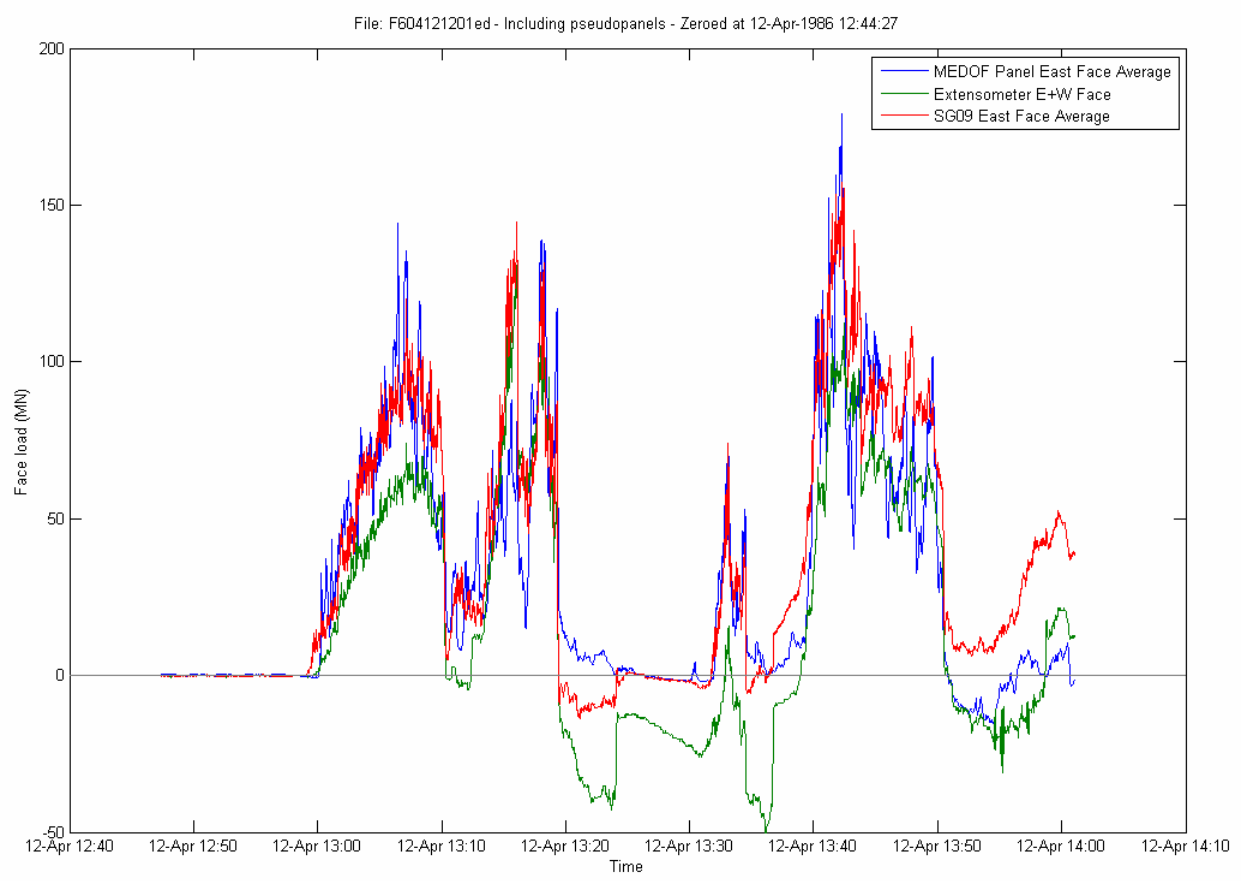

Figure 54 April 12 - East face loading, Event 0412C

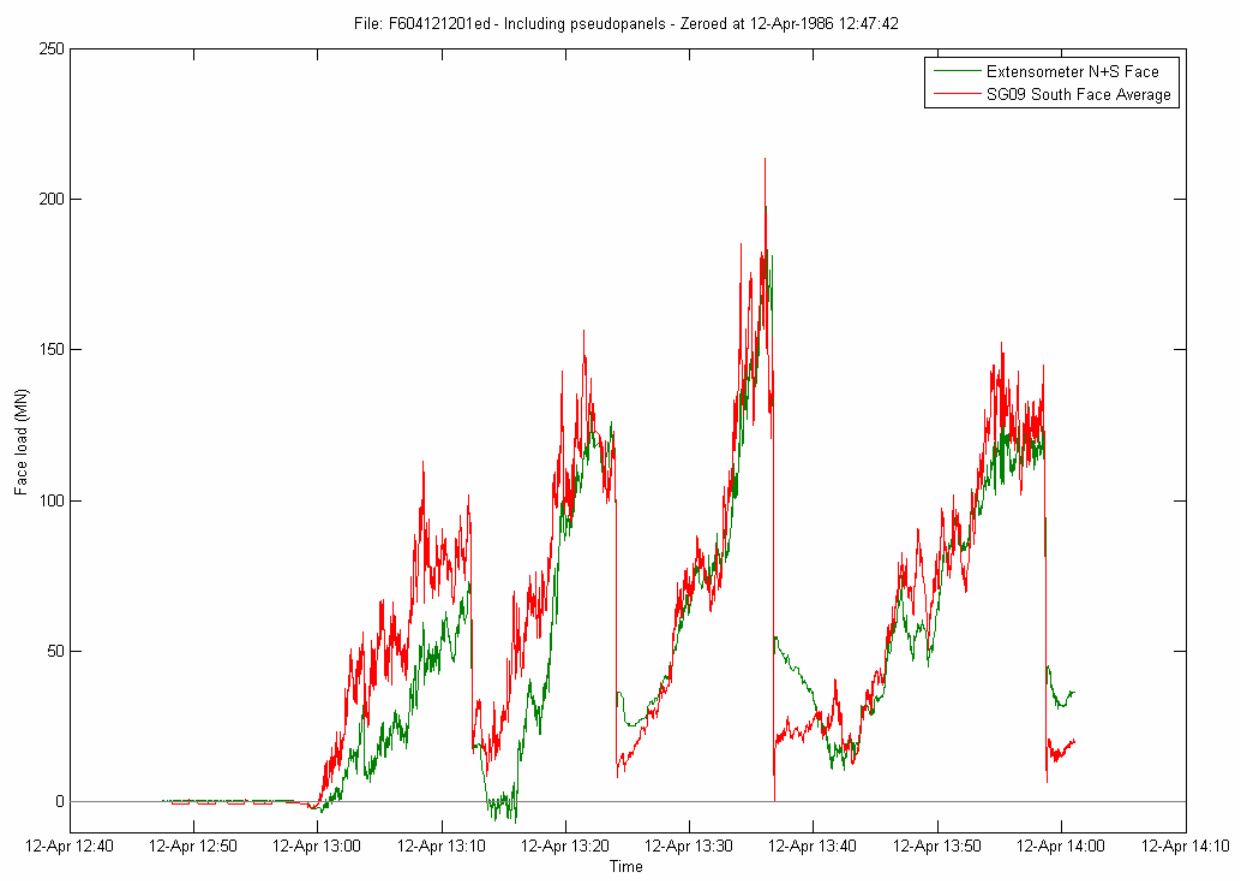

Figure 55 April 12 - South face loading, Event 0412C

Event **0412D** had loading on both east and south faces, but with lower loads.

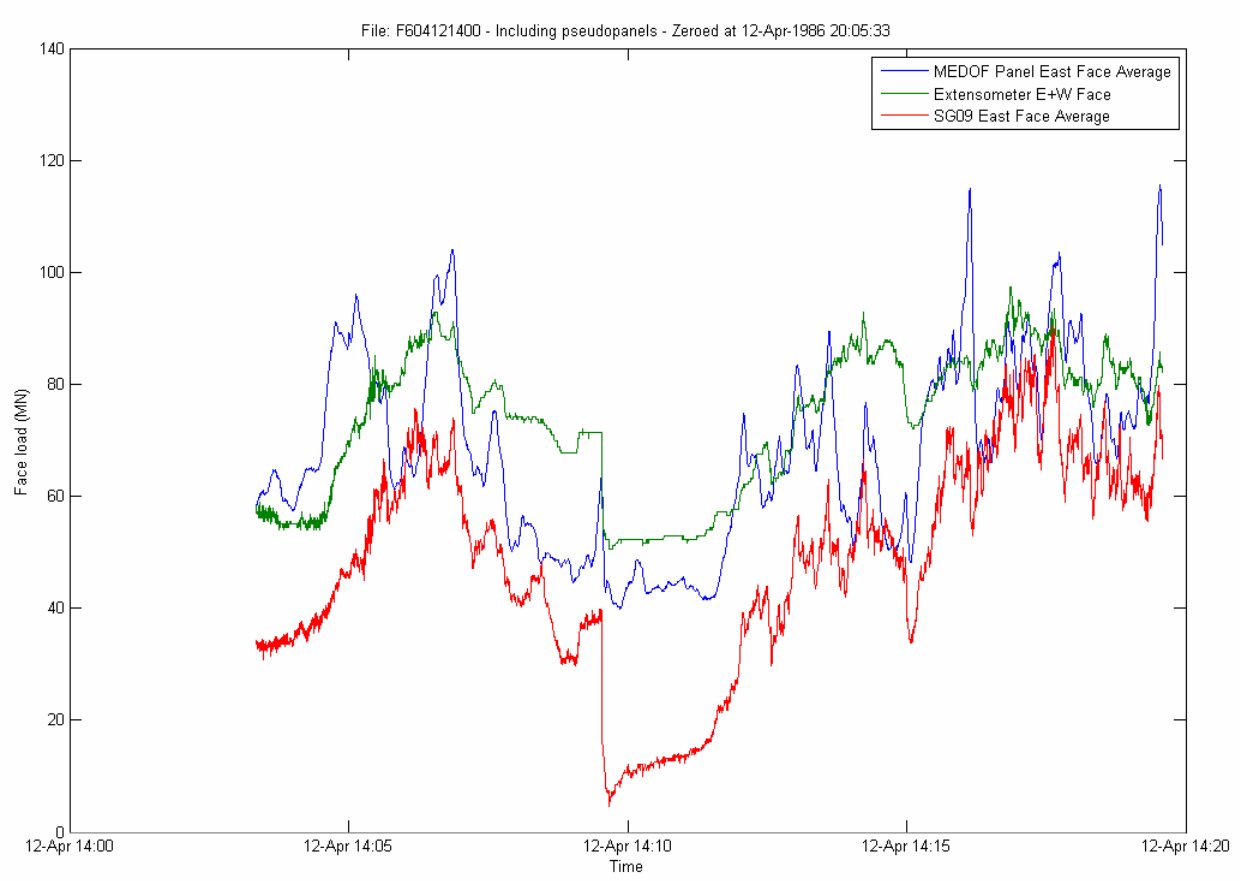

Figure 56 April 12 - East face loading, Event 0412D

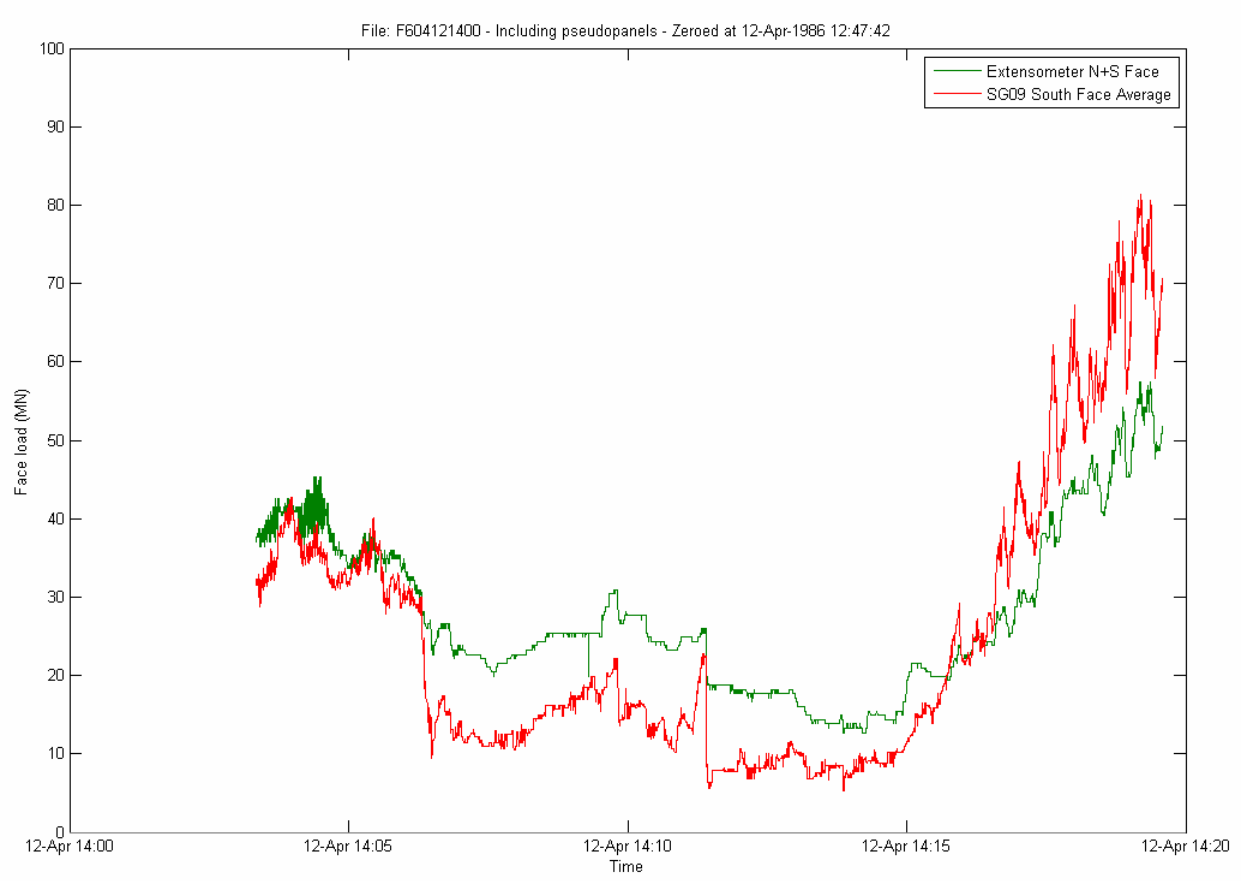

Figure 57 April 12 - South face loading, Event 0412D

Event **0412E** also involved loading on east and south faces late in the afternoon.

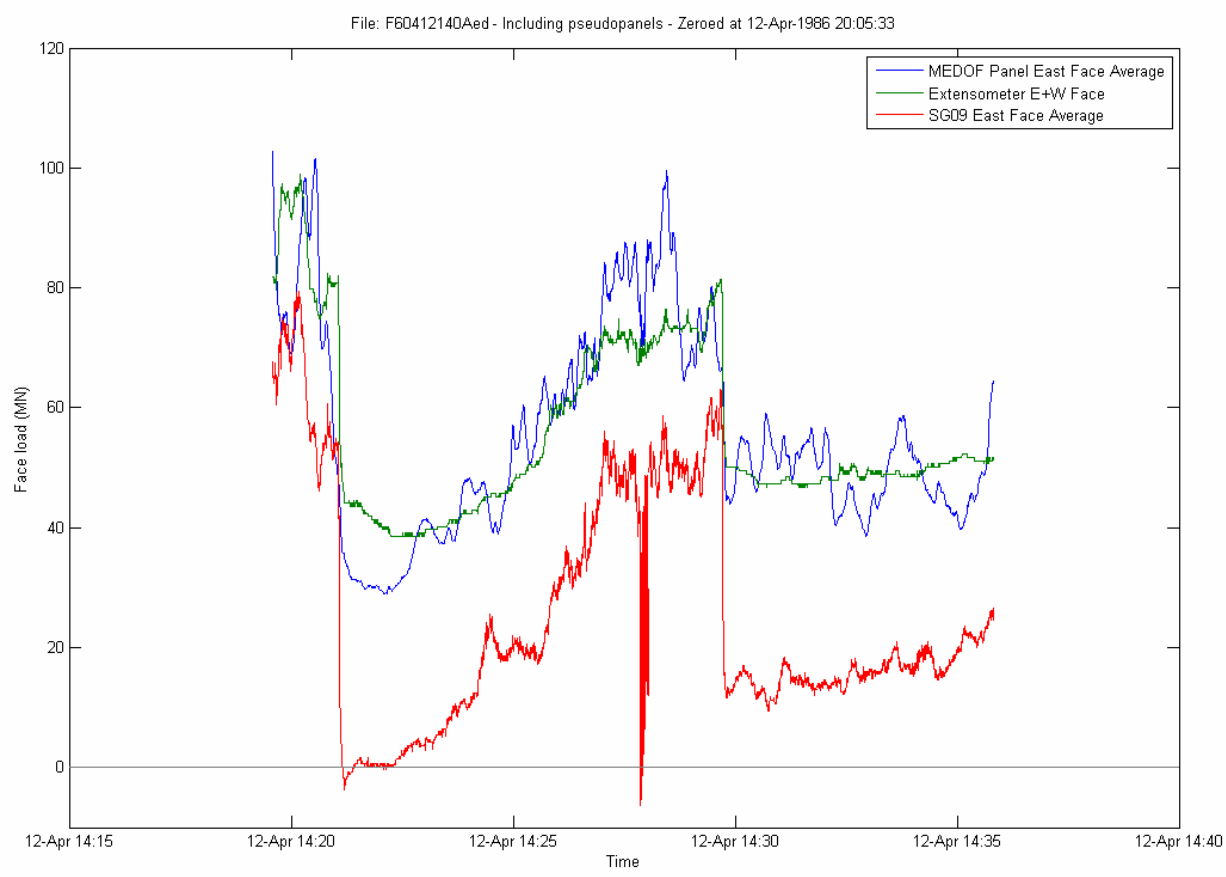

Figure 58 April 12 - East face loading, Event 0412E

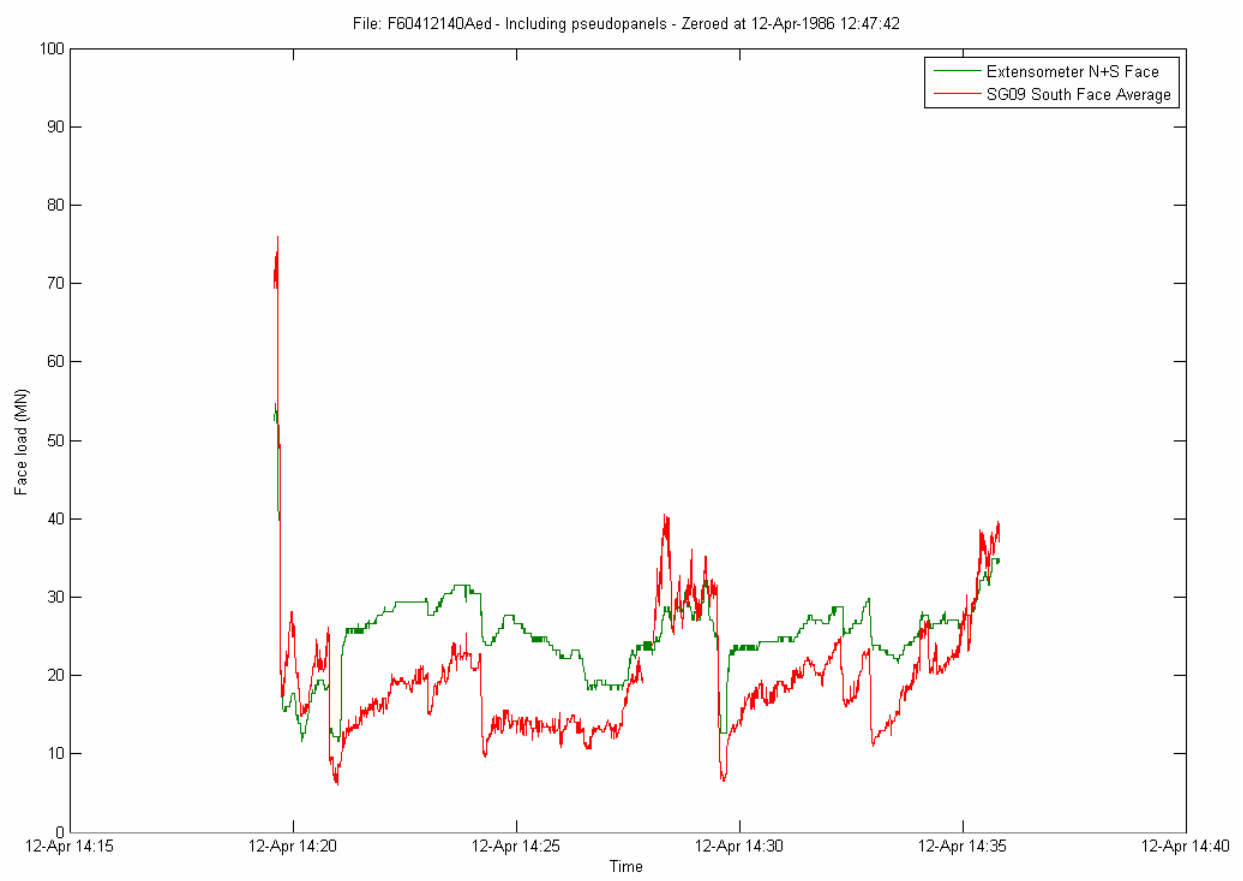

Figure 59 April 12 - South face loading, Event 0412E

11.12 May 12, 1986

11.12.1 Description of ice conditions and loading events

On May 12, it has been reported that a large floe of thick first-year ice with multi-year inclusions impacted the Molikpaq after open water conditions. The average air temperature for the preceding three days was -6 C, so this could be described as relatively warm ice. This event was documented in Timco et al (2005). Results of a helicopter survey carried out shortly after the event are presented in Figure 60. The actual area of the floe is outlined in red. Viewing the video and consultations with Michelle Johnston caused us to change the description of the floe to be second-year ice (Johnston, personal communication 2009). This did not have any affect on the estimated mass of the floe, but it gave an improved basis for estimating the thickness of the ice interacting during the event; most likely second-year ice in the thickness range 2.5 to 3 m. From descriptions in the NRC Ice Load Catalogue (Timco et al, 1999), ice thicknesses of 2.5, 2.7 and 3 m were taken successively during the interaction. If a multi-year inclusion impacted the structure, it may have been inclusion A (see Figure 60) at the end of the event ~03:27 when the floe had stopped. Notes by V. Neth found in the Gulf Canada files describing the May 12 event report for 03:01 “ice impact – thick FY ice (1.7-2.0 m). Started HP9845 at 4 Hz. Missed MY floe impact by 200 meters.”

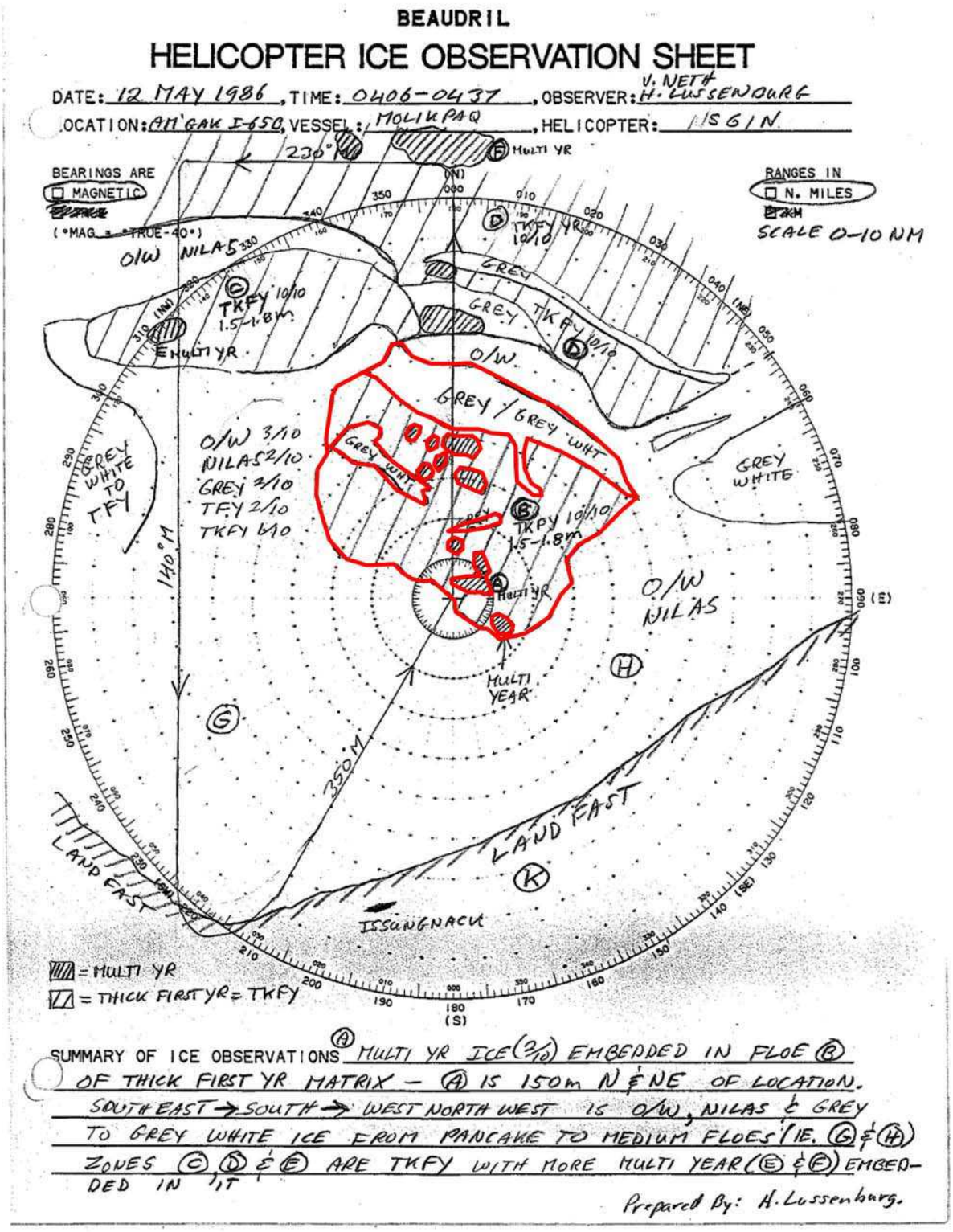

Figure 60 Description of floe impact Molikpaq on May 12

The edge of the floe was angled, so that initial contact was on the northeast corner and progressed westwards across the north face. Figure 61 shows the position of the floe at the end of the impact. The

floe did not advance any more that 150 m along the east side of the structure, by which time it stopped moving. Close examination of the acceleration record indicates floe movement stopped at 03:25:15.

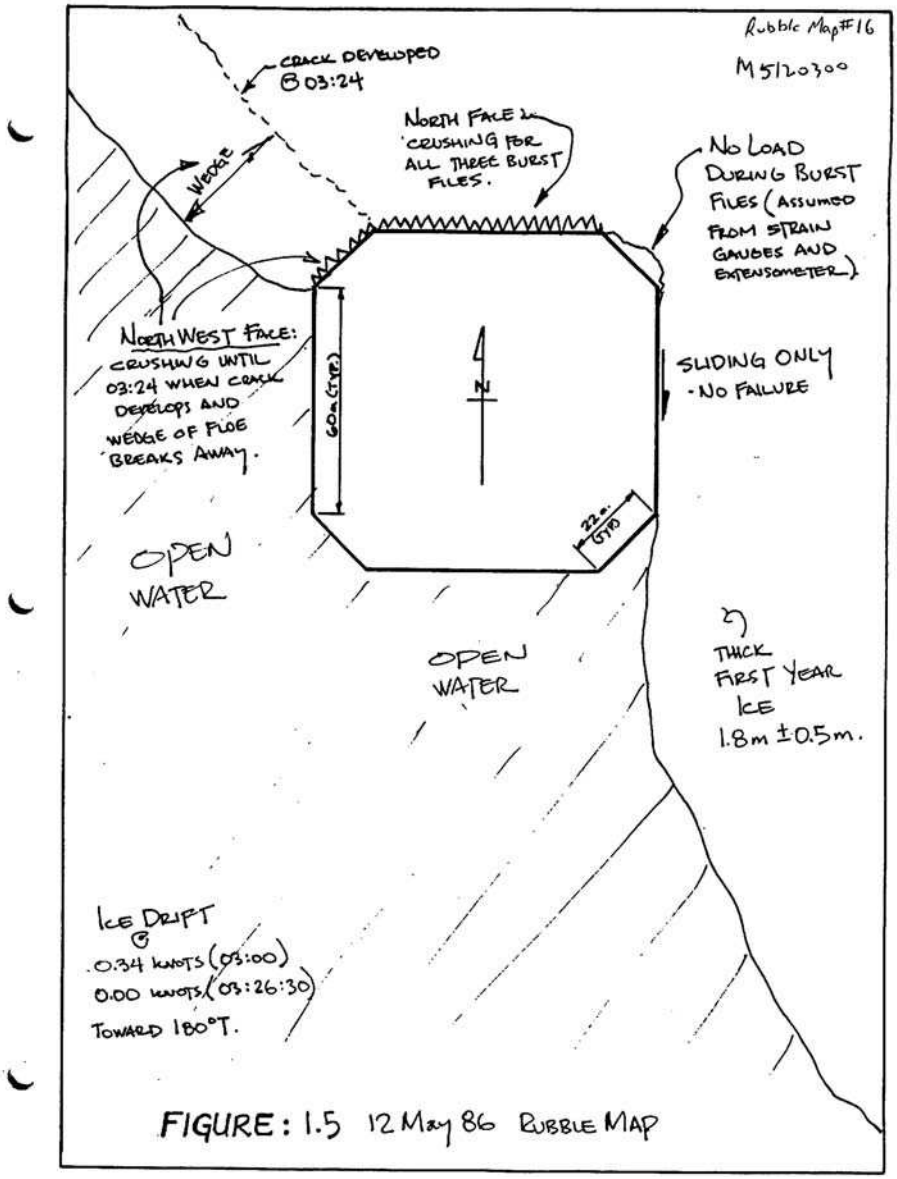

Figure 61 Sketch of the floe edge impact with Molikpaq.

A summary of the ice interaction is provided in Table 29.

Table 29 Summary of ice loading on May 12, 1986

Time period # (and Event ID if applicable)	Time		Drift speed, direction	Ice type & thickness	Ice conditions and failure behaviour
	From	To			
16 (0512A)	03:00	03:10	0.17 m/s, to 185º	FY with MY inclusions; level FY ice thickness 1.7 - 2m, MY ridge height average 1.5m, max 2.5m	Large floe (7 by 15 km) impacts Molikpaq at approximately 03:00. Initial contact on east corner of north face, and NE face. Prior to the impact a large grounded rubble pile was present off the east face. At 3:02 the rubble pile begins to slide across east face towards the south until it is clear of the face at 03:10.
	03:12	03:28	0.17 m/s to creep, to 185º	FY with MY inclusions; level FY ice thickness 1.7 - 2m, MY ridge height average 1.5m, max 2.5m	At 03:12 the floe makes full contact on the north face. On the western half of the north face, ice failure is mainly breaking into 2m blocks resulting in rubble build-up. On the NE face and eastern half of the north face, ice is crushing. By 03:20 the floe is slowing down and the Molikpaq experiences vibrations due to “hammering” movement of floe. By 03:28 the floe has virtually stopped moving.
	03:28	04:30	creep	FY with MY inclusions; level FY ice thickness 1.7 - 2m, MY ridge height average 1.5m, max 2.5m	Slow movement or pressure of ice floe causes low loads on north and east faces.

11.12.2 Event analysis

A DAY file starting on May 11 was used to establish zeros for instrument responses on May 12. It also indicated that significant loads were generated in the 15 minutes before the start of the FAST File at 03:10. The Sub-events identified in the video analysis of Section 10 were used to describe time periods, ice thickness, ice velocity, and failure mode in Table 30.

It has been previously been reported that significant loads were applied below the MEDOF panels so that face load estimates from the MEDOF panels are likely to be low (Klohn-Crippen, 1995). Our own review indicated that when the lower MEDOF panel (1010) was experiencing large loads the two neighbouring panels above it (1008 and 1009) were experiencing low loads. This is also supported by Johnston’s advice on ice thickness.

Table 30 Description of event and sub-events for May 12

Event ID	Sub-event number	Time Period	Ice thickness (m)	Ice velocity (m/s)	Failure Mode
0512A	full event	03:10:16 – 03:58:24	2.6m average	0.1 to creep	CR, MM & SLW
0512A-1	1	03:10:16 – 03:16:28	2.5	0.1	MM
0512A-2	2	03:16:29 – 03:19:28	2.5	0.09	CR
0512A-3	3	03:19:29 – 03:22:23	2.5	0.08	MM
0512A-4	4	03:22:24 – 03:27:33	2.7	0.08 to creep	CR
0512A-5	5	03:27:34 – 03:58:24	3.0	creep	SLW

The thick ice resulted in significant load application below the MEDOF panels so that face load estimates from the MEDOF panels are likely to be low (Klohn-Crippen, 1995).

The time series plot for Event **0512A** shows significant loading from linear averaging of MEDOF and strain gauge data, as well as the extensometers. The first part of the event until about 03:28 is crushing, followed after that by slow pressure on the north face.

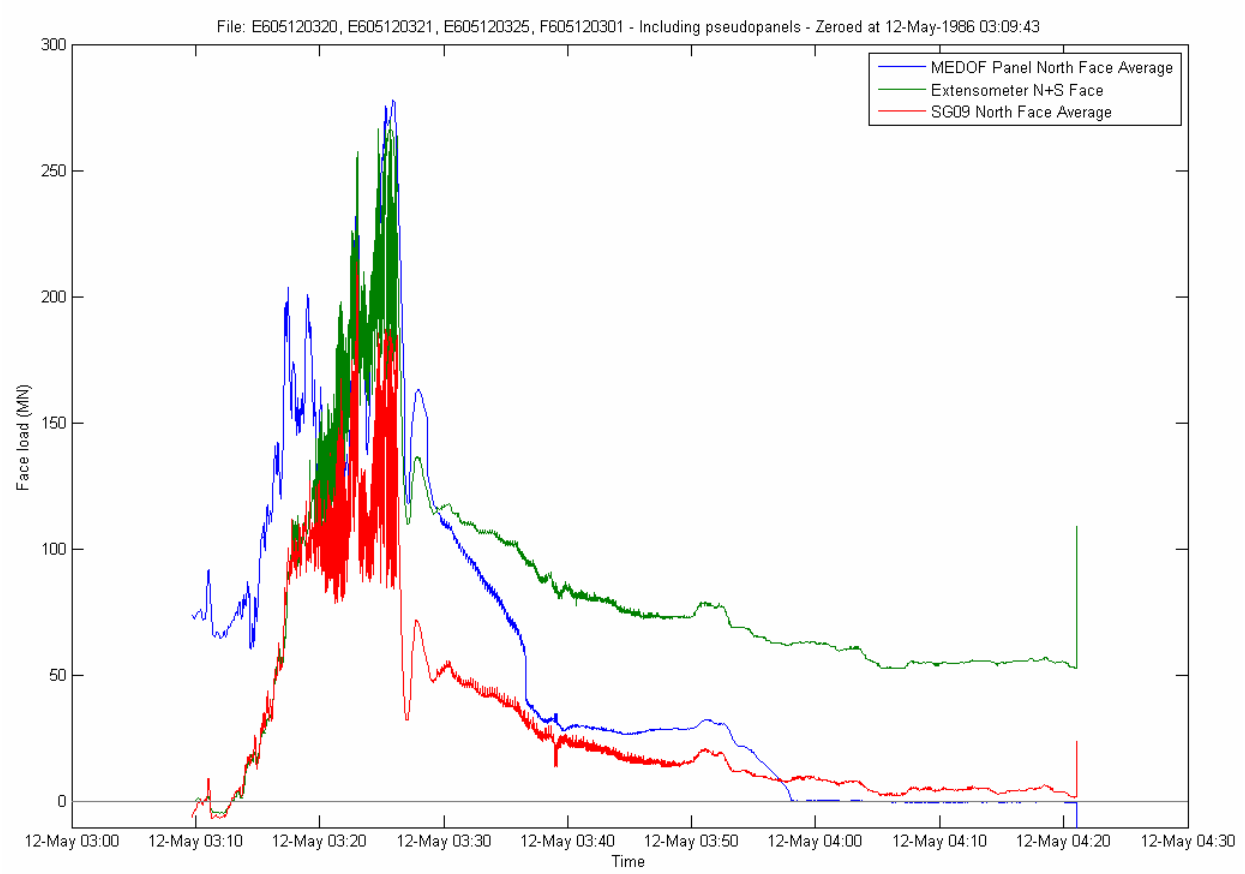

Figure 62 May 12 Event 0512A – North face loading

Loads determined from MEDOF panels, extensometers and strain gauges have been re-plotted on an expanded time scale in Figure 63 to facilitate comparison of the results depending on the instrument. While there is general similarity of the results between the different instruments, the time of peak loads do not correspond. The maximum load from the strain gauges was about 214 at 03:23. MEDOF panels and

extensometers also had a load peak at the same time, but it was not the largest one. The maximum load from extensometers was 267 MN at about 03:25.

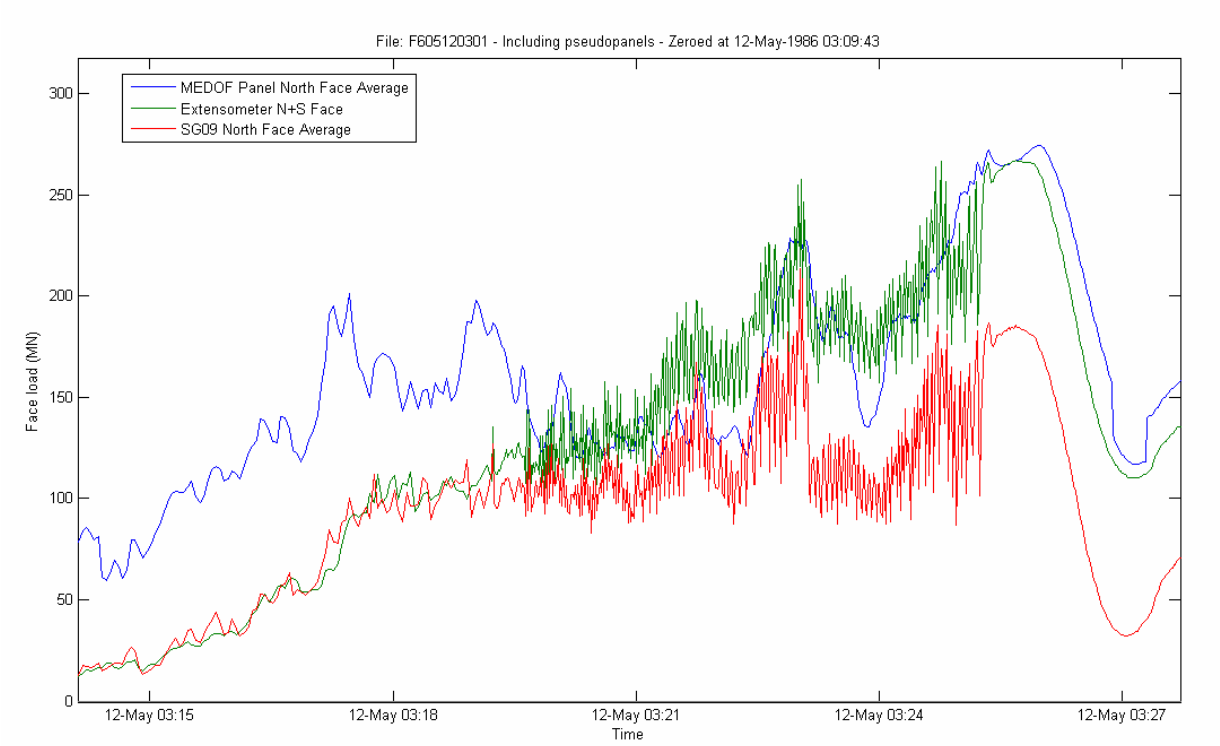

Figure 63 May 12 Event 0512A – North face loading with expanded time scale

11.12.3 Maximum Force Based on Floe Deceleration and Ring Deformation (IJA team)

This Section is taken from Section 5.2.2 of the Ian Jordaan & Associates report (Appendix B).

Approach

The maximum force during the May 12 event was calculated based on the floe deceleration, assuming that an accurate time trace of the relative force can be obtained from the extensometer readings. The floe velocity $v(t)$ at any time t is

$$v(t) = v(0) - \int_0^t a(t)\,dt \qquad \textbf{(11-1)}$$

where v(0) is the initial velocity and $a(t)$ is the acceleration at time t. At $t = t_{end}$ the floe is stopped so

$$0 = v(t_{end}) = v(0) - \int_0^{t_{end}} \frac{F(t)}{M_T}\,dt \qquad \textbf{(11-2)}$$

where $F(t)$ is the interaction force and M_T is the mass of the floe, including added mass. Assuming that the Molikpaq ring distortion is linearly related to the interaction force, i.e.

$$F(t) = K\Delta(t) \quad \textbf{(11-3)}$$

where $\Delta(t)$ is the distortion at time t and K is the corresponding stiffness, one obtains

$$\int_0^{t_{end}} \frac{K\Delta(t)}{M} dt = v(0) \quad \textbf{(11-4)}$$

or

$$K = \frac{M \cdot v(0)}{\int_0^{t_{end}} \Delta(t)\, dt} \quad \textbf{(11-5)}$$

Calculations

It is necessary to determine the appropriate combination of extensometer readings to represent the variation in load. The stiffness is determined by calibration such that the resulting load causes the floe to stop in the observed time.

Following Timco et al. (2005), the mass of the floe is estimated assuming a rectangular floe with length 15000 m, width 7000 m, average thickness 2.5 m, and density of ice equal to 1000 kg/m3 as 260 million tonnes. The initial floe velocity was taken as 0.18 m/s and that the floe was observed to effectively stop after 27 minutes.

The effect of added mass has been taken into account using the relationship:

$$M_T = \left(1 + \frac{h_s}{2W_D - h_s}\right) M \quad \textbf{(11-6)}$$

from Marcellus and Morrison (1982), where h_s is the floe draft; W_D is the water depth and M is the mass of the floe. A value of 5 m was used for the floe draft, giving an added mass of 8.8%.

Day file data that covers the period immediately before and through the first 9 minutes of the impact was also considered. The combined day file and fast file data up to the end of the impact are shown in the figure below. The day file data consists of the average, maximum and minimum values over the 5 minutes preceding each record. It appears that there could have been some loading before 3:01 a.m. on May 12th but we have used 3:01 a.m. as the impact start time in further analysis.

Dynamics of Interaction

The interaction was characterized by dynamic action induced by the ice compressive failure at the loaded face. The variation of load, as expressed by the extensometer readings (appropriately scaled) has been

taken into account in the analysis. Local fluctuations in displacement will take place at the contact zone, as the load rises and rapidly falls after each pulverization event. In the analysis, the situation further back into the floe was accounted for, where the movement would be steady. The dynamic action does not involve movements of the structure as a whole; it is confined to movements of the structure wall and a small amount of liquefied soil behind. The inertial mass involved in the vibration is therefore relatively small.

Further analysis of the dynamic situation would be useful and interesting, but is beyond the scope of the present work. We do not consider that a significant change to the present estimates of load would result.

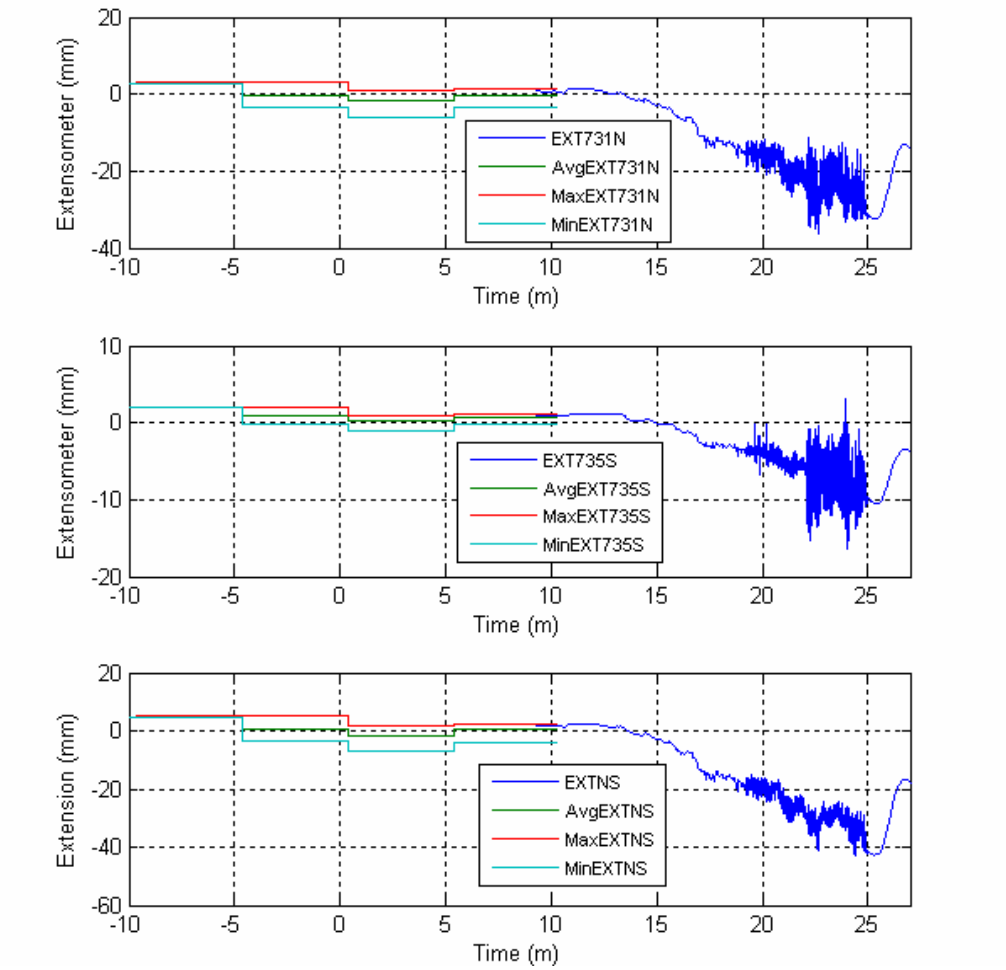

Figure 64 Combined Day File and Fast File Information for May 12th Impact

The method previously documented has been used to determine the load trace necessary to stop the floe in 27 minutes, assuming that the load is proportional to the North-South ring distortion. Figure 65 below shows a time trace of the North-South distortion, corrected for the initial offsets shown at time -10 minutes in Figure 64 above, and shows the load trace required to stop the floe in 27 minutes. The necessary global stiffness was 2.19 MN/mm and the maximum load was 105 MN. It is possible but not certain that the floe underwent some rotation during the event; this would have the effect of reducing the kinetic energy involved in failure of the ice.

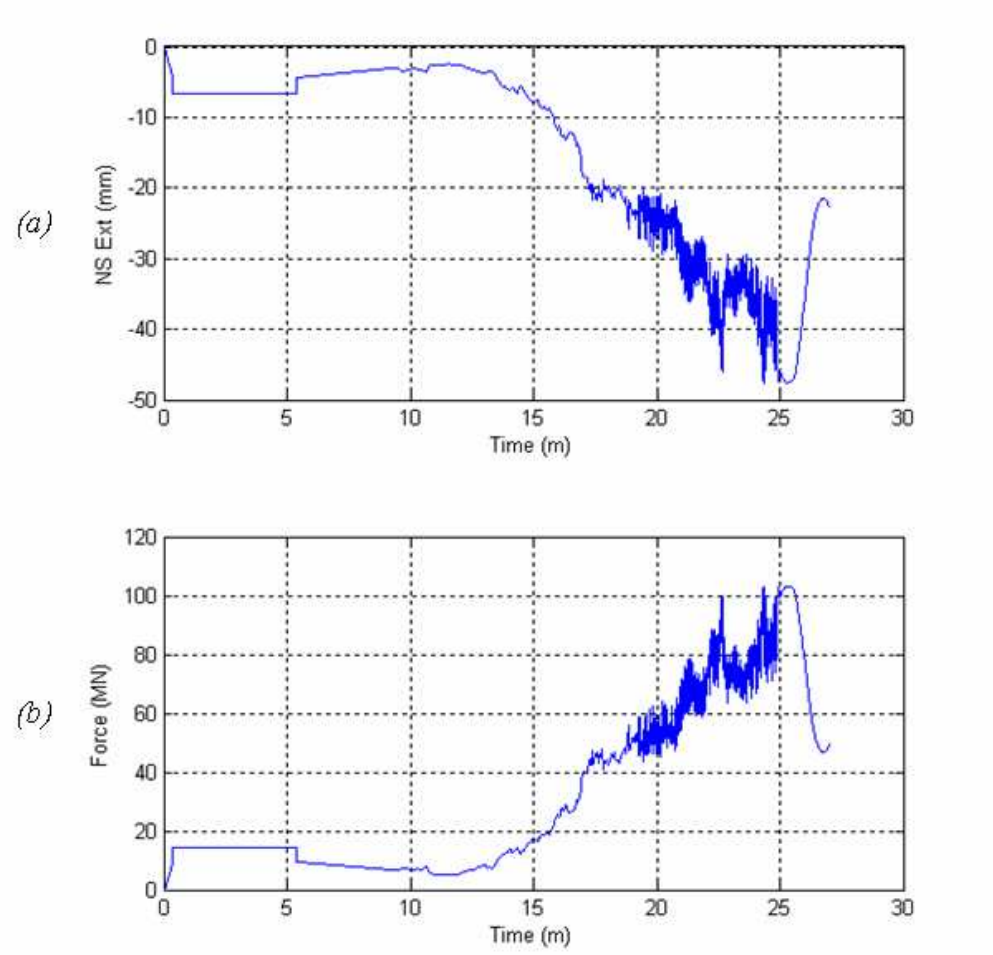

Figure 65 (a) North-South distortion, corrected for initial extensometer offsets; (b) corresponding load trace required to stop the floe in 27 minutes.

An analysis of possible uncertainty in the time during which the floe deceleration proper occurred has been carried out. To reflect this, an alternative approach removing the first 12 minutes of the impact has been considered. The contribution for the first 12 minutes appears to correspond to small loads based on the extensometer ring distortion. The results of this approach can be seen in Figure 66 which leads to an increased global stiffness and maximum global load required to stop the floe in 15 minutes as opposed to the 27 minute approach described previously. A structural stiffness of 2.89 MN/mm with a maximum global load of 130 MN is the result of this.

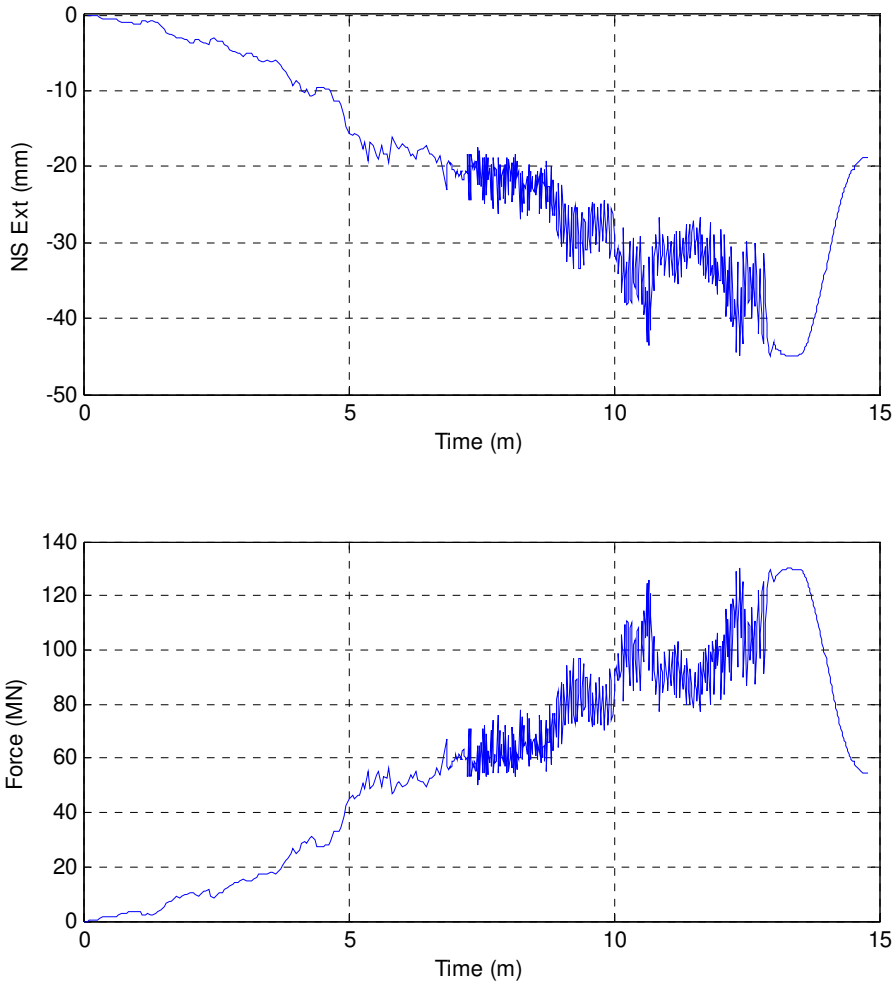

Figure 66 (a) North-South distortion, adjusted such that 12 minute segment with low loading is removed; (b) corresponding load trace required to stop the floe in 15 minutes.

11.13 May 22, 1986

11.13.1 Description of ice conditions and loading events

On May 22, 1986, multi-year ice loaded the east, northeast and north faces. The mean air temperature for the three preceding days was -9ºC. The Ice Observer reports indicated ice had been stationary for several days before it began to drift to the west at 0.1 to 0.2 knots. The ice cover was described as $2/10^{th}$ medium (100-500 m) multi-year floes in thick first-year ice. More detailed description of the ice interacting with the structure is given in Table 31.

Table 31 Summary of ice loading on May 22, 1986

Time period # (and Event ID if applicable)	Time		Drift speed, direction	Ice type & thickness	Ice conditions and failure behaviour
	From	To			
17 (0522A)	08:30	09:45	Creep to 210º	MY ice, 2 – 3 m thick	Crushing and rubble pile-up on north, northeast and east faces. Some sliding on east face. Lead on southern part of east face (location E3).
18 (0522B)	14:30	16:00	0.05 m/s to 240º	MY ice, 3 – 4 m, with ridges up to 2m high	Crushing and sliding begins on east face; no loading on north and northeast. At an undetermined time (most likely approximately 15:00), crushing begins on northeast and north face. By 16:00 there is no load on east face, and the north and northeast faces are fully loaded.

11.13.2 Event analysis

In characterizing the factors affecting loads, the events and Sub-events identified in the video analysis of Section 10 are described in terms of time period, ice thickness, ice velocity, and failure mode in Table 32.

Table 32 Description of events and sub-events for May 22

Event ID	Sub-event number	Time Period	Ice thickness (m)	Ice velocity (m/s)	Failure Mode
0522A	full event	08:39:23 – 09:50:27	2.5	creep	SLW & MM (North face)
0522A -1	1	08:39:23 – 09:16:56	2.5	creep	SLW
0522A -2	2	09:16:57 – 09:21:25	2.5	creep	MM
0522A -3	3	09:21:26 – 09:29:50	2.5	creep	SLW
0522B	full event	13:58:07 – 15:11:32	3.5	creep to 0.05	CR, SLD & SLW (North face)
0522B -1	1	13:58:07 – 14:01:04	3.5	creep	CR
0522B -2	2	14:01:05 – 14:06:43	3.5	creep	CR
0522B -3	3	14:06:44 – 14:54:50	3.5	0.05	SLD
0522B -4	4	14:54:51 – 14:56:54	3.5	0.05	CR
0522B -5	5	14:56:55 – 15:01:58	3.5	0.05	CR
0522B -6	6	15:01:59 – 15:11:32	3.5	0.05	SLW

The DAY file preceding Event **0522A** did not have any loading on the north face, but there were a few lower level, ~50 MN, loading events on the east face between 05:00 and 07:25 on May 22. It was also used to establish zeros for the FAST file. Between 08:00 and the beginning of Event **0522A** at 08:39 significant load developed on N3 and NE. From the beginning of Event **0522A,** loading was on the north face, with load levels exceeding ~100 MN. Then at 09:37 loading switched to the east face and magnitudes of ~40 MN, see Figure 67 and Figure 68. The extensometer record in Figure 67 indicates a negative load on the east face between 09:20 and 09:37, which is not possible. However during this time

there was a large load on the north face which caused the East-West diameter of the caisson to increase. Producing an apparent negative load. None of the lower MEDOF panels experienced any significant loading during this event, which supports taking an average ice thickness of 2.5 m for this event. The DAY file between this event and Event **0522B** did not indicate any loading on the north face, but there were several loadings, up to ~50 MN on the east face. There was also active loading on the northeast corner for this period.

For Event **0522B,** Figure 69 and Figure 70 show loading was initially on the north face with a maximum of ~140 MN until 14:07 when loading switched completely to the east face. Around 14:55 loading began to pickup on the north face again. Then at about 15:00 the loading switched back to the north face, while the load on the east face dropping off rapidly. Between 15:00 and 15:10 the maximum load on the north face was ~140 MN. The northeast corner experience loading during most of this event. Only the lower MEDOF panel on the north face experienced any significant loading during this event and that was for the last 10 minutes of the record of the event, to 15:11.

Loading for the two May 22 events was on either the north or east faces, in combination with loading on the northeast corner. When there was loading on both faces at the same time it was much lower than when loading was exclusively on one face.

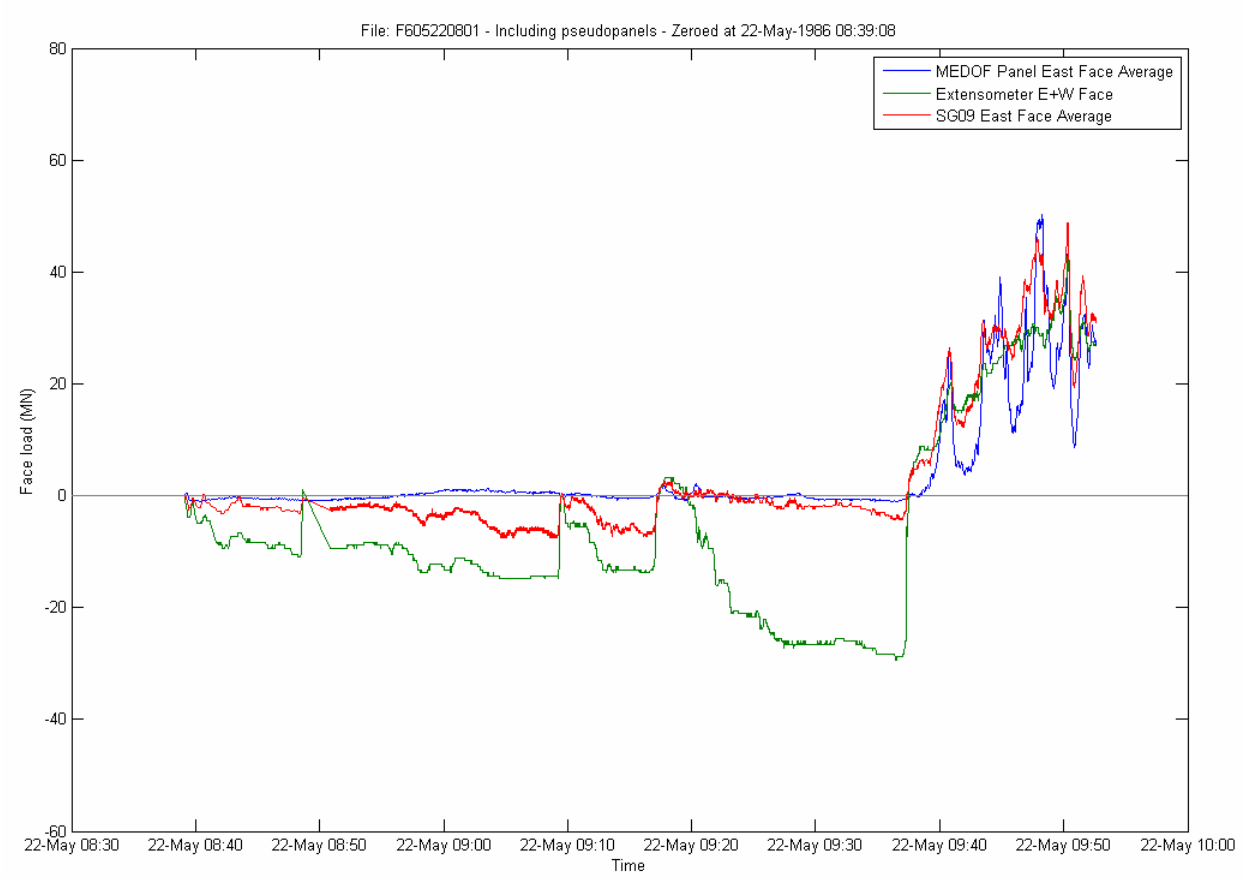

Figure 67 May 22 East Face loading, Event 0522A

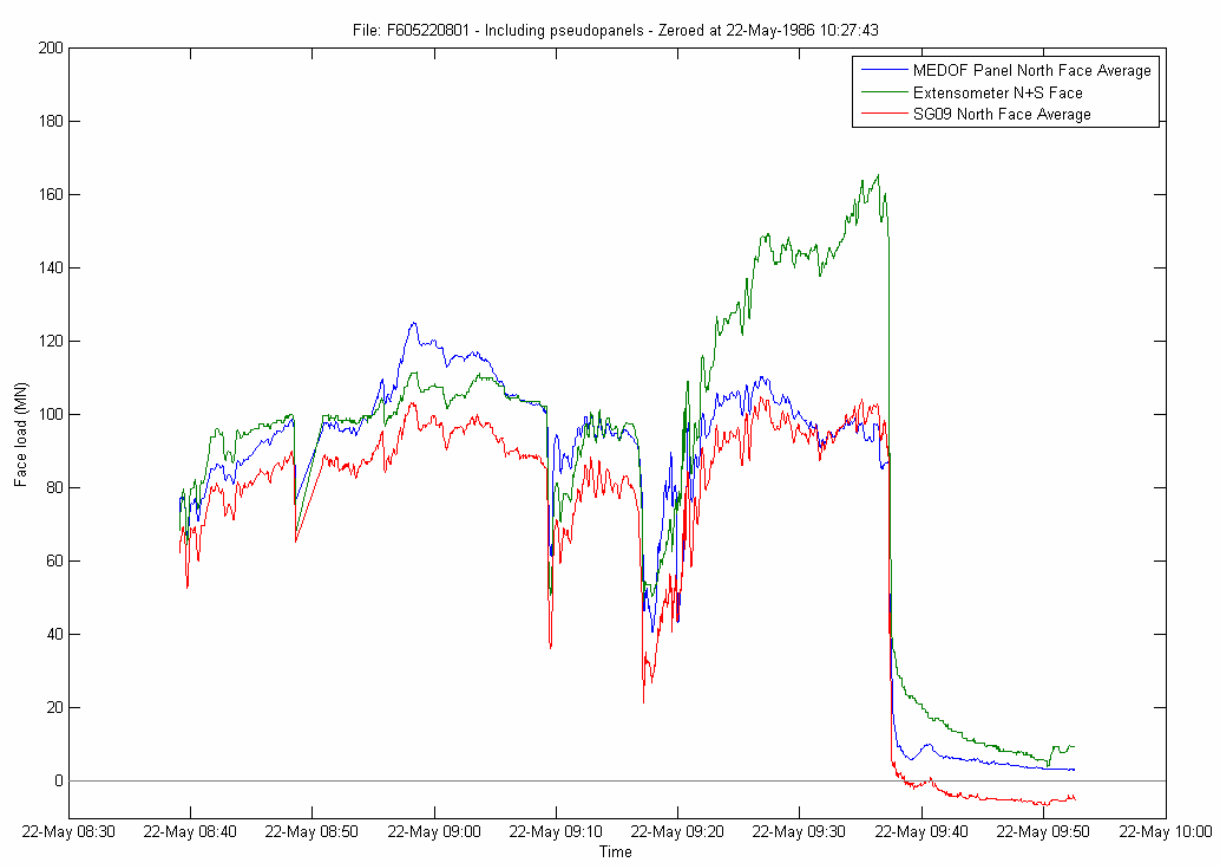

Figure 68 May 22 North Face loading, Event 0522A

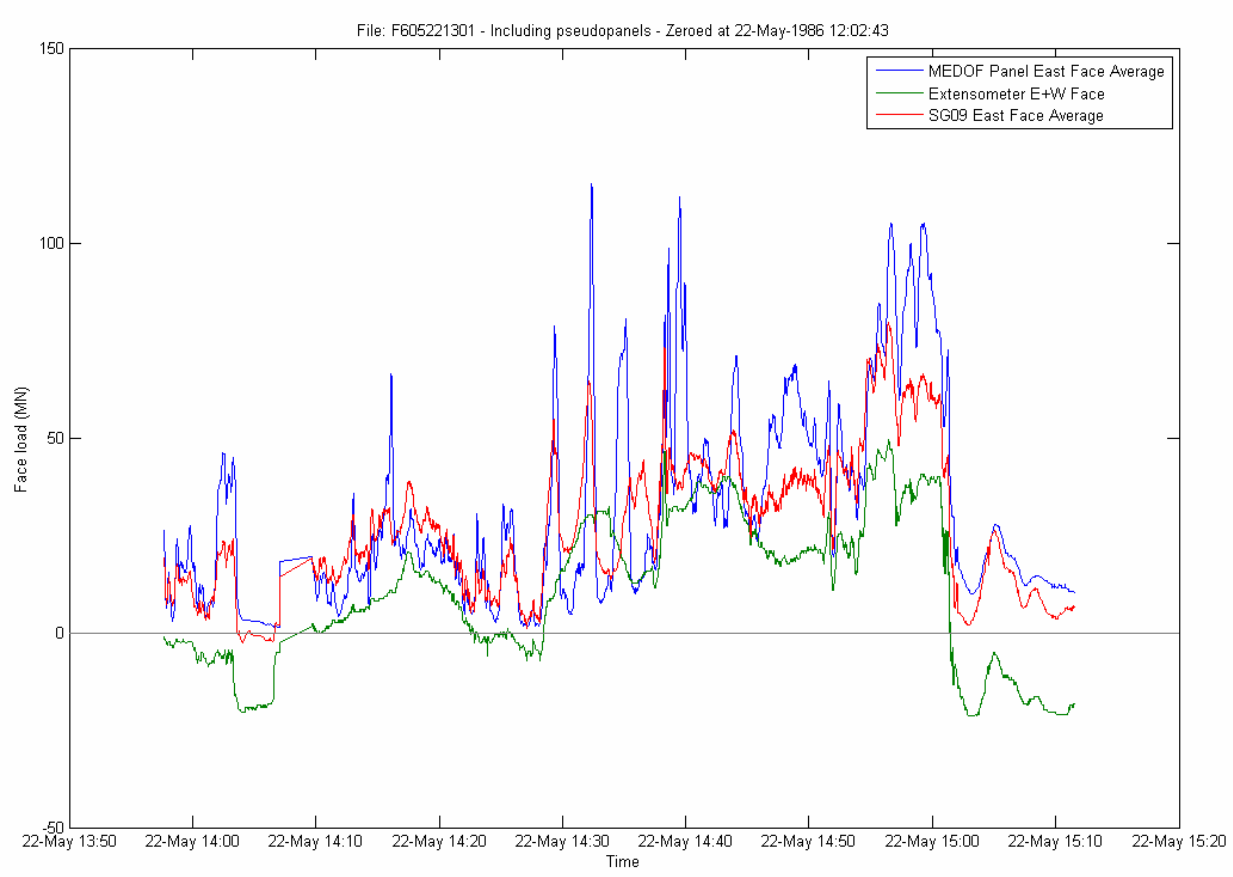

Figure 69 May 22 East Face loading, Event 0522B

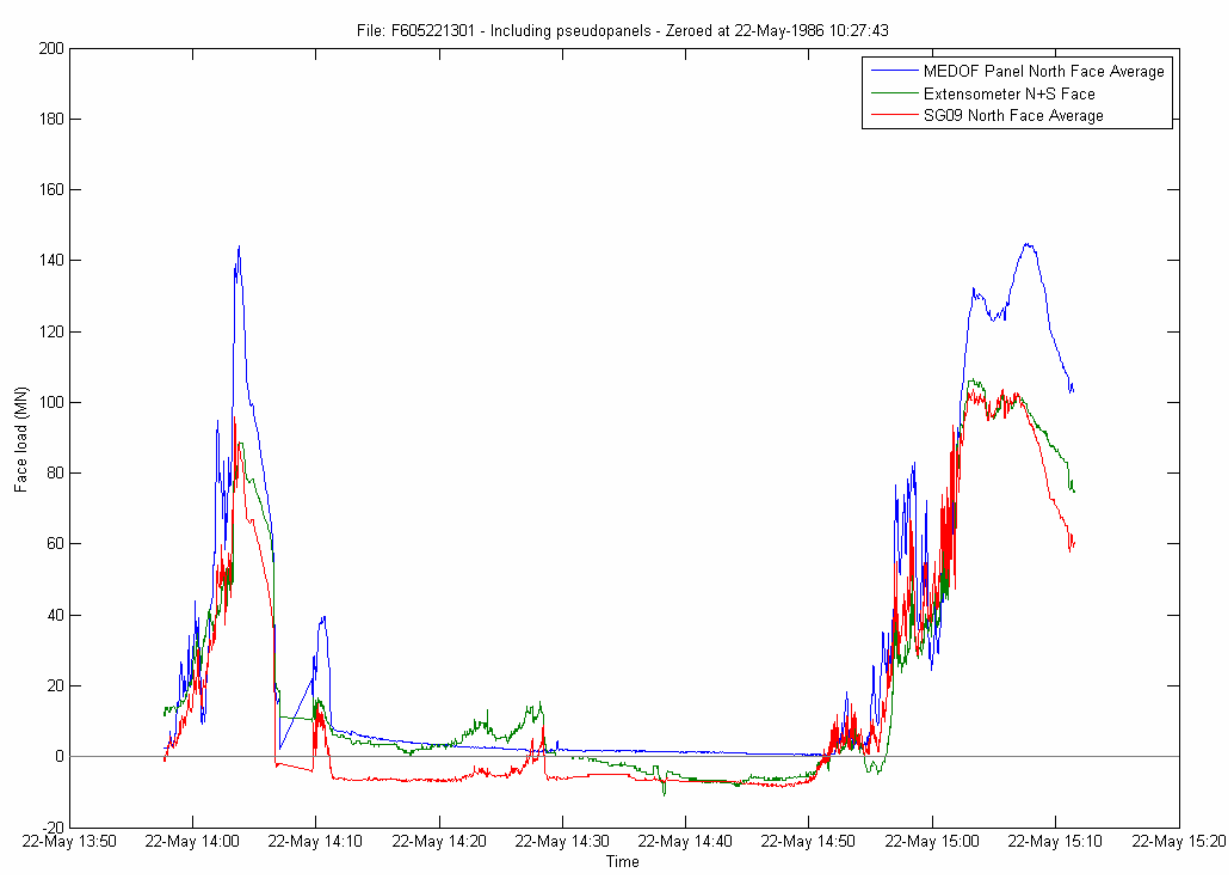

Figure 70 May 22 North Face loading, Event 0522B

An interesting loading feature was noted on the east face between 14:27 and 14:37, where Figure 69 shows 3 successive load peaks in the MEDOF and strain gauge derive loads, but much lower loads from the extensometer record. Closer examination of the MEDOF group and SG09 strains, Figure 71, shows what can be interpreted as a moving local ice load, most likely a corner of a multi-year floe. The load moves southwards from E1 to E2 to E3, a distance of about 40 m in 6 minutes, at a speed of about 0.1 m/s. During this period that was no loads at all on any of the north face or northeast corner MEDOF panels or SG09 strain gauges. This is a case where attributing the load measured on one MEDOF panel group or SG09 strain gauge, which represents a width of about 2 m, to a width of about 20 m gives a grossly exaggerated load. In this case the extensometer gives the best indication of the load on the east face. The record also shows the difference in the response of the MEDOF panels and SG09 strain gauges to a localized load. MEDOF panels only respond when there is load directly on them, whereas the SG09 strain gauge on a bulkhead already responds to load some distance from it due to structural interconnectivity. This is illustrated by the SG09 strain-based peaks, which are wider than the MEDOF panel based load peaks.

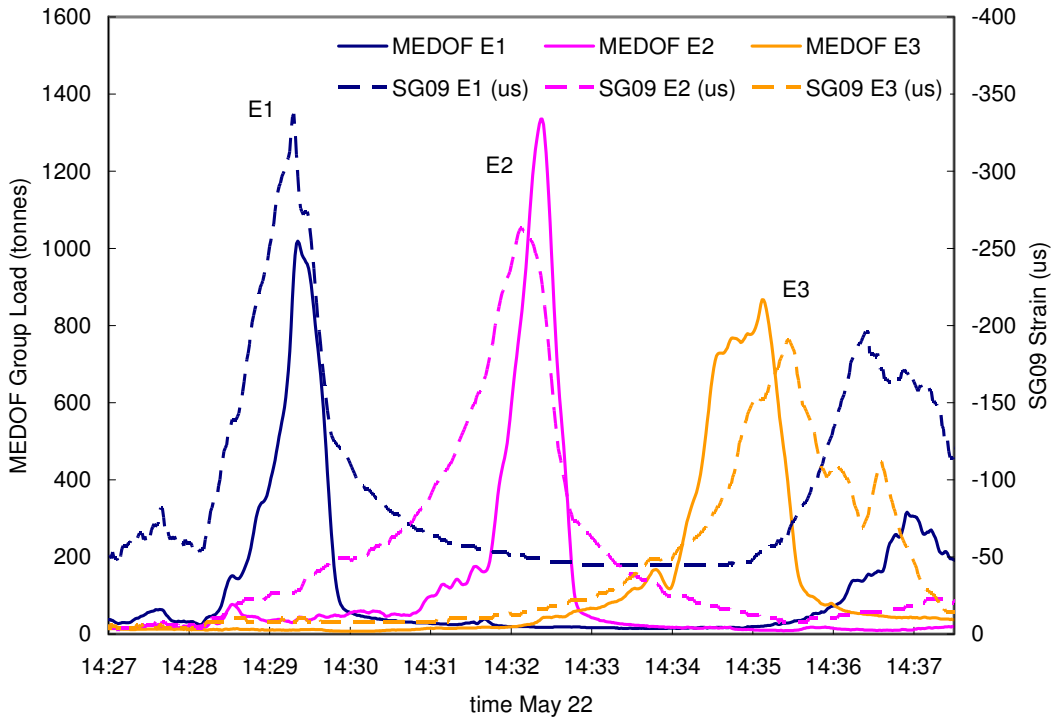

Figure 71 May 22 East Face moving load (time expansion of Event 0522B)

11.14 June 2, 1986

11.14.1 Description of ice conditions and loading events

On June 2, a vast floe of medium to thick first-year ice with 2/10^{ths} multi-year inclusions made contact with the Molikpaq (Klohn-Crippen, 1995). Ice movement was from the east at a relatively low velocity. The average air temperature for the previous three days was -2 C, so this could be described as a warm ice loading . The floe moved against the Molikpaq during the two time periods described in Table 33. No rubble maps are available for this interaction.

Table 33 Summary of ice loading on June 2, 1986

Time period # (and Event ID if applicable)	Time		Drift speed, direction	Ice type & thickness	Ice conditions and failure behaviour
	From	To			
19 (0602A)	13:00	14:20	Creep – 0.01 m/s, to 250º	FY ice with 2/10^{ths} MY inclusions; thickness: 1.8 – 2.5 m	Vast floe impacts the Molikpaq. Examination of video shows a slow push on the east face until the ice begins moving at 13:11. Interaction on east face involved creep loading, then crushing and sliding and sliding of the ice toward the south. By the end of the time period, crushing was occurring only on the southern third of the structure (MEDOF panel group E3), while the rest of the east face is in open water.
20 (0602B)	20:00	21:30	Creep – 0.01 m/s, to 250º	FY ice with 2/10^{ths} MY inclusions; thickness: 1.8 – 2.5 m	Ice begins moving against the east face of the Molikpaq once again. Examination of video shows a slow push on the east face until the ice begins crushing on the southern half of the east face at 20:37. Flooding around northern part of east face (MEDOF panel group E1). Flexural failure occurs behind MEDOF panel groups E2 and E3 at 20:42, followed by mixed modal failures and periods of crushing across various parts of the east face. By 21:02 loads have dropped off and brash and small fractured floes slide northwards on the east face. Considerable areas of open water.

11.14.2 Event analysis

In characterizing the factors affecting loads, the events and Sub-events identified in the video analysis of Section 10 are described in terms of time period, ice thickness, ice velocity, and failure mode in Table 34.

Table 34 Description of events and sub-events for June 2

Event ID	Sub-event number	Time Period	Ice thickness (m)	Ice velocity (m/s)	Failure Mode
0602A	full event	13:02:26 – 14:16:45	2 (est.)	creep to 0.01	CR, MM, SLW & SLD
0602A -1	1	13:02:26 – 13:11:30	2	creep	SLW
0602A -2	2	13:11:31 – 13:32:05	2	0.01	CR
0602A -3	3	13:32:06 – 13:41:08	2	0.01	SLD & MM
0602A -4	4	13:41:09 – 13:51:53	2	0.01	CR
0602A -5	5	13:51:54 – 13:55:09	2	0.01	CR
0602A -6	6	13:55:10 – 13:58:04	2	0.01	SLD
0602A -7	7	13:58:05 – 14:10:16	2	0.01	CR
0602A -8	8	14:10:17 – 14:16:45	2	0.01	CR
0602B	full event	20:16:55 – 21:24:33	FY ice 2m (est.), with MY inclusions	creep to 0.01	SLW, CR & MM
0602B -1	1	20:16:55 – 20:40:19	2	creep	SLW
0602B -2	2	20:40:20 – 20:43:53	2	0.01	CR
0602B -3	3	20:43:54 – 21:00:50	2	0.01	MM
0602B -4	4	21:00:51 – 21:24:33	2	0.01	SLD

The DAY file preceding Event **0602A** showed a steady increase of loading on the east face starting mid-afternoon on May 1. The DAY file after Event **0602B** showed all loading was off by midnight on June 2, however it was noted that there was about 4 mm of permanent movement of the caisson to the west over this period.

For Event **0602A,** loading was exclusively on the east face, with no loading on either the northeast or south-east corners. The event was divided into 8 Sub-events based on video analysis. The highest load was 120 MN, as determined from MEDOF panels during crushing failure, Figure 72, otherwise maximum loads were in the range 70 to 80 MN.

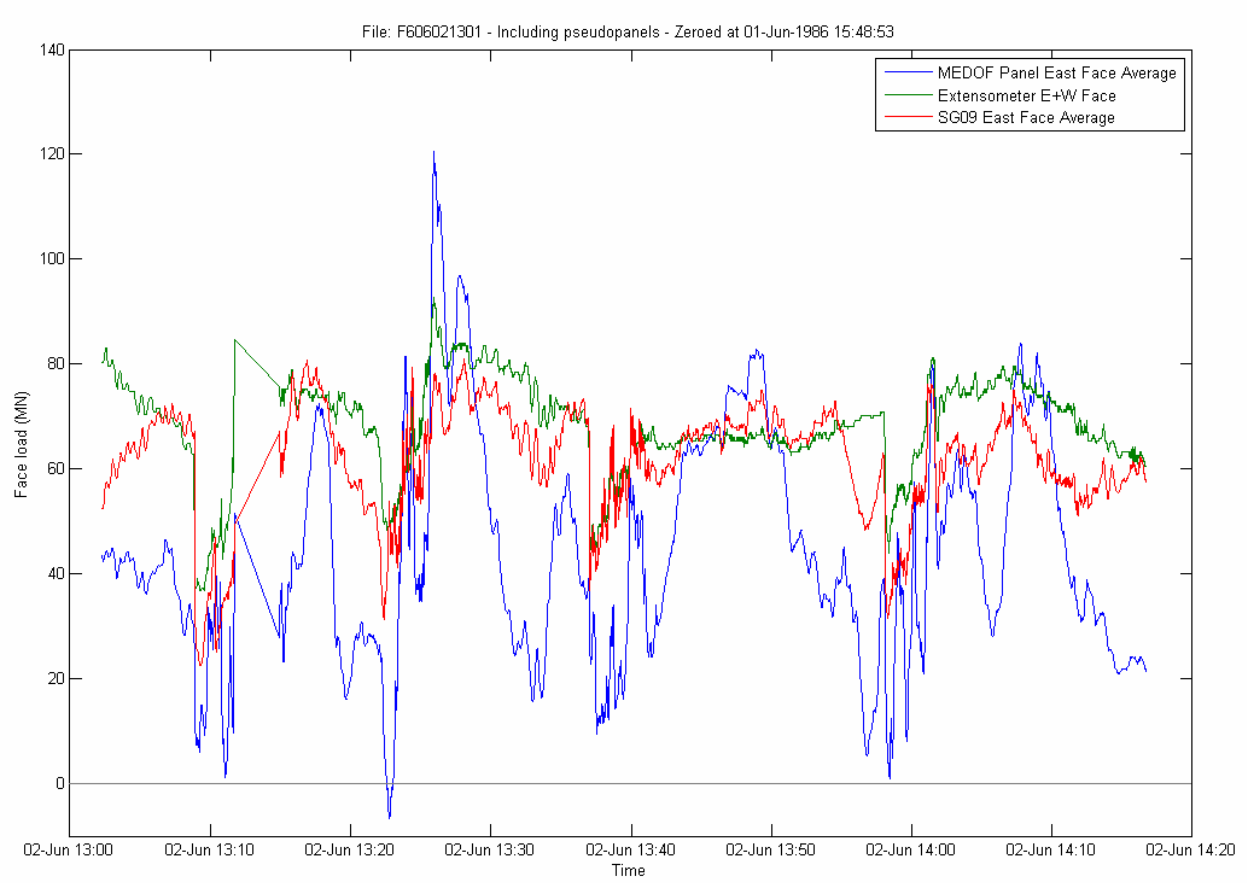

Figure 72 June 2 - East face load for Event 0602A

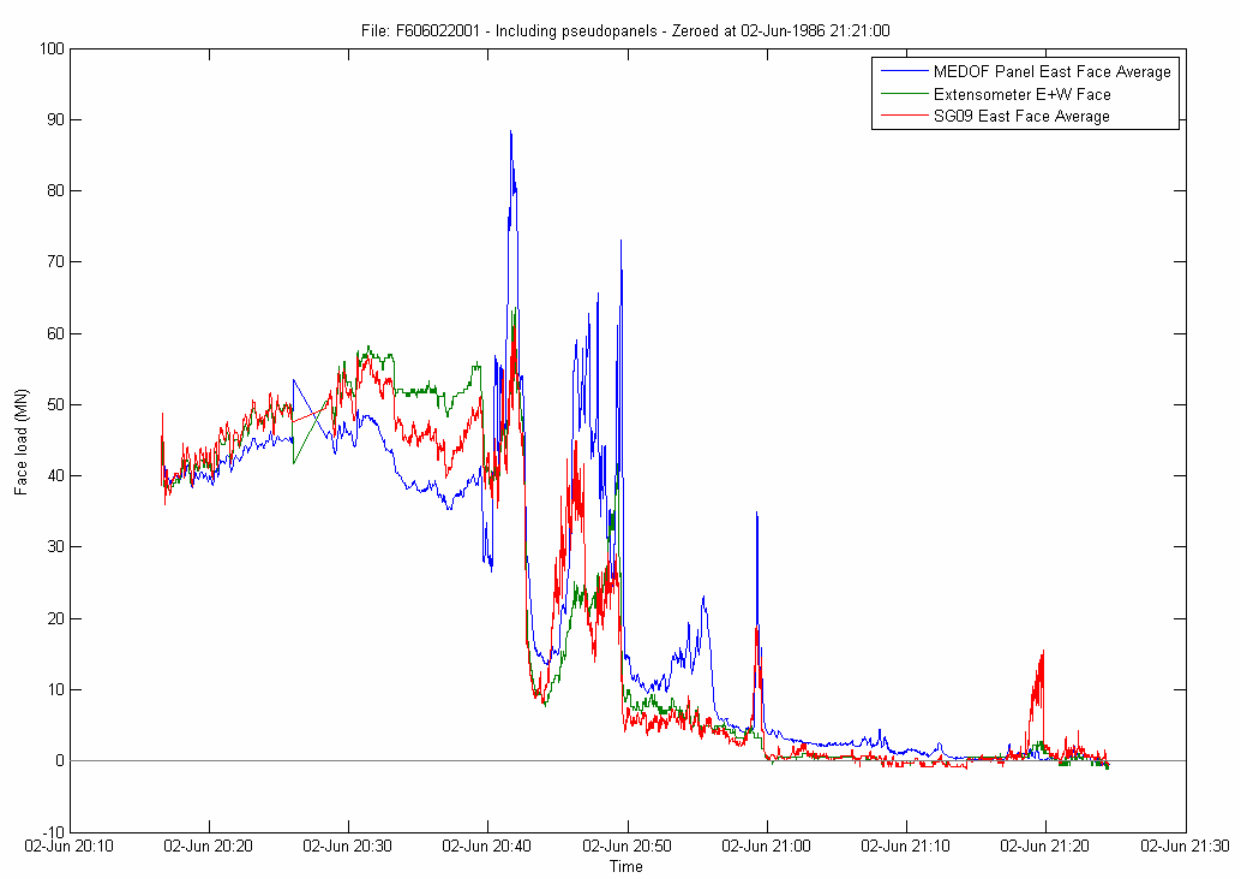

Figure 73 June 2 - East face load for Event 0602B

11.15 June 25, 1986

11.15.1 Description of ice conditions and loading events

On June 25, 1986 the west face was loaded with either first-year or second-year ice (Klohn-Crippen, 1995). No rubble maps are available from the time of this event. The hourly reports of ice surrounding the Molikpaq indicate thick FY ice with SY inclusions ($1/10^{th}$). Video is available for the north face, but the ice type cannot be established from this record. Since this event involves late-season warmer ice it is more difficult to distinguish the ice type. Note that the average air temperature for the preceding three days was +6 C.

Table 35 Summary of ice loading on June 25, 1986

Time period # (and Event ID if applicable)	Time		Drift speed, direction	Ice type & thickness	Ice conditions and failure behaviour
	From	To			
21 (0625A)	05:30	06:45	0.2 m/s – creep, to 100º	1.5 – 2.5 m	Thick FY or SY ice crushes against west and SW faces of Molikpaq. Dynamic loading thought to be from SY ice.

11.15.2 Event analysis

To describe the factors affecting loads, the event identified in the video analysis of Section 10 are described in terms of time period, ice thickness, ice velocity, and failure mode in Table 36.

Table 36 Description of event for June 25

Event ID	Sub-event number	Time Period	Ice thickness (m)	Ice velocity (m/s)	Failure Mode
0625A	full event	05:31:17 – 06:44:56	2 (est.)	0.2 to creep	CR, SLW

The DAY file preceding the FAST file, which started at 05:30, showed several loading events starting at 02:20. These events were on the west face, and since the maximum value of the strain and extensometer readings were several times the average value for the 5-minute recording intervals, failure behaviour in these events was crushing. Figure 74 for Event **0625A** indicates the maximum west face load was almost 120 MN from the three west strain gauges, and 95 MN from the extensometer. At the time of maximum load, the distribution of loads on the west face was strongly towards the north end of the face, W3. SG09 strain gauge data indicated that the largest strains were at W3, with lower strains at W2. Strains were even lower at W1, SW and S3, but of similar magnitude. The strains on the SW corner and S3, suggest that the actual loading direction was more like 80º, than the 100º drift direction reported.

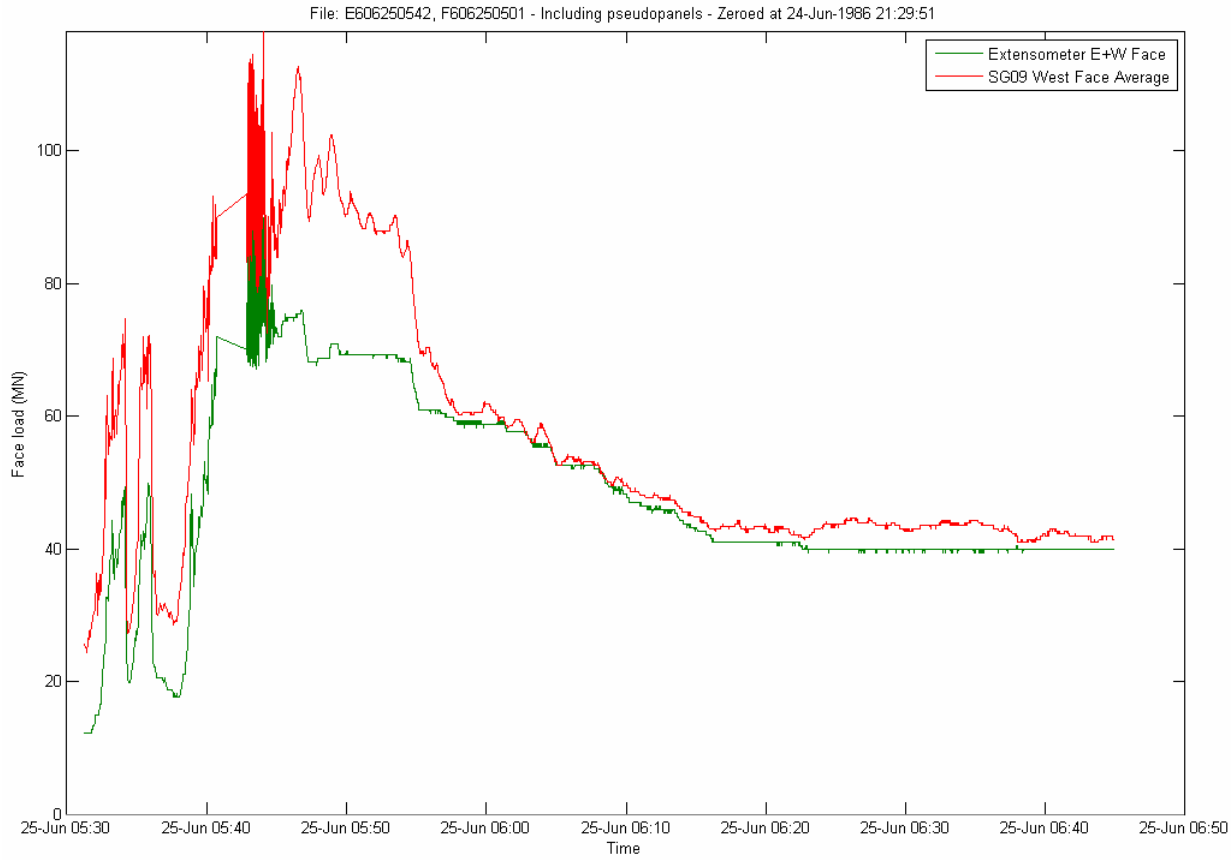

Figure 74 June 25 - West Face loading, Event 0625A

12. EFFECT OF PHASE LOCK ON ICE LOADS

Phase lock refers to the cyclic response of the Molikpaq to ice loading in which loads across the whole face are in phase (Jefferies and Wright, 1988). It is also sometimes referred to as "simultaneous" crushing. This behaviour was observed on several occasions during the 1985-86 season, and was most clearly defined during the May 12 event, in which the full complement of instruments, including three Main Bulkhead SG09 strain gauges on each face, were connected to the data acquisition system and a near complete record was obtained. It was also necessary for the recording system to be in EVENT mode (50 Hz) in order to conclusively capture the full characteristics of the cycling behaviour, and the simultaneity of the structure responses. It may also be possible to infer the occurrence of phase lock at times before the strain gauge instrumentation was not as complete by examining strain, extensometer and acceleration records. While phase lock was identified and associated with multi-year loading events in the 1985-86 season, it also occurred during first-year loading events. It also likely occurred during the 1984-85 season, where notes on ice events refer to "hammering", a term also used to describe the April 12 and May 12 events. The issue addressed within this report is identifying where phase lock was occurring at the time of peak ice loads. Note that phase lock discussed here is not cyclic crushing identified in the video analysis in Section 10 of this report.

12.1 Example of phase lock events on May 12

The influence of phase lock on the structure can be seen in Figure 75 which plots the output of the three SG09 strain gauges, N1, N2 and N3 on the north face, for EVENT File E603120320 recorded at 50 Hz. Ice was crushing against the north face during the whole of the almost 54 s duration of the file. Part of the time the three SG09 gauges on main bulkheads are responding in a synchronized fashion (times 03:19:11-14, 03:19:37-42 and after 03:19:48-57). Part of the time it is also clear that the strain gauges are responding quite independently of each other. To make the synchronous behaviour of the strains clearer, a 10-second record centred on 03:19:12 is illustrated in Figure 76. It can be clearly seen that the N1, N2 and N3 strains are closely synchronized for the interval 03:19:11-14.

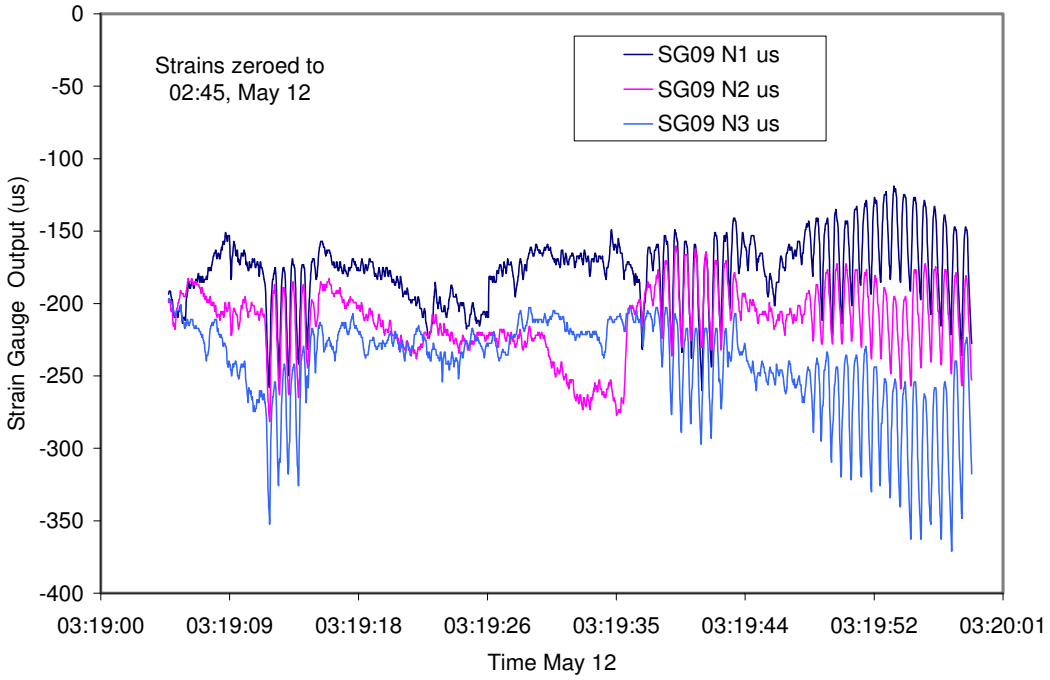

Figure 75 Time series record of North face strains for EVENT File E605120320

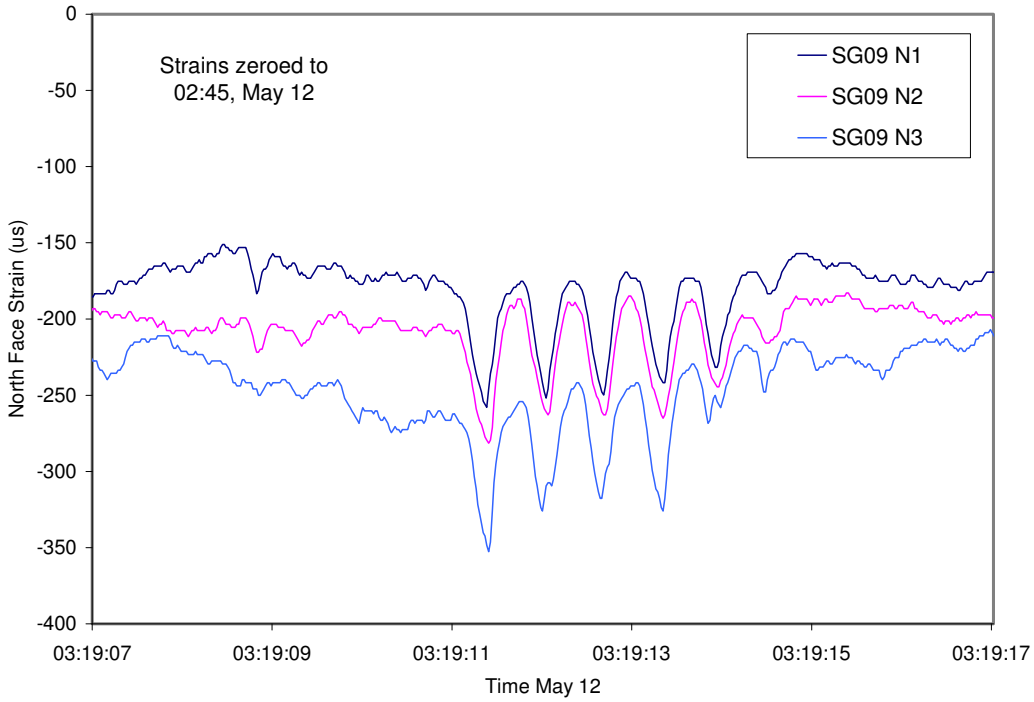

Figure 76 Expansion of time series of strain for phase lock event around 03:19:12

It is useful to also examine the acceleration record for the same time period. Acceleration in the north-south direction of an accelerometer 2 m above the base of the caisson in a pump room near the back-side and centre of the north face is plotted in Figure 77. Acceleration amplitude is less that 0.5% g for random crushing, compared to being greater than 1% g during periods of phase lock. The magnitude and relative regular period of the accelerations could also be considered an indicator of phase lock.

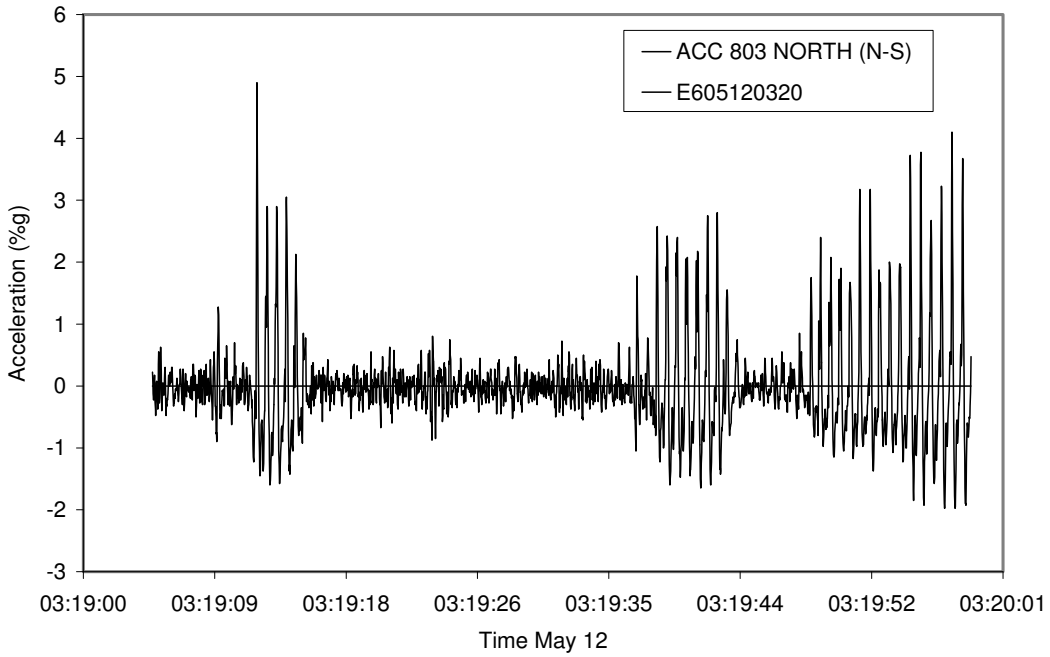

Figure 77 North-south accelerations of an accelerometer in the North face for EVENT File E605120320

The other issue which relates to phase lock is the increase in peak ice load when it is occurring. Based on the "historical" case, total load on the north face, calculated from both the three north face strain gauges and the extensometers on the north and south faces, is plotted in Figure 78. The peak ice load during the interval of phase lock around 3:19:12 from the strain gauges is about 160 MN, compared to 120 MN prior to phase lock. Later, around 3:19:40 the increase was from about 110 MN to 140 MN. In these two instances the increase is about 30%.

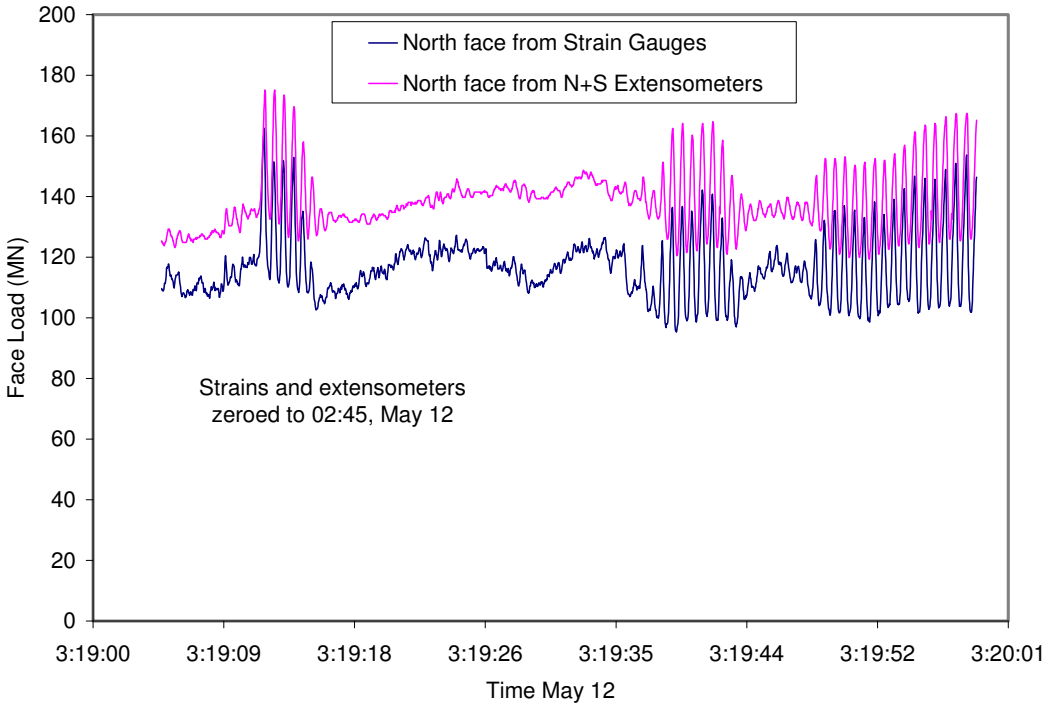

Figure 78 North face loads determined using strain gauge and extensometer data

To quantify the increase in peak load during periods of phase lock, the ratio of the maximum load to the average load, both over the same two-second interval, was calculated and plotted in Figure 79. The periods of phase lock correspond to periods when the ratio of peak to mean loads is greater than 1.1 and in the range 1.2 to 1.3.

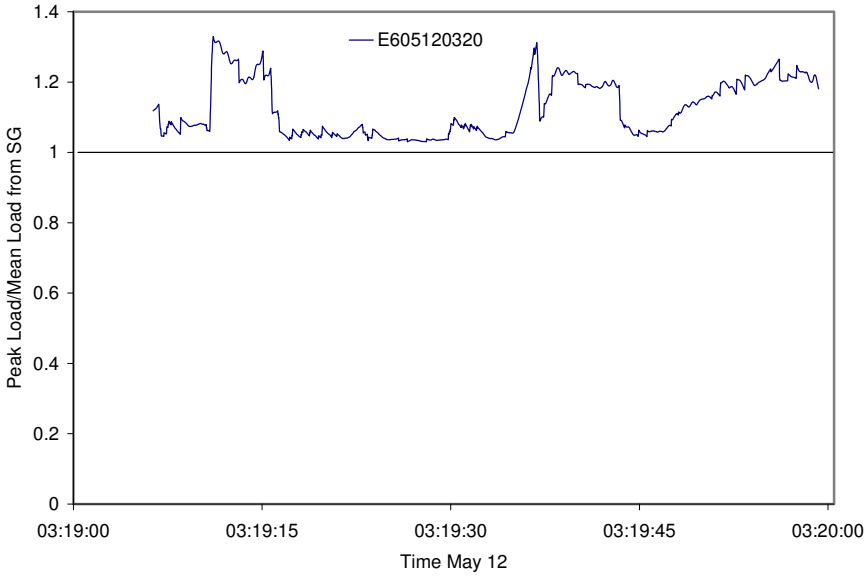

Figure 79 Ratio of peak load to one-minute average load

The loading and acceleration during the whole event is compared, and the times of the EVENT files noted in Figure 80. This is a FAST file, so the recording frequency is only 1 Hz, however periods where accelerations are greater than about ±1%g during a FAST file generally correspond to periods when phase lock is occurring. Periods when accelerations in FAST files exceed 1%g may be taken as indicators of possible occurrences of phase lock.

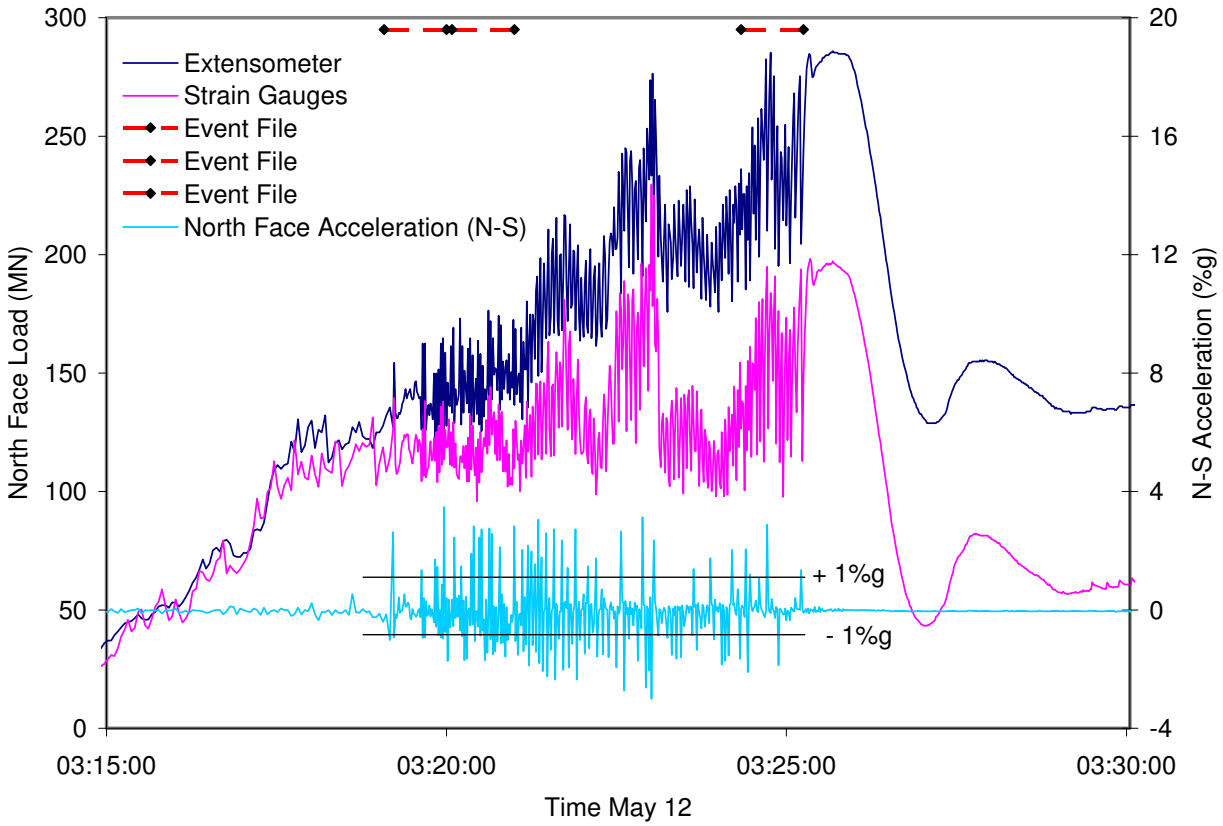

Figure 80 Comparison of May 12 loads and acceleration for phase lock

12.2 Periods of phase lock

The first step in identifying periods of phase lock was to examine all EVENT files for evidence of phase lock occurring. As discussed in Section 12.1, the most conclusive evidence is when two or three strain gauges have synchronized signals, but this is only possible for records after April 12. For records up to and including April 12, accelerations greater than 1 %g and systematic cyclic signals were considered indicative of phase lock. The assessment of the 25 EVENT files examined is summarized in Table 37. Eight of the files did not have any evidence of phase lock. Additionally, acceleration records in FAST files were examined for times when accelerations were greater than 0.5%g. These time intervals are noted in Table 38. These FAST file intervals that contained EVENT files are marked with an *.

Table 37 EVENT files showing evidence of phase lock

Date	EVENT File	time; hh:mm	Phase Lock
1986-Mar-07	E603070345	03:45	no
	E603070532	05:32	no
	E603070725	07:25	no
1986-Mar-07	E603071529	15:29	no
	E603071549	15:49	yes
	E603071551	15:51	yes
	E603071638	16:38	yes
	E603071641	16:41	yes
	E603071645	16:45	yes
1986-Mar-08	E603081612	16:12	yes
	E603081623	16:23	yes
	E603081731	17:31	yes
	E603082120	21:20	no
	E603082225	22:25	no
1986-Apr-12	E604120823	08:23	yes
	E604120827	08:27	yes
	E604120828	08:28	yes
	E604121322	13:22	no
	E604121354	13:54	yes
1986-May-12	E605120320	03:20	yes
	E605120321	03:21	yes
	E605120325	03:25	yes
1986-May-22	E605221429	14:29	no
1986-Jun-02	E606022040	20:40	yes
1986-Jun-25	E606250542	05:42	yes

Table 38 FAST files and time intervals with accelerations greater than 0.5%g

Date	FAST File	time interval	Acceleration
Mar-07	F603071520	15:21-15:31*	1%g
		15:47-16:07*	1 - 2%g
		16:18-16:25	1%g
		16:28-16:31	1%g
	F603071603	16:39-16:42*	>0.5%g, <1%g
		16:44-15:45*	>0.5%g, <1%g
		17:08-17:11	>0.5%g, <1%g
		17:13-17:16	>0.5%g, <1%g
		17:19-17:20	>0.5%g, <1%g
Mar-08	F603081603	16:13-16:15*	1%g
	F603081731	17:32-18:19*	1 - 2%g
Apr-12	estimate	08:15-08:35*	3 - 6%g
	F604121101	11:39-11:43	2%g
	F604121201	13:23-13:24	< 1%g
		13:54-13:55*	>1%g
	F604121400	14:03-14:06	>1 %g
	F60412140A	14:19-14:21	< 0.5%g
May-12	F605120301	03:09-03:19	< 0.2%g
		03:19-03:26*	1-3%g
May-22	F605221301	14:51-14:54	< 0.5%g
		14:57-14:58	1%g
		15:00-15:01:45	2%g
Jun-02	F606021301	14:15-14:16	< 0.4%g
	F606022001	20:41:43-20:20:43:07*	< 0.5%g
Jun-25	F606220501	05:43:08-05:44:25*	2%g
		05:44:25:05:44:56	< 0.3%g

* EVENT files in this interval

12.3 Events where peak loads coincided with phase lock

Strain gauge and extensometer results from EVENT files can conclusively indicate when phase lock has occurred. As pointed out in Section 12.1, instances of phase lock in EVENT files were associated with high accelerations, generally greater than ± 0.5 %g. This provides a means for using the accelerations recorded in FAST files to identify additional possible times when phase lock was occurring, but for which there were no EVENT files. Both approaches were used to identify peak loads which coincided with phase lock. Table 39 identifies the event, or sub-event, time, values of peak loads using "Historical Case" calibration factors and whether an EVENT file of and acceleration record from a FAST file was used. No effort has been made to adjust estimated loads to account for phase lock, since that was beyond the scope of the JIP.

Table 39 Peak loads coinciding with phase lock

Event ID	Extensometer		SG09 Strain gauges		EVENT file	FAST file Acceleration
	Time	Load (MN)	Time	Load (MN)		
0307A-3	16:01:59	231 (W)				X
0307A-5	16:29:54	135 (N)				X
0307B-1	16:41:22	175 (N)	16:41:24	244 (N)	X	X
0307B-2	16:45:19	145 (N)	16:45:16	175 (N)	X	X
0308A	16:13:55	145 (N)	16:13:55	154 (N)	X	X
0412A-1	08:24:35	196 (E)	08:24:36	214 (E)	X	X
0412A-2	08:28:10	314 (E)	08:28:08	389 (E)	X	X
0412A-3	08:29:54	388 (E)	08:28:46	304 (E)	X	X
0412A-4	08:34:18	321 (E)	08:34:18	151 (E)		X
0412C-9	13:55:12	138 (S)	13:55:11	153 (S)	X	X
0412D-1	14:06:31	93 (E)	14:06:11	76 (E)		X
0412E-1	14:20:12	99 (E)	14:20:11	79 (E)		X
0412E-2	14:20:49	82 (E)	14:29:40	63 (E)		X
0412E-1	14:19:37	55 (S)	14:19:39	76 (S)		X
0512A-2	03:19:14	135 (E)	03:19:14	127 (E)	X	X
0512A-3	03:21:44	198 (E)	03:21:44	167 (E)	X	X
0512A-4	03:25:41	267 (E)	03:23:01	214 (E)	X	X
0522B-5	15:01:42	93 (N)	15:01:41	94 (N)		X
0602B-2	20:41:55	64 (E)	20:41:54	61 (E)	X	X
0625A	05:43:23	95 (W)	05:44:03	118 (W)	X	X

13. ICE LOAD ESTIMATES

13.1 "Historical Case" ice loads and global pressures

"Historical Case" ice loads are presented since they generally relate to previously published results, with relatively small differences due to different treatment of the influence of the lower level MEDOF panels and refined factors for converting strains to local ice loads. The "Historical Case" also provides a means for establishing the relation between loads from MEDOF panels, strain gauges and extensometers.

Time series plots with "Historical Case" loads for the MEDOF panels, strain gauges and extensometers are presented in Appendix K for each event. The loads for the "Historical Case" scenario are based on the face load calculation methods presented in Section 4. The strain gauges and extensometers were calibrated as detailed in Sections 5.2 and 5.3, respectively.

The table in Appendix K provides a summary of each Event or Sub-event, including ice load values related to periods when the size, thickness and shape, and speed of multi-year ice features are relatively uniform or defined; e.g. a hummock. Loading from the south and west, where there were no MEDOF panels, was analysed using the available extensometer and/or strain gauge data. Figure 81 presents a summary plot of the maximum face loads over the time interval of the event. Note that strain gauge based loads up to and including April 12, data from only one or two strain gauges were available, but in these cases load has been extrapolated to the full face width (see markings with * or ** in Figure 81). The maximum face load estimated based on the "Historical Case" was approximately 390 MN.

For events before April 12, 1986, the strain gauge based north face load is calculated using two strain gauges instead of the usual three (as explained in detail in Section 4.2). For Event **0412A** on April 12, the strain gauge based east face load is extrapolated using results from one strain gauge, SG09 E2 (also explained in Section 4.2). The face load for this event was reduced by 20% (from 486 MN to 389 MN), to account for the general tendency of the central strain gauge to measure higher loads than the other two gauges during high load, crushing events. Frederking and Sudom (2006) analysed ice loading for April 12 events for which all three SG09 gauges were available, and found that for forces greater than 150 MN, face forces calculated from SG09 E2 alone were at least 25% greater than face forces calculated from all three strain gauges on a face. Therefore it is considered reasonable to reduce the face load for April 12 Event **0412A** by 20%.

In Figure 81, if significant loading (>15 MN) occurred on more than one face, the load on each face is plotted. For events with loads on more than one face, the maximum face loads on different faces do not necessarily occur at the same point in time.

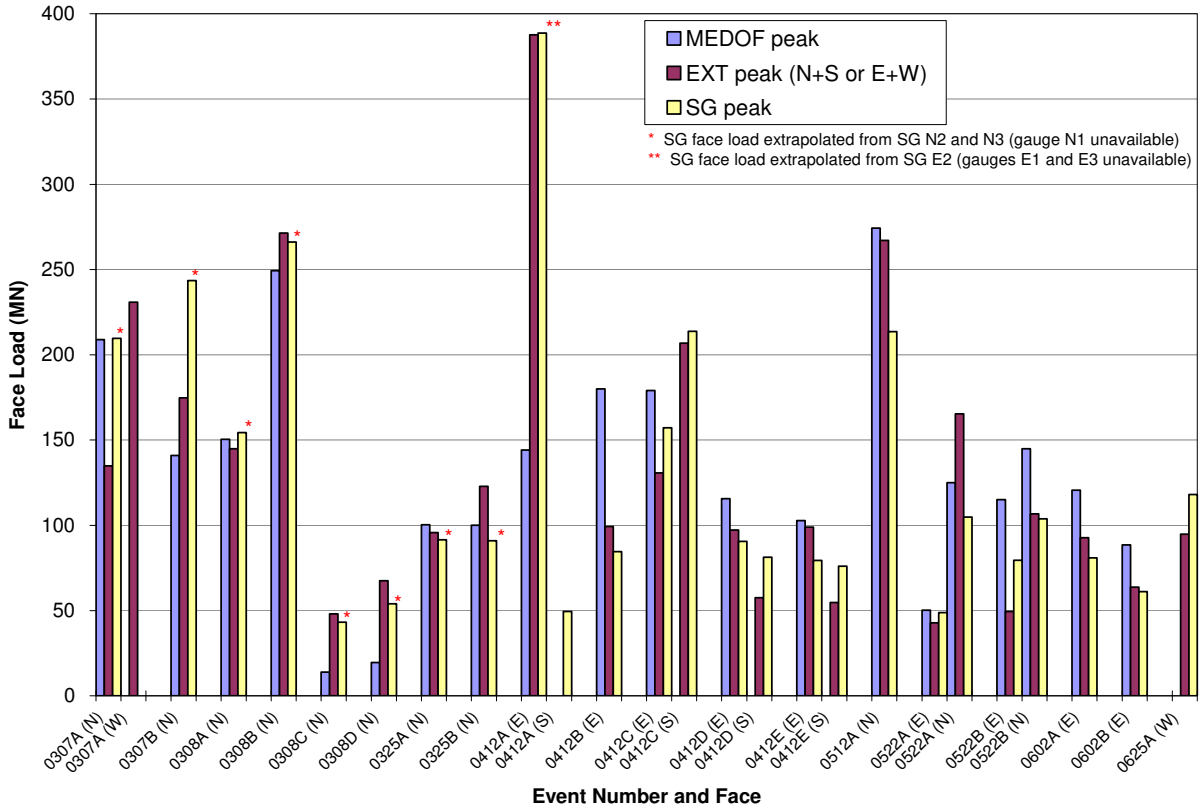

Figure 81 "Historical Case" peak face loads

Figure 82 shows the peak global ice pressures for each event. Global pressures are calculated as

$$P = F/A \qquad \textbf{(13-1)}$$

where F is the face load [MN] and A is the area [m^2]. This area is the average ice thickness across the width of the face multiplied by the width of the face (58 m). Global pressures are based on the face load, or extrapolated face load in cases where only one or two strain gauges are available.

The high global pressure for Event **0512A** on May 12, 1986 stands out in Figure 82. For this event, the measured face load was much lower than that for April 12 hummock Event **0412A**; however the observed ice thickness was lower on May 12, resulting in a higher global pressure.

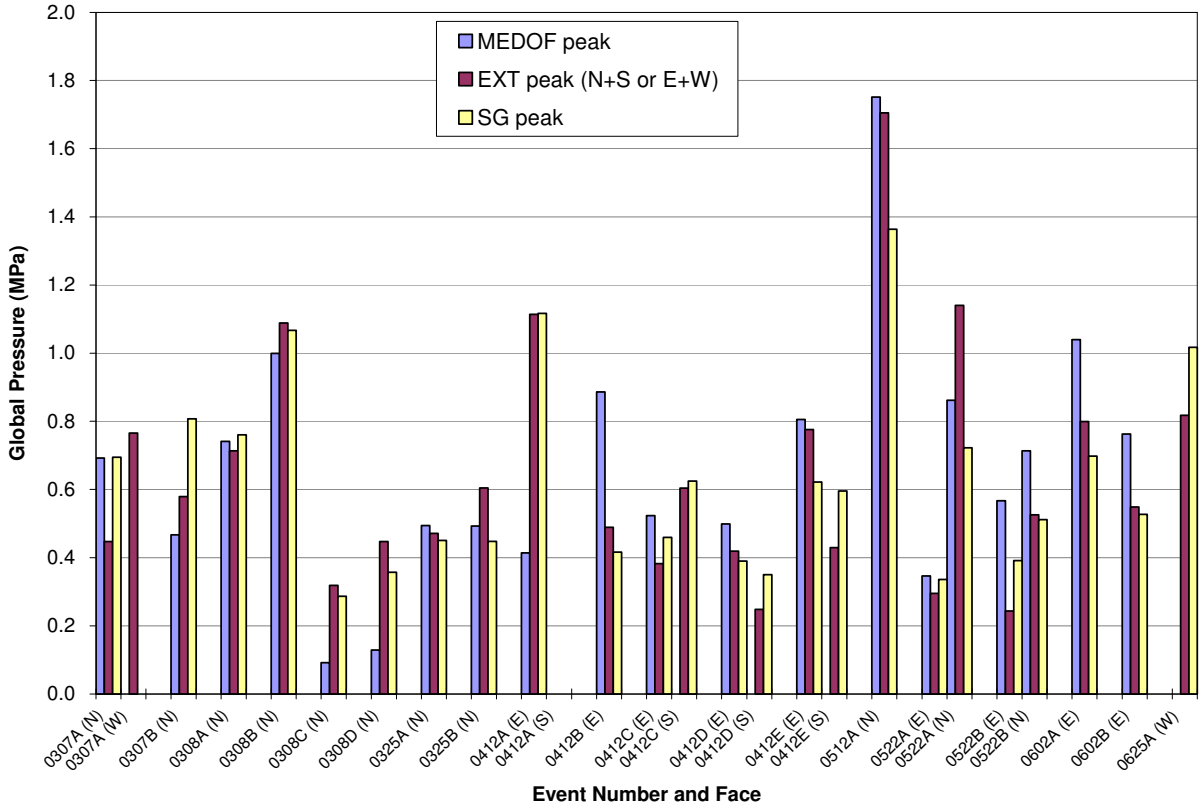

Figure 82 "Historical Case" peak global ice pressures on 58 m face width

Figures 83, 84 and 85 show ice pressure plotted against average ice thickness for the MEDOF panel, extensometer, and strain gauge based data, respectively. The pressures are categorized by the ice failure mode which was predominant during the time periods of analysis (Event or Sub-event). The failure modes for most events and Sub-events were identified by Brian Wright from video records of the east and north faces (see Section 10.2.3 and Appendix G). These time periods are the Events and Sub-events of Appendix K.

The pressures are calculated using Equation 13-1, however the width of the structure over which the pressure is determined is different for the strain gauge based calculations several cases. For the MEDOF panels and extensometers this width is always the full structure width of 58 m. For events before April 12, 1986 and for Event **0412A** on April 12, the strain gauge based pressure is calculated over a shorter width corresponding to the tributary area of the available strain gauges. For the east face there was just one strain gauge, E2, and for the north face there were two strain gauges, N2 and N3. This is noted in Table 1 of Appendix K and on Figure 85. For all other events, all three strain gauges are available and the strain gauge based pressure is calculated over the full structure width.

The general trend of decreasing global ice pressure with increasing ice thickness is apparent from the results of all three instruments. However, the global ice pressures for ice ~2 m thick, all late season June events, stand out as being lower than expected. Closer examination of these global pressure results could be done, but is beyond the scope of this project. Note that all these pressures will be halved for the "Best Estimate" case as will be described in Section 13.2.

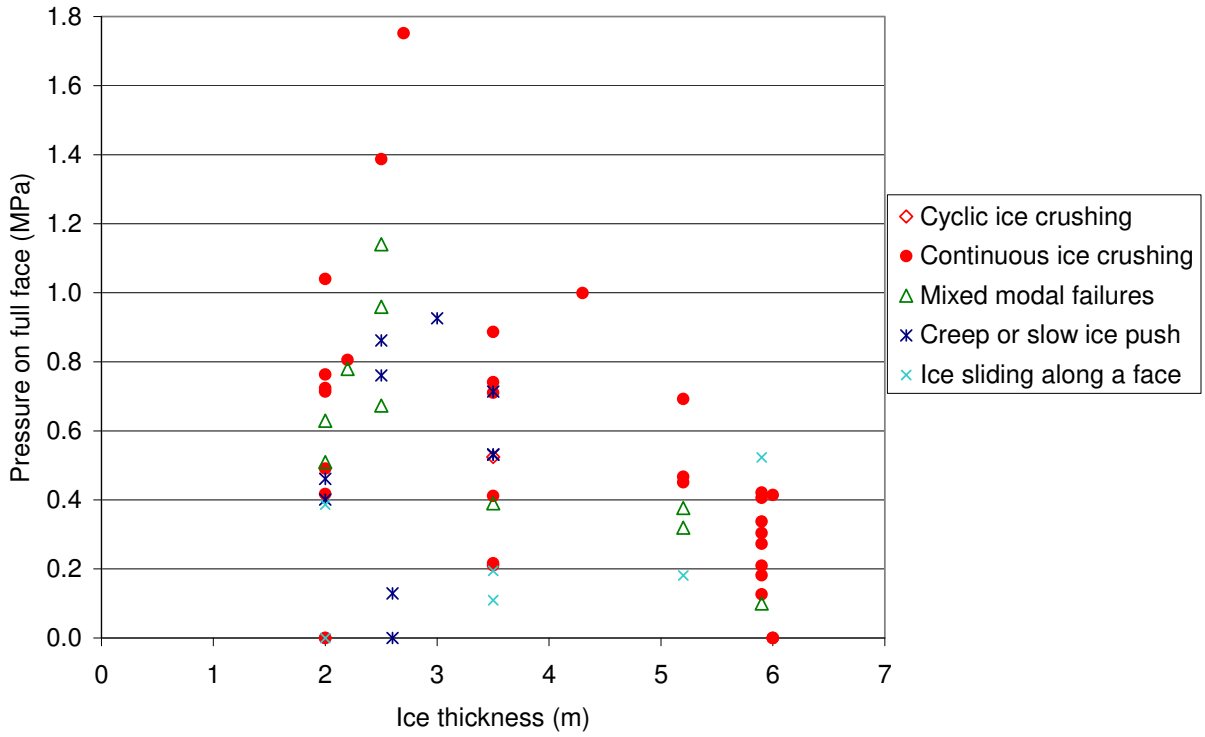

Figure 83 "Historical Case" pressures based on MEDOF panel loads, categorized by failure mode

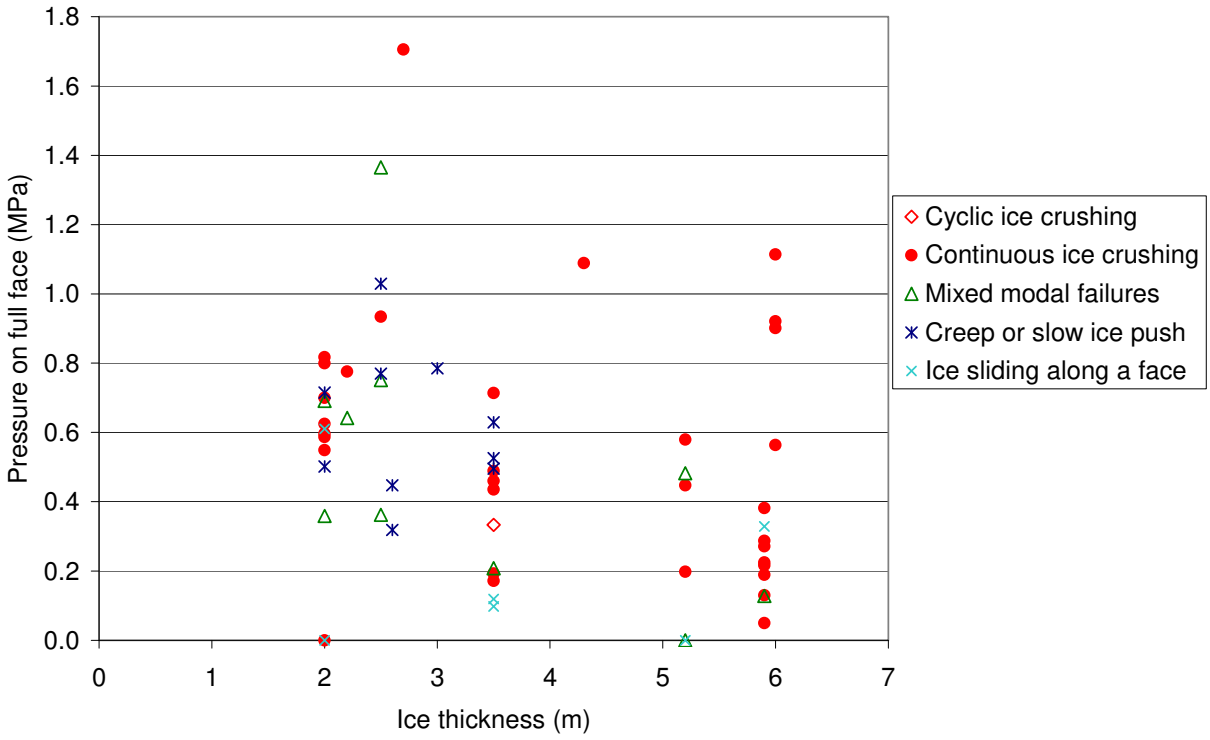

Figure 84 "Historical Case" pressures based on extensometer results, categorized by failure mode

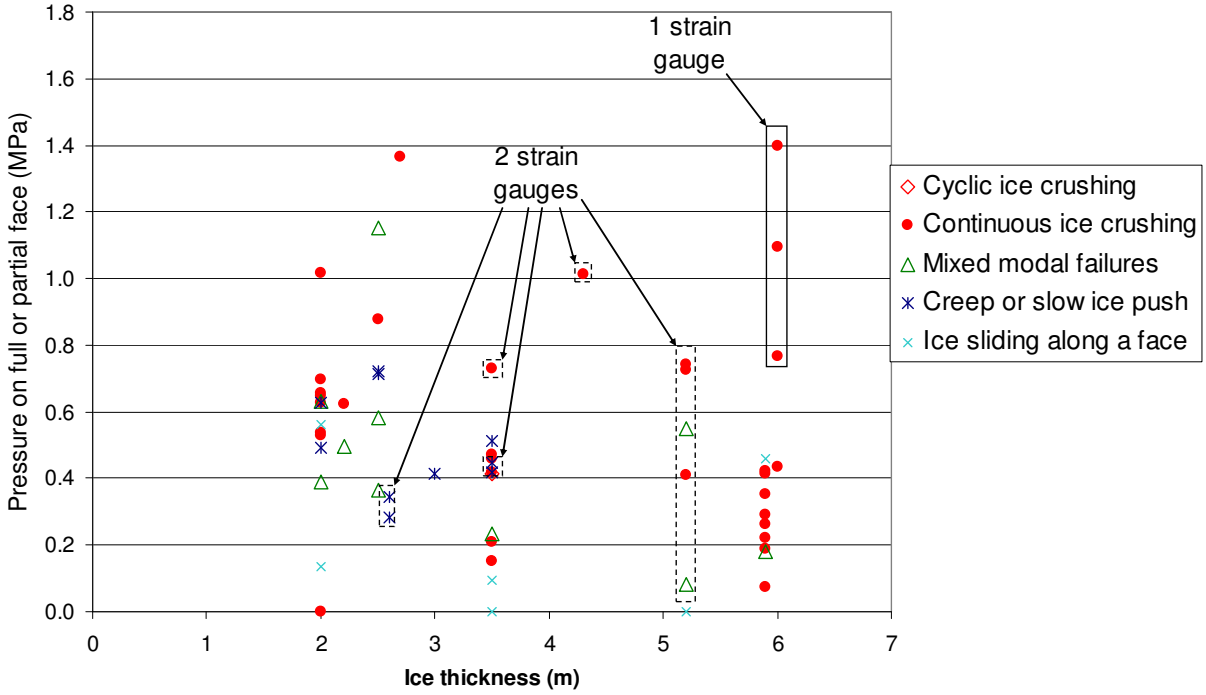

Figure 85 "Historical Case" pressures based on strain gauge results, categorized by failure mode

13.2 "Best Estimate" ice loads

As already pointed out in this report there are four factors which lead us to establish a "Best Estimate" of ice loads which is 50% of those found by the "Historical Case" approach:

- Sand core as placed was in a loose state, so that at the small deformations measured, resistance was provided mainly by base friction of the caisson.
- Softening of polyurethane buttons in the MEDOF panels lead to their overestimation of ice forces.
- Free-floating floe impact of May 12 gave substantially lower ice impact force.
- Local ice pressure from MEDOF panels substantially higher than the STRICE local pressures for equivalent ice thickness.

We have selected a calibration factor for the extensometers of 3 MN/mm, 50% of the 6 MN/mm used in the "Historical Case" calculations, for face loads as a basis for recalculating face loads and pressures. Note that the value of 3 MN/mm is towards the upper limit of the range of extensometer factors that were determined, but was selected at this level to be prudent. Loads from MEDOF panels and strain gauges are similarly scaled down by 50%. "Best Estimate" face loads are presented in Figure 86. The March 7 event **0307B** face load from application of the extensometer measure of north-south relative deformation gave a peak face load of about 85 MN. Applying the biaxial matrix method developed by the IJA team, the global load for that event was determined to be 95 MN. On May 12 the "Best Estimate" peak loads were 137 MN, 134 MN and 107 MN, respectively for MEDOF panel, extensometer and strain gauge based determinations. The highest force estimated by the IJA team for the May 12 event, using an assessment of floe deceleration was, 126 MN.

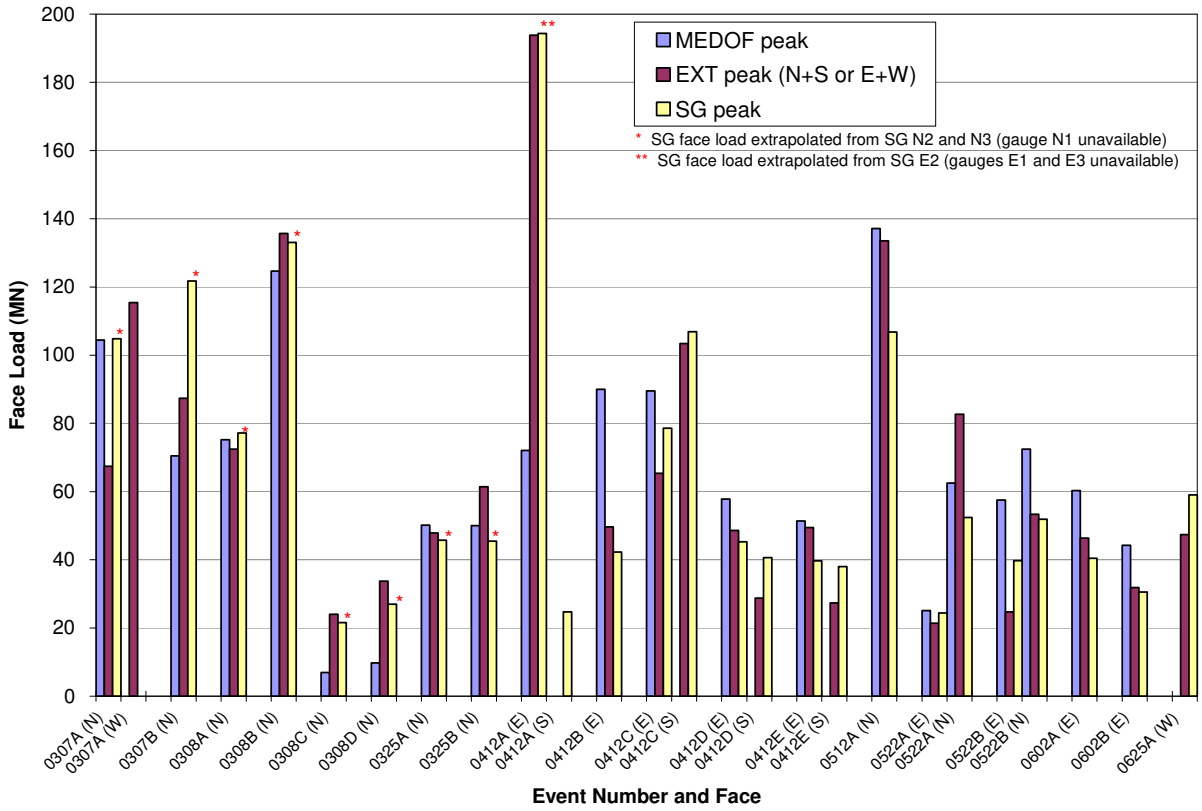

Figure 86 "Best Estimate" peak face loads

Using the same methodology as for the "Historical Case" described in Section 13.1, and Equation 12-1, global pressures were calculated and are plotted in Figure 87. Again, the May 12 global ice pressures stand out from those of other events.

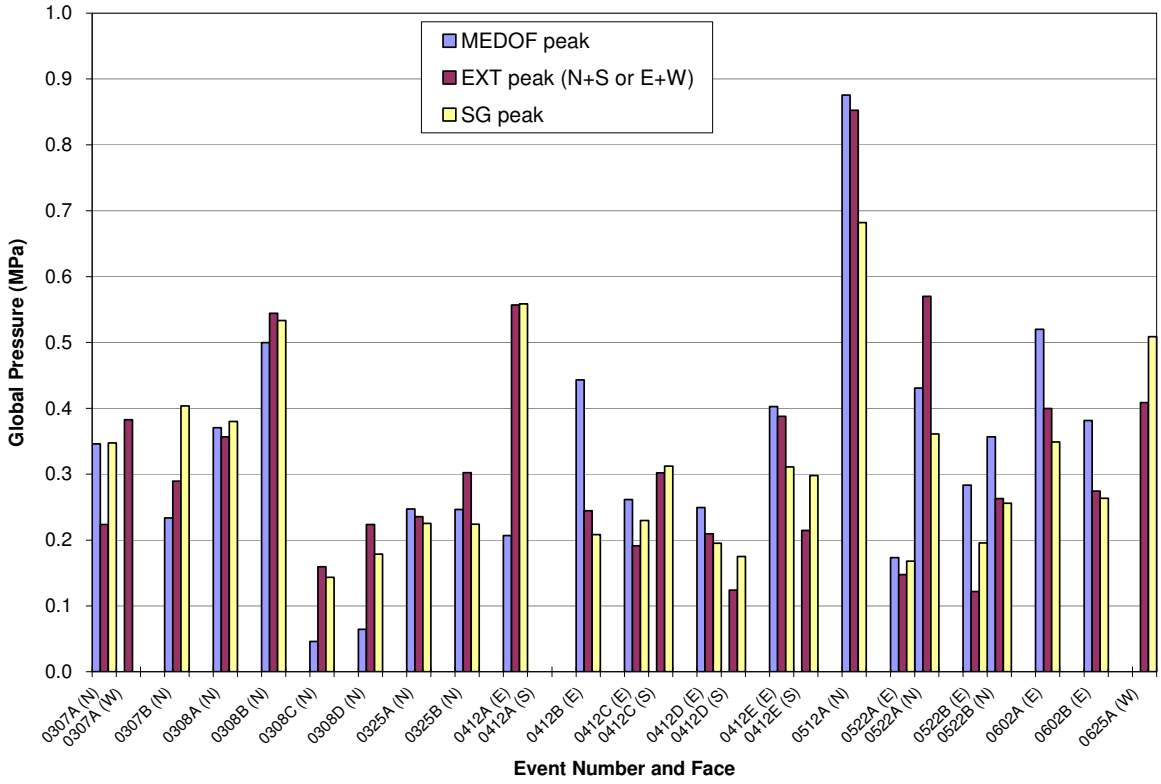

Figure 87 "Best Estimate" peak global face pressures on 58 m width

14. SUMMARY

Twenty-one time periods of interest where multi-year or second-year ice was present were investigated. A detailed video analysis of failure behaviour identified 13 of the events to be further broken down into Sub-events by failure mode. Loads from MEDOF panels, strain gauges and extensometers have been calculated and presented separately in Appendix K. Each Event or Sub-event includes a time series record of load related to periods when the size, thickness and shape and speed of multi-year ice features are relatively uniform or defined; e.g. a hummock. Loading from the south and west, where there were no MEDOF panels, was analysed using strain gauge and/or extensometer data. The analysis in Appendix K has been done by NRC-CHC using linear averaging and calibration factors for strain gauges and extensometers from original MEDOF panel calibrations for the "Historical Case". Figure 81 has presented a summary plot of the maximum face loads for each Event. The time series traces for all events in Figure 81 are given in Appendix K, along with a summary table.

Figure 88 presents a comparison of the "Historical Case" global pressures with the pressure-area curve for a 58 m wide structure determined from ISO/DIS 19906 Eqn [A.8-22] (ISO, 2009).

$$p_o = C_R\, h^n\, (w/h)^m$$

where p_o = global average pressure, MPa
w = width of structure, m
h = ice thickness, m
m = empirical coefficient = -0.16
n = empirical coefficient = -0.3 for $h \geq 1$ m
C_R = ice strength coefficient = 2.8 for Beaufort Sea conditions

The "Historical Case" pressures are calculated as described in Section 13.1, and are the same global pressures plotted in Figure 82. The thickness used in pressure calculations is our best estimate of the average ice thickness; the actual average ice thickness could vary by ± 25 to 33%. As shown in Figure 88, the Historical Case pressures generally fall below the ISO curve. The one exception is the calculated ice pressure for Event **0512A** on May 12, 1986.

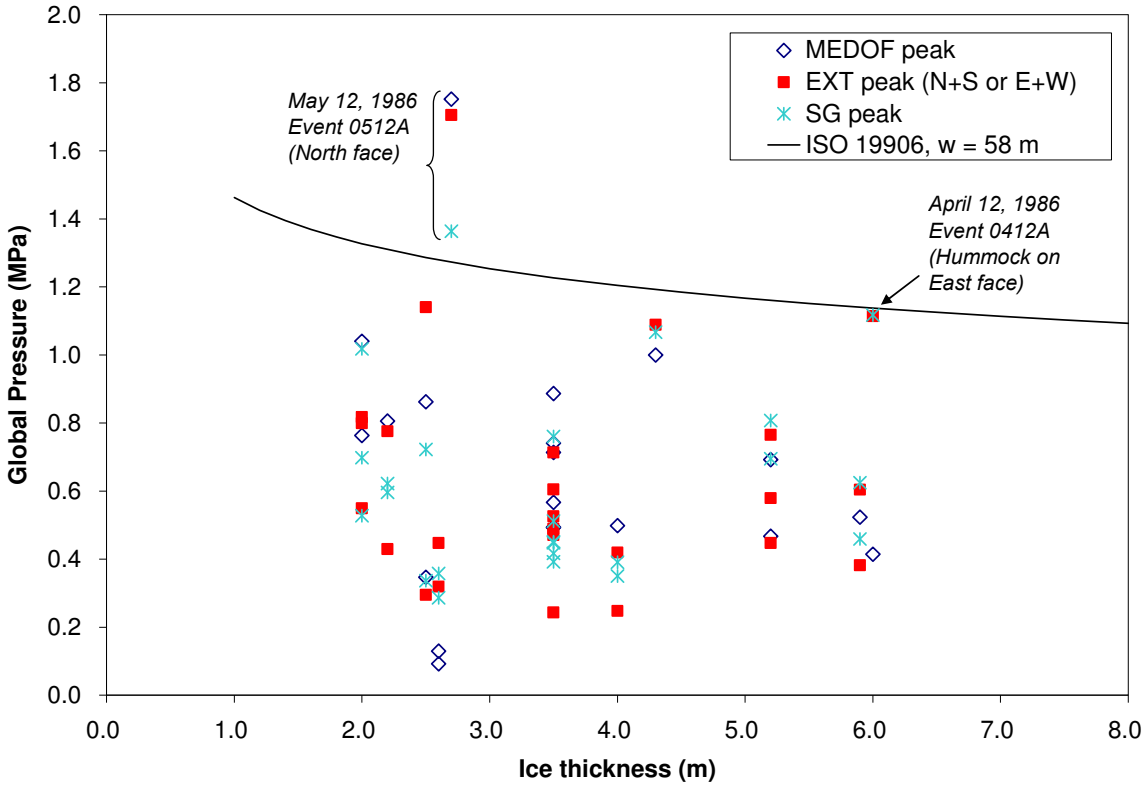

Figure 88 Comparison of "Historical Case" global pressures with global pressure curve from ISO/DIS 19906 for a structure of the same face width as the Molikpaq, 58 m

Careful and critical review of all reports and information related to the original 1986 JIP has resulted in a reassessment of ice loads. Geotechnical analysis indicated that due to the low relative density of the sand core and the small deformations, the majority of resistance derived from base friction of the caisson on the berm, and loads must be lower than previously estimated. A plausible mechanism for softening of the MEDOF panels explains why they would over-predict ice forces. Local ice pressures from the MEDOF panels gave higher pressures than the local ice pressures from other data sources for comparable ice thicknesses. Analysis of deceleration of a free-floating second-year floe on May 12 gave substantially lower loads than that in previous determinations. It is our judgement that historical MEDOF panel derived ice loads are of the order of two times too high. Loads from strain gauges, extensometers and MEDOF panels have all been reduced by 50% to provide our "Best Estimate"

In Figure 89 global pressures for our "Best Estimate" case are plotted against average ice thickness. The ISO global pressure curve for Arctic/Beaufort conditions now lays above all our data. Nevertheless, we do not suggest at this time that the ISO equation or the strength coefficient for Beaufort conditions, C_R = 2.8, be reduced.

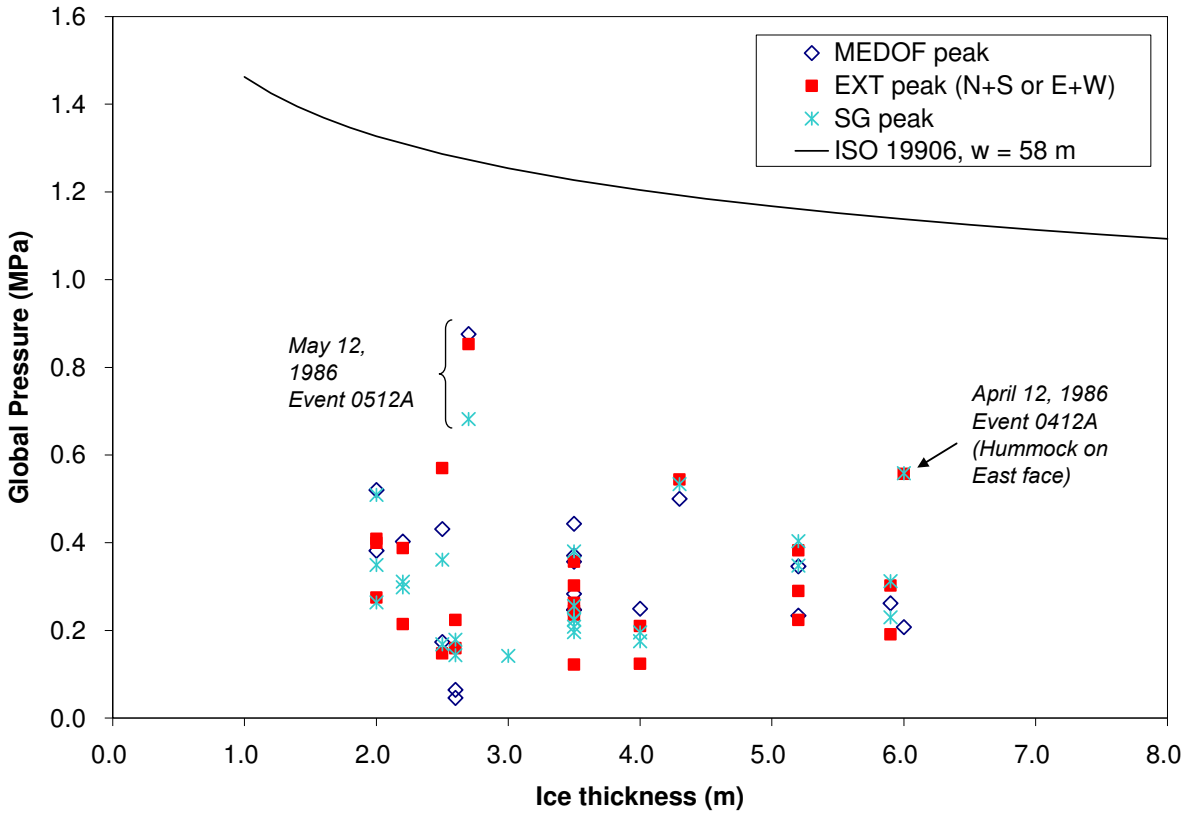

Figure 89 Comparison of "Best Estimate" global face pressures with global pressure curve from ISO/DIS 19906 for a structure of face width 58 m

In terms of trends that could be derived from the results, a reduction in peak global pressure with increasing ice thickness is evident for the three instruments used to determine ice loads. This trend is clearest for MEDOF panel and extensometer derived pressures, but less so for strain gauge derived pressures. There is some evidence of late season (June events) giving lower global pressure than would be expected, given the thickness of the ice. Finally it should be kept in mind that the results presented in this report are for a relatively large structure, and caution should be used in applying them to narrow structures.

Almost 25 years since the data were collected, the 1985-86 deployment of the Molikpaq at Amauligak I-65 represents one of the most comprehensive data sets on ice interactions with a large offshore structure. Further analysis could be carried out on individual events and that would yield insights into the mechanics of ice-structure interaction processes, however in terms of reducing uncertainty, future efforts would be best directed towards new field measurement projects. There have been significant improvements in instrumentation, measurement techniques and analysis methods since the 1980s, which would make new field projects attractive. Future work on specifying loading from large ice features interacting with offshore structures would be best directed towards measurement opportunities on new or existing structures, or natural features such as Hans Island.

15. ACKNOWLEDGEMENTS

We would like to thank ConocoPhillips Canada for making the 1985-86 Molikpaq data available for analysis within this JIP.

16. REFERENCES

Altaee, A. and Fellenius, B.H. 1994. Modelling the performance of the Molikpaq, Can. Geotech. J., Vol. 31, pp 649-660.

Bercha, F. & Associates, Klohn-Crippen, Sandwell Inc., and Wright, B. & Associates, 1994. Molikpaq dynamic characteristics and ice loading events. (CHC 14-58)

Brown, T.G., Wright, B.D., Rogers, B., Jefferies, M. and Bruce, J.R., 1992. A Model for Dynamic Ice Interaction with Molikpaq, Proceedings of IAHT Ice Symposium, Banff, Alberta, Vol. , pp 1289-1303

Frederking, R., Masterson, D.. Wright, B., and Spencer, P., 2002. Ice load measuring panels – the next generation, Ice in the Environment: Proceedings of the 16th IAHR International Symposium on Ice Dunedin, New Zealand, 2nd–6th December 2002, Vol. 1, pp 450-457.

Frederking, R. and Sudom, D., 2006. Maximum ice force on the Molikpaq during the April 12, 1986 event. Cold Regions Science and Technology 46 (3), 147-166.

Frederking, R. and Sudom, D., 2008. Local ice pressure distributions during 1990 Hobson's choice ice island multi-year ice indentation tests, Proceedings of the 19th IAHR International Symposium on Ice, July 6 to 11, 200, Vancouver, BC, Canada, Vol. 2, pp 815-827.

Frederking, R. and Sudom, D., 2009. Flux of multi-year ice past the Molikpaq in the Beaufort Sea, 1985-86 season, Proceedings of the 20th International Conference on Port and Ocean Engineering under Arctic Conditions, June 9-12, 2009, Luleå, Sweden, paper POAC09-118.

Gulf Canada Frontier Development Division, 1989. Ice tests, observations, rubble maps and ice load calculations. (CHC 14-63)

Gulf Canada Resources Ltd., 1987a. Dynamic horizontal ice loading on an offshore structure; Phase 1A: Molikpaq performance at Amauligak I-65, Vol. 3 – Instrumentation. (CHC 14-3)

Gulf Canada Resources Ltd., 1987b. Dynamic horizontal ice loading on an offshore structure; Phase 1A: Molikpaq performance at Amauligak I-65, Vol. 4 – Validation of ice force measurement. (CHC 14-4)

Hewitt, K.J., 1994. Molikpaq ice interactions: Predicted and actual performance, Proceedings IAHR Ice Symposium, Trondheim, Norway, August 23-26, Vol. 3, pp. 993-1002.

ISO, 2009. Draft International Standard ISO/DIS 19906: Petroleum and natural gas industries – Arctic offshore structures, International Organization for Standardization.

Jefferies, M.G. and Wright, W.H., 1988. Dynamic response of Molikpaq to ice-structure interaction. Proc. 7th Int. Conf. Offshore Mech. and Arctic Eng., Houston, USA, Vol. 4, pp. 201-220.

Jefferies, M.G. and Spencer, P.A., 1989. Dynamic ice/structure interaction with the Molikpaq at Amauligak I-65, Phase 1B, Main Report, Vol. 1 of 2. Gulf Canada Resources Ltd., July 1989. (CHC 14-13)

Jefferies, M., Kärnä, T. and Løset, S. 2008. Field data on the magnification of ice loads on vertical structures, 19th IAHR International Symposium on Ice "Using New Technology to Understand Water-Ice Interaction" Vancouver, British Columbia, Canada, July 6 to 11, 2008, Vol. 2, pp 1325-1343.

Jeyatharan, K. 1991. 'Partial Liquefaction of Sand Fill in a Mobile Arctic Caisson Under Ice Loading.' Cambridge University Doctoral Thesis.

Johnston, M. 2008 "Thickness and material Properties of Multi-Year Ice Sampled during the CAT Study, August 2007" report CHC-TR-067, January 2008, 57 pages plus 4 appendices.

Jordaan, I.J., Li, C., Mackey, T. and Nobahar, A. 2006 "Design Ice Pressure-Area Relationships; Molikpaq Data", Report prepared for Canadian Hydraulics Centre, National Research Council of Canada, Version 2.0

Klohn-Crippen, 1995. Molikpaq ice loading events, Amauligak I-65: Summary tables and selected sheets showing strain gauge and extensometer response. Report for Gulf Canada Resources Ltd. (CHC 14-55)

Klohn-Crippen, 1998. DynaMAC: Molikpaq Ice Loading Experience, Report to Program on Energy Research and Development, March 1998, PERD/CHC Report 14-62.

McCreath, WE, Hodge, WE, and Harrington, AG., 1982. 'Geotechnical Design Considerations for the Gulf Oil Mobile Arctic Caisson, Beaufort Sea.' Second Canadian Conference on Marine Geotechnical Engineering, Halifax, June 1982. Canadian Geotechnical Society.

Qu, H.J. and Boyce, M.C., 2005. Stress-strain behaviour of thermoplastic polyurethanes, Mechanics of Materials, Vol. 37, pp. 817-839.

Rogers, B.T., and Jefferies, M.G., 1986. Molikpaq multi-year ice event report, April 12, 1986 at Gulf et al. Amauligak I-65. Frontier Development Division, Gulf Canada Resources. November 1986. p. 24. (CHC 14-35)

Rogers, B.T, Graham, C.A. Been, K. and Jefferies M.G., 1991a. Dynamic ice/structure interaction with the Molikpaq at Amauligak I-65; Phase 2, Vol. 1 of 2 – Characterization of Sand Core Behaviour on April 12, 1986. Gulf Canada Resources Ltd., April 1991. (CHC 14-23)

Rogers, B.T, Spencer, P.A. and Hardy, M.D., 1991b. Dynamic ice/structure interaction with the Molikpaq at Amauligak I-65; Phase 2, Vol. 2 of 2 – Load measurement on the Molikpaq at Amauligak I-65. Gulf Canada Resources Ltd., April 1991. (CHC 14-24)

Rogers, B.T., Hardy, M., Jeffries, M. and Wright, B., 1998. DynaMAC: Molikpaq Ice Loading Experience. PERD project report by Klohn-Crippen, March 1998. (CHC 14-62)

Sandwell, 1991. See Appendix C of Rogers et al (1991b)

Sladen, J.A. 1989. Problems with interpretation of sand state from cone penetration test, Geotechnique, Vol. 39, No. 2, pp. 323-332.

Sladen, J.A. and Hayley, D.W. 1988. Molikpaq Geotechnical Study. Assessment of in situ sand state and implications for predicted performance. Natural Resources Canada Open File Report

Sladen, J.A. and Hewitt, K.J. 1989. Influence of placement method on the in situ density of hydraulic sand fills, Canadian Geotechnical Journal, Vol. 26, No. 3, pp. 453-462

Smyth, M.W. and Spencer, P.A., 1987. Review of Ice Load Measurement Techniques on the Gulf Molikpaq, Final Report for Gulf Canada Resources by GEOTECHnical Resources Ltd., June 1987. (CHC 14-44)

Spencer, P.A., Jefferies, M.G., Neth, V., Sopczak, L.L. and Wells, W.W., 1989. Dynamic ice/structure interaction with the Molikpaq at Amauligak I-65, Phase 1B, Appendix A: Detailed Review of MEDOF and Strain Gauge Calibration. Gulf Canada Resources Ltd., May 1989. (CHC 14-15)

Timco, G.W., Johnston, M.E., and Frederking, R., 1999. The NRC Ice Load Catalogue, National Research Council-Canadian Hydraulics Centre Controlled Technical Report HYD-CTR-058, Vol. 1 & 2, January, 1999.

Timco, G.W., Johnston, M.E., and Wright, B.D., 2005. Multi-year ice loads on the Molikpaq: May 12, 1986 event. Proceedings, 18th International Conference on Port and Ocean Engineering under Arctic Conditions (POAC'05), Vol. 1, pp. 453-462, Potsdam, NY, USA.

Timco, G. W. and Johnston, M. 2003. Ice loads on the Molikpaq in the Canadian Beaufort Sea, Cold Regions Science and Technology, Vol. 37, pp 51– 68

Timco, G. W. and Johnston, M. 2004. Ice loads on the caisson structures in the Canadian Beaufort Sea, Cold Regions Science and Technology, Vol. 38, pp 185– 209

Timco, G.W. and Croasdale, K.R., 2006. How Well Can We Predict Ice Loads?, Proceedings 18th International Symposium on Ice, IAHR'06, Vol. 1, pp 167-174, Sapporo, Japan.

Vanmarcke, E., 1983. "Random Fields: Analysis and Synthesis", MIT press.

Wright, B.D. and Timco, G.W. 2001. First-year ridge interaction with the Molikpaq in the Beaufort Sea, Cold Regions Science and Technology, Vol. 32, pp 27–44.

APPENDICES

Appendix A **List of Time Periods with SY or MY Ice**

Appendix B **Molikpaq Analysis Report (by Ian Jordaan & Associates)**

Appendix C **MEDOF Panel Performance Assessment**

Appendix D **Extensometer Sign Convention**

Appendix E **Background to Strain Gauge and Extensometer Calibrations**

Appendix F **Strain Gauge and Extensometer Calibration Factors from MEDOF Panels**

Appendix G **Video Analysis (by Brian Wright & Associates)**

Appendix H **Ice Thickness Documentation**

Appendix I **Geotechnical Analysis (by Kevin Hewitt & Associates)**

Appendix J **Review of Molikpaq Geotechnical Material (by Dr. Tim Law of Carleton University)**

Appendix K **Event Summary Table and Face Load Plots**

Please see subdirectories for Appendix contents